

NUREG/CR-2229
EPRI NP-1783
GEAP-24962-1
Vol. 1

BWR Large Break Simulation Tests — BWR Blowdown/Emergency Core Cooling Program

Volume 1

Prepared by L. S. Lee, G. L. Sozzi, S. A. Allison

**Nuclear Engineering Division
General Electric Company**

**Prepared for
U.S. Nuclear Regulatory Commission**

**and
Electric Power Research Institute**

**and
General Electric Company**

NOTICE

This report was prepared as an account of work sponsored by an agency of the United States Government. Neither the United States Government nor any agency thereof, or any of their employees, makes any warranty, expressed or implied, or assumes any legal liability or responsibility for any third party's use, or the results of such use, of any information, apparatus product or process disclosed in this report, or represents that its use by such third party would not infringe privately owned rights.

Available from

GPO Sales Program
Division of Technical Information and Document Control
U. S. Nuclear Regulatory Commission
Washington, D. C. 20555

Printed copy price: \$10.00

and

National Technical Information Service
Springfield, Virginia 22161

NUREG/CR-2229
EPRI NP-1783
GEAP-24962-1
Vol. 1
R2

BWR Large Break Simulation Tests — BWR Blowdown/Emergency Core Cooling Program

Volume 1

Manuscript Completed: March 1981
Date Published: April 1982

Prepared by
L. S. Lee, G. L. Sozzi, S. A. Allison

Nuclear Engineering Division
General Electric Company
San Jose, CA 95125

Prepared for
Division of Accident Evaluation
Office of Nuclear Regulatory Research
U.S. Nuclear Regulatory Commission
Washington, D.C. 20555
NRC FIN No. B3014

and
Electric Power Research Institute
3412 Hillview Avenue
Palo Alto, CA 94303

and
Nuclear Engineering Division
General Electric Company
San Jose, CA 95125

NOTICE

Availability of Reference Materials Cited in NRC Publications

Most documents cited in NRC publications will be available from one of the following sources:

1. The NRC Public Document Room, 1717 H Street, N.W.
Washington, DC 20555
2. The NRC/GPO Sales Program, U.S. Nuclear Regulatory Commission,
Washington, DC 20555
3. The National Technical Information Service, Springfield, VA 22161

Although the listing that follows represents the majority of documents cited in NRC publications, it is not intended to be exhaustive.

Referenced documents available for inspection and copying for a fee from the NRC Public Document Room include NRC correspondence and internal NRC memoranda; NRC Office of Inspection and Enforcement bulletins, circulars, information notices, inspection and investigation notices; Licensee Event Reports; vendor reports and correspondence; Commission papers; and applicant and licensee documents and correspondence.

The following documents in the NUREG series are available for purchase from the NRC/GPO Sales Program: formal NRC staff and contractor reports, NRC-sponsored conference proceedings, and NRC booklets and brochures. Also available are Regulatory Guides, NRC regulations in the *Code of Federal Regulations*, and *Nuclear Regulatory Commission Issuances*.

Documents available from the National Technical Information Service include NUREG series reports and technical reports prepared by other federal agencies and reports prepared by the Atomic Energy Commission, forerunner agency to the Nuclear Regulatory Commission.

Documents available from public and special technical libraries include all open literature items, such as books, journal and periodical articles, and transactions. *Federal Register* notices, federal and state legislation, and congressional reports can usually be obtained from these libraries.

Documents such as theses, dissertations, foreign reports and translations, and non-NRC conference proceedings are available for purchase from the organization sponsoring the publication cited.

Single copies of NRC draft reports are available free upon written request to the Division of Technical Information and Document Control, U.S. Nuclear Regulatory Commission, Washington, DC 20555.

Copies of industry codes and standards used in a substantive manner in the NRC regulatory process are maintained at the NRC Library, 7920 Norfolk Avenue, Bethesda, Maryland, and are available there for reference use by the public. Codes and standards are usually copyrighted and may be purchased from the originating organization or, if they are American National Standards, from the American National Standards Institute, 1430 Broadway, New York, NY 10018.

NUREG/CR-2229
EPRI NP-1783
GEAP-24962-1
March 1981
DRF E00-66

BWR LARGE BREAK SIMULATION TESTS
BWR BLOWDOWN/EMERGENCY CORE COOLING PROGRAM

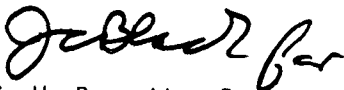
Volume 1

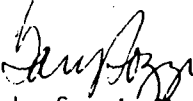
L. S. Lee
G. L. Sozzi
S. A. Allison

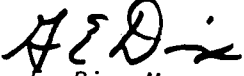
Contributors:

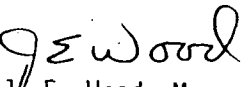
J. Ashjaee
D. W. Danielson

W. S. Hwang
D. A. Wilhelmson

Approved: 
G. W. Burnette, Program Manager
BWR BD/ECC Program

Approved: 
G. L. Sozzi, Manager
LOCA System Technology

Approved: 
G. E. Dix, Manager
Safety and Thermal Hydraulics
Technology

Approved: 
J. E. Wood, Manager
Nuclear Core Technology

Prepared for the
U.S. Nuclear Regulatory Commission
and Electric Power Research Institute
Under Contract NCR-04-76-215

Printed in the United States of America
Available from
National Technical Information Service
U.S. Department of Commerce
5285 Port Royal Road
Springfield, VA 22161

NUCLEAR ENGINEERING DIVISION • GENERAL ELECTRIC COMPANY
SAN JOSE, CALIFORNIA 95125

GENERAL  ELECTRIC

LEGAL NOTICE

This report was prepared by the General Electric Company as an account of work sponsored by the Nuclear Regulatory Commission, the Electric Power Research Institute, and the General Electric Company. No person acting on behalf of the NRC, the Institute, or members of the Institute, or General Electric Company:

- A. Makes any warranty or representation, express or implied, with respect to the accuracy, completeness, or usefulness of the information contained in this report, or that information, apparatus, method or process disclosed in this report may not infringe privately owned rights, or*
- B. Assumes any liabilities with respect to the use of, or for damages resulting from the use of any information, apparatus, method or process disclosed in this report.*

ABSTRACT

The BD/ECC Program is an experimentally based program jointly sponsored by the Nuclear Regulatory Commission, the Electric Power Research Institute, and the General Electric Company. The BD/ECC 1A Test Phase of this program involves investigating the integral systems effects of emergency core coolant injection during a hypothetical LOCA. Tests were conducted in a BWR system simulator, the Two-Loop Test Apparatus (TLTA), which features a full-size electrically heated bundle. Fluid delivery systems were included to simulate emergency coolant injections.

Tests conducted under this program include large break (design basis accident), small break, and core uncover under slow loss-of-coolant (boil-off) transient. Three separate topical reports are issued, one for each type of test. This topical covers the large break results.

ACKNOWLEDGMENTS

This report was completed as a team effort. In addition to those listed whose contributions were integrated into the report, credits are due the following persons: S. D. Stevens for reducing the data and preparing figures, H. Ngo for assisting in conducting the tests as well as contributing to data reduction. Gratefully acknowledged are technical guidance rendered by Dr. G. E. Dix and B. Maztner and the Program Management Group: Dr. W. D. Beckner of NRC, Dr. S. P. Kalra of EPRI, and G. W. Burnette of GE.

SUMMARY

The BWR system simulator, Two-Loop Test Apparatus (TLTA), has been used to experimentally investigate the system thermal hydraulic and bundle heat transfer responses over a wide range of simulated BWR LOCA conditions. The facility was originally built in 1974 under the BWR Blowdown Heat Transfer Program in which early system blowdown responses were extensively evaluated. During the ensuing years, the facility was modified under the BWR Blowdown/Emergency Core Cooling (BD/ECC) Program. The modifications were made to accommodate changes in BWR fuel and system designs and for investigations extending into the emergency core cooling (ECC) injection period of a BWR LOCA (with an 8x8 bundle). An earlier phase of this BD/ECC Program, 8x8 BDHT, has been reported previously.

The objectives of the test phase herein reported were to obtain a physical understanding of the BWR system thermal hydraulic and bundle heat transfer responses during a LOCA simulation, and to provide a data base for evaluating the models and assumptions used in BWR analyses. To meet these objectives, 14 tests were conducted under this test phase: 11 tests simulated a large break (DBA) LOCA; two tests simulated a small break LOCA; and one test series simulated low-flow, core uncover heat transfer. The latter two test series were reported separately. The significant findings from the large break test series are:

- The phenomenon of counter-current flow limitation at the bundle inlet was found to play an important part in removing energy from the bundle. Early in the transient, the bundle inventory was prevented from draining completely by the counter-current flow limiting condition at the bundle inlet. Because of this inventory retention, the stored energy in the rods was almost completely removed before the bundle dried out. A few rods entering into film boiling were quickly rewetted by inventory redistribution following lower plenum bulk flashing. Later in the transient, the CCFL condition at the bundle inlet contributed to early bundle reflood.
- The subcooled ECC injection was sufficient to condense all the steam generated in the core region and led to CCFL breakdown at the top of the core. Consequently, the bundle was reflooded rapidly, the system refilled, and the upper plenum emptied.
- The bundle heated to a maximum temperature that was quite low: less than 700°F (310°C) for an average power bundle and less than 1000°F (538°C) for a peak power bundle receiving nominal rates of ECC injection. These

low temperatures are attributable to: (a) dry-out delay caused by bundle inlet CCFL; (b) rod rewets and enhanced cooling caused by core spray, and (c) early bundle reflood, which was promoted by the CCFL condition at the bundle inlet.

CONTENTS

<u>Section</u>	<u>Page</u>
1 INTRODUCTION	1-1
1.1 Background	1-1
1.2 Program Objectives	1-2
1.3 Report Objective and Scope	1-5
2 FACILITY DESCRIPTION	2-1
2.1 Test Facility Description	2-1
2.1.1 General Description	2-1
2.1.2 Scaling Considerations and Compromises	2-4
2.2 Test Apparatus Modifications	2-7
2.2.1 Leakage Paths	2-11
2.2.2 Recirculation Line Volume	2-11
2.2.3 Separator Liquid Reservoir	2-11
2.2.4 Bundle Power Supply Controller	2-15
2.2.5 Instrumentation	2-15
2.3 Measurement System	2-16
2.3.1 Measurement Objectives	2-16
2.3.2 Measurement Approach	2-16
2.3.3 Measurement Methods	2-16
2.3.4 Instrumentation	2-17
2.3.5 Accuracy of Data	2-17
2.4 Test Operation	2-27
3 EXPERIMENTAL RESULTS	3-1
3.1 Test Plan and Summary	3-1
3.2 Scenario of System Response	3-1
3.2.1 Description of the Reference Test (6425 Run 2)	3-1
3.2.2 Highlights of Other Tests	3-23
3.3 System Simulation Effects	3-68
3.3.1 Effect of Bundle Power	3-68
3.3.2 ECC Injection Effects	3-74

<u>Section</u>	<u>Page</u>
3.3.3 Geometric Effects	3-93
3.3.4 Miscellaneous Effects	3-96
3.4 Analysis and Evaluation	3-112
3.4.1 CCFL Characteristics	3-112
3.4.2 System Depressurization	3-120
3.4.3 TLTA Break Flow Evaluation	3-122
3.4.4 Heat Transfer Coefficient	3-130
3.4.5 Comparison of Heat Transfer Coefficients	3-135
3.4.6 Local Flow Conditions	3-137
3.4.7 Comparison of Heat Transfer Coefficients (Prediction vs. Data)	3-142
4 UTILIZATION OF RESULTS	4-1
5 SUMMARY AND CONCLUSIONS	5-1
6 REFERENCES	6-1
APPENDIX A WORK SCOPE FOR BD/ECC PROGRAM - CONTRACT NO. NRC-04-76-215	A-1
APPENDIX B BD/ECC PROGRAM: LIST OF REPORTS	B-1
APPENDIX C DATA UNCERTAINTY ANALYSIS	C-1
APPENDIX D EFFECTS OF VALUE FAILURE IN TEST 6426 RUN 1	D-1
APPENDIX E VAPOR GENERATION DUE TO FLASHING	E-1
APPENDIX F COUNTER CURRENT FLOW LIMITATION ANALYSIS	F-1
APPENDIX G THE SYSTEM DEPRESSURIZATION EQUATION	G-1
APPENDIX H TLTA BLOWDOWN FLOW MEASUREMENTS AND UNCERTAINTIES	H-1

TABLES

<u>Table</u>	<u>Page</u>
1-1 BD/ECC Original Program Test Phases and Objectives	1-2
1-2 Chronological Summary of Results from BDHT and BD/ECC Programs	1-3
2-1 Flow Areas and Correlations for TLTA Large Break Tests	2-5
2-2 Relative Volume Distributions	2-6
2-3 TLTA Test Configurations	2-8
2-4 Estimated Data Uncertainty of Primary Measurements	2-25
3-1 Summary of Tests Conducted under the BD/ECC 1A Program	3-2
3-2 Brief Description of Goals for Each of the Tests Conducted under the BD/ECC 1A Program	3-3
3-3 Initial Conditions of the BD/ECC 1A Reference Test (6425 Run 2)	3-5
3-4 Sequence of Events for 6425 Run 2 (Avg. Power, Avg. ECC)	3-6
3-5 Peak Power, Average ECC (6424 Run 1) Initial Conditions	3-31
3-6 Sequence of Events for 6424 Run 1 (Peak Power, Avg. ECC)	3-32
3-7 BD/ECC 1A Test 6426 Run 1 Initial Conditions	3-42
3-8 Sequence of Events for 6426 Run 1 (Avg. Power, No ECC)	3-43
3-9 Test 6423 Run 3 Initial Conditions	3-52
3-10 Sequence of Events for 6423 Run 3 (Peak Power, Low Rate/High Temperature ECC)	3-53
3-11 Comparison of Initial Conditions for Average Power, Average ECC Tests	3-107
3-12 Comparison of Timing of Events for Average Power, Average ECC Tests	3-108
3-13 Sensitivity of System Depressurization to Variation of System Parameters	3-123

ILLUSTRATIONS

<u>Figure</u>	<u>Page</u>
2-1 TLTA5 (Two-Loop Test Apparatus Configuration 5) with ECCS	2-2
2-2 TLTA Simulation of BWR Regions and Flow Paths	2-3
2-3 Comparison of Jet Pump Size and Elevation between TLTA and BWR	2-10
2-4 Two-Loop Test Apparatus Configuration 5A (TLTA 5A) with Emergency Core Cooling Systems	2-12
2-5 Flow Paths at Inlet Region of a BWR Fuel Bundle and the TLTA Simulation	2-13
2-6 Steam Separator Liquid Reservoir Which Was Removed for TLTA 5A	2-14
2-7 TLTA 5 Primary Measurements	2-19
2-8 TLTA 5A Primary Measurements	2-21
2-9 Temperature and Differential Pressure Measurements in TLTA 5A	2-23
2-10 Comparison of Measurements from 10 psid (DP20) and 2 psid (DP20A) Pressure Transducers	2-26
2-11 Core Inlet Flow for Average Power, Average ECC Test (6425)	2-28
2-12 Core Inlet Flow for Peak Power, Average ECC Test (6424)	2-29
3-1 Controlled Parameter Responses of Reference Test (6425 Run 2, Average Power, Average ECC)	3-7
3-2 System Responses in the Early Stage of the Blowdown Transient for the Reference Test (6425 Run 2, Average Power, Average ECC)	3-8
3-3 System Pressure Response at Steam Dome	3-10
3-4 Two-Phase Mixture Level Response along the Parallel Flow Paths: Bundle and Bypass	3-11
3-5 Fluid Conditions at Selected Instances for Test 6425 Run 2	3-12
3-6 Fluid Temperature Measurement above Bundle Outlet UTP	3-17
3-7 Fluid Temperature Measurement at Bundle Inlet SEO and Lower Plenum Saturation Temperature	3-18

<u>Figure</u>	<u>Page</u>
3-8 Peak Power Region Cladding Temperatures for TLTA 5A Reference Test (Average Power, Average ECC)	3-19
3-9 Mixture Level Response along the Lower Plenum/Bundle/Upper Plenum Path for Test 6425 Run 2	3-20
3-10 Mixture Level Response along the Guide Tube/Bypass/Upper Plenum Path for Test 6425 Run 2	3-21
3-11 Mixture Level Response in the Annular Downcomer Region for Test 6425 Run 2	3-22
3-12 Pressure Drops across Steam Separator Showing Reversed Flow Caused by ECC Condensation	3-24
3-13 Mass Inventory Response at Various Regions for Test 6425 Run 2	3-25
3-14 Break Flow Measurements for the Reference Test	3-26
3-15 ECC Injection Rates for Test 6425 Run 2	3-27
3-16 Bundle Temperature Response at Selected Elevations for Test 6425 Run 2	3-28
3-17 Peak Cladding Temperature for Test 6425 Run 2	3-29
3-18 System Pressure Response for Test 6424 Run 1, Peak Power, Average ECC	3-33
3-19a Two-Phase Mixture Level Response for Test 6424 Run 1 along LP/Bundle/UP Path	3-34
3-19b Two-Phase Mixture Level Response for Test 6424 Run 1 along Guide Tube/Bypass/UP Path	3-35
3-20 Regional Mass Responses for Test 6424 Run 1	3-36
3-21 ECC Injection Rates for Test 6424 Run 1	3-37
3-22 Break Flows from Turbine Meter and Drag Disc Measurements for Test 6424 Run 1	3-38
3-23 Peak Cladding Temperature Response for Test 6424 Run 1	3-39
3-24 Bundle Temperature Responses at Selected Elevations for Test 6424 Run 1	3-40
3-25 System Pressure Response for 6426 Run 1 (Avg. Power, No ECC)	3-44
3-26a Two-Phase Mixture Level Response along Bundle Path for Test 6426 Run 1	3-45
3-26b Two-Phase Mixture Level Response along Bypass Path for Test 6426 Run 1	3-46
3-27 Mass Inventory Responses at Various Regions for Test 6426 Run 1	3-47

<u>Figure</u>	<u>Page</u>
3-28 Break Flows from Turbine Meter and Drag Disc Measurements for Test 6426 Run 1	3-48
3-29 Bundle Temperature Response at Peak Power Regions for Test 6426 Run 1	3-49
3-30 Bundle Temperature Response at Peak Power Regions for Test 6421 Run 2 (Average Power, No ECC)	3-50
3-31 System Pressure Response for Test 6423 Run 3 (Peak Power, Low Rate/High Temperature ECC)	3-54
3-32a Two-Phase Mixture Level Response along Bundle Path for Test 6423 Run 3	3-55
3-32b Two-Phase Mixture Level Response along Bypass Path for Test 6423 Run 3	3-56
3-33 Regional Mass Responses for Test 6423 Run 3	3-58
3-34 ECC Injection Rates for Test 6423 Run 3	3-59
3-35 Peak Cladding Temperature Response for Test 6423 Run 3	3-60
3-36 System Pressure Responses for Scoping Series Tests 6406 Run 1 and 6406 Run 3	3-62
3-37 Mixture Level Responses for Average Power Tests with and without ECC of Scoping Series	3-63
3-38 Mass Inventory Responses for Average Power Tests with and without ECC of Scoping Series	3-64
3-39a Temperature Responses in Lower Half of Bundle for Average Power Tests with and without ECC of Scoping Series	3-65
3-39b Temperature Responses in Upper Half of Bundle for Average Power Tests with and without ECC of Scoping Series	3-66
3-40 Cladding Temperatures at Peak-Power Elevation (71 in.) for Scoping Series Tests	3-67
3-41 Comparison of System Pressure Responses for Average ECC Tests with Average Power (6425/2) and Peak Power (6424/1)	3-69
3-42 Comparison of Regional Inventory Responses for Average ECC Tests with Average Power (6425/2) and Peak Power (6424/1)	3-70
3-43 Comparison of Pressure Difference across the Bundle for Average ECC Tests with Average Power (6424/2) and Peak Power (6424/1)	3-71
3-44 Comparison of Mixture Level Response along the Bundle Path for Average ECC Test with Average Power (6425/2) and Peak Power (6424/1)	3-72
3-45 Comparison of ECC Injection Rates for Average ECC Tests with Average Power (6425/2) and Peak Power (6424/1)	3-73

<u>Figure</u>	<u>Page</u>
3-46 Comparison of Peak Cladding Temperature Responses for Average ECC Tests with Average Power (6425/2) and with Peak Power (6424/1)	3-75
3-47 Comparison of Peak Cladding Temperatures for Tests with and without ECC	3-76
3-48 Comparison of Regional Masses for Tests 6425/2 (Average Power, Average ECC) and 6426/1 (Average Power, No ECC)	3-78
3-49 Comparison of System Pressures for Average Power Tests with and without ECC	3-79
3-50 Comparison of Lower Plenum Mass Inventories for Average Power Tests with and without ECC	3-80
3-51 Comparison of Bundle Mass Inventories for Average Power Tests with and without ECC	3-81
3-52 Comparison of Upper Plenum Mass Inventories for Average Power Tests with and without ECC	3-82
3-53 Comparison of Guide Tube Mass Inventories for Average Power Tests with and without ECC	3-83
3-54 Comparison of Bypass Region Mass Inventories for Average Power Tests with and without ECC	3-84
3-55 Comparison of Annulus Region Mass Inventories for Average Power Tests with and without ECC	3-85
3-56 Comparison of Calculated Fluid Densities (Based on Turbine Meter and Drag Disc Measurements) at the Drive Line Break for Tests with and without ECC	3-87
3-57 Comparison of Volumetric Flowrates through the Suction Line Break for Average Power Tests with and without ECC	3-88
3-58 Comparison of Volumetric Flowrates through the Drive Line Break for Average Power Tests with and without ECC	3-89
3-59 Comparison of System Pressure Responses for Peak Power Tests with Average ECC (6424/1) and Low Rate/High Temperature ECC (6423/3)	3-90
3-60 Comparison of ECC Injection Rates for Peak Power Tests with Average ECC (6424/1) and Low Rate/High Temperature ECC (6423/3)	3-91
3-61 Comparison of Two-Phase Levels along the Bundle Path for Peak Power Tests with Average ECC (6424/1) and Low Rate/High Temperature ECC (6423/2)	3-92
3-62 Comparison of Peak Cladding Temperatures for Peak Power Tests with Average (6424/1) and Low (6423/3) ECC	3-94
3-63 Comparison of Mixture Level Responses for Average Power, Average ECC Tests in TLTA 5 and TLTA 5A	3-95

<u>Figure</u>	<u>Page</u>
3-64 Comparison of System Pressure Responses for Average Power, No ECCS Tests in TLTA 5 and TLTA 5A	3-97
3-65 Comparison of System Pressure Responses for Large and Small Break Tests	3-99
3-65a Comparison of System Pressure Responses Following Vapor Flow Initiation	3-100
3-66 Comparison of Mixture Level Responses along the Bundle Path for Large and Small Break Tests	3-101
3-67 Typical Cladding Temperature Response at Selected Elevations for Second Small Break Test (6432) with Degraded ECCS	3-102
3-68 Comparison of Mass Depletion Showing Faster Mass Depletion Rate in LP	3-104
3-69 Estimated Heat Addition from Vessel to Fluid Based on Figure 3-68	3-105
3-70 Comparison of System Pressure Responses for Average Power, Average ECCS Tests	3-109
3-71 Comparison of Level Response along Bundle Path for Average Power, Average ECC Tests	3-110
3-72 Comparison of Regional Mass Responses for Average Power, Average ECCS Tests	3-111
3-73 Counter Current Flow Limiting Conditions at Inlet and Outlet of Bundle Measured at Atmospheric Pressure	3-113
3-74 Limiting Vapor Flows at CCFL Locations	3-115
3-75 Comparison of Lower Plenum Vaporization with Limiting Vapor Flow at SEO for Test 6425 Run 2	3-116
3-76 Comparison of Guide Tube/Bypass Vapor Generation with Limiting Vapor Flow at Bypass Outlet for Test 6425 Run 2	3-117
3-77a Estimated Liquid Downflow at the Bundle Inlet SEO for Test 6425 Run 2	3-118
3-77b Estimated Vapor Flow Corresponding to the Liquid Flow at the SEO for Test 6425 Run 2	3-118
3-78a Estimated Liquid Downflow into Bundle through UTP for Test 6425 Run 2	3-119
3-78b Estimated Vapor Flow Corresponding to Liquid Flow at UTP for Test 6425 Run 2	3-119
3-79 Blowdown Loop Break Flow Measurement Locations in TLTA 5A	3-124
3-80 Total Break Flow Determined from Inventory Method for Average Power Tests with (6425/1) and without (6426/1) ECC	3-125

<u>Figure</u>	<u>Page</u>
3-81a Suction Line Break Flow from TM/DD Measurements for Average Power Tests with (6425/2) and without (6426/1) ECC	3-126
3-81b Drive Line Break Flow from TM/DD Measurements for Average Power Tests with (6425/2) and without (6425/1) ECC	3-127
3-82 Suction Line Break Flow from Blowdown Nozzle DP Measurements for Average Power Test with (6425/2) and without (6426/1) ECC	3-129
3-83 Selected Bundle Locations for Heat Transfer Coefficient Evaluation for TLTA 5A Tests	3-131
3-84 Measured Temperatures and Calculated Heat Transfer Coefficients for Test 6421 Run 2	3-132
3-85 Measured Temperature and Calculated Heat Transfer Coefficient for Test 6422 Run 3	3-133
3-86 Measured Temperature and Calculated Heat Transfer Coefficient for Test 6423 Run 3	3-134
3-87 Comparison of Heat Transfer Coefficients for Tests 6421 Run 2, 6422 Run 3, 6423 Run 3	3-136
3-88 Core Inlet Mass Flux Used for MAYU Calculation of Test 6423 Run 3 Local Conditions	3-138
3-89 Local Mass Flux Determined by MAYU for Selected Elevations of Peak Power Low ECC Test (6423/3)	3-139
3-90 Local Void Fraction Determined by MAYU at Selected Elevations for Peak Power Low ECC Test (6423/3)	3-139
3-91 Measured Inside Cladding Temperatures at Selected Elevations for Peak Power, Low ECC Test (6423/3)	3-140
3-92 HCODE Determined Heat Transfer Coefficients at Selected Elevations for Peak Power, Low ECC Test (6423/3)	3-141
3-93 Comparison of Heat Transfer Coefficients Between Those Determined from Data and Those from EM Methodology	3-144

LIST OF ACRONYMS

BD/ECC	blowdown/emergency core cooling
BP	bypass region
BWR	boiling water reactor
CCFL	counter current flow limitation (flooding)
DBA	design basis accident (a double-ended guillotine break of the recirculation line)
ECC	emergency core cooling
EL	elevation (axial location with reference to a datum such as bottom of vessel)
EM	evaluation models (currently used for BWR licensing calculations)
EPRI	Electric Power Research Institute
GE	General Electric Company
HPCS	high pressure core spray
HTC	heat transfer coefficient
LOCA	loss-of-coolant accident
LP	lower plenum
LPCI	low-pressure coolant injection
LPCS	low-pressure core spray
LPF	lower plenum flashing
NRC	Nuclear Regulatory Commission
POS	heater rod position in the bundle
SEO	bundle inlet side entry orifice
TLTA	Two-Loop Test Apparatus, scaled BWR system simulator
UP	upper plenum
UTP	bundle outlet upper tie plate

Section 1

INTRODUCTION

1.1 BACKGROUND

The BWR Blowdown/Emergency Core Cooling (BD/ECC) Program is an experimentally based program to investigate the integral system response under hypothetical loss-of-coolant accident conditions. This program is part of a continuing effort for improving and advancing safety technology. It is sponsored by the Nuclear Regulatory Commission (NRC), the Electric Power Research Institute (EPRI), and the General Electric Company (GE).

The BD/ECC program can be considered an extension of the BWR Blowdown Heat Transfer (BDHT) Program (1) which was completed in late 1975. The BD/ECC program is divided into several test phases (Table 1-1) which are designed to investigate different portions or variations of the BWR LOCA responses. A building block approach to evaluate the effects of various ECC systems, operating independently and in combination, was adopted.

The first test phase of the BD/ECC Program, 8x8 BDHT, has been completed and reported (2). The BD/ECC 1A Test Phase is the subject of this current report. A comprehensive summary of tests conducted and results obtained from the two programs is shown in Table 1-2.

The tests were conducted in the BWR system simulator, the Two-Loop Test Apparatus (TLTA), located in San Jose, California (GE). Main features of this system simulator include a full-size, electrically heated bundle and coolant injection systems to supply the emergency core cooling fluid. The TLTA was modified to meet the overall objectives of each testing phase with the overall objective of maintaining a real-time, thermal-hydraulic response. Each modification is assigned a different designation, as evident from Table 1-2.

Table 1-1

BD/ECC ORIGINAL PROGRAM TEST PHASES AND OBJECTIVES

Test Phase	Test Conditions and Objectives
1. 8x8 BDHT	- 8x8 test bundle, no ECCS operation, stepwise scaling basis from BWR/4 to BWR/6. Investigate BDHT system performance of scaled BWR/4 and BWR/6.
2. BD/ECC-1A	- Investigate effectiveness of high-pressure core spray (HPCS) and low-pressure core spray (LPCS).
3. BD/ECC-1B*	- Investigate reflooding phenomenon in the TLTA system.
4. BD/ECC-2*	- Parametric variations at high cladding temperature, if required.
5. Non-jet pump plant BD/ECC*	- Investigate the ECC interaction with the system during blowdown in a representative non-jet pump test system configuration.

*NOTE: These test phases have been eliminated. The program has been restructured, and the test facility is being upgraded.

1.2 PROGRAM OBJECTIVES

The principal objective of the BD/ECC Program is to obtain and evaluate basic BD/ECC data from test system configurations which have performance characteristics similar to a BWR during a hypothetical LOCA. Other objectives include the determination of the degree of proficiency to which the current LOCA models describe the observed phenomena and, where necessary, the development of improved physical interpretation of the governing phenomena. Specific objectives of the program are included in Appendix A, where an excerpt from the Contract Project Agreement is presented.

The objective of the BD/ECC 1A Test Phase was to obtain integral system thermal-hydraulic responses and to evaluate the effect of ECC injection. The period of the LOCA transient of primary interest ranges from break initiation through core spray systems operation. While the original test plan emphasized the large break, hypothetical design basis accident, two tests were included to investigate the more probable small pipe break transient. The execution of the planned small break (3) tests was advanced in response to interest generated by the accident at TMI-2. In

Table 1-2

CHRONOLOGICAL SUMMARY OF RESULTS FROM BDHT AND BD/ECC PROGRAMS

Program Phase	TLTA Configuration	Objective	Status	Simulation Bases	Results
7 x 7 BDHT	TLTA-1	Baseline BWR Data	Completed 1975	- BWR/4 - BDHT only - 7 x 7 full-size bundle - Full bundle power (4.55 MW)	<ul style="list-style-type: none"> ● Bundle heatup governed by uncover ● PCT margin identified ($\sim 1000^{\circ}\text{F}$) ($540^{\circ}\text{C}$) ● Improved phenomena understanding
8 x 8 BDHT	TLTA-2	Bundle Variation	Completed 1976	- BWR/4 - BDHT only - 8 x 8 full-size bundle - Full bundle power (6.5 MW)	<ul style="list-style-type: none"> ● PCT for 8 x 8 bundle < PCT for 7 x 7 ● No new phenomena
	TLTA-3	BWR/4 and 6 Tie Back	Completed 1977	- BWR/6 - BDHT only - 8 x 8 full-size bundle - Full bundle power (5.05 & 6.5 MW)	<ul style="list-style-type: none"> ● BWR/6 depressurization slower compared with BWR/4 as expected
BD/ECC-1A	TLTA-4	Baseline Data with No ECC	Completed 1978	- BWR/6 - BDHT only - 8 x 8 full-size bundle - Full bundle power (5.05 & 6.5 MW) - Upper tie plate mockup	<ul style="list-style-type: none"> ● System depressurization slower with improved jet pump simulation (extended tail pipe) ● CCFL at bundle inlet holds up inventory in bundle, delays uncover, and enhances heat transfer
	TLTA-5	Early (<100 sec.) ECC Interaction	Completed 1979	- BWR/6 - ECCS injection, multiple failure - 8 x 8 full-size bundle - Full bundle power (2.6 to 6.5 MW) - ECCS parameter variations	<ul style="list-style-type: none"> ● System depressurization slower with ECC injection ● ECCS effective in reducing PCT ● CCFL at bundle inlet delays heat-up
	TLTA-5A	BD/ECC Interaction with Improved Simulation (Reflood & Power)	Completed 1980	- BWR/6 - ECCS injection, multiple failure - 8 x 8 full-size bundle - Full bundle power (5.05 & 6.5 MW) - ECCS parameters variation	<ul style="list-style-type: none"> ● ECCS effective in cooling bundle ● Max. PCT < 1000°F (540°C) ● Bundle refloods early (before LP refills completely) because of CCFL at bundle inlet
	TLTA-5B	Small Break Scoping Test	Completed 1980	- BWR/6 - High-pressure ECC injection on high drywell pressure - 8 x 8 full-size bundle - Full bundle power after 7 sec.	<ul style="list-style-type: none"> ● ECCS effective in maintaining level above core region. ● No new phenomena

Table i-2 (Continued)

CHRONOLOGICAL SUMMARY OF RESULTS FROM BDHT AND BD/ECC PROGRAMS

<u>Program Phase</u>	<u>TLTA Configuration</u>	<u>Objective</u>	<u>Status</u>	<u>Simulation Bases</u>	<u>Results</u>
	TLTA-5C	Small Break Test Baseline Data	Completed 1980	<ul style="list-style-type: none"> - BWR/6 multiple failure - HPCS deactivated for degraded test - ADS activated and delayed 120 sec. - LPCS plus 2/3 LPCI - 8 x 8 full-size bundle 	<ul style="list-style-type: none"> ● Bundle inventory maintained by ECC fluid and CCFL at SEO ● No bundle heat-up ● System refilled
	TLTA-5A	Bundle Uncovery, Boil-Off Separate Effects	Completed 1980	<ul style="list-style-type: none"> - BWR/6 - 8 x 8 full-size bundle - Decay heat bundle power - Steady system pressure variation - Steady decay heat variation 	<ul style="list-style-type: none"> ● Heat transfer rates well predicted by standard correlations (e.g., Dittus-Boelter) ● Void distribution agrees well with drift-flux model

addition, this test phase was expanded to include core uncover (boil-off) tests (4) under slow loss of inventory transients.

1.3 REPORT OBJECTIVE AND SCOPE

This report is written with these objectives in mind:

- a. provide a comprehensive summary of the program,
- b. describe the scenario of system response in large break tests, and
- c. provide an interpretation and evaluation of the observed phenomena.

This report is separated into two volumes. Volume I contains the summary, discussion, analyses, and conclusions. The BWR system simulator used for the tests is briefly described. Test results are synthesized and presented in phenomenological descriptions of scenarios. Effects of test parameters and effectiveness of ECC injection are discussed. Further evaluation and analysis of data are included. Utilization of results is put into perspective. Additional details and comprehensive sets of data are provided in the Appendices. Volume II contains the data reports.

Other reports from this program are listed in Appendix B.

Section 2

FACILITY DESCRIPTION

The BWR system simulator, Two-Loop Test Apparatus (TLTA), is described in detail in the facility description report (5). Recapitulated below are key features and significant compromises of TLTA. Also included are additions to and modifications of the TLTA and an updated description of measurements and uncertainties.

2.1 TEST FACILITY DESCRIPTION

The BWR system simulator, TLTA, is shown in Figure 2-1. Configurations 5 and 5A (TLTA 5 and 5A) were used for the BD/ECC 1A large break tests. Described below are common features of Configurations 5 and 5A. Modifications made to TLTA 5 to make it TLTA 5A are described in Subsection 2.2.

2.1.1 General Description

Salient features of TLTA 5 and 5A are:

- a. integral system,
- b. full-size bundle,
- c. full power,
- d. typical BWR operating pressure and temperature, and
- e. emergency core cooling systems.

The full-size electrically heated bundle (which is capable of duplicating the power output of a BWR fuel bundle from full initial power to the decay heat power) is enclosed in a pressure vessel. Also contained inside the vessel are such BWR counterparts as guide tube, jet pumps, and steam separator, as shown in Figure 2-1. Connected to the vessel outside are two recirculating loops, a feedwater system, and a steam line with pressure regulation capability.

The configurations of the TLTA simulate the reference BWR system in all the major regions. Figure 2-2 depicts the TLTA representation of the BWR regions. These regions include the lower plenum, guide tube, core region (viz., the bundle and

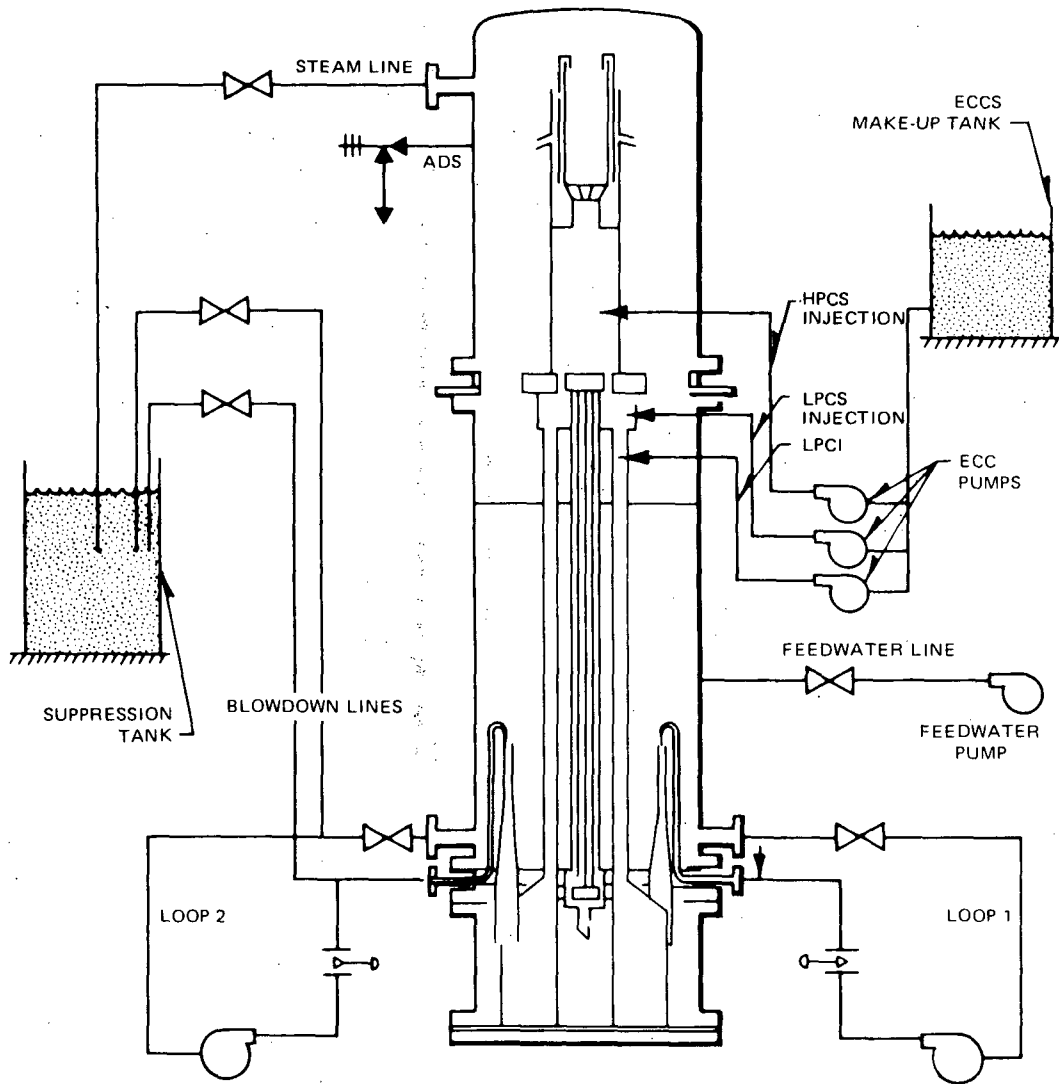


Figure 2-1. TLTA5 (Two-Loop Test Apparatus Configuration 5) with ECCS

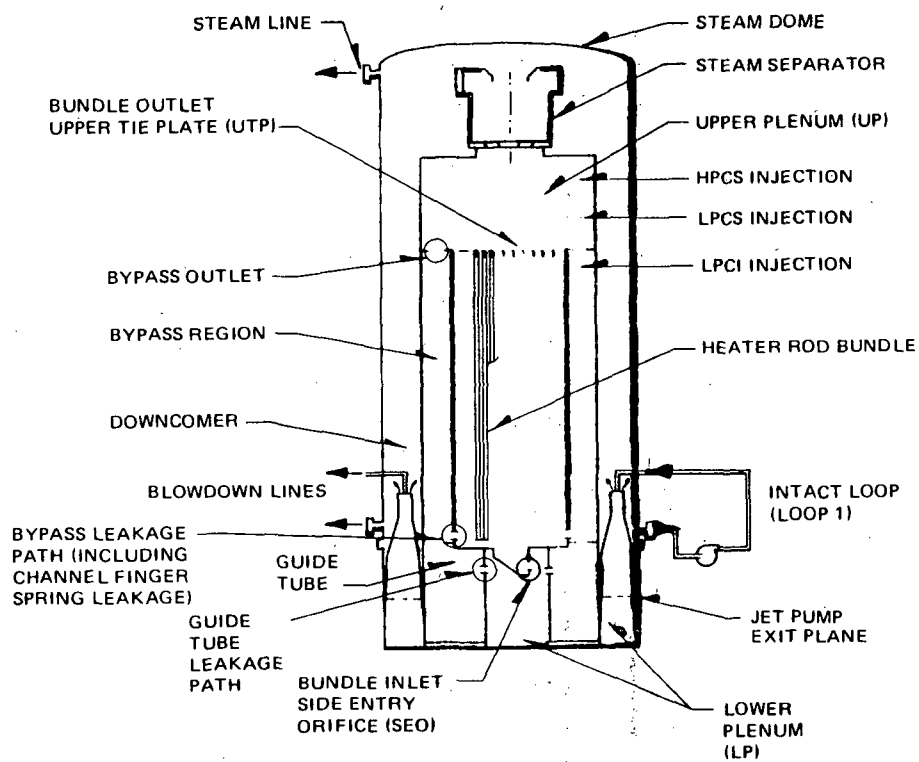


Figure 2-2. TLTA Simulation of BWR Regions and Flow Paths

bypass region), upper plenum, steam separator, steam dome, annular downcomer, recirculation loops, and ECC injection systems. The regional fluid volumes and their relative distributions within the reference BWR system are simulated.

All significant internal flow paths between adjacent regions are preserved. These paths are identified in Figure 2-2; the flow areas are given in Table 2-1. Key elements along the flow paths are provided to ensure that the anticipated phenomenon is preserved. In an effort to preserve the CCFL characteristics at the bundle inlet and exit, for instance, a typical side entry orifice and a simulated upper tie plate are used in TLTA. The leakage paths, as will be discussed later, were modified during the program to improve the simulation.

The external flow paths are also simulated to give close simulation to a BWR system. These include the steam line flow, recirculation flow, feedwater flow, break flow, and ECC flow. The steam line contains a pressure regulator which duplicates the function of a reactor pressure control system and the main steam isolation valve. The intact loop recirculation pump has coastdown characteristics similar to the BWR counterpart. The broken loop recirculation lines are connected to the two blowdown lines. Flow limiters are installed in the blowdown lines to simulate and vary the break size. The ECC injection systems have flow characteristics (6) similar to those of a BWR system. The feedwater system is not representative, however.

2.1.2 Scaling Considerations and Compromises

The fundamental scaling consideration in TLTA is to achieve the real-time response objective. Both Configurations 5 and 5A of TLTA were scaled to a reference BWR/6 - 218 having 624 fuel bundles. Each bundle consists of 64 rods in an 8x8 array. The ratio of TLTA to BWR bundles is 1/624. This same ratio is the basis for scaling the regional volumes, masses, energies, and flow rates.

The TLTA was designed with the constraint of accommodating a full-size test bundle and to achieve the fundamental objective of real-time response. A number of compromises have been made in order to satisfy these scaling considerations and geometric limitations. The compromises on the regional volumes, as can be seen from Table 2-2, are the larger steam space and the recirculation loops. The larger steam space was found (5) to have a negligible effect on the system response. The large recirculation loop volume can be expected to retard the system depressurization because the larger fluid mass will flash into vapor and interact with the rest of the system.

Table 2-1

FLOW AREAS AND CORRELATIONS FOR TLTA LARGE BREAK TESTS

<u>Flow Location</u>	<u>Flow Area</u> (in ²)	<u>Correlation*</u> W(lbm/sec), ΔP(psi), ρ(lbm/ft ³)
Bundle inlet orifice	4.638	$W = 2.48 [\Delta P \times \rho]^{1/2}$
Bypass leakage	0.2732	$W = 0.119 [\Delta P \times \rho]^{1/2}$ forward flow $W = 0.113 [\Delta P \times \rho]^{1/2}$ reverse flow
Guidetube leakage	0.0908	$W = 0.0379 [\Delta P \times \rho]^{1/2}$
Bypass outlet	0.160	
Bundle outlet (UTP)	11.3	
Bundle	15.15	
Bypass	15.83	
Steam line orifice	3.237	
Suction line break nozzle	0.4336	
Drive line break orifice	0.0804	
HPCS orifice	0.1307	$W = 0.0645 [\Delta P \times \rho]^{1/2}$
LPCS orifice	0.1706	$W = 0.069 [\Delta P \times \rho]^{1/2}$
LPCL orifice	0.1225	$W = 0.0515 [\Delta P \times \rho]^{1/2}$

*Note: Determined from single-phase water calibration data.

Table 2-2
RELATIVE VOLUME DISTRIBUTIONS

Region	Volumes (ft ³)	
	"Ideal" TLTA ^a	TLTA 5 and 5A
Lower Plenum	2.97	3.09
Core	1.38	1.38
Upper Plenum	2.34	2.78
Separation Region	8.21	11.76
Downcomer	2.88	2.88
Recirculation Loop No. 2	0.48	2.09
Recirculation Loop No. 1	0.48	2.79 (0.53) ^b
Bypass	1.05	1.01
Steam Dome	5.09	5.29
Guide Tube Volume	2.03	1.90
<u>Fluid Volumes Governing Key Events Timing</u>		
Volume of saturated liquid in the separation region	3.26	3.26
Volume from jet pump support plate to jet pump throat	1.37	1.37
Volume of inventory in annulus	6.15	6.15
Volume of subcooled liquid in annulus	2.89	2.89

^aIdeal TLTA Volumes = BWR/6 Volumes ÷ 624.

^bTLTA-5A recirculation loop volume after isolation valves closed.

Additional compromises included flow area to fluid volume ratio and the boundary surface area to volume ratio, the flow area being larger in the downcomer region and the lower plenum. This larger flow area renders the fluid velocity slower. However, in both the BWR and TLTA the fluid velocities are typically very low. The higher surface to volume ratio can lead to higher heat addition from the vessel stored energy to the fluid.

In order to assure realistic recirculation flow coastdown performance for the early portion of the blowdown transient, the jet pumps were linearly scaled to height and diameter (5). The resultant TLTA jet pumps are much shorter than the BWR counterparts. However, the mass flux through these jet pumps was scaled to produce the typical mass flux as in the BWR. Other fluid regions in the TLTA, typically in the downcomer region, were correspondingly made shorter to produce a real-time response. The size of the TLTA jet pumps and vessel relative to the reference BWR can be seen in Figure 2-3. The short jet pumps result in a lower hydrostatic head. This lower head can have a significant effect during the reflooding phase of the transient. The height of the jet pumps can affect the height to which the bundle region can be reflooded because the bundle is in a hydraulic path parallel with the jet pumps. The elevation distortion can also affect the level response even though the timings of the controlling events in the early transient are preserved in TLTA.

Finally, any radial or parallel channel effects which might exist in the multi-bundle BWR would be much less prominent in the single bundle TLTA. Effects such as core spray injection on CCFL breakdown and parallel channel hydraulics on bundle reflood are expected to be important after ECC injection. They are not well represented in TLTA.

2.2 TEST APPARATUS MODIFICATIONS

The TLTA has been modified to meet the primary objective of each test phase with the overall objective of maintaining a real-time, thermal-hydraulic system response. Each modification of TLTA is assigned a number to identify with that configuration. The evolution of the configurations is summarized in Table 2-3.

The key features of TLTA 5 are the ECC injection systems and the simulated upper tie plate. The significant modifications made to TLTA to transform Configuration 5 to 5A were: improved leakage path simulations and improved bundle power supply controller. Other modifications include recirculation line isolation and removal of the separator liquid reservoir. These modifications have been reported previously (7) and are recapitulated below. A schematic of the TLTA Configuration 5A is shown

Table 2-3

TLTA TEST CONFIGURATIONS

TLTA Configuration Number	Scaling Basis	Design Considerations
1	BWR/4, 560 bundles, 7x7 BDHT base line	1. TLTA design used in the 7x7 BDHT program.
2	BWR/4, 560 bundles, 8x8 BDHT base line	<ol style="list-style-type: none"> 1. Replace 7x7 bundles with 8x8 bundles in TLTA. 2. Modify bundle electrode plate and include new electrode connector design.
3	BWR/6, 624 bundles, 8x8 BDHT (same scaling basis as TLTA-1 for BWR/4)	<ol style="list-style-type: none"> 1. Modify lower plenum volume to match BWR/6. 2. Adjust initial mixture level in annulus to match hydraulic timing of BWR/6. 3. Lower feedwater sparger to provide the proper amount of subcooled liquid in downcomer. 4. Steam line pressure control characteristics of BWR/6. 5. Initial power for 8x8 bundle in BWR/6. 6. Break geometry modified to provide scaled BWR/6 break flow for entire transient (including the subcooled discharge regime). 7. Scaled single side entry orifice for core inlet flow.
4	BWR/6, 624 bundles, 8x8 BDHT, base line design for BD/ECC	1. Modify flow geometry at core exit and at bypass exit to account for counter-current flow limiting (CCFL) phenomena along these flow paths.

Table 2-3

TLTA TEST CONFIGURATIONS (Continued)

TLTA Configuration Number	Scaling Basis	Design Considerations
4 (cont)		<ol style="list-style-type: none"> 2. Lower the jet pump suction inlet and extend the jet pump diffuser/tailpipe into the lower plenum to preserve the timing of the coast-down period and to achieve a more representative lower plenum geometry. 3. Provide for more representative stored heat effects by adding insulation to lower plenum.
5	BWR/6, 624 bundles, BD/ECC 1A, early ECC interaction scoping series	<ol style="list-style-type: none"> 1. Implemented ECCS injection systems.
5A	BWR/6, 624 bundles, BD/ECC 1A, ECC interaction with improved simulation	<ol style="list-style-type: none"> 1. Add bundle to bypass leakage paths to improve simulation of the flow paths at the inlet region of a BWR/6. 2. Include an isolation valve in both the suction and drive lines of the intact recirculation loop to improve simulation of post lower plenum flashing response. 3. Remove the separator liquid reservoir to improve transient simulation. 4. Improve power control by using a new controller for the bundle power supply.

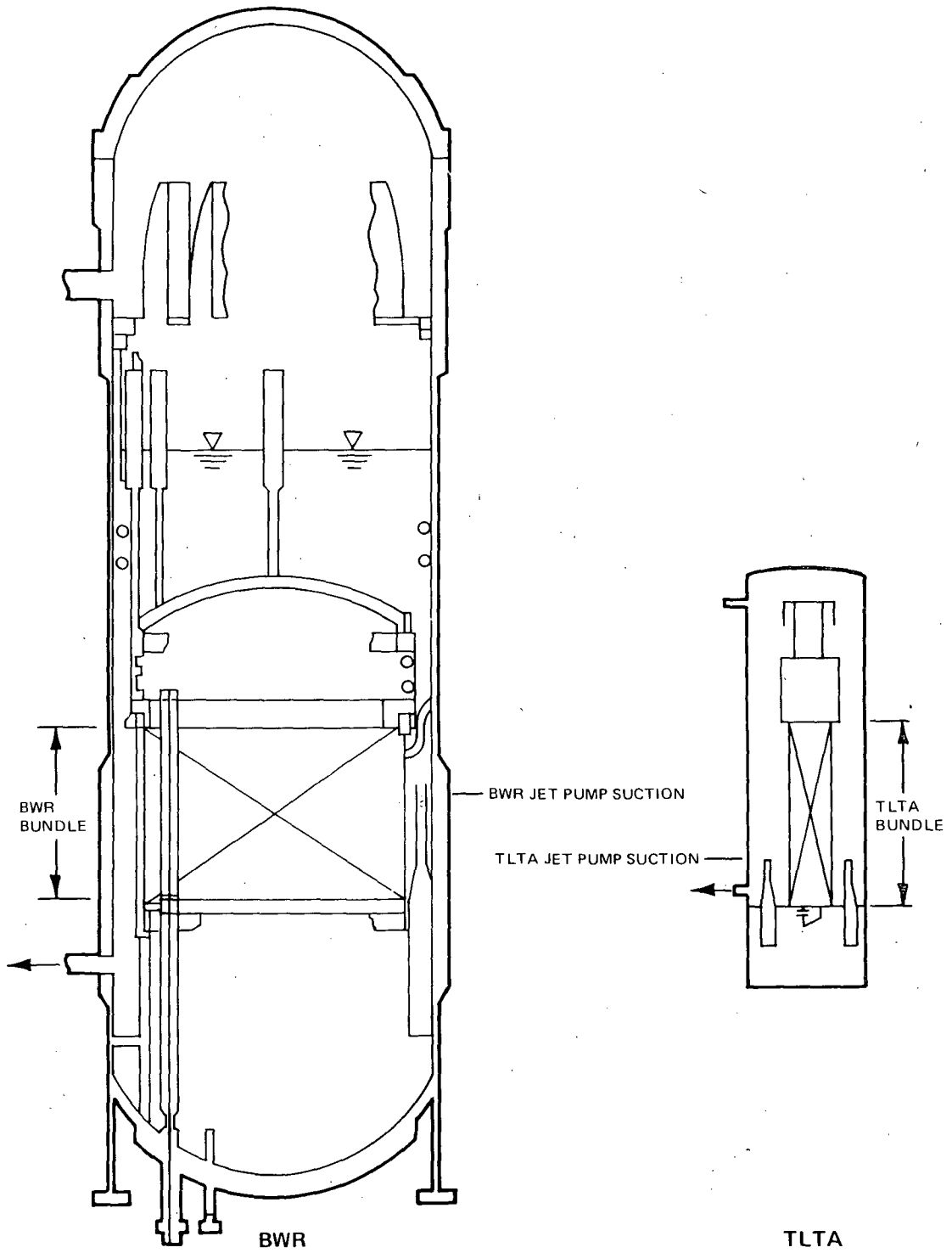


Figure 2-3. Comparison of Jet Pump Size and Elevation between TLTA and BWR (Height Only to Scale, Width Not to Scale)

in Figure 2-4. During the course of TLTA 5A tests there were also other minor additions: improved break flow instrumentation and improved pressure control simulation. These are discussed later.

2.2.1 Leakage Paths

The inlet region of a BWR fuel bundle and that of TLTA 5A are shown in Figure 2-5. Various flow paths of a fuel bundle and the TLTA representations are shown.

Two core-bypass flow paths are included in TLTA 5A. One path allows a proportion of the bundle inlet flow that passes through the side entry orifice to be diverted to the bypass region. Another path permits fluid to flow from the lower plenum through the guide tube and into the bypass region. The orifices (Table 2-1) in each path have been sized to give the correct flow rates under normal operating conditions.

2.2.2 Recirculation Line Volume

The volume of the intact recirculation line was 2.79 ft^3 in TLTA 5. In comparison, the volumetrically scaled value is 0.48 ft^3 . The excessive volume of fluid flashes into steam and interacts with the pressure vessel as the blowdown transient progresses. The added steam generation tends to retard the system depressurizations.

In order to improve the simulation of the post lower plenum flashing response, two isolation valves were used in TLTA 5: one each in the suction and drive lines of the intact recirculation loop. These valves were closed after the recirculation pumps coasted down (at ~ 20 sec). This isolated the major portion of the excess volume, with the remaining volume of $\sim 0.53 \text{ ft}^3$ being close to the desired scale volume.

The blowdown loop has only one valve that closes at the beginning of the transient. This valve does not isolate the mass in the loop but only stops the flow through the recirculating pump.

2.2.3 Separator Liquid Reservoir

The separator liquid reservoir in TLTA-5 (Figure 2-6) contained $\sim 0.52 \text{ ft}^3$ of saturated liquid which, upon flashing, could affect the system response. It was initially installed to assure that the separator would perform the desired function. Subsequent testing after this reservoir was removed showed that the desired function could still be realized. It was removed in TLTA 5A to improve the blowdown response simulation.

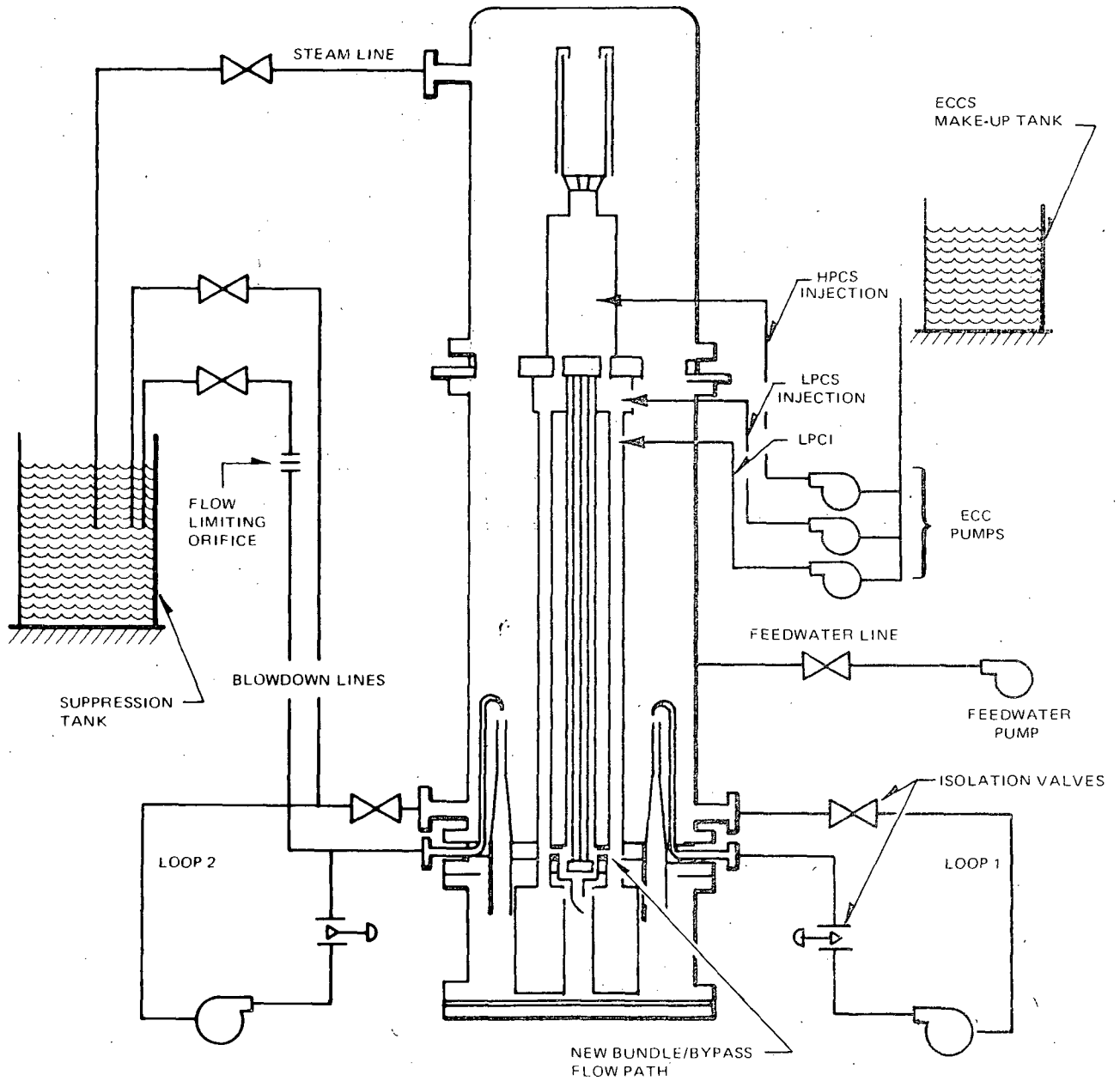


Figure 2-4. Two-Loop Test Apparatus Configuration 5A (TLTA 5A) with Emergency Core Cooling Systems

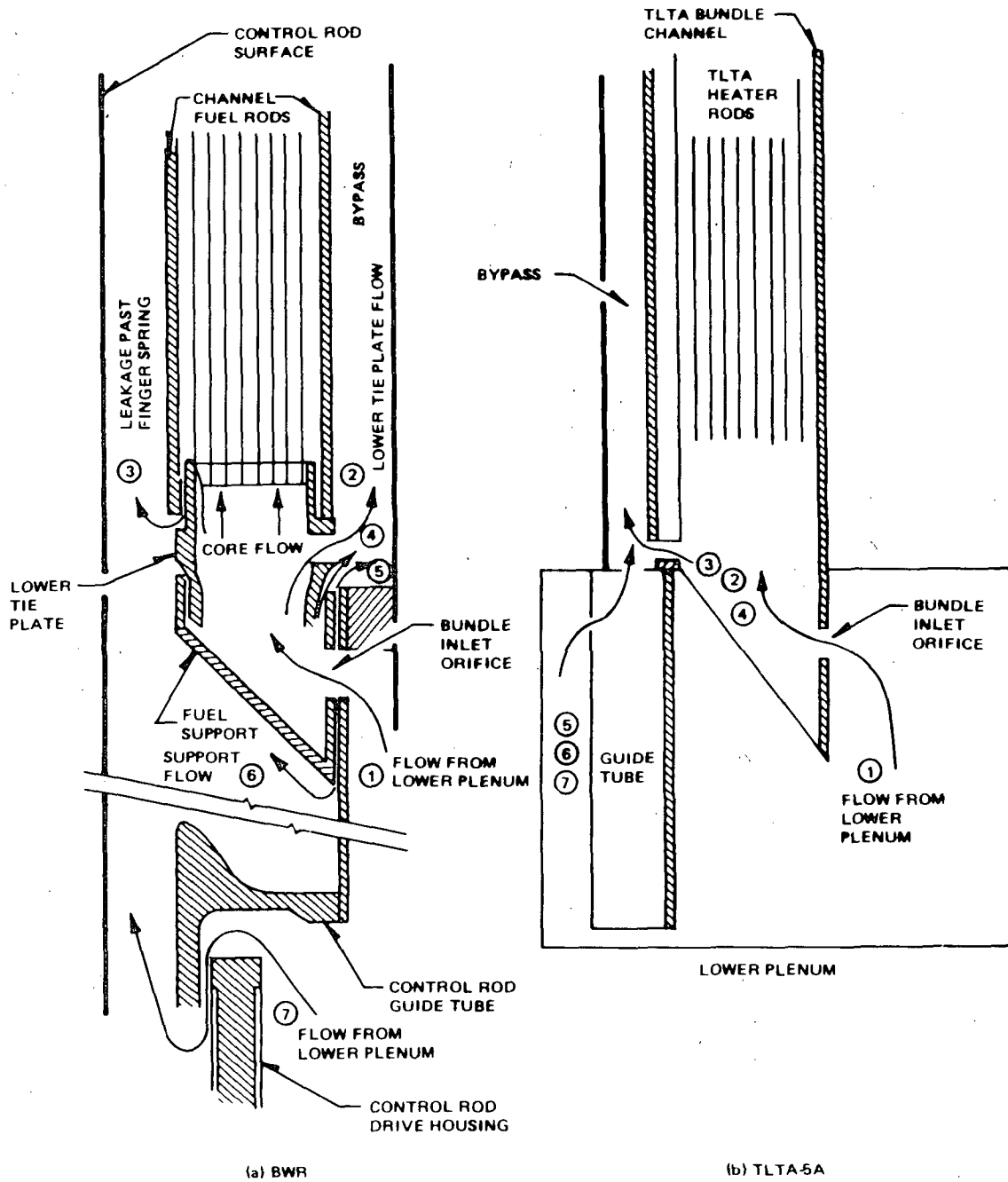


Figure 2-5. Flow Paths at Inlet Region of a BWR Fuel Bundle and the TLTA Simulation

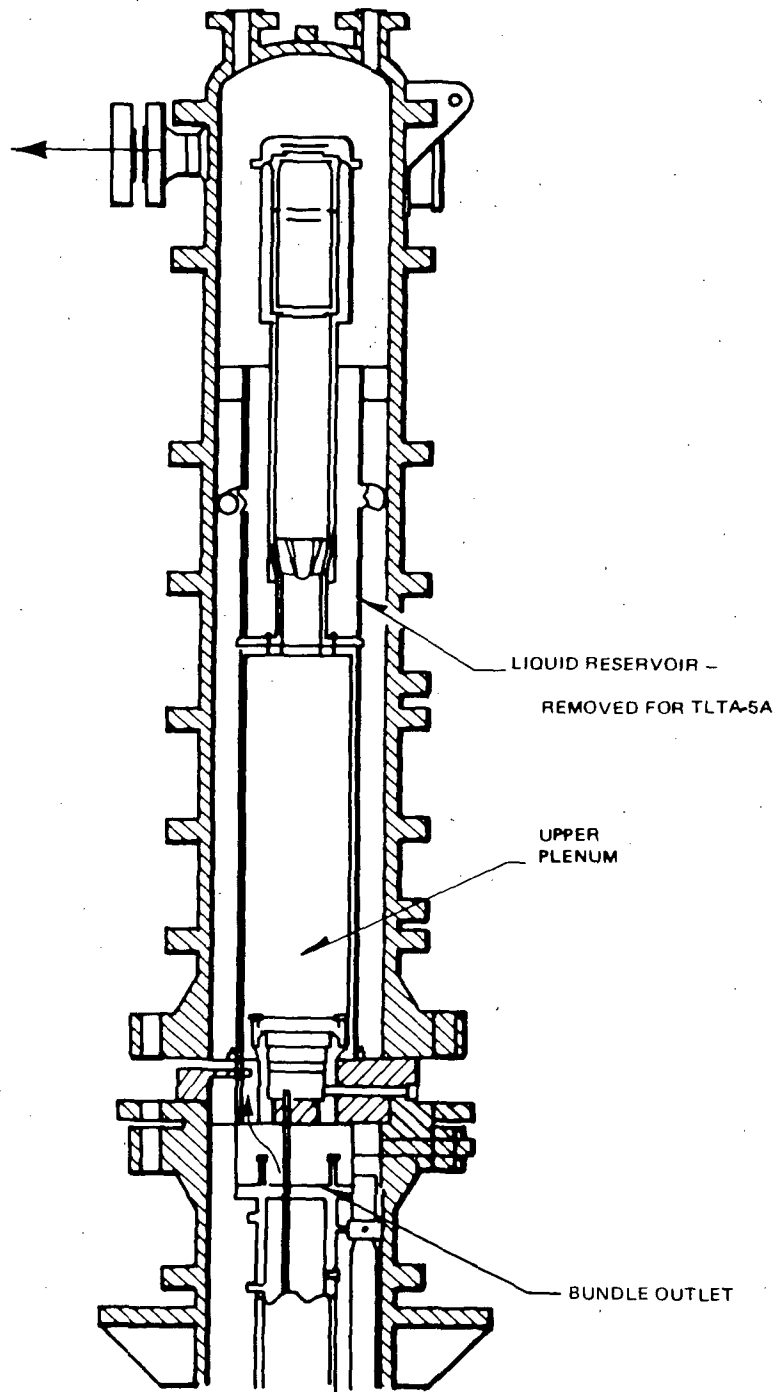


Figure 2-6. Steam Separator Liquid Reservoir Which Was Removed for TLTA 5A

2.2.4 Bundle Power Supply Controller

A new controller was used in TLTA 5A for the bundle power supply. It improved the power control for more accurate simulation for the entire test (~300 sec). The controller used in the previous tests could control power for only 50 seconds, after which the power was held constant.

The power decay of the bundle was calculated on the best estimate value for fission decay heat. The power input also takes into consideration the stored energy effects (8).

2.2.5 Instrumentation

The instrumentation scheme was modified for improved in TLTA 5A measurements as follows:

- a. Flow Measurements. The data obtained from six turbine meters and two drag discs installed in a series of scoping tests was disappointing. Only two turbine meters and one drag disc provided any qualitative data. Post-test evaluation of these instruments identified several problems mostly associated with instrument failures caused by the high temperature environments. Therefore, the free-field turbine meters used at the bundle inlet, the jet pump discharge tail pipes, and the steam separator were replaced with pitot tubes (annubars) in TLTA 5A.
- b. Heat Addition Characteristics. Heat addition from various parts of the test vessel to the fluid can contribute to steam generation and affect the depressurization rate. In order to better characterize the heat addition, thermocouples were installed on the walls of the downcomer, lower plenum, and bundle channel. The insulation installed on the walls during the previous test series appears to have performed satisfactorily after post-test examination. This insulation was also used in the TLTA 5A.
- c. Fluid Temperature Measurements. Additional thermocouples have been installed to the upper plenum and the bypass region to provide additional measurements of fluid temperature and temperature distribution in these regions.
- d. Bundle Temperatures. Thermocouples were added to three heater rods at elevations just above the grid spacers. Previous test data showed that a liquid continuum persisted in the bundle for ~40 seconds during the blowdown with a transition to a vapor continuum thereafter. These thermocouples provide additional information on the distribution of the fluid within the bundle.
- e. Differential Pressures. Several differential pressure measurements were added to aid in data interpretation (see also Figure 2-8 discussed later). They are: DP23 and DP25 along the bundle; DP69 across the limiting flow orifice in the drive/blowdown line; DP42 across the new core-bypass flow path; and DP36 in the annular downcomer region.

2.3 MEASUREMENT SYSTEM

The measurement system used in the BD/ECC 1A program was derived from the methodology evolved from the BDHT Program. The basic philosophy of this methodology is one of obtaining sufficient measurements in order to characterize the system response and perform a mass and energy balance throughout the system. The quantities measured in TLTA include: system pressure, nodal (controlled volume) differential pressure, flow differential pressure, fluid conductivity, fluid temperature, cladding temperature, vessel temperature, valve positions, pump speed, power supply, volume flow, and momentum flux.

The measurement system and its application have been described in detail in the Facility Description Report (5). A summary is provided below.

2.3.1 Measurement Objectives

The measurement system of BD/ECC 1A was developed in keeping with the following objectives:

- a. assure that the initial conditions specified for each test were established;
- b. measure the bundle temperature distribution and the power input;
- c. measure fluid conditions in various regions; and
- d. measure the global system pressure response and obtain sufficient data to perform, as practicable, mass and energy balance on the total system and on key components, e.g., lower plenum.

2.3.2 Measurement Approach

The approach adopted to achieve these measurement objectives was to divide the TLTA into a number of measurement "nodes." In general, these "nodes" are defined by the geometry of the internal vessel hardware and were chosen to correspond to regions within the vessel where changes in cross-sectional area are small. This approach is also used usually for computer code noding in predicting system blow-down response for LOCA analysis.

2.3.3 Measurement Methods

In general, the measurement techniques were the same as those used in the previous BDHT Program (1). Where necessary, alternate measurement techniques were used to supplement these basic measurements.

Schematic drawings of the instrumentation for TLTA Configurations 5 and 5A are shown in Figures 2-7 and 2-8, respectively. The thermocouples and differential pressure transducers are installed in the test bundle as shown in Figure 2-9.

2.3.4 Instrumentation

The instruments used to collect various data in the BD/ECC 1A tests include four pressure transducers, 70 differential pressure transducers, 30 loop thermocouples, 80 cladding thermocouples, 10 conductivity probes, and various other devices such as turbine meters, drag discs, potentiometer (valve position), tachometer, amp-meter, voltmeter, and wattmeter. The output signals from these measuring devices were recorded on a Hewlett-Packard data acquisition system and reduced for further processes on a Honeywell H-6070 system. The details of the function, installation, and application of these instruments are documented elsewhere (5).

2.3.5 Accuracy of Data

Two types of data are presented in this report: direct measurements and derived quantities. The direct measurements are self-evident to interpret. Their accuracy depends primarily upon the instrument and its application in the test system, the associated electronics, and overall measurement and recording system response. Examples of direct measurements are: pressure, differential pressure, temperature, liquid levels in downcomer and lower and upper plena, bundle power, and output signals from the drag discs and turbine meters.

Derived quantities are generally a result of combining one or more direct measurements. These quantities usually require assumptions on interpretation associated with the phenomena for which the measurement is intended. The derived quantities must be interpreted with an understanding of the system response and the governing phenomena. Derived quantities include density, void fraction, mass inventory, and flow rates (volumetric and mass flow).

The overall measurement accuracy of the directly measured quantities, e.g., pressure and differential pressure, is dependent upon the combined effects of the static and dynamic uncertainties. The accuracy of the derived quantities is, of course, also dependent on the overall accuracy of the direct measurements. In addition, because the derived quantities require additional assumptions, they are time- and space-dependent. Their interpretation must be based on understanding of the system response and the governing phenomena.

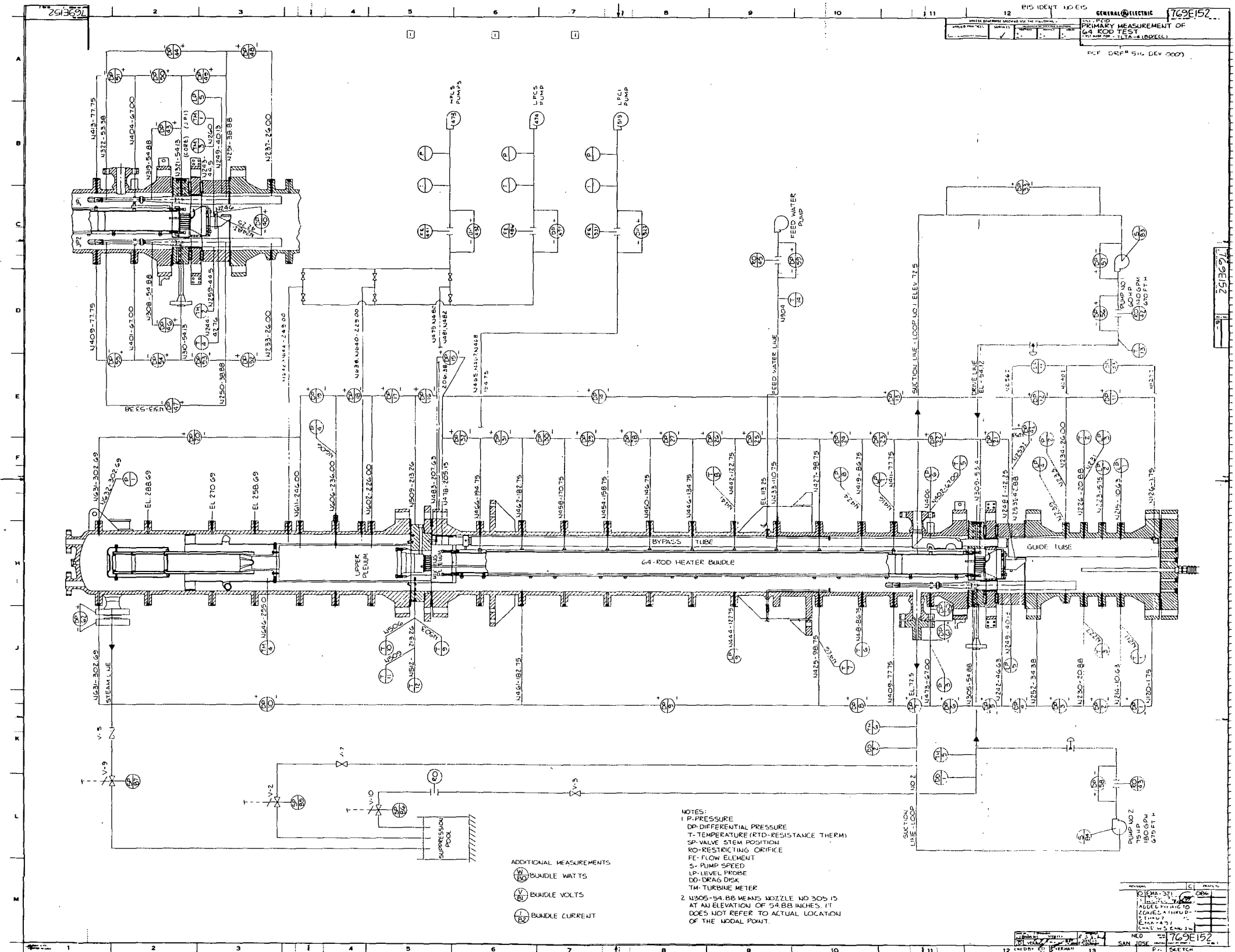
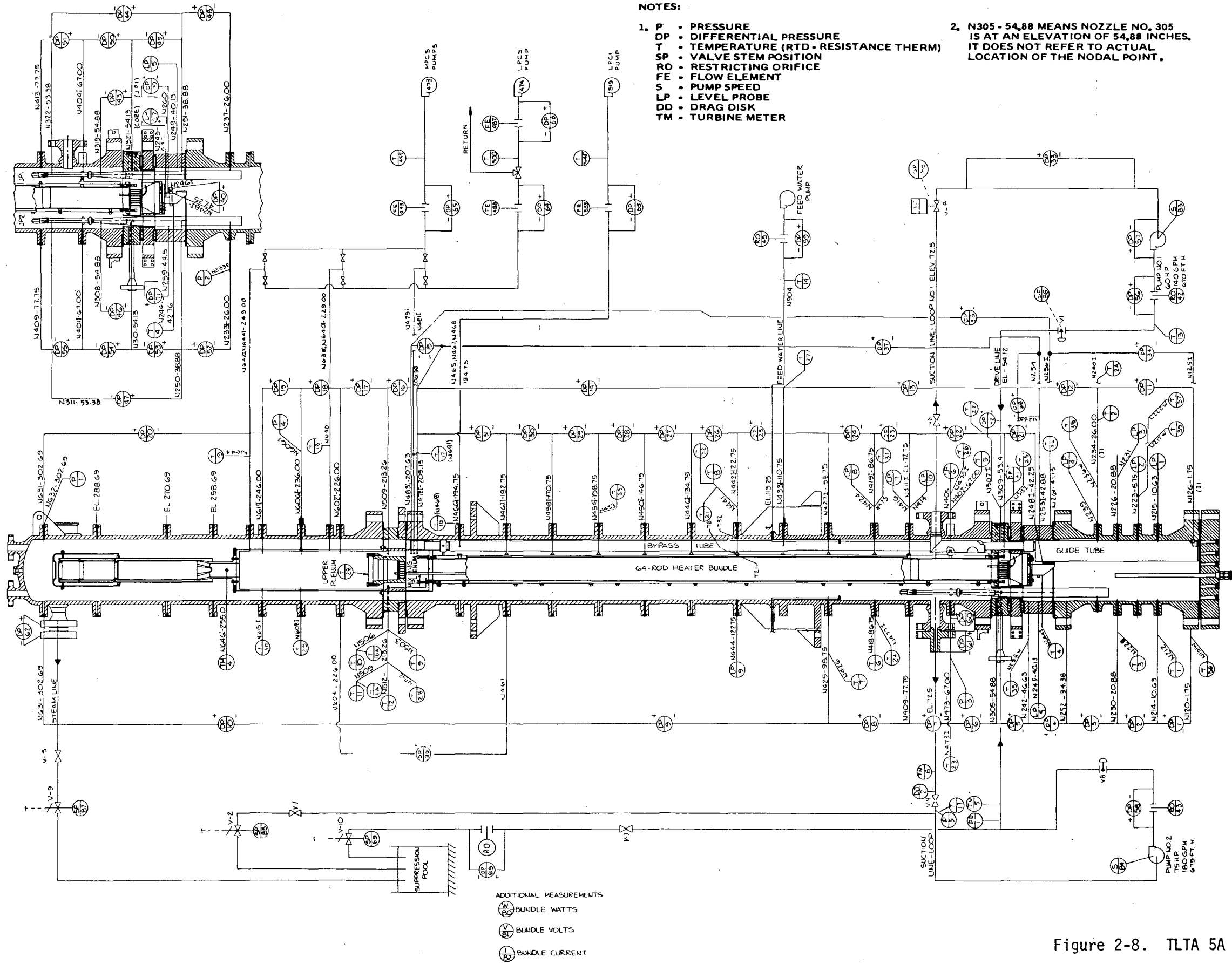


Figure 2-7. TLTA 5 Primary Measurements



- NOTES:**
- P • PRESSURE
 - DP • DIFFERENTIAL PRESSURE
 - T • TEMPERATURE (RTD - RESISTANCE THERM)
 - SP • VALVE STEM POSITION
 - RO • RESTRICTING ORIFICE
 - FE • FLOW ELEMENT
 - S • PUMP SPEED
 - LP • LEVEL PROBE
 - DD • DRAG DISK
 - TM • TURBINE METER
 - N305 - 54,88 MEANS NOZZLE NO. 305 IS AT AN ELEVATION OF 54,88 INCHES. IT DOES NOT REFER TO ACTUAL LOCATION OF THE NODAL POINT.

Figure 2-8. TLTA 5A Primary Measurements

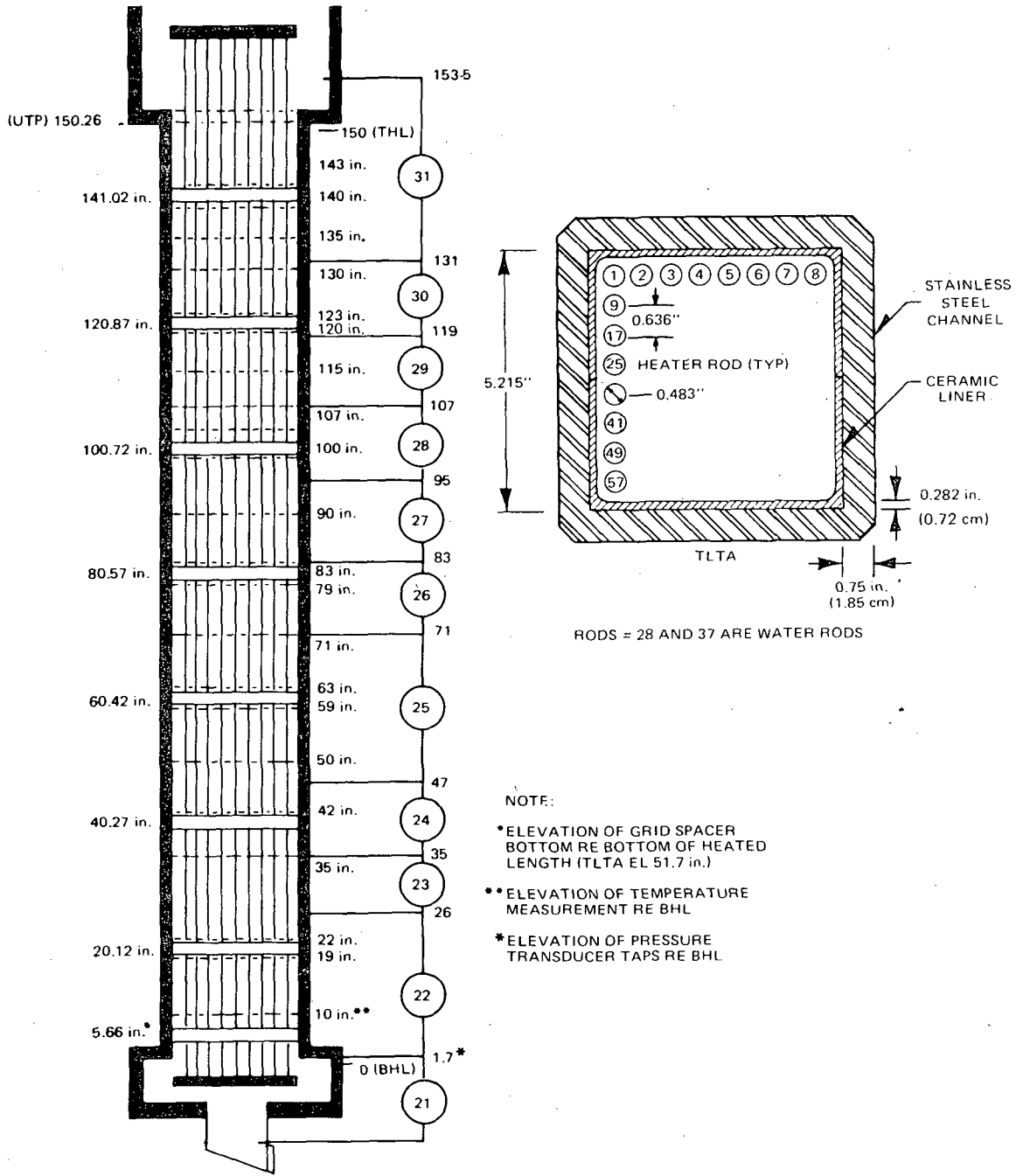


Figure 2-9. Temperature and Differential Pressure Measurements in TLTA 5A

2.3.5.1 Accuracy of Direct Measurements. A comprehensive analysis of measurement uncertainties has been previously performed (9). An updated analysis for the BD/ECC IA program is included in Appendix C.

Results from these analyses showed that the uncertainties in the measurements are acceptably small. Also, redundant information is available for cross reference. Examples of redundant information are: larger differential pressure measurement to supplement a string of smaller ones, and conductivity probe measurements in conjunction with differential pressures for estimating the mixture level.

The uncertainties for the primary measurements are summarized in Table 2-4. The bases for the values in the table are in Appendix C-1.

The sensitivity of the differential pressure measurement was evaluated in one of the tests. Two transducers, one with a range of 10 psid and the other 1 psid, were connected to the same taps. The resulting measurements, shown in Figure 2-10, indicate that the larger range transducer provides comparable sensitivity except at very low, near-zero pressure drops.

2.3.5.2 Accuracy of Derived Quantities. The accuracies of two key derived quantities that will be discussed below are core flow (± 15) and break flow (from $\pm 15\%$ to $\pm 25\%$)

An example of estimating the uncertainty for derived quantities is included in Appendix C-2. The system mass determination and the associated uncertainty estimation are shown. The system mass response is determined from nodal differential pressure measurements. The uncertainty on the mass is estimated from assessing the validity of the assumption that the pressure difference is due primarily to the hydrostatic head.

Shown in Appendix C-3 is the breakflow determined from the system mass balance. The breakflow is the net balance of inflow from ECCS and mass balance in the vessel.

The uncertainties associated with derived quantities are in general estimated as for the system mass and system mass outflow (breakflow). Uncertainty bands included for all the derived quantities are somewhat subjectively estimated as per the examples given.

Table 2-4

ESTIMATED DATA UNCERTAINTY OF PRIMARY MEASUREMENTS

Electrical Power to Bundle

Steady-State: $\pm 0.5\%$ of reading, $\pm 7\text{KW}$

Transient: ± 0.1 sec time constant

Pressures

Steady-State: ± 6 psi

Transient: Time constant 0.02 second

Differential Pressures

Steady-State:

Core Inlet (DP-40) ± 0.05 psid

Bypass Orifice (DP-41, 42): ± 0.08 psid

Jet Pump Diffuser:

#1 (DP-43): ± 0.11 psid

#2 (DP-46): ± 0.08 psid

Lower Plenum: (DP-1,2,3,4): ± 0.03 psid

Bundle: (DP-21,31): ± 0.03 psid

ECCS Flow Orifice

HPCS (DP-65) ± 0.17 psid

LPCS (DP-66) ± 0.08 psid

LPCI (DP-63) ± 0.20 psid

Transient: Studies indicate time constants of 0.1 second or less.

Loop Temperatures: $\pm 4^\circ\text{F}$

Bundle Temperatures: $\pm 0.8\%$ of reading

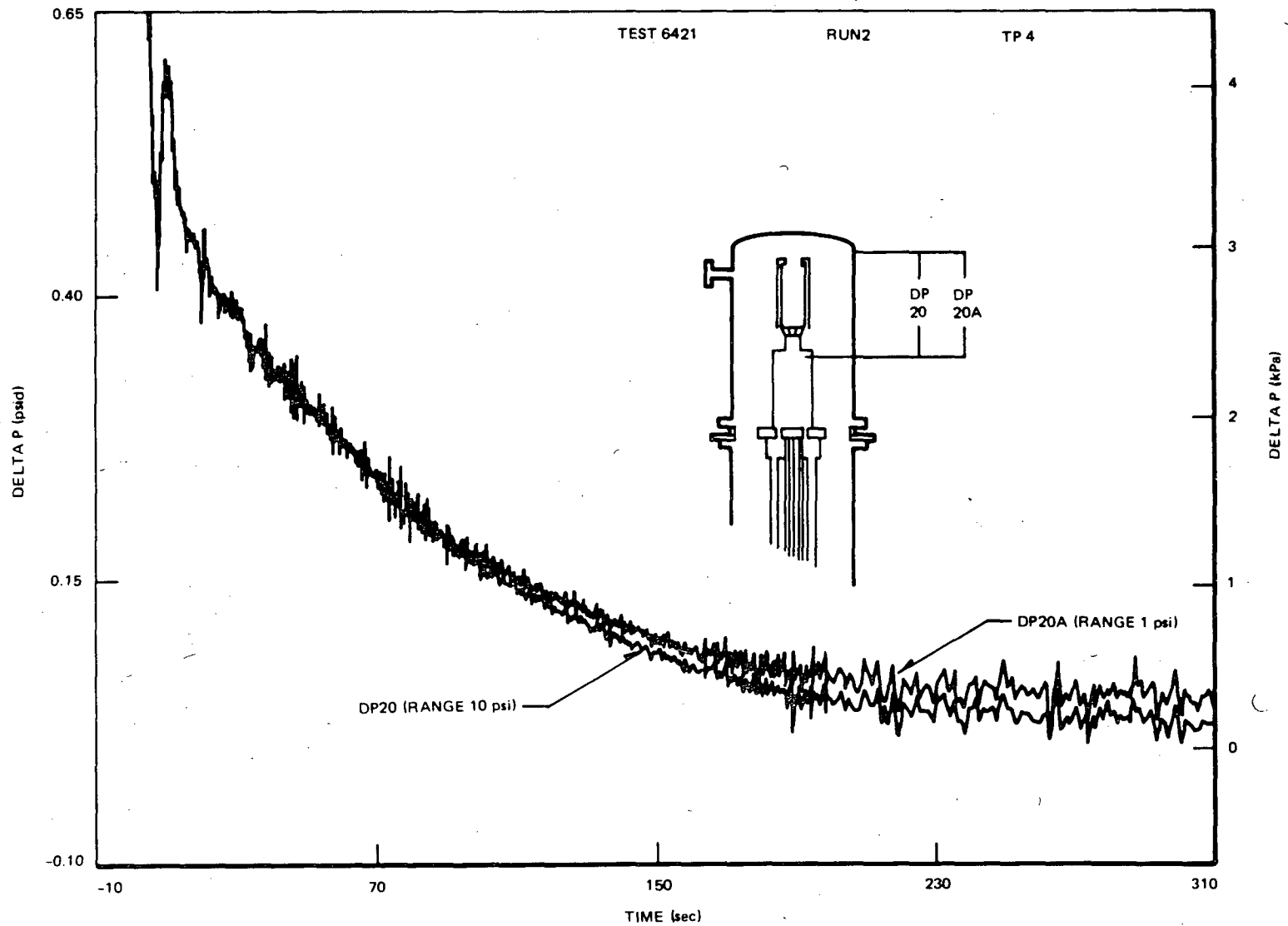


Figure 2-10. Comparison of Measurements from 10 psid (DP20) and 1 psid (DP20A) Pressure Transducers

A more detailed estimate of the core inlet flow is detailed in Appendix C-4. Three methods of determining the core flow are: (a) based on direct DP measurements across the inlet orifice, (b) based on direct measurements with an annubar at core inlet, and (c) based on measurements other than at the core inlet. In all cases the basic measurement, DP, is used in combination with a fluid density in a correlation to determine the flow rate. The accuracy of the flow then depends on the measurement, the correlation, and the fluid density determined from other measurements.

The bundle inlet flow for the first 20 seconds (shortly after lower plenum flashing) are plotted for two typical tests in Figures 2-11 and 2-12. These figures show the values to be nearly identical. The accuracy of the bundle inlet flow at this time span is estimated to be better than $\pm 15\%$.

A more detailed estimate of the breakflow and the associated uncertainty is discussed in Subsection 3.4.3. Four methods were used in determining the flow through the break: (a) system mass balance (as discussed above), (b) combined drag disc and turbine meter measurements, (c) suction line flow limiting nozzle measurements, and (d) the mass increase in the blowdown (suppression) tank. The uncertainties estimated for the methods are: $\pm 15\%$ for mass balance, $\pm 25\%$ for drag disc/turbine-meter, and $\pm 30\%$ for suction nozzle. The suppression pool method shows potential for further development.

2.4 TEST OPERATION

The following is a synopsis of the test operation that is defined in the Facility Description Report (5).

A number of separate effects tests were conducted to calibrate flow paths and determine the performance of the "as-built" equipment. These tests included

- a. flow calibration of orifices for core bypass and bundle inlet (see Table 2-1),
- b. confirmatory calibration of jet pumps,
- c. determination of pump and system characteristics of simulated ECC systems (6), and
- d. CCFL characteristic tests of certain components (10).

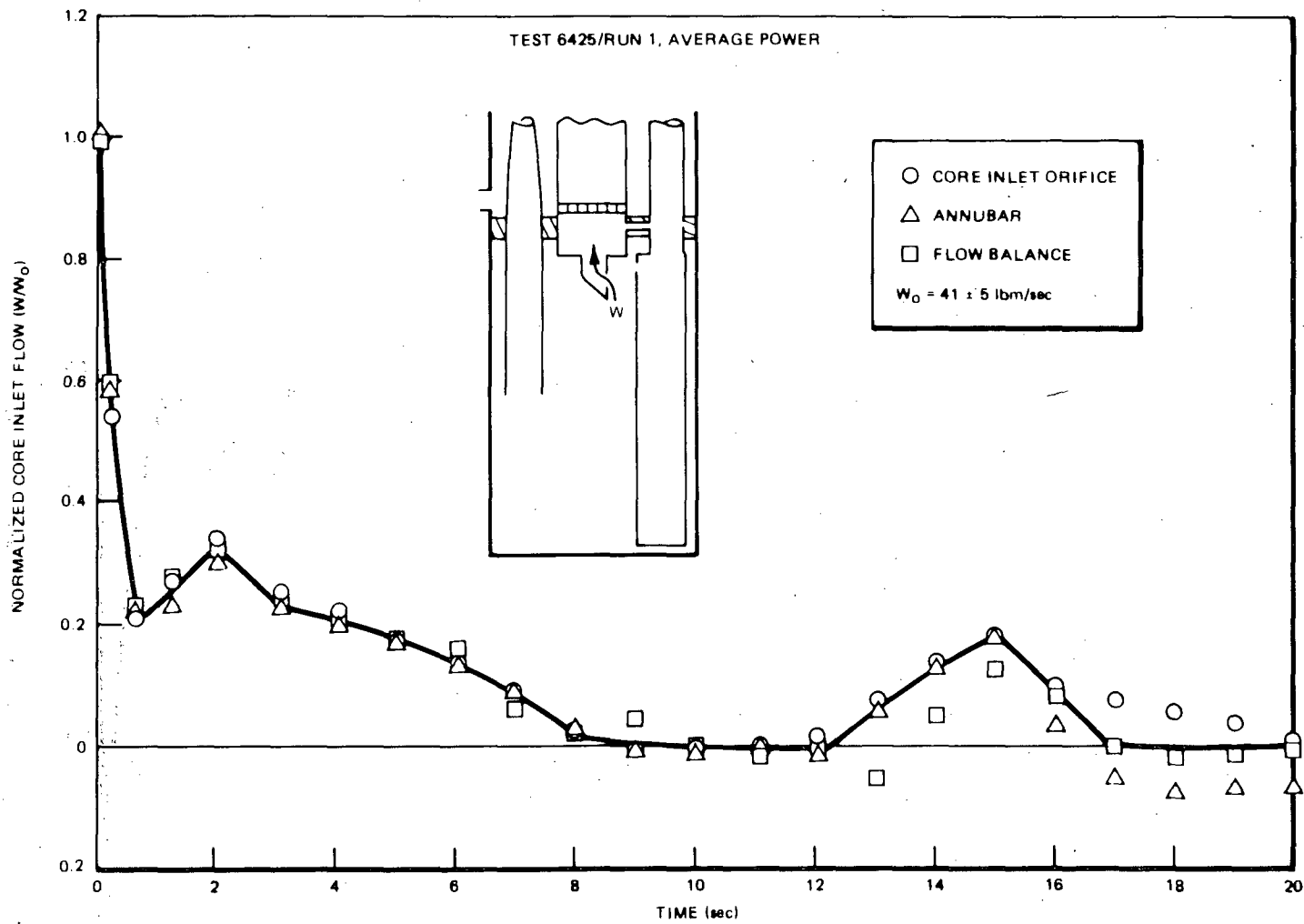


Figure 2-11. Core Inlet Flow for Average Power, Average FCC Test (6425)

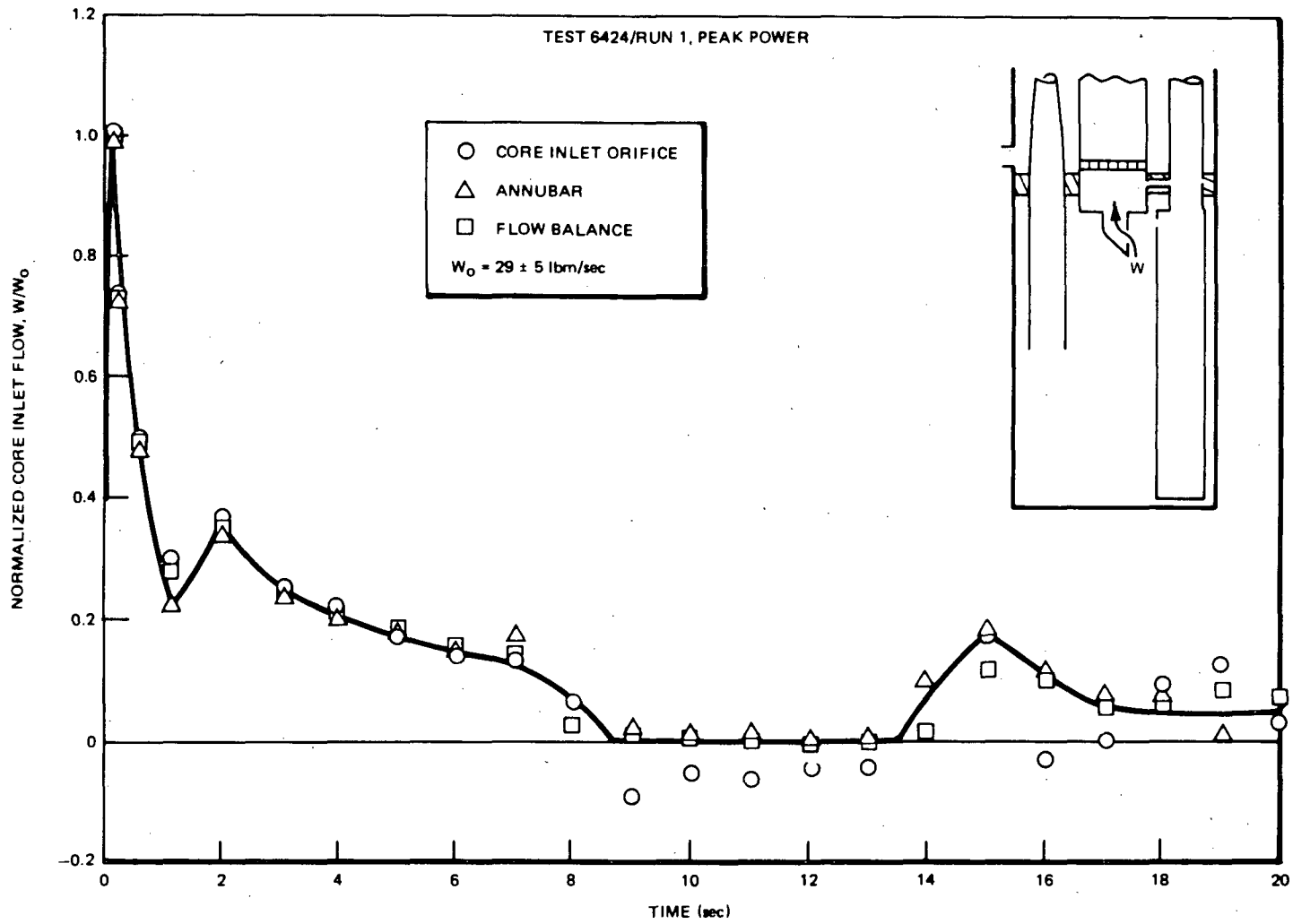


Figure 2-12. Core Inlet Flow for Peak Power, Average ECC Test (6424)

The matrix tests were conducted in three stages to obtain the desired initial conditions.

Stage 1 - establishes the lower plenum temperature.

Stage 2 - establishes subcooling in the lower plenum with steam flow and feedwater flow.

Stage 3 - establishes test initial conditions.

The test procedure used for the test makes certain that a complete instrumentation check is made prior to initiating each test. With the system at operating pressure, all instruments are checked for proper reading with zero flow and with rated flow. Pressure and flow balances throughout the system are checked.

The stages might be repeated a number of times before actual blowdown. This allows the initial conditions to be verified against specified limits. It might also be necessary to fine-tune some of the control settings such as core flow or feedwater flow. After confirmation that the conditions set in Stage 3 bring about the desired initial conditions, the test is started.

Section 3
EXPERIMENTAL RESULTS

3.1 TEST PLAN AND SUMMARY

Tests conducted under the BD/ECC 1A Program are summarized in Table 3-1. A brief description of the test objectives is shown in Table 3-2.

Table 3-1 shows that 14 tests were conducted as compared with the original (11) matrix of 26 tests. Of the 14 tests, the first five were conducted in TLTA 5 in 1978 to scope the outcome of the original matrix. The next four tests were from the series of six tests selected for the improved facility, TLTA 5A. The second small break test (6432) and the boil-off test were inserted in response to a surge of interest for data pertaining to the Three Mile Island kind of accident. The last three tests were conducted with improved instrumentation for measuring break flows.

Results and the reference test data report from the scoping series are included in Appendix I. The small break tests (3) (6431 and 6432) and the boil-off test (4) are the subjects of separate topical reports.

The large break tests conducted in the improved system configuration (TLTA 5A) are reported herein. The average power, average ECC test with improved break-flow measurements (6425 Run 2) is the reference test and is discussed in detail. Highlights of the system response from other tests are also presented.

3.2 SCENARIO OF SYSTEM RESPONSE

3.2.1 Description of the Reference Test (6425 Run 2)

The initial conditions for the reference test are shown in Table 3-3. These conditions are typical of those in a BWR/6. Other controlled conditions, the transient response of which has been designed to simulate that of a BWR, are shown

Table 3-1

SUMMARY OF TESTS CONDUCTED UNDER THE BD/ECC 1A PROGRAM

Test ID	Bundle Power (MW)	Spray Rate	ECC Temp	Break Size	TLTA Configuration	Test Date
6401 Run 4	2.63	high	nominal	DBA	5	Jun 78
6405 Run 3	5.05	average	nominal	DBA	5	Jul 78
6406 Run 1	5.05	average	nominal	DBA	5	Aug 78
6406 Run 3	5.05	-	-	DBA	5	Sep 78
6414 Run 3	6.49	low	high	DBA	5	Sep 78
6421 Run 2	5.05	-	-	DBA	5A	Sep 79
6422 Run 3	5.05	average	nominal	DBA	5A	Oct 79
6423 Run 3	6.49	low	high	DBA	5A	Nov 79
6431 Run 1	2 ^a	average	nominal	small	5B	Dec 79
6432 Run 1	2 ^a	average	nominal	small	5C	Mar 80
6441	(Boil-off test)				5A	Jun 80
6424 Run 1	6.49	average	nominal	DBA	5A ^b	Jul 80
6425 Run 2	5.05	average	nominal	DBA	5A ^b	Jul 80
6426 Run 1	5.05	-	-	DBA	5A ^b	Sep 80

^aBundle power for small break tests was held at 2MW for 7 seconds, then decayed in accordance with the 5.05 MW initial power decaying curve.

^bWith turbinometer and drag disc measurements for break flow and new automatic pressure controller.

Table 3-2

BRIEF DESCRIPTION OF GOALS FOR EACH OF THE TESTS
CONDUCTED UNDER THE BD/ECC 1A PROGRAM

Test	TLTA	Description	Goal
6401 Run 4	5	Peripheral bundle (2.63 MW) with high spray rates at nominal temperature.	Establish system response for the more favorable conditions expected at the periphery of the core.
6405 Run 3	5	Average central bundle with below average spray rates at nominal temperature.	Establish sensitivity of system response to variation of spray rate.
6406 Run 1	5	Average central bundle with average spray rates at nominal temperature.	Establish system response for representative conditions (reference case).
6406 Run 3	5	Average central bundle with <u>no</u> ECC.	Establish system response for a benchmark test to evaluate effects of ECC injection.
6414 Run 3	5	Peak Power bundle with low spray rates at high temperature.	Establish system response for the worst case to bound the problem.
6421 Run 2	5A	Average central bundle with <u>no</u> ECC.	Reestablish system response for the benchmark test to evaluate effects of ECC under improved system simulation.
6422 Run 3	5A	Average central bundle with average spray rates at nominal temperature.	Reestablish system response for representative conditions (reference case).
6423 Run 3	5A	Peak power bundle with low spray rates at high temperature.	Reestablish system response for the bounding case in the improved system simulation.
6431 Run 1	5B	Small break, average central bundle power. All ECCS available.	Establish suitability of TLTA for small break test.
6432 Run 1	5C	Small break, average central bundle power. HPCS assumed inoperative.	Obtain system response of small break under degraded conditions.
6441	5A	Boil-off test at steady bundle powers and system pressures.	Separate effects test to obtain data on bundle heat transfer without forced coolant circulation.

Table 3-2

BRIEF DESCRIPTION OF GOALS FOR EACH OF THE TESTS
CONDUCTED UNDER THE BD/ECC IA PROGRAM (Continued)

Test	TLTA	Description	Goal
6424 Run 1	5A	Peak power bundle with average spray rates at nominal temperature.	Establish system response for realistic condition; also enable evaluation of ECC effects.
6425 Run 2	5A	Average central bundle with average spray rates at nominal temperature.	Reestablish reference test with improved break flow measurements (comparable to Test 6422 Run 3).
6426 Run 1	5A	Average central bundle with no ECC.	Reestablish system response for the benchmark test with improved break flow measurements (comparable to Test 6421 Run 2).

in Figure 3-1: bundle power decay, steam line flow, ECC flows, and drive pump coastdown.

Sequence of significant events for the LOCA simulation test is shown in Table 3-4. This table, along with Figures 3-3 through 3-8, will facilitate the phenomenological description of the system response. Additional details of system response then follow. A complete set of data for the reference test is included in Appendix J.

3.2.1.1 Phenomenological Description of System Response for Reference BWR/6 Simulation (Test 6425 Run 2). The early blowdown, i.e., flow coastdown through low plenum flashing (LPF), has been studied extensively in previous TLTA tests (1,2). The early responses for this present series of tests are identical to those reported previously. These early responses are governed by the break flow and the resulting decrease of the mixture level in the downcomer region, as illustrated in Figure 3-2. The mixture level reaches the jet pump suction inlet at 6.7 sec and the recirculation line suction at 9.4 sec (Figure 3-2a). The bundle inlet flow

*Under the single failure criterion, only one of the three LPCI systems is assumed operational for simulation.

Table 3-3

INITIAL CONDITIONS OF THE BD/ECC 1A REFERENCE TEST (6425 Run 2)

Initial Conditions	TLTA	
Bundle power	5.05 ^a ± 0.03 MW	
Steam dome pressure	1044 ± 5 psia	(7198 kPa)
Lower plenum pressure	1071 ± 5 psia	(7384 kPa)
Lower plenum enthalpy	528 ± 5 Btu/lbm	(1228 Kj/Kg)
Initial water level ^b	73 ± 6 in. E1	(1.85m)
Feedwater enthalpy	41 ± 2 Btu/lbm	(95 Kj/Kg)
Bundle inlet to outlet DP	17 ± 2 psi	(117 Pa)
Steam flow	6 ± 1 lbm/sec	(2.7 Kg/s)
Feedwater flow	1.4 ± 0.3 lbm/sec	(0.5 Kg/s)
Drive Pump 1 flow	9.1 ± 1 lbm/sec	(4.1 Kg/s)
Drive Pump 2 flow	8.4 ± 1 lbm/sec	(3.8 Kg/s)
Jet Pump 1 flow	22 ± 2 lbm/sec	(10 Kg/s)
Jet Pump 2 flow	20 ± 2 lbm/sec	(9 Kg/s)
Bundle inlet flow	39 ± 5 lbm/sec	(18 Kg/s)

All uncertainty bands are judged from the maximum of data fluctuation and/or absolute uncertainties of the measurements.

^aNOTE: 5.05 MW is central average bundle power; core average power is 4.60 MW for BWR/6.

^bNOTE: Relative to jet pump support plate.

Table 3-4

SEQUENCE OF EVENTS FOR 6425 RUN 2 (AVG. POWER, AVG. ECC)

<u>Events</u>	<u>Time (sec.)</u>
Blowdown valves open	0.0
Bundle power decay initiated	0.5
Blowdown loop jet pump flow reverses	0.5
Feedwater flow stops	0.5
Bypass flow reverses	1.7
Jet pump suction uncovers	6.7
Steamline valve completely closed	9.0
Recir. suction line begins to uncover	9.4
Lower plenum bulk flashing	11
Guide tube flashing	11.2
Core inlet uncovers (SEO center line)	20
Loop 1 isolated	20
HPCS injection begins	27
Lower plenum mixture level reaches jet pump exit plane	35
LPCS, LPCI activated	37
LPCS flow begins	64
LPCI flow begins	75
Bypass/guide tube region begins to refill	85
CCFL breaks down at bypass outlet	95
Bundle begins to refill	114
Bypass region refilled	125
Bundle reflood with two-phase mixture	130
CCFL breaks down at upper tie plate	125
Bundle quenched	150
End of test	400

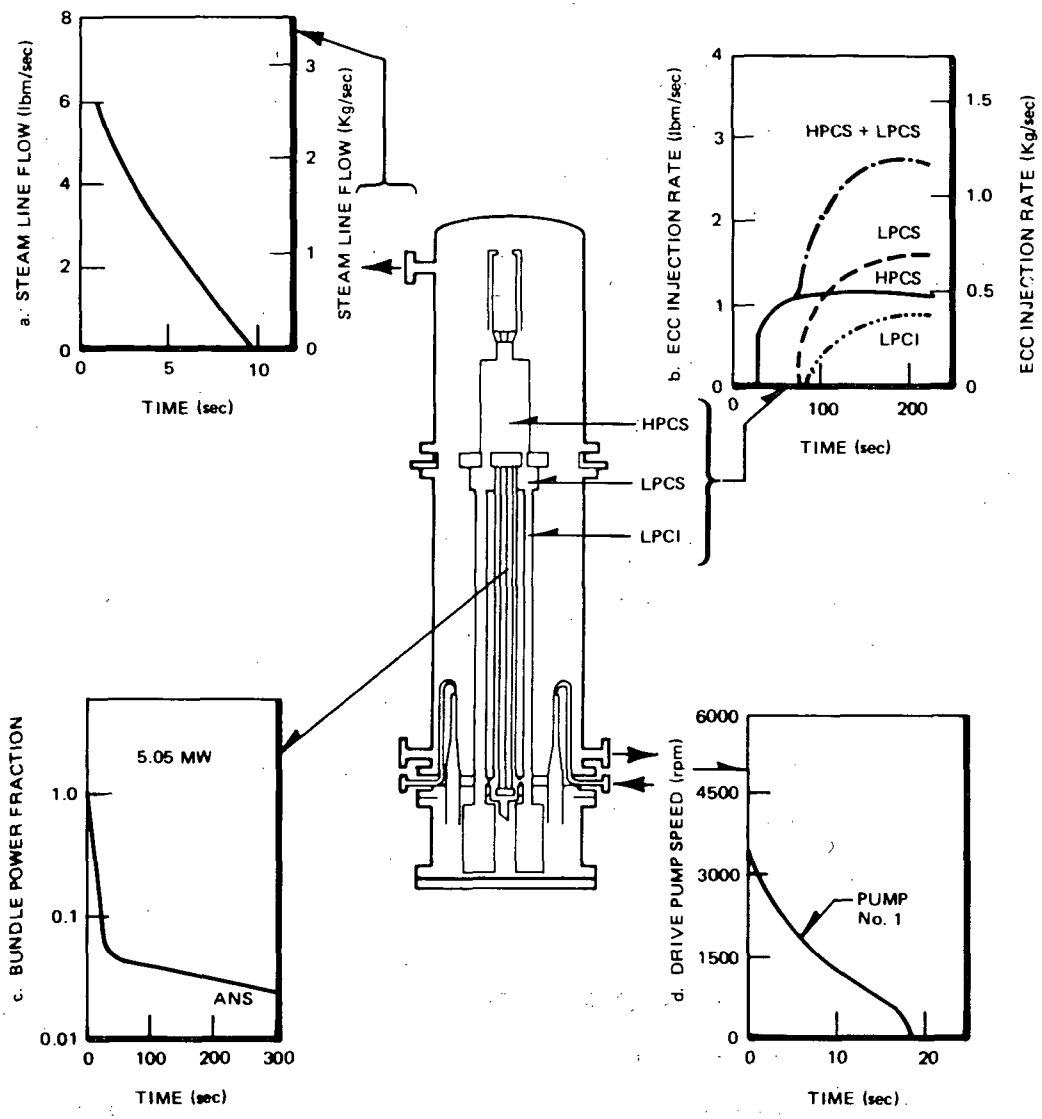


Figure 3-1. Controlled Parameter Responses of Reference Test (6425 Run 2, Average Power, Average ECC)

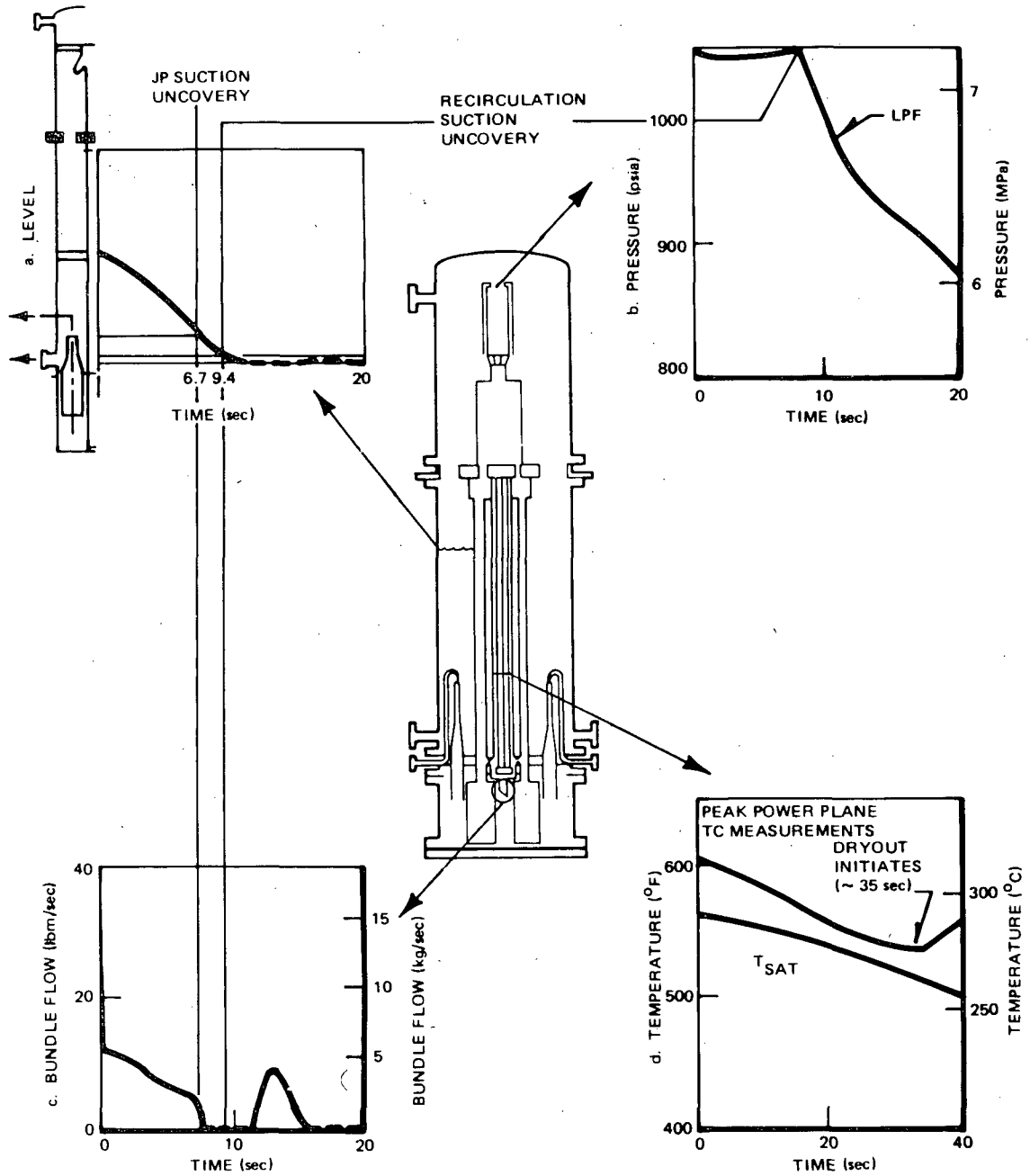


Figure 3-2. System Responses in the Early Stage of the Blowdown Transient for the Reference Test (6425 Run 2, Average Power, Average ECC)

drops in response to the loss of jet pump flow in the broken loop; it then decreases (Figure 3-2c) as the drive pump coasts down (Figure 3-1d). The flow becomes nearly zero when the jet pump suction is uncovered at 6.7 sec. The flow surge associated with lower plenum flashing occurs shortly after recirculation line suction uncover, at 11 sec.

The system pressure as measured at the steam dome is shown in Figure 3-3. The system depressurization rate increases after the recirculation line suction uncover (Figure 3-2b) because of the increased volumetric discharge that accompanies this transition from predominantly liquid to vapor blowdown. The system pressure quickly drops to the saturation pressure of the lower plenum fluid which is initially subcooled. Bulk flashing of this fluid, referred to as lower plenum flashing (LPF), occurs at ~11 seconds. The volume expansion accompanying LPF redistributes mass inventories into various regions of the system (additional details are discussed later with Figures 3-4 and 3-5). As the system pressure blows down farther, the subcooled fluid injection begins first through the high-pressure system and later through the low-pressure ECC systems. Low-pressure core spray (LPCS) flow into the upper plenum begins at 64 seconds and augments the injection from the high-pressure core spray which begins at 27 seconds. Low-pressure coolant injection (LPCI) into the bypass region begins at 75 seconds.

The response of the system fluid inventory is shown in the mixture level plots in Figure 3-4. These plots were deduced from DP measurement strings. They show that the bundle refloods completely at 130 seconds, and the upper plenum is empty.

The scenario of the system response is described and explained with the aid of a series of pictorial depictions of the system fluid conditions in Figure 3-5. System conditions at selected instances are characterized. The initial system condition, Figure 3-5a, shows the existence of two free fluid surfaces (mixture levels): one inside the core region at the top of the separator and one outside the core region above the jet pumps.

Following LPF, which redistributes inventory in the various regions, phase separation occurs, and two-phase mixture levels are maintained by counter current flow limiting (CCFL) conditions at the regional boundaries where the flow paths connecting the regions are geometrically restrictive. Under CCFL conditions, the liquid in the upper region is restricted from draining into the lower region because of the upflowing vapor generated (primarily from flashing) in the lower region.

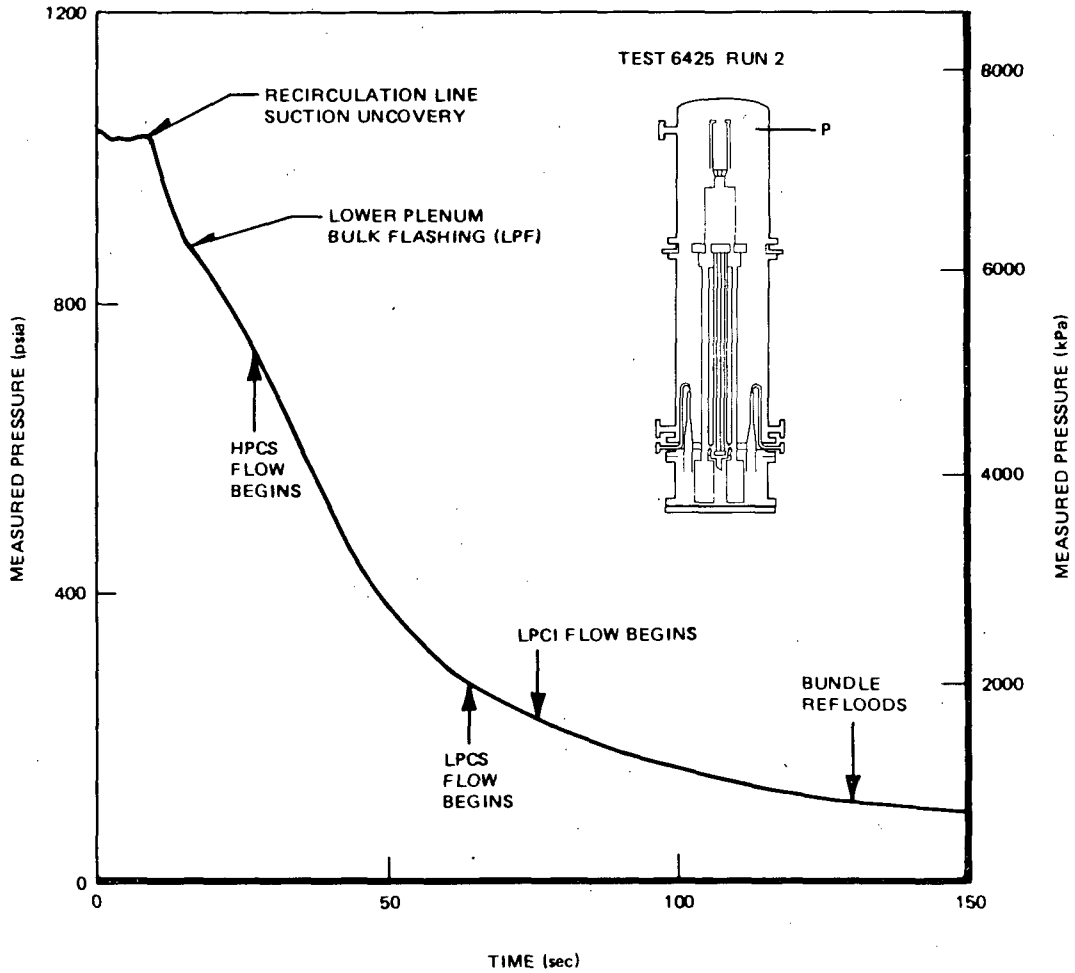


Figure 3-3. System Pressure Response at Steam Dome

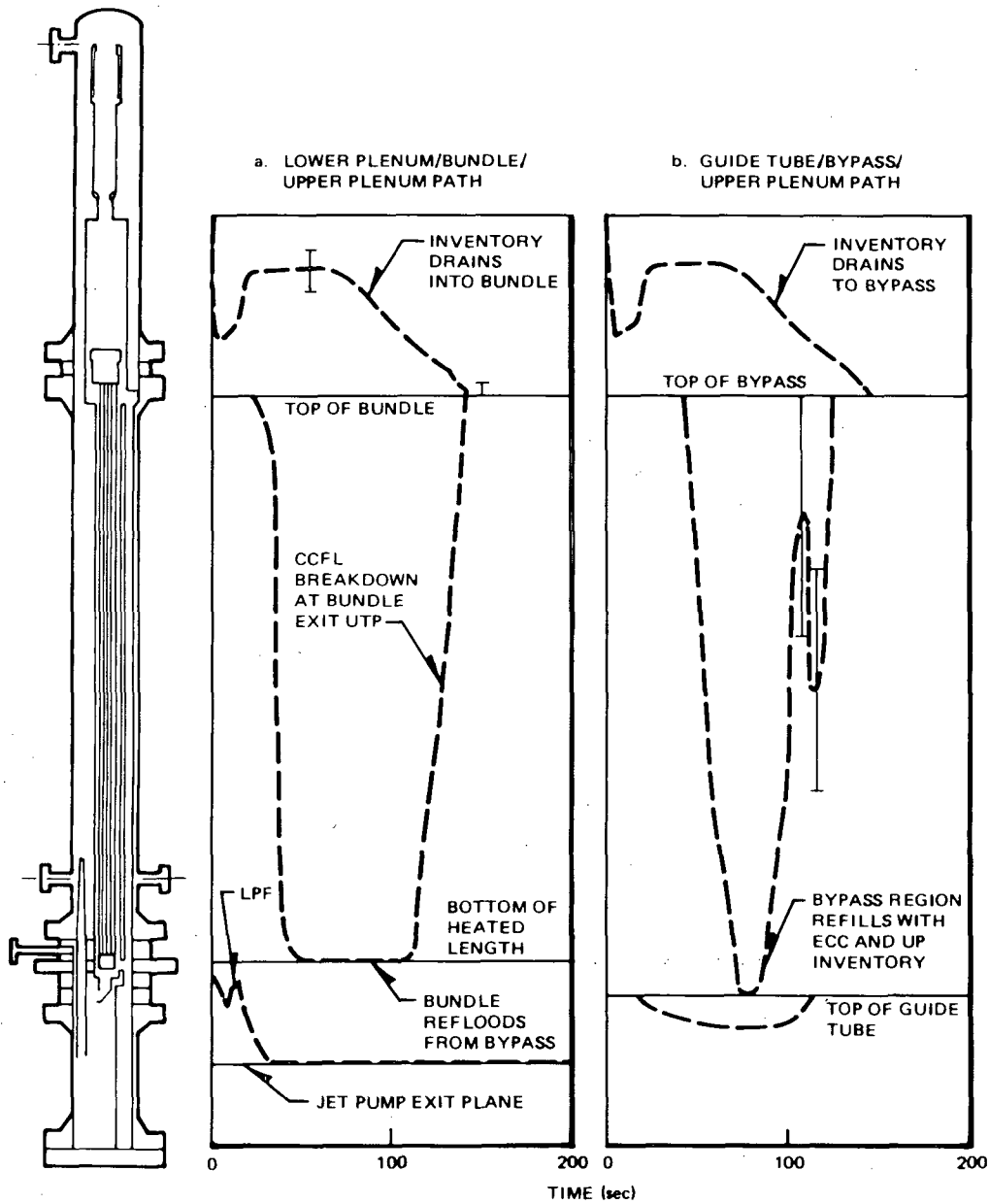


Figure 3-4. Two-Phase Mixture Level Response along the Parallel Flow Paths: Bundle and Bypass

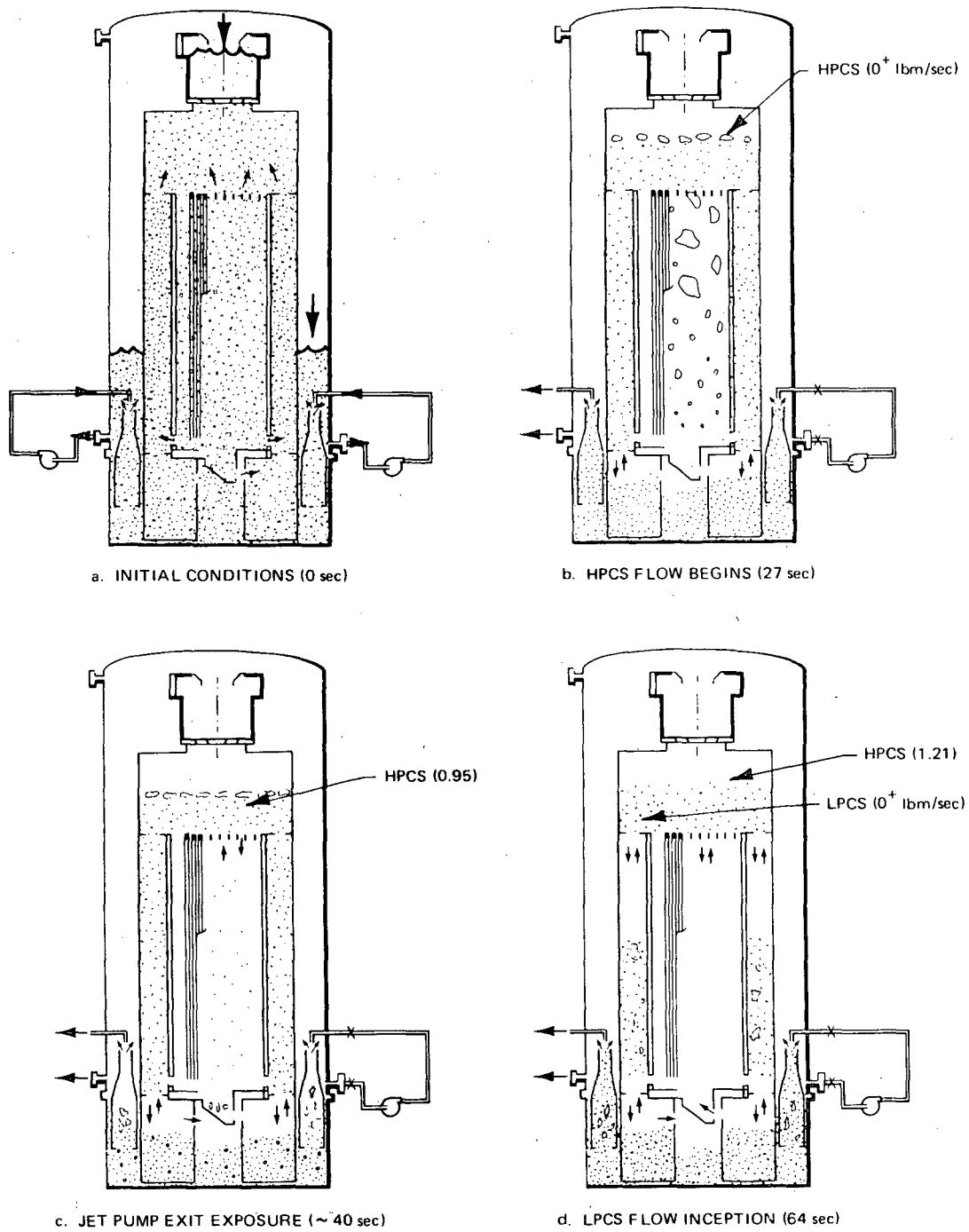
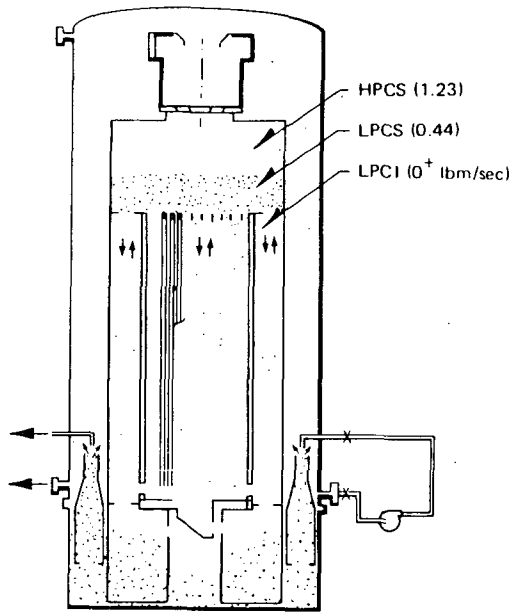
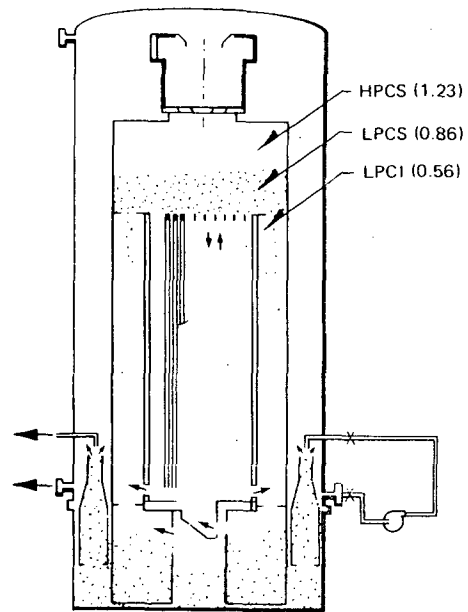


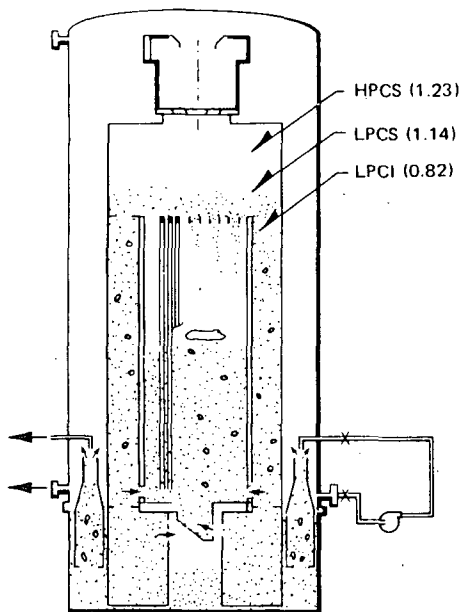
Figure 3-5. Fluid Conditions at Selected Instances for Test 6425 Run 2



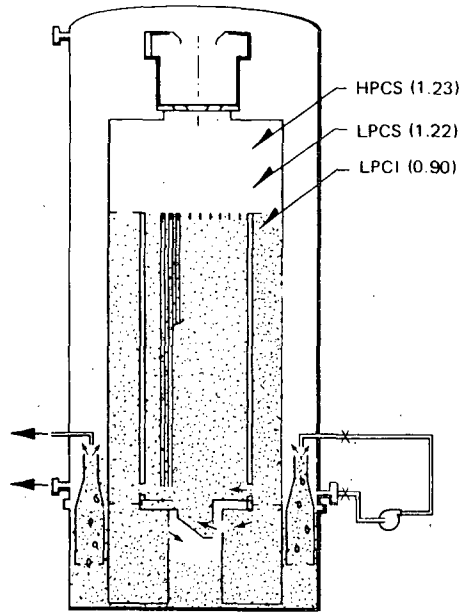
e. LPCI FLOW BEGINS (75 sec)



f. CCFL BREAKS DOWN AT BYPASS OUTLET (90 sec)



g. CCFL BREAKS DOWN AT UTP (~ 125 sec)



h. BUNDLE COMPLETELY REFLOODED, UP EMPTY, LP PARTIALLY FILLED (150 sec)

Figure 3-5. Fluid Conditions at Selected Instances for Test 6425 Run 2 (Continued)

Figure 3-5b depicts the fluid conditions at the instant shortly after LPF and when the HPCS flow is about to begin (27 seconds). The bundle inventory is held up by the CCFL conditions at the inlet side entry orifice (SEO). Similarly, CCFL condition at the upper tie plate together with that at the bypass outlet holds up the upper plenum inventory which was transported there as a result of LPF. Because of CCFL at the bundle inlet, a two-phase liquid continuum is maintained in the bundle to keep the rods well cooled.

The mixture level in the bundle drops at ~35 seconds when the mixture level in the lower plenum reaches the jet pump exit plane (Figure 3-4). Before 35 seconds, the inventory in the lower plenum is lost because of continued flashing and discharge through the jet pump. Both of these contribute to the drop in mixture level in the lower plenum. When the level reaches the jet pump exit plane, an alternative path for LP vapor to escape becomes available. A portion of lower plenum vapor then discharges through the jet pump, thus decreasing the vapor through the bundle SEO. The diminished vapor upflow can no longer hold up (because of CCFL) the liquid continuum in the bundle. The liquid continuum is depleted, and the mixture level falls below the bottom of the heat length (BHL) at ~40 seconds (Figure 3-4).

The system conditions at 40 seconds are shown in Figure 3-5c. The bundle is filled with a vapor continuum and some entrained droplets, and bulk dryout of heater rods has begun (see also discussion in conjunction with Figure 3-8 later).

CCFL conditions at the UTP maintain an upper plenum mixture, with ECCS injection replenishing the liquid that drains into the bundle. The lower plenum inventory is also maintained, with liquid draining through the bundle replacing the loss of inventory discharging through the jet pump. The bypass region is still filled with a two-phase mixture. This mixture continues to flow into the bundle through the leakage path near the bottom of the core region. CCFL at the bottom of the bypass prevents the bypass fluid from completely draining into the guide tube region below while CCFL at the outlet prevents upper plenum liquid from draining into the bypass.

The CCFL condition at the UTP changes as the vapor flow decreases at the bundle outlet. This decrease results from a decrease of vapor flow from the lower plenum and a reduction in the vapor generation, caused by bundle dryout, within the bundle. Consequently, more liquid from the upper plenum drains into the bundle which contributes to rewetting some of the previously dried-out rods. Figure 3-5 is a pictorial representation of the system at that instant (64 sec). The mass inventory and mixture level in the bypass region have decreased substantially. By contrast, conditions in the lower plenum, upper plenum, and guide tube remain

relatively steady. The mixture level in the lower plenum remains at the jet-pump exit plane (Figure 3-4).

When LPCI begins to inject at 75 seconds, the system conditions are as illustrated in Figure 3-5e. By this time the bypass region has become voided. The leakage flow reverses to the forward direction, and the jet pump fluid becomes more dense. The guide tube and the plena inventories, however, remain unchanged from 65 seconds even though the LPCS flow rate has been increasing. This indicates that an increasing amount of injected ECC fluid drains into and then discharges from the lower plenum through the jet pump and therefore causes the jet pump fluid density to increase.

The vapor flow through the jet pump decreases in response to the increase in pressure drop because of fluid density increase. The lower plenum vapor finds a less resistive path through the voided bypass. Therefore, the bypass flow reverts to an upward direction as some of the lower plenum vapor flows into the bundle and passes through the leakage path to the bypass. This causes the vapor flow at the bundle outlet to decrease. The decrease contributes to a more favorable CCFL condition for liquid to drain into the bundle through the UTP. Rewetting of dried-out rods becomes more evident (Figure 3-8). The LPCS injection, however, has not yet reached sufficient capacity to condense all the vapor to break down CCFL at the UTP.

At ~90 seconds, the LPCI flowrate has reached sufficient capacity to condense the vapor in the bypass region. CCFL breaks down at the top of the bypass. The system conditions are depicted in Figure 3-5f. The following events ensue: the upper plenum inventory drains into the bypass, and the upper plenum level drops. The bypass region then refills from the combined upper plenum drainage and the increasing flow of LPCI fluid. The bypass level rises rapidly.

The guide tube fills as the subcooled LPCI fluid penetrates to the bottom of the bypass region, condenses the vapor from the guide tube, and eventually breaks down CCFL at this regional boundary (Figure 3-4). The bypass level drops momentarily, then resumes refilling. The leakage flow into the bundle from that point consists mainly of liquid. The flow from the bypass enters the bottom of the bundle where some of the liquid accumulates, while the remainder drains through the SEO into the lower plenum.

The influx of liquid in the lower plenum causes the level to rise slightly and blocks the path of the vapor discharging through the jet pump. The situation is a reversal of what took place at ~35 seconds when the lower plenum level fell to the

jet pump exit plane. As more liquid is forced through the jet pump, more vapor is forced up the bundle through the inlet orifice. CCFL at the SEO holds up the inventory and allows more liquid from the bypass leakage flow to accumulate. The bundle refloods as the level rises.

The extent of the bundle reflood is dictated by the pressure drop across the jet pump path.* This can be explained by consideration of the pressure drop components across the parallel paths as follows: the liquid influx into the lower plenum increases the liquid fraction of the fluid discharging through the jet pump. The hydrostatic component of the pressure drop increases. The vapor flow adjusts accordingly to the prevalent condition of the system. The vapor upflow through the SEO increases. This renders the CCFL condition at the SEO less favorable for liquid to drain. The liquid downflow at the SEO decreases, and inventory accumulates in the bundle. The increases hydrostatic head in the bundle compensates for the drainage of fluid and, hence, the decreased head in the upper plenum. The combined hydrostatic head and the flow pressure drop in the bundle adjust to balance the pressure drop across the jet pump.

The bundle reflood is accelerated at ~ 125 seconds when CCFL breaks down at the UTP because of condensation (Figure 3-4). Evidence of subcooling that is indicative of condensation can be seen in Figure 3-6 which shows temperature measurements above the UTP. The system conditions at this instant are shown in Figure 3-5g. The bundle has reflooded more than halfway up. The upper plenum inventory of two-phase mixture has drained almost completely into the bypass. The HPCS and LPCS injections, which have been increasing in rate and condensing local voids, become more accessible to the UTP. The subcooled HPCS and LPCS fluid is augmented by the subcooled LPCI fluid when overflowing of the bypass diverts the latter to the upper plenum. As a result, the combined capacity of the three ECC injections produces sufficient subcooling to condense the vapor flow out of the bundle. CCFL breaks down at the upper tie plate and allows the fluid to flow directly from the upper plenum into the bundle. The bundle becomes completely reflooded at ~ 130 seconds.

The system conditions at 150 seconds are shown in Figure 3-5h. A substantial amount of inventory is held up in the bundle by CCFL at the bottom SEO. The upper plenum is essentially empty. The guide tube and bypass are filled with high-density fluid close to the saturated liquid density. The combined ECC injection capacity during this period is passing through the bundle (core region) and into the lower plenum. From there it flows out the jet pump into the annular downcomer and out the break.

*NOTE: For the short TLTA jet pump, both the hydrostatic head component and the flow loss component of the pressure drop are lower than that in an actual BWR.

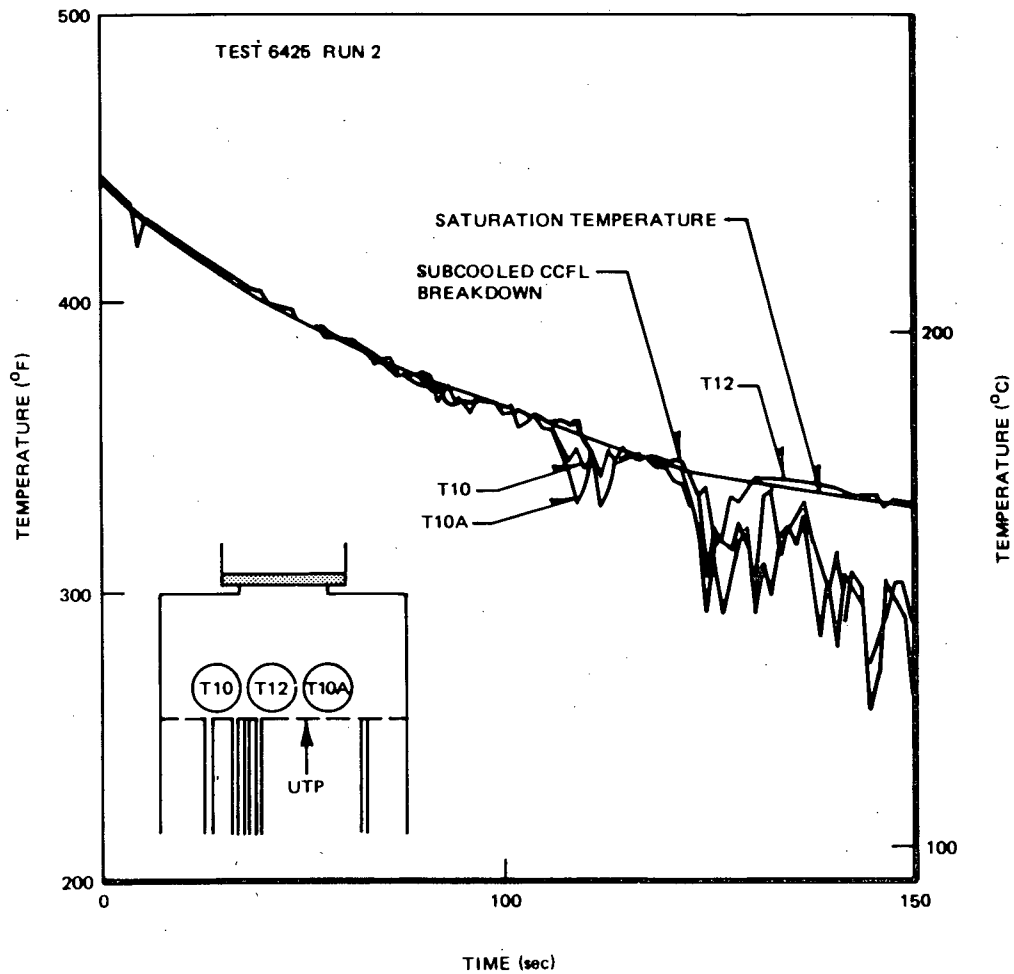


Figure 3-6. Fluid Temperature Measurements above the Bundle Outlet UTP

Eventually there is sufficient flow to actually begin refilling the downcomer above the break. Yet the lower plenum remains at essentially the same level reached at 35 seconds, i.e., near the jet pump exit.

The fluid temperature at the SEO is shown in Figure 3-7, which indicates that no subcooling reaches the SEO. Consequently, CCFL persists at the SEO because the fluid there does not have sufficient condensation potential to break down CCFL.

The bundle thermal response is represented by Figure 3-8, which shows cladding temperature measurements at the peak power plane. The effect of CCFL at the SEO in delaying bundle drainage (until ~35 sec) can be observed. Some of the rods at the

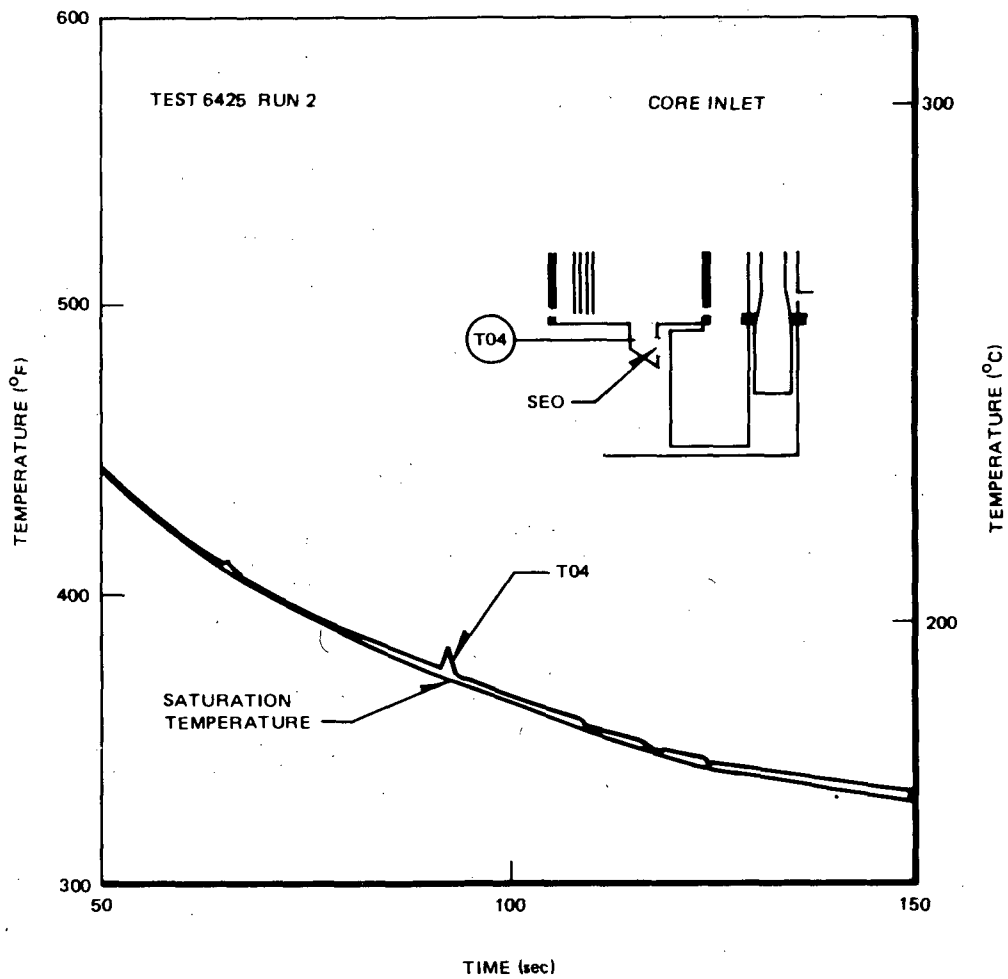


Figure 3-7. Fluid Temperature Measurement at Bundle Inlet SEO and Lower Plenum Saturation Temperature

peak power location (and a few other locations nearby) dryout earlier, but they all rewet as the fluid in the bundle redistributes following LPF. The rewetting occurs prior to widespread heat-up, as can be seen from Figure 3-8. The bundle is quenched following reflood. Even during the period when CCFL at the UTP limits the amount of ECC fluid entering the bundle, rewetting of dried-out rods keeps the cladding temperature relatively low. As a result, the maximum cladding temperature during the test was less than 700°F (370°C).

3.2.1.2 Additional Details of System Response for Test 6425 Run 2. The mixture level responses presented previously (Figure 3-4) are farther extended in Figures 3-9 and 3-10. The mixture levels along the bundle path and the bypass path

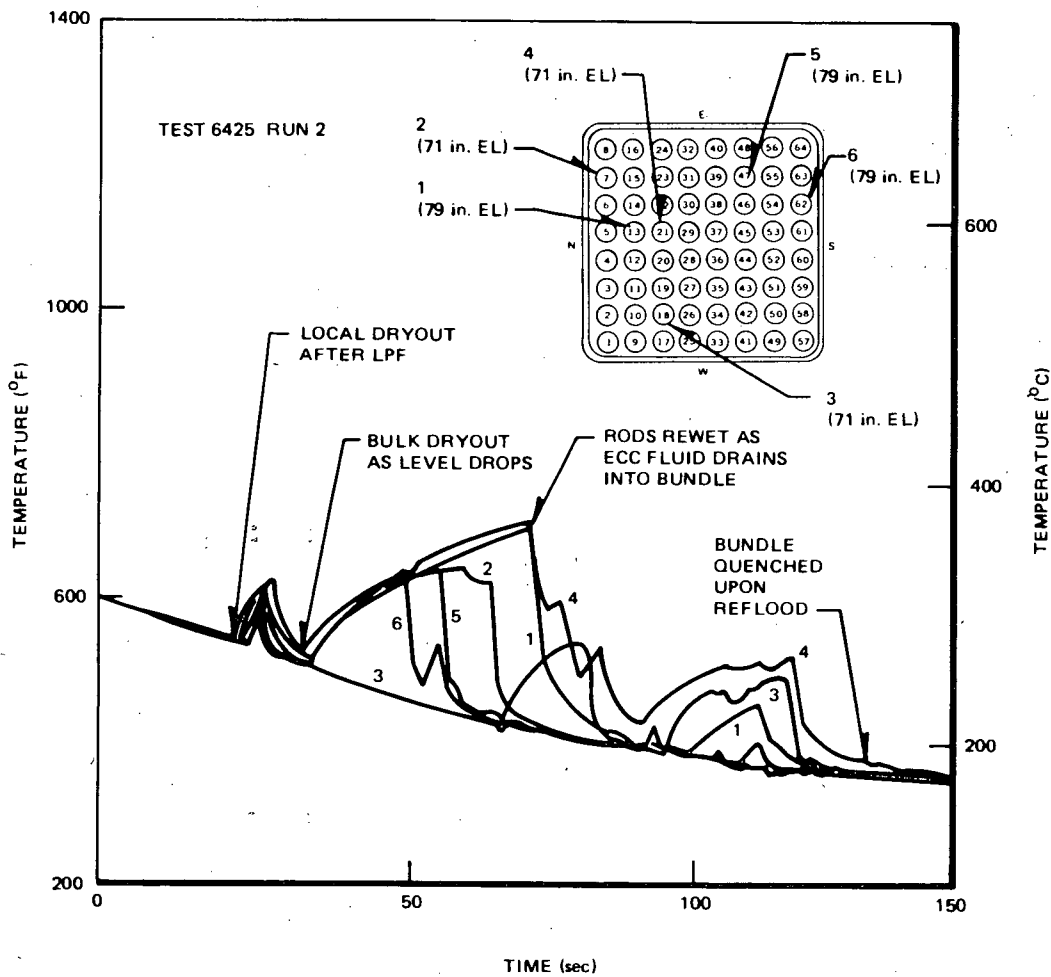


Figure 3-8. Peak Power Region Cladding Temperatures for TLTA 5A Reference Test (Average Power, Average ECC)

for the complete transient are shown in these figures. In addition the level response in the annulus is included in Figure 3-11.

Referring to Figure 3-11, the fluid level in the downcomer region at the end of the transient is seen to rise above midcore height. The level covers the recirculation line suction inlet at ~200 seconds and the drive line outlet (jet pump suction) at ~250 seconds. Consequently, the break flows from both lines are low quality two-phase rather than highly dispersed vapor flow after those times. The system pressure nevertheless continues to decrease because of condensation by the ECC fluid. This condensation effect is evident from the pressure drop measurements across the

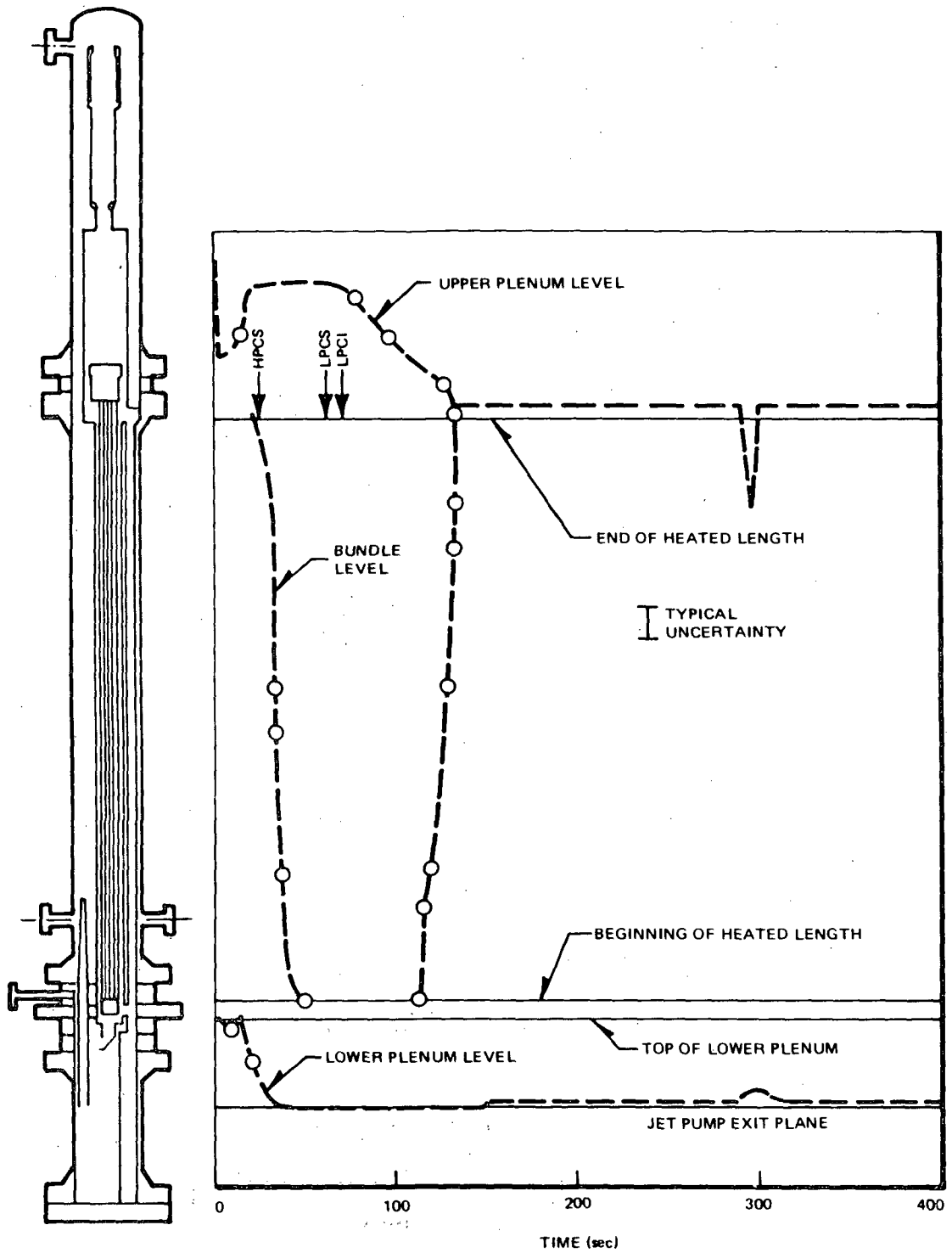


Figure 3-9: Mixture Level Response along the Lower Plenum/Bundle/Upper Plenum Path for Test 6425 Run 2 (Avg. Power, Avg. ECC)

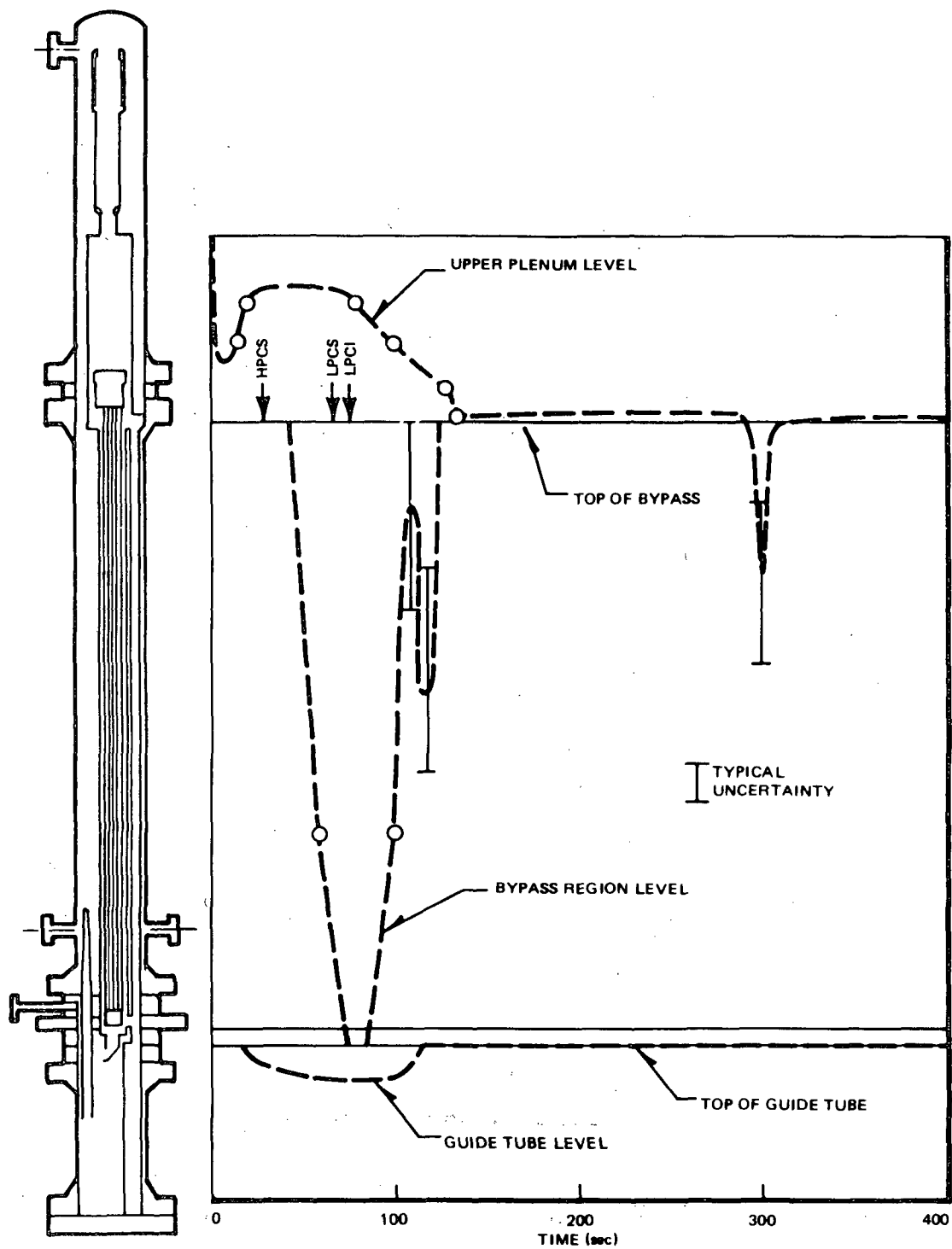


Figure 3-10. Mixture Level Response along the Guide Tube/Bypass/Upper Plenum Path for Test 6425 Run 2 (Avg. Power, Avg. ECC)

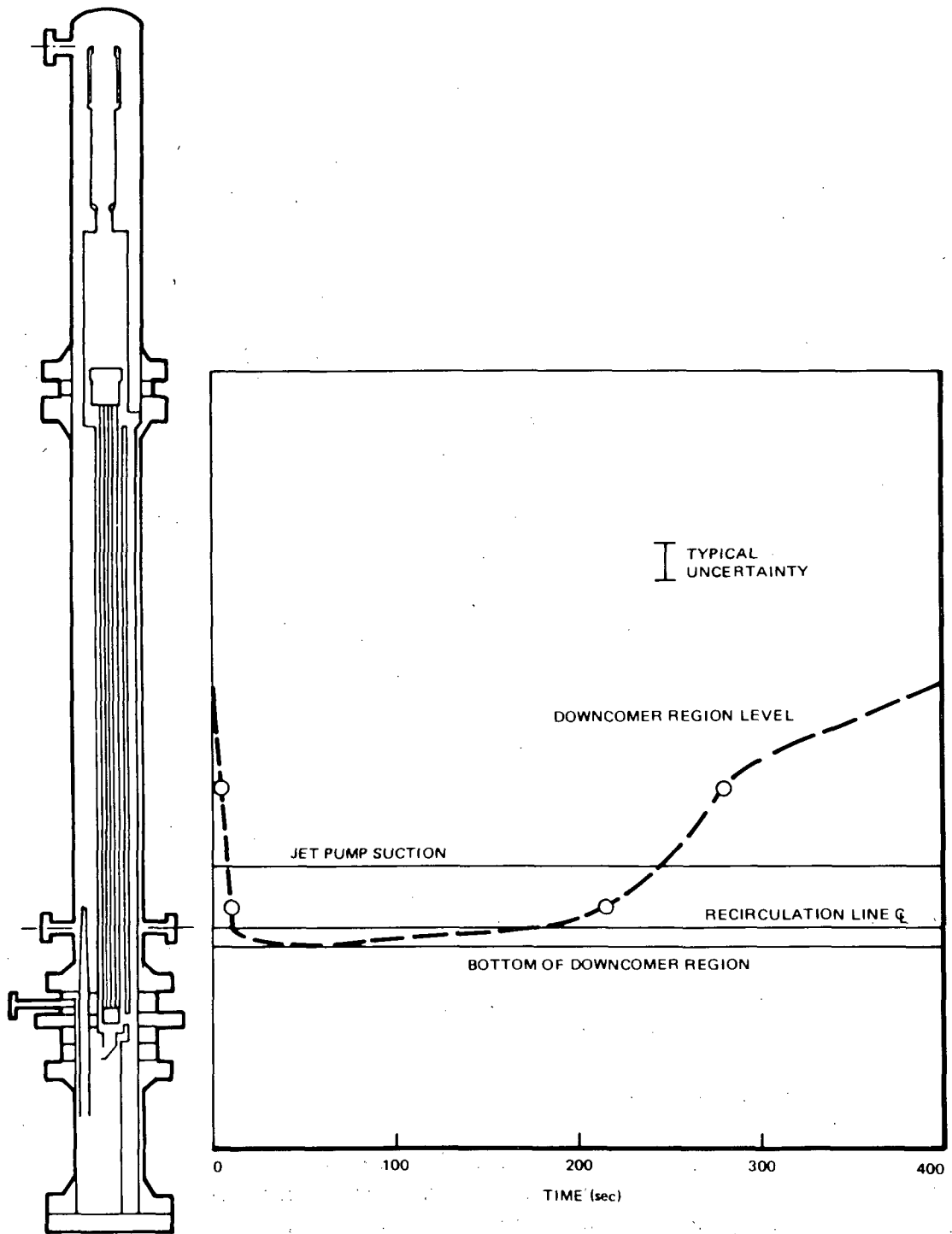


Figure 3-11. Mixture Level Response in the Annular Downcomer Region for Test 6425 Run 2 (Avg. Power, Avg. ECC)

steam separator: DP20 and the flow pressure drop measurement (annubar) shown in Figure 3-12, which indicate a net steam flow into the upper plenum.

Mass histories in different regions are shown in Figure 3-13. These mass plots provide supplementary information to the level plots. For reference, the mass of each region if it were full of saturated liquid is also indicated.

The break flows are presented in Figure 3-14. The break flow through the suction line is seen to increase at ~120 seconds (Figure 3-14b). This increase is due to the increased amount of liquid which becomes available upstream of the break in the downcomer region, as illustrated in Figure 3-11. Also, as pointed out in Appendix H, the break flow determined from the drag disc and turbine meter measurements beyond ~100 seconds becomes erroneously high.

The break flow through the drive line does not show any discernible change when the downcomer level submerges the drive flow nozzle. This suggests that the flow to the nozzle and out the break could have been a two-phase fluid throughout this time.

The individual and total ECC injection rates are included in Figure 3-15. The low-pressure ECC systems were activated at 37 seconds, but the system pressure was higher than the shutoff head of the pumps until 64 seconds for LPCS and 75 seconds for LPCI.

Cladding temperatures along the length of the bundle are shown in Figure 3-16. The peak cladding temperature for the entire bundle is shown in Figure 3-17. The maximum cladding temperature of ~700°F is indicated. This maximum temperature occurs at ~75 seconds, about the same time as LPCI flow begins. The bundle becomes well cooled at ~130 seconds, and, because of the continual supply of subcooled ECC fluid, the cladding surfaces are actually cooled to below the saturated temperature and become subcooled after the bundle refloods (Figure 3-16).

3.2.2 Highlights of Other Tests

3.2.2.1 Peak Power, Average Spray Rate (6424 Run 1). System response of this test is similar to that of the reference test: the bundle refloods completely at ~150 seconds following the bypass region refill from LPCI flow and CCFL breakdown. The maximum cladding temperature of ~1060°F (571°C) results from the boiling transition during the pump coastdown period. The maximum cladding temperature caused by subsequent dryout is limited to ~810°F (432°C).

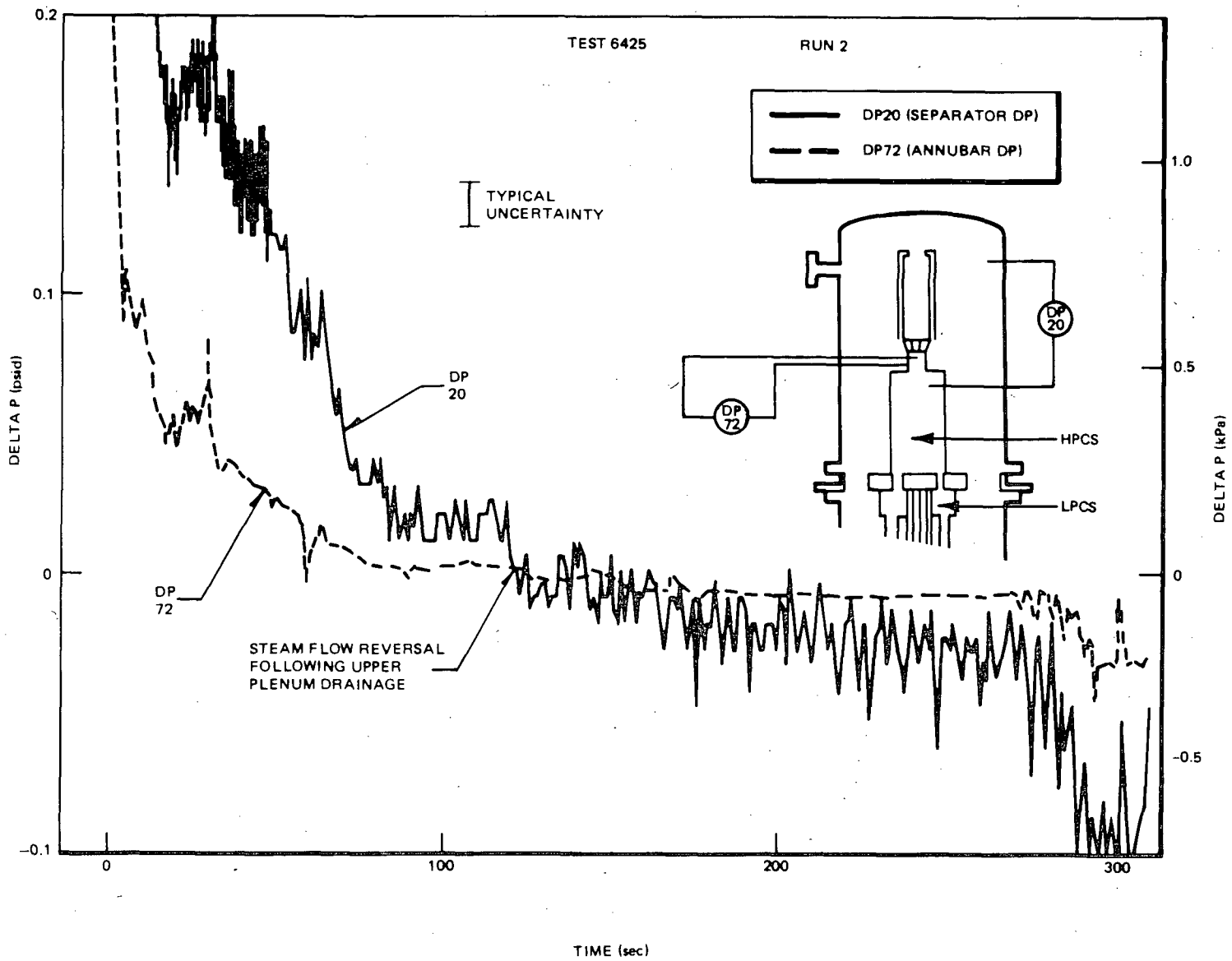


Figure 3-12. Pressure Drops across Steam Separator Showing Reversed Flow Caused by ECC Condensation

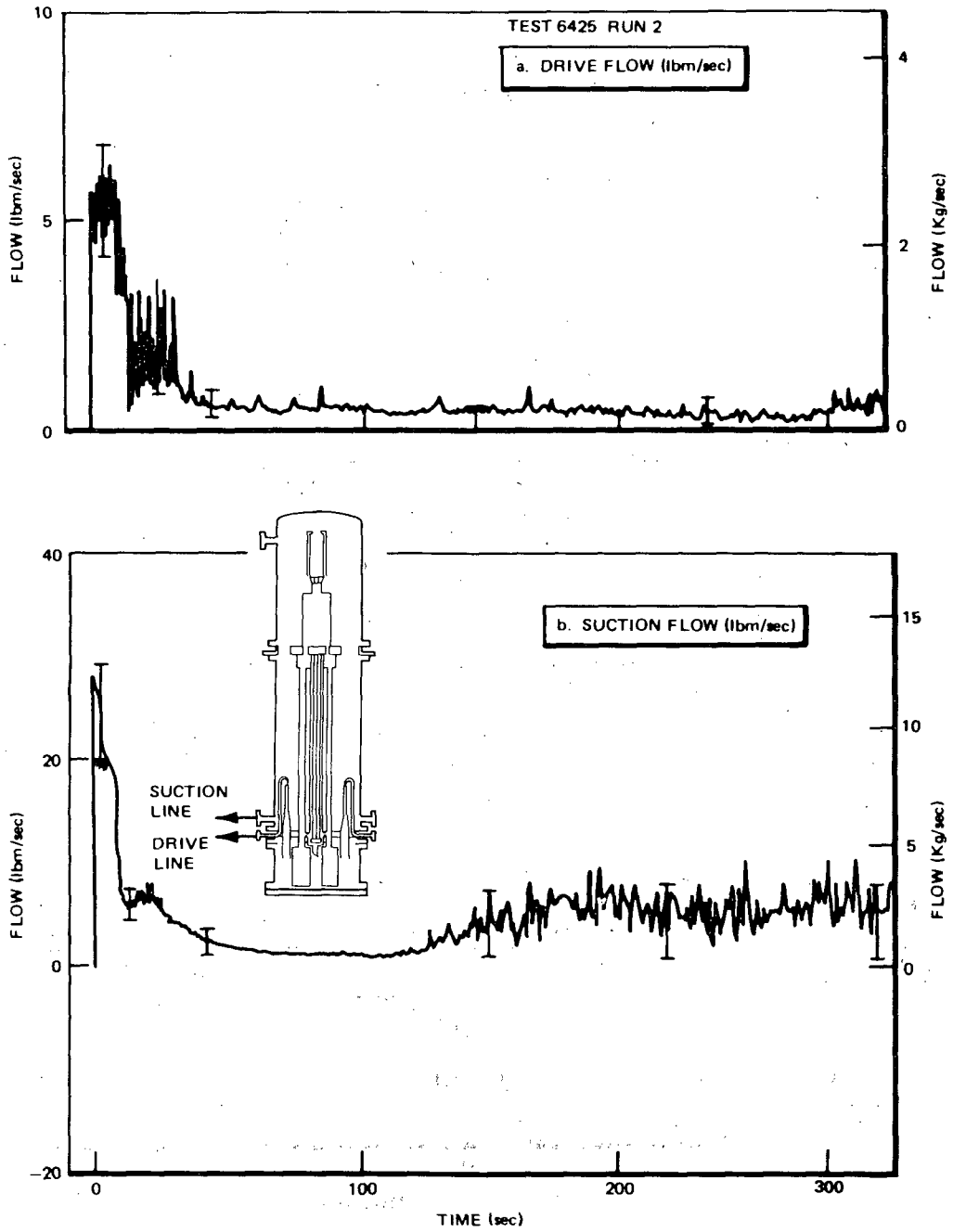


Figure 3-14. Break Flow Measurements for the Reference Test. (Based on Drag Disc and Turbine Meter Measurements.) As Pointed Out in Appendix H, the Break Flow Determined from These Measurements Becomes Too High after ~100 sec

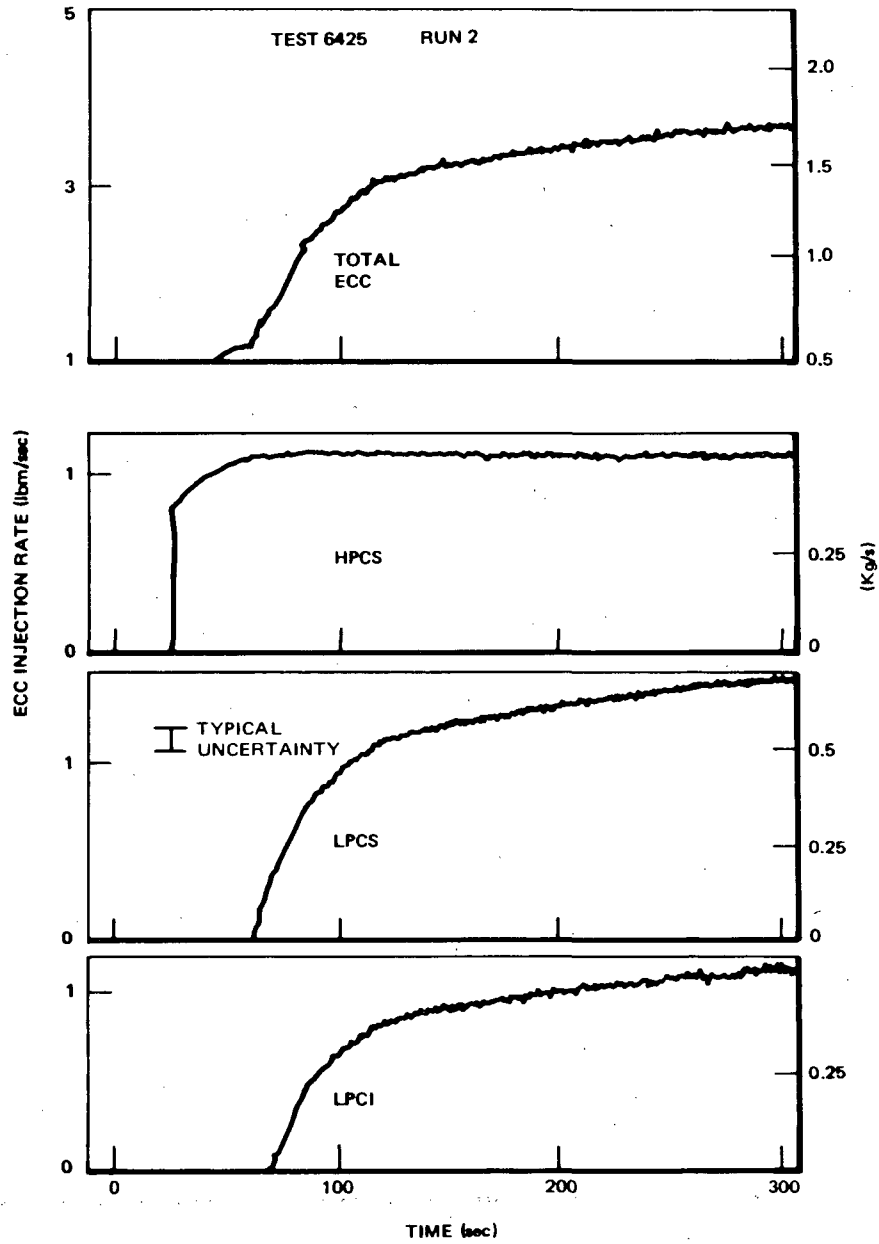
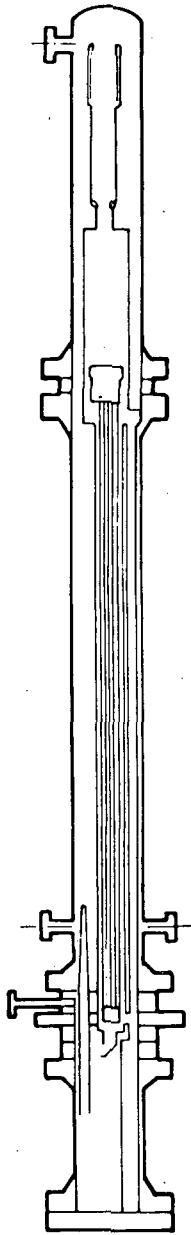


Figure 3-15. ECC Injection Rates for Test 6425 Run 2 (Avg. Power, Avg. ECC)

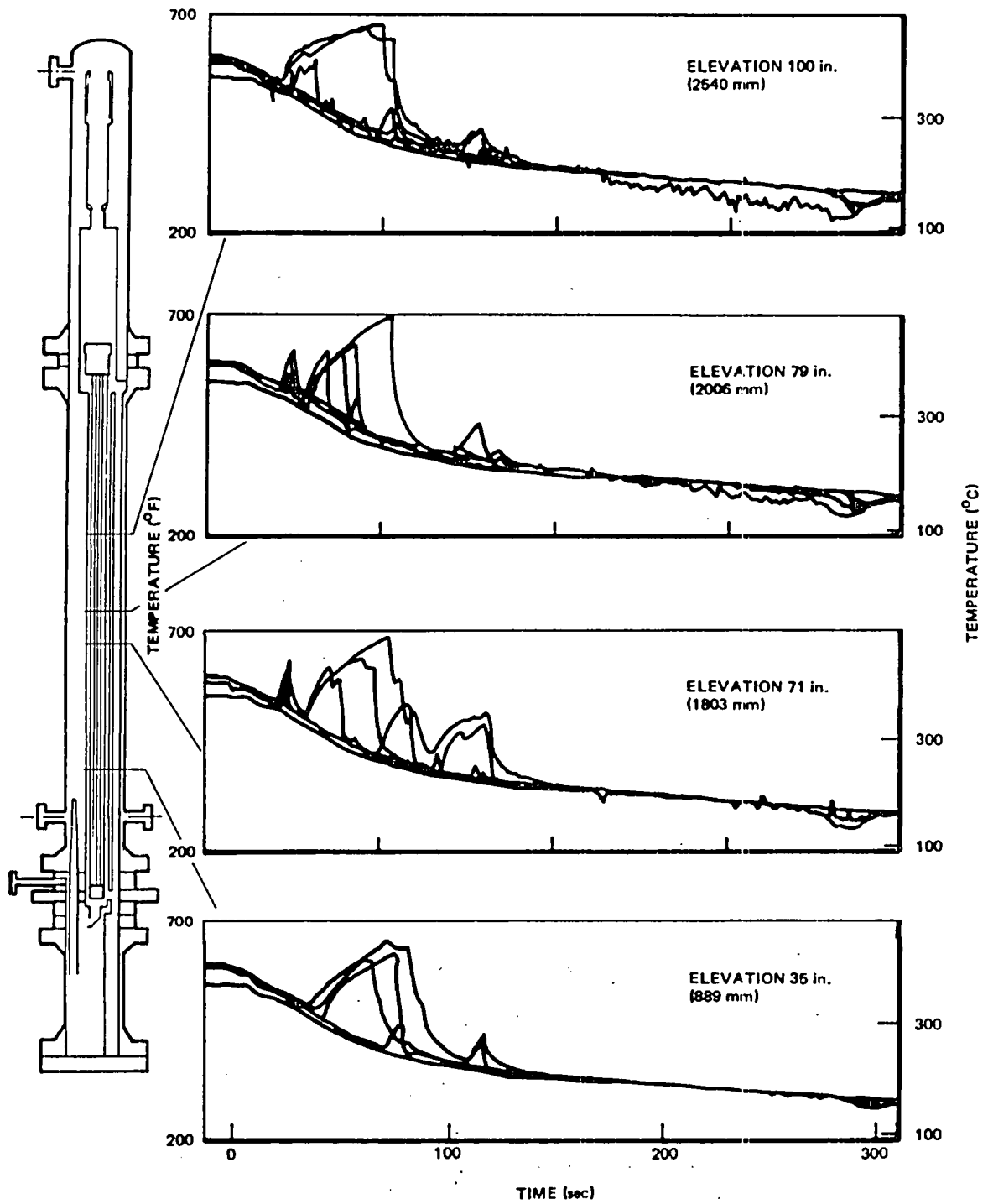


Figure 3-16. Bundle Temperature Response at Selected Elevations for Test 6425 Run 2 (Avg. Power, Avg. ECC)

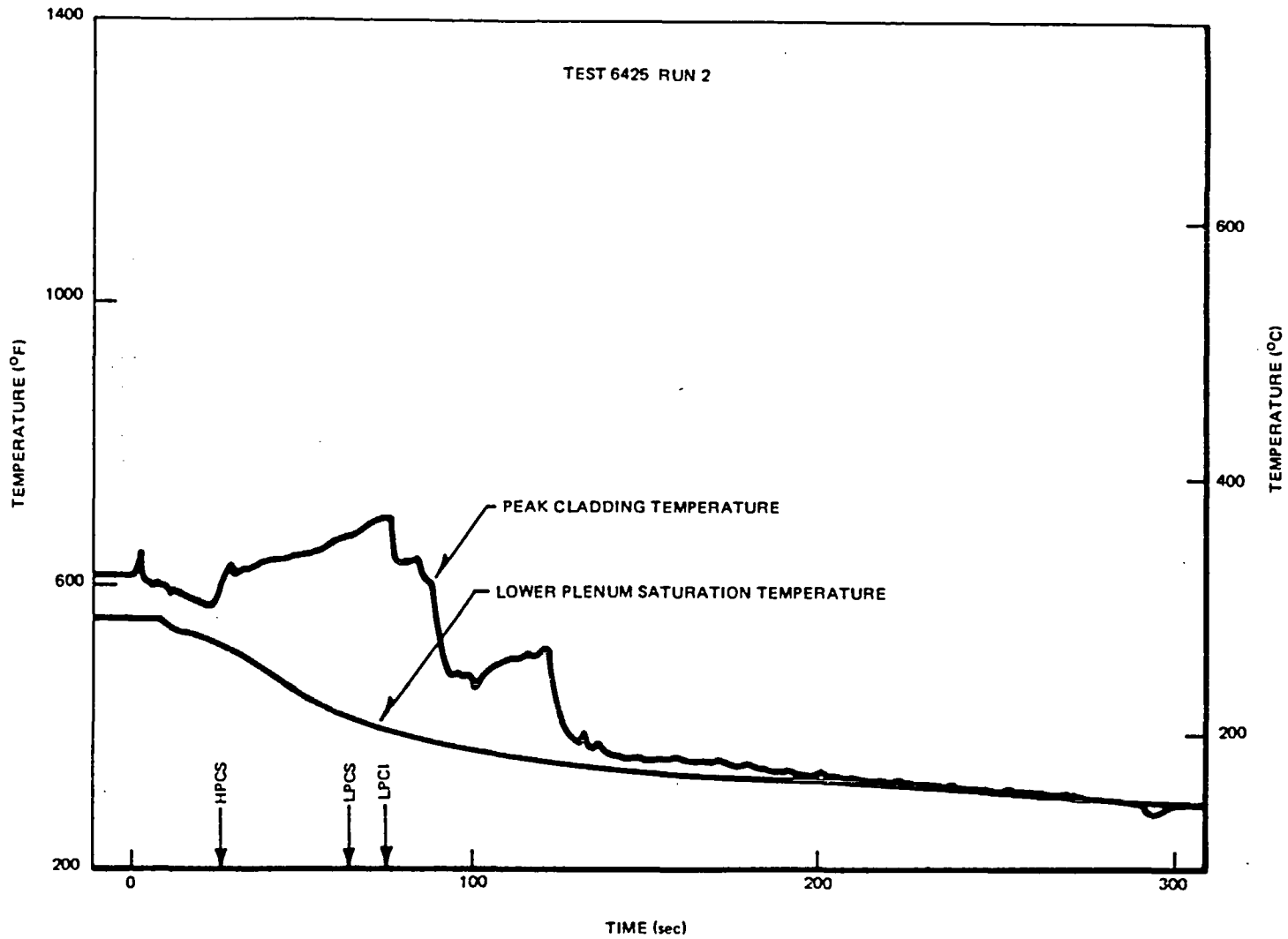


Figure 3-17. Peak Cladding Temperature for Test 6425 Run 2 (Avg. Power, Avg. ECC)

The initial conditions for this test are as shown in Table 3-5. The sequence of events is depicted in Table 3-6. An overview of the system response is conveyed in plots of the system pressure (Figure 3-18), two phase mixture levels in different regions (Figure 3-19), and regional mass responses (Figure 3-20). Bundle reflooding can be seen to occur at ~150 seconds in Figure 3-19.

The injection rates of the ECC systems are shown in Figure 3-21. The low-pressure ECC systems begin to flow at 63 seconds (LPCS) and 71 seconds (LPCI).

The break flows are shown in Figure 3-22. The break flow through the suction line begins to increase from ~100 seconds, thereby reflecting the increase of liquid fraction of the fluid in the downcomer region. However, the break flow through the drive line shows no discernible change, suggesting a continuing flow of two-phase fluid.

Thermal response of the bundle is represented by the plot of peak cladding temperature in Figure 3-23, and temperature responses at selected elevations in Figure 3-24. The maximum cladding temperature of 1060°F (571°C) is seen to occur at 10 seconds because of the boiling transition which occurs during the very early flow coastdown period. This is not expected to be representative of the BWR because the fluid inertia in the TLTA jet pumps is atypically low, which leads to the very rapid coastdown and the boiling transition exhibited in Figure 3-23. The ensuing temperature is rapidly reduced to ~650°F, caused primarily by lower plenum flashing at 14 seconds. The maximum cladding temperature resulting from subsequent heat-up is ~810°F (432°C). The bundle becomes well cooled when it refloods completely at ~150 seconds.

A complete set of data for this test is included in Appendix K. Further discussions on the results of this test can be found in Subsection 3.3.1 in relation to bundle power effects on system response.

3.2.2.2 Average Power, No ECC Test (6426 Run 1). This test was intended to provide benchmark data for evaluating the effects of ECC. Without ECC injection, the system inventory depletes continuously as expected. Bundle heat-up continues following level collapse when the jet pump exit uncovers at ~33 seconds to open an alternate path for the lower plenum vapor. The maximum cladding temperature reached ~1400°F (760°C) when the test was terminated at 294 seconds.

Table 3-5

PEAK POWER, AVERAGE ECC (6424 RUN 1) INITIAL CONDITIONS

<u>Initial Conditions</u>	
Bundle power	6.49 ± 0.03 MW
Steam dome pressure	1056 ± 5 psia
Lower plenum pressure	1081 ± 5 psia
Lower plenum enthalpy	554 ± 5 Btu/lbm.
Initial water level	124 ± 6 in. El
Feedwater enthalpy	45 ± 2 Btu/lbm
Bundle inlet to outlet DP	30 ± 2 psi
Steam flow	8 ± 1 lbm/sec
Feedwater flow	1.1 ± 0.3 lbm/sec
Drive Pump 1 flow	7 ± 1 lbm/sec
Drive Pump 2 flow	8 ± 1 lbm/sec
Jet Pump 1 flow	14 ± 2 lbm/sec
Jet Pump 2 flow	18 ± 2 lbm/sec
Bundle inlet flow	29 ± 5 lbm/sec
ECC fluid temperature	120 ± 15°F

All uncertainty bands are judged from the maximum of data fluctuation and/or absolute uncertainties of the measurements.

Table 3-6

SEQUENCE OF EVENTS FOR 6424 RUN 1
(Peak Power, Avg. ECC)

<u>Events</u>	<u>Time (sec.)</u>
Blowdown valves open	0.0
Bundle power decay initiated	0.5
Feedwater flow stops	0.5
Bypass flow reverses	1.2
Steamline valve completely closed	8.0
Lower plenum bulk flashing	14
Loop 1 isolated	20
HPCS injection begins	27
Lower plenum mixture level reaches jet pump exit plane	34
LPCS, LPCI activated	37
LPCS flow begins	63
LPCI flow begins	71
Bundle quenched	150
End of test	400

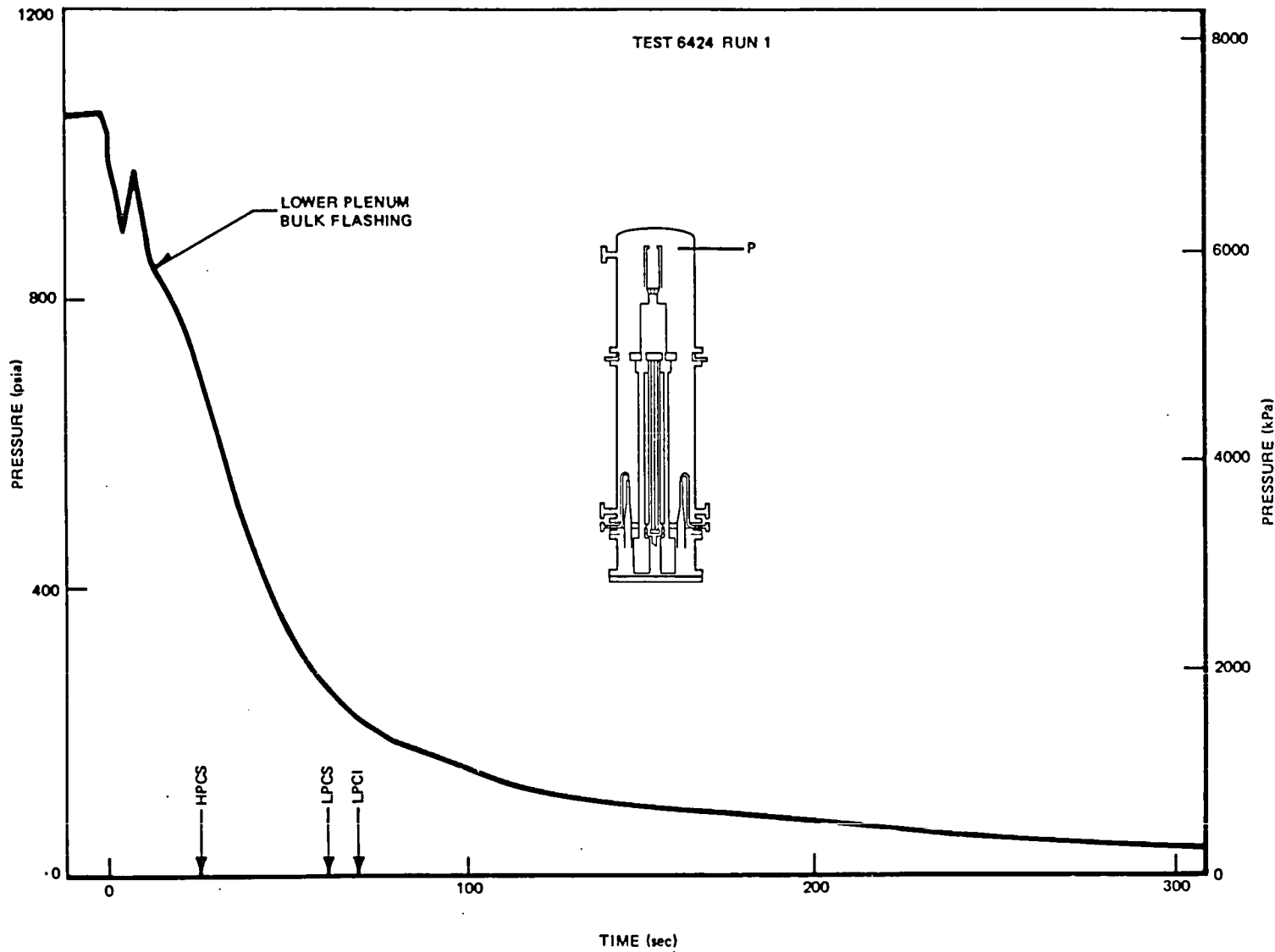


Figure 3-18. System Pressure Response for Test 6424 Run 1, Peak Power, Average ECC

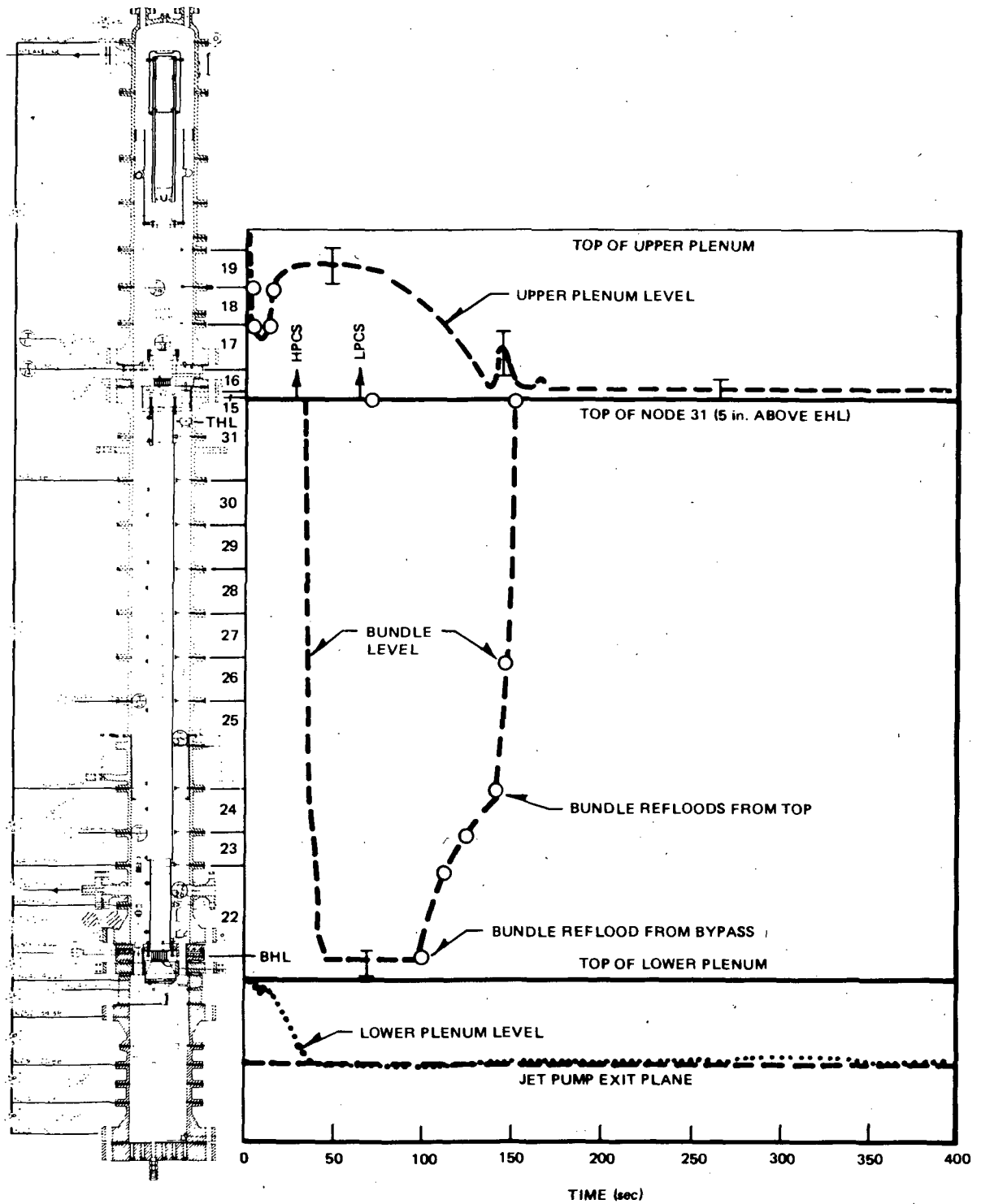


Figure 3-19a. Two-Phase Mixture Level Response for Test 6424 Run 1 (Peak Power, Avg. ECC) along Lower Plenum/Bundle/Upper Plenum Path

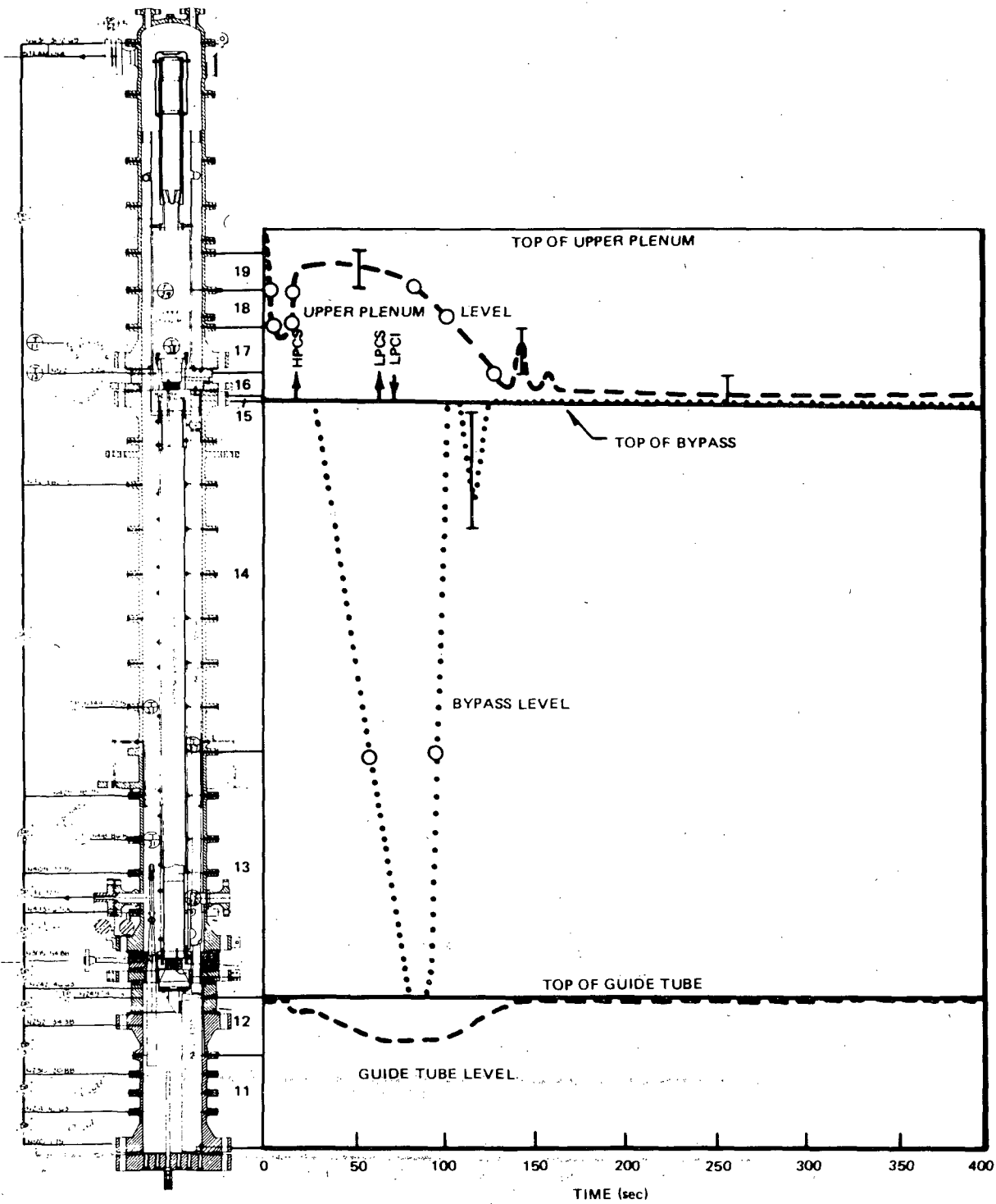


Figure 3-19b. Two-Phase Mixture Level Response for Test 6424 Run 1 (Peak Power, Avg. ECC) along Guide Tube/Bypass/Upper Plenum Path

TYPICAL
UNCERTAINTY

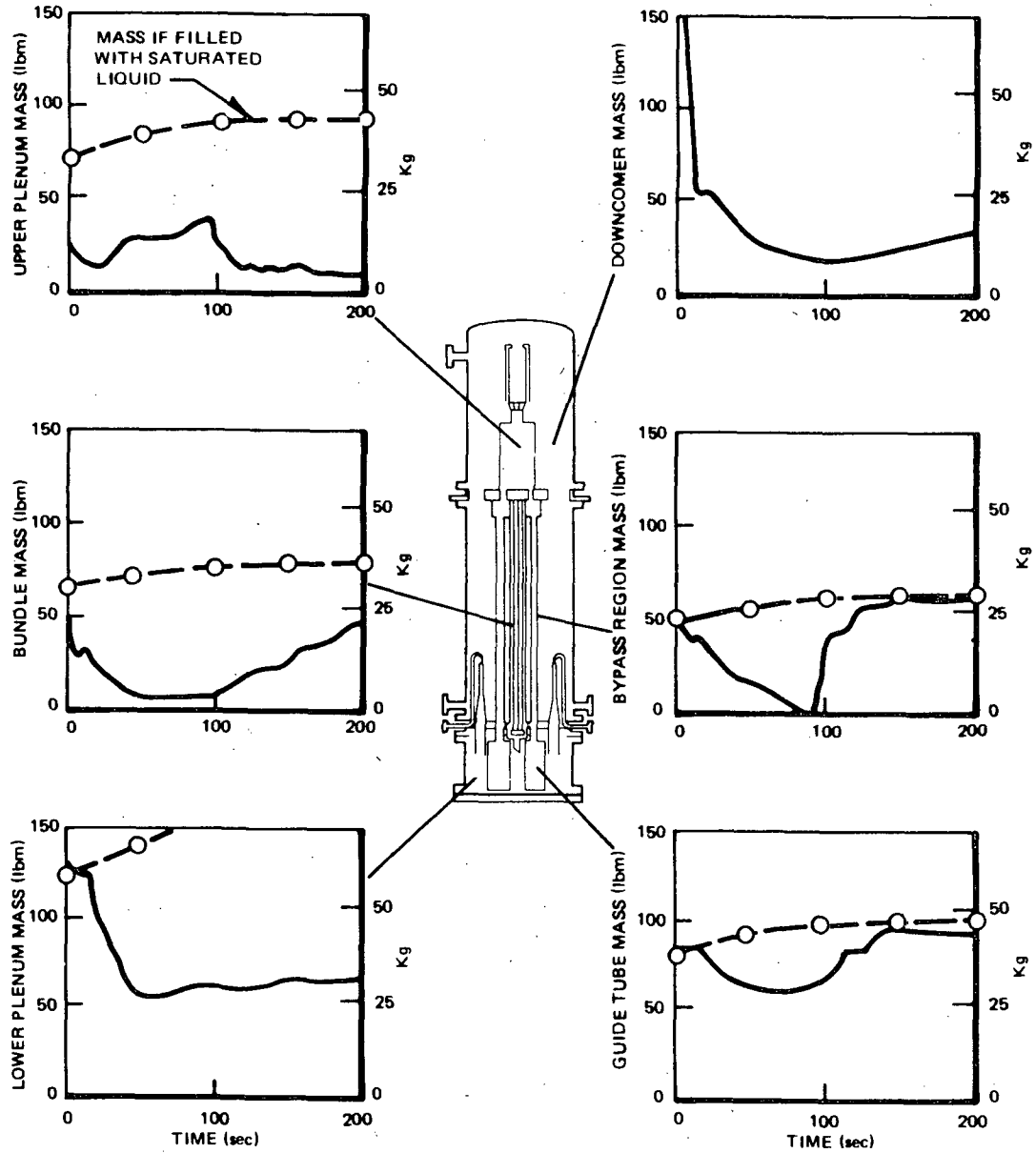


Figure 3-20. Regional Mass Responses for Test 6424 Run 1 (Peak Power, Avg. ECC)

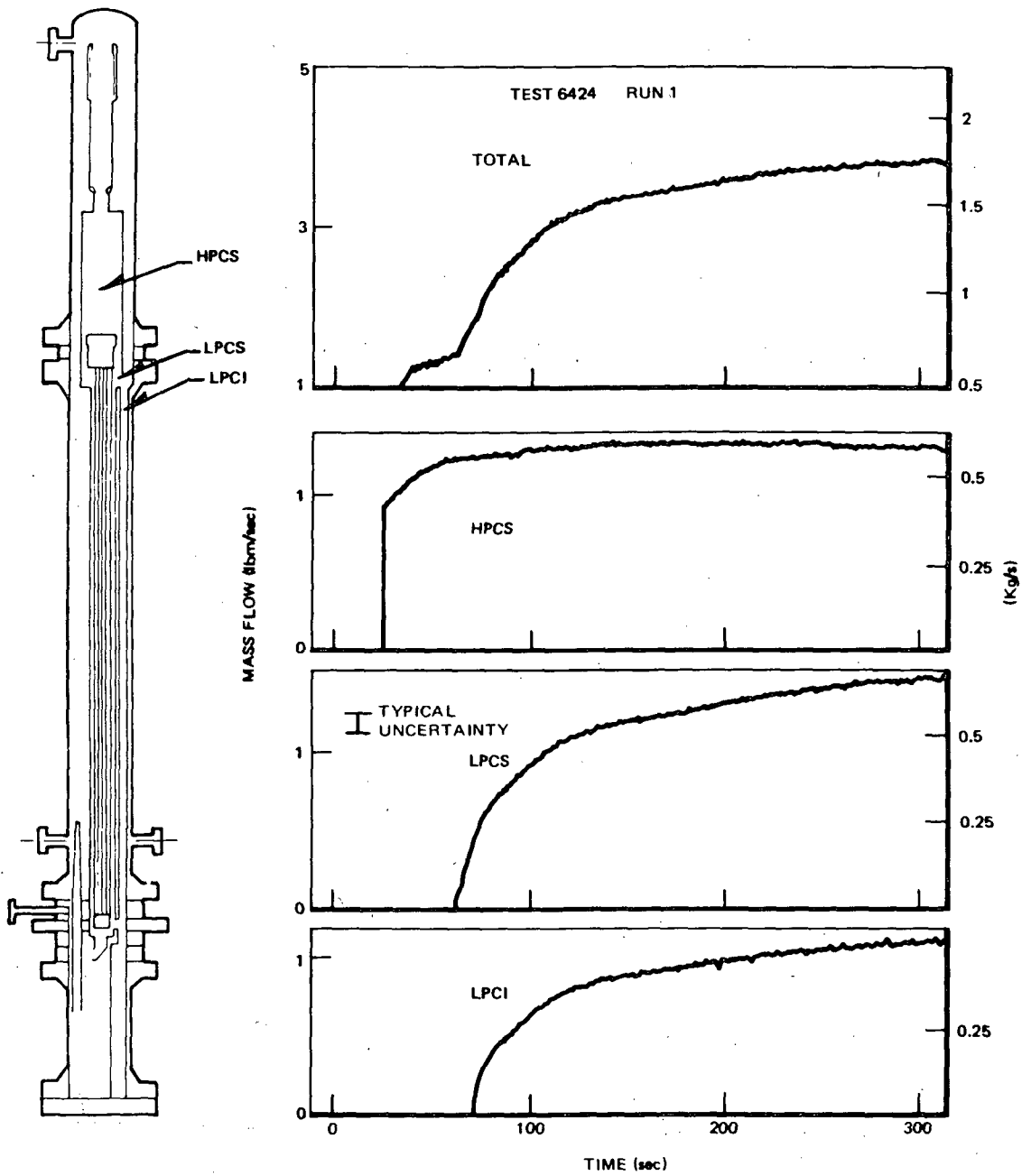


Figure 3-21. ECC Injection Rates for Test 6424 Run 1 (Peak Power, Avg. ECC)

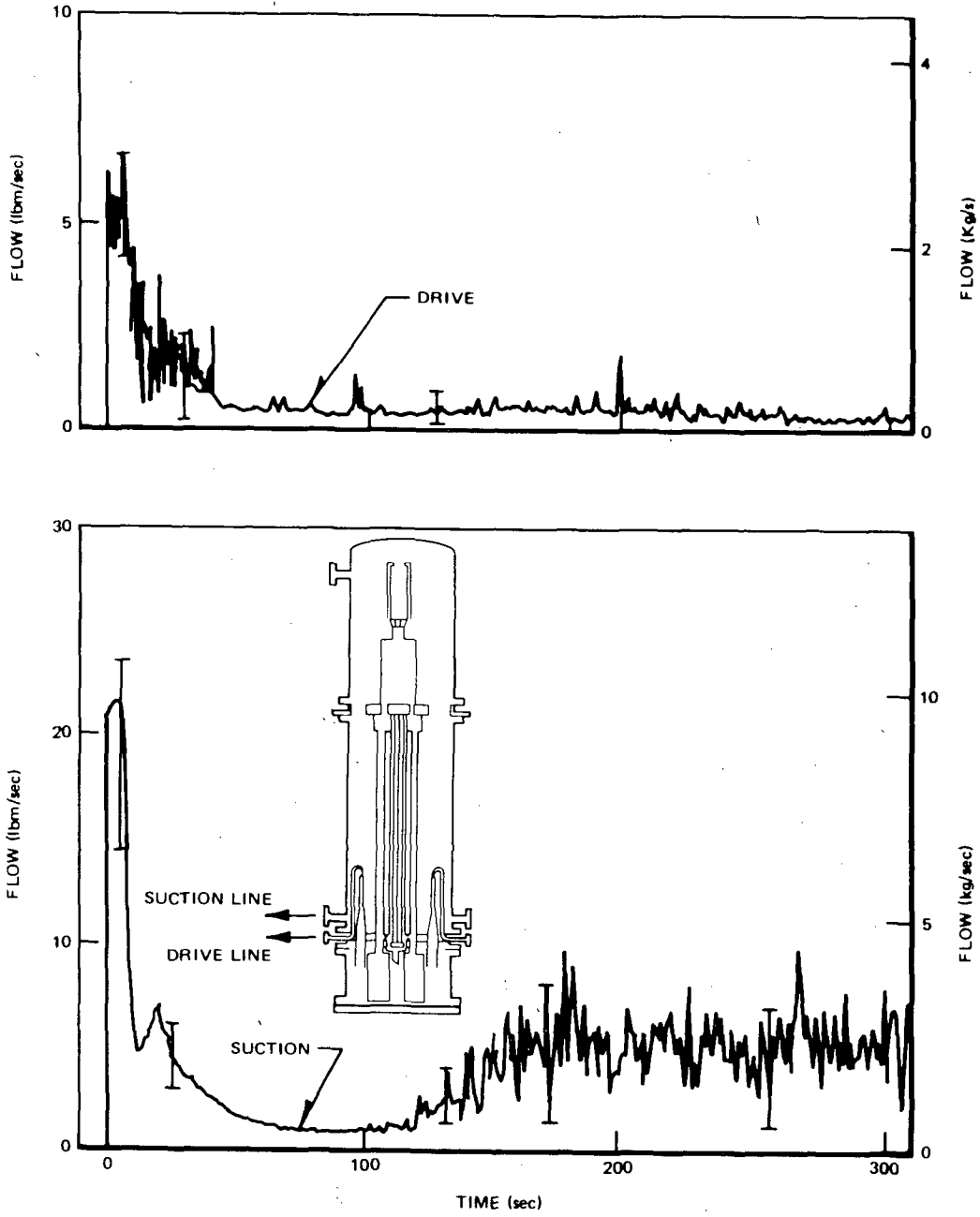


Figure 3-22. Break Flows from Turbine Meter and Drag Disc Measurements for Test 6424 Run 1 (Peak Power, Avg. ECC)

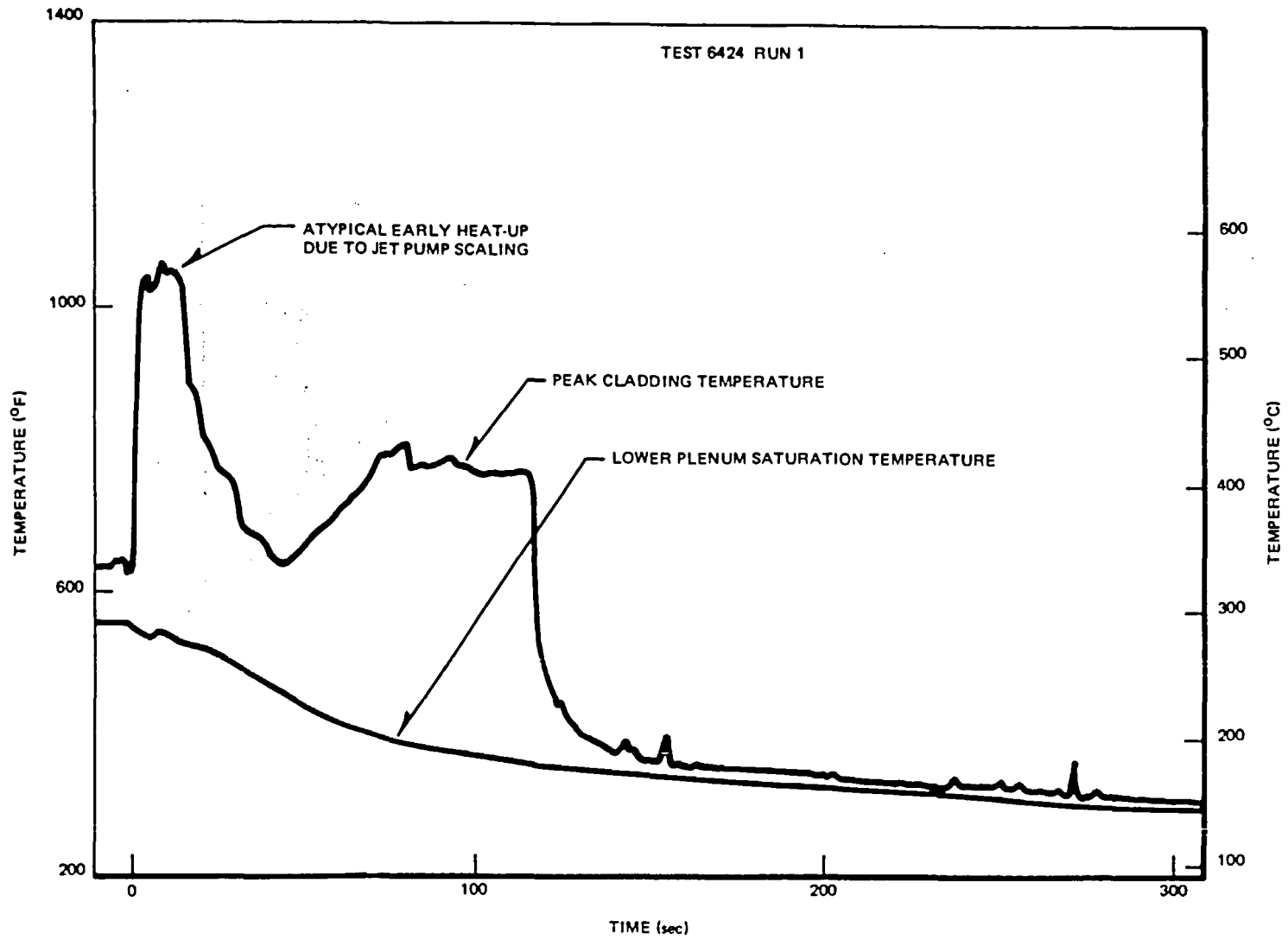


Figure 3-23. Peak Cladding Temperature Response for Test 6424 Run 1 (Peak Power, Avg. ECC)

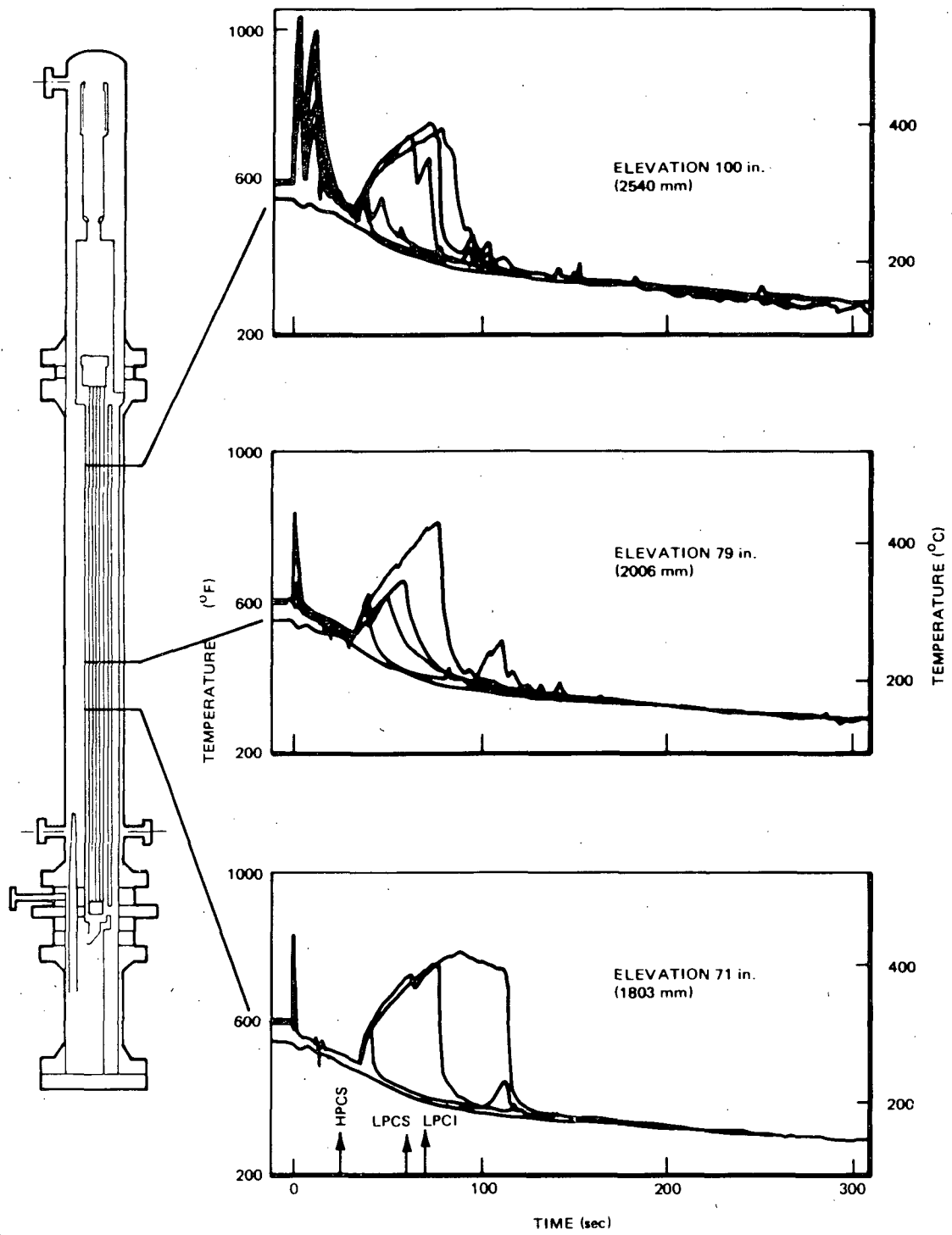


Figure 3-24. Bundle Temperature Responses at Selected Elevations for Test 6424 Run 1 (Peak Power, Avg. ECC)

The initial conditions for this test are presented in Table 3-7 and the sequence of events is depicted in Table 3-8. Figures 3-25 through 3-27 provide an overview of the system response with plots of system pressure (Figure 3-25), two-phase mixture levels (Figure 3-26), and regional mass inventories (Figure 3-27).

The break flow measurements are shown in Figure 3-28. Except for these measurements, this test (6426 Run 1) was intended to be a repeat of Test 6421 Run 2. After the test was completed, however, it was found that the isolation valve (V8) in the blowdown loop, which should have been closed at the beginning of blowdown, failed to close in this test (because of a faulty controller). It was not clear whether the valve did close later. The effect on global response, however, seemed diminished after that time. More detailed discussions on the valve failure are included in Subsection 3.3.2 and Appendix D.

The bundle thermal responses of this test (6426/1) differ from those of a comparable test (6421/2) in two aspects. The heat-up time of Test 6426/1 (valve failure), as seen in Figure 3-29, occurs earlier than that of Test 6421/2, as well as other tests. The heat-up rate of Test 6426/1 is also higher, as can be seen from comparing Figures 3-29 and 3-30. The heat-up rate difference is attributable to the difference in bundle power history discussed in Appendix L-3.

The reason for the heat-up time difference, on the other hand, is not as clear. The power difference that causes the difference in heat-up rate is not clearly attributable as a cause for the earlier heat-up time because the heat-up time for the peak power test (6424/1) is later (Figure 3-24). This leaves the valve failure as the most likely cause. It could be argued that although the global effect of system response caused by valve failure diminishes after ~ 25 seconds, there are on the bundle mass inventory some local effects which persist until ~ 40 seconds. Such effects can be seen from the comparative plot of bundle mass inventory in Figure 3-51, which shows that the inventory is slightly less for the test with valve failure at about 20 seconds. Consequently, some of the rods experiencing early boiling transition were not rewetted by redistribution of inventory following lower plenum flashing.

On the other hand, the bundle thermal response from this test has a rather large uncertainty because of an erratic multiplexer. A large number of thermocouple measurements were clearly erroneous (e.g., initial cladding temperature was less than saturation temperature). The remaining ones appear reasonable, but there is no way of verifying them. Therefore, data from this test (6426/1) Appendix L-1) which

Table 3-7

BD/ECC 1A TEST 6426 RUN 1 INITIAL CONDITIONS
(Avg. Power, No ECC)

<u>Initial Conditions</u>	
Bundle power	5.05 ± 0.03 MW
Steam dome pressure	1044 ± 5 psia
Lower plenum pressure	1068 ± 5 psia
Lower plenum enthalpy	526 ± 5 Btu/lbm
Initial water level	123 ± 6 in. El
Feedwater enthalpy	66 ± 2 Btu/lbm
Bundle inlet to outlet DP	15 ± 2 psi
Steam flow	6 ± 1 lbm/sec
Feedwater flow	1.3 ± 0.3 lbm/sec
Drive Pump 1 flow	8.2 ± 1 lbm/sec
Drive Pump 2 flow	8.4 ± 1 lbm/sec
Jet Pump 1 flow	16 ± 2 lbm/sec
Jet Pump 2 flow	20 ± 2 lbm/sec
Bundle inlet flow	33 ± 5 lbm/sec

All uncertainty bands are judged from the maximum of data fluctuation and/or absolute uncertainties of the measurements.

Table 3-8

SEQUENCE OF EVENTS FOR 6426 RUN 1
(Avg. Power, No ECC)

<u>Events</u>	<u>Time (sec.)</u>
Blowdown valves open	0.0
Bundle power decay initiated	0.5
Blowdown loop jet pump flow reverses	0.1
Feedwater flow stops	0.5
Bypass flow reverses	1.5
Jet pump suction uncovers	6.5
Steamline valve completely closed	7.9
Recirc. suction line begins to uncover	9.2
Lower plenum bulk flashing	13.3
Guide tube flashing	13.8
Core inlet uncovers (SEO center line)	20
Lower plenum mixture level reaches jet pump exit plane	33
End of test	294

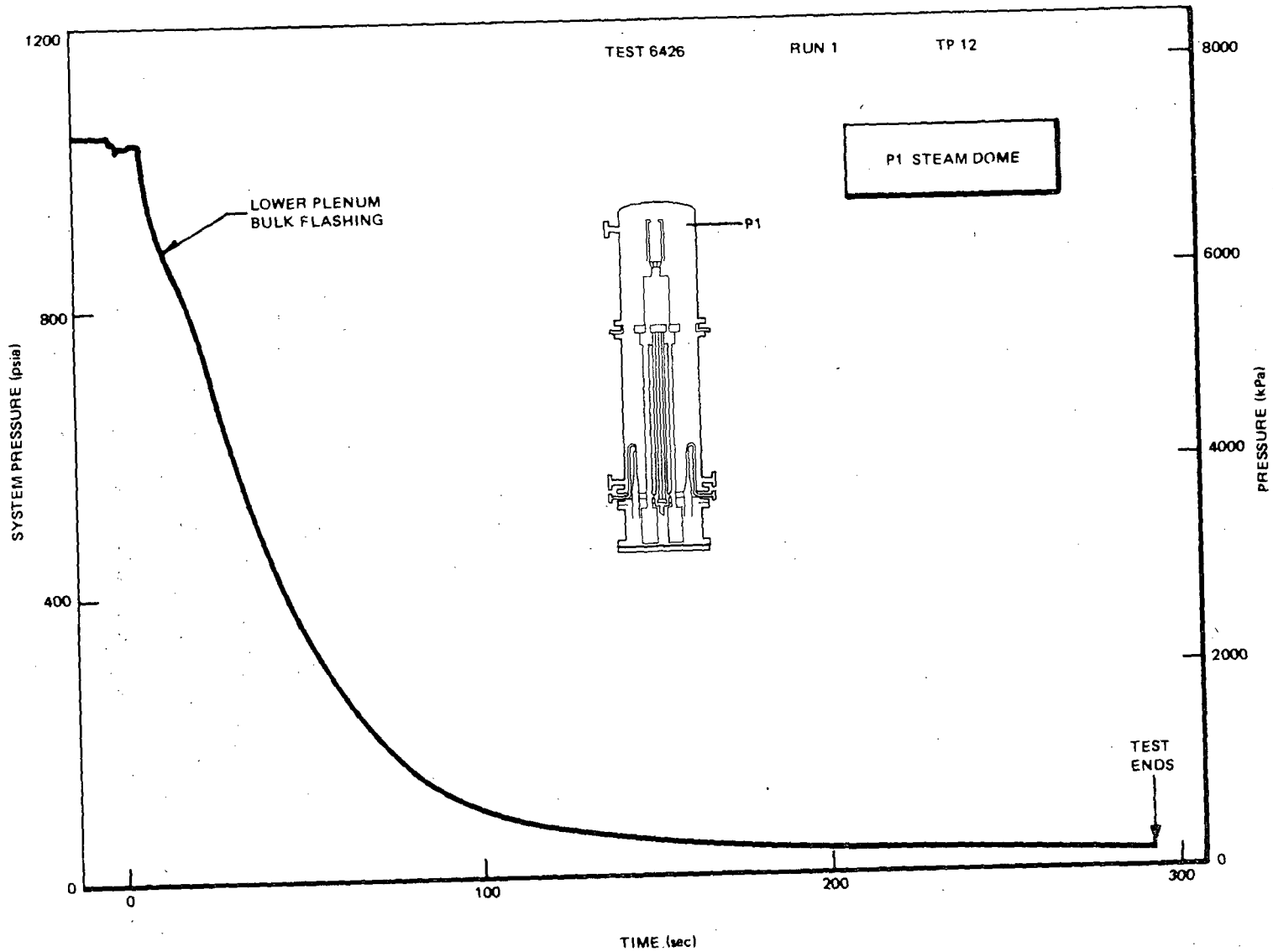


Figure 3-25. System Pressure Response for 6426 Run 1 (Avg. Power, No ECC)

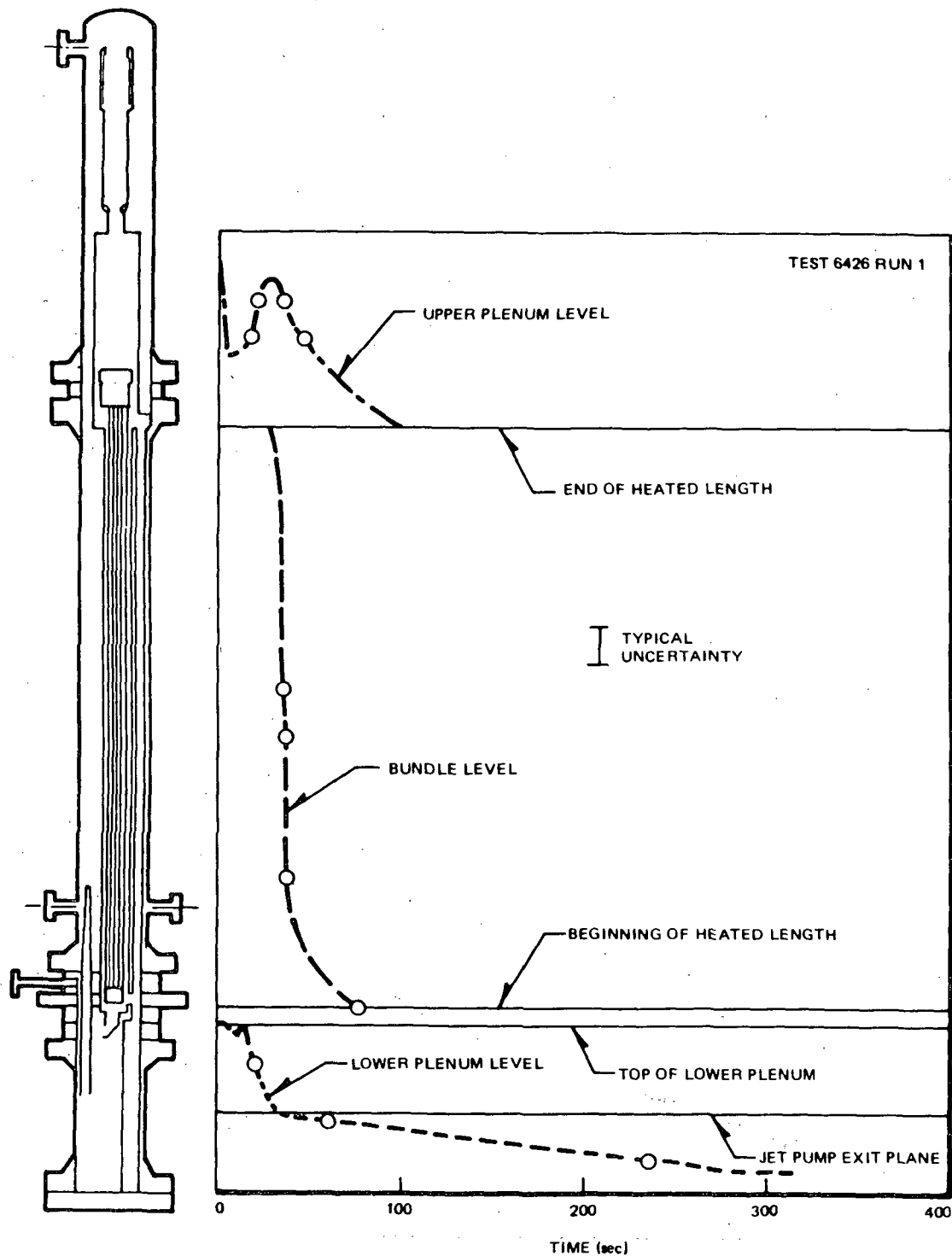


Figure 3-26a. Two-Phase Mixture Level Response along Bundle Path for Test 6426 Run 1 (Avg. Power, No ECC)

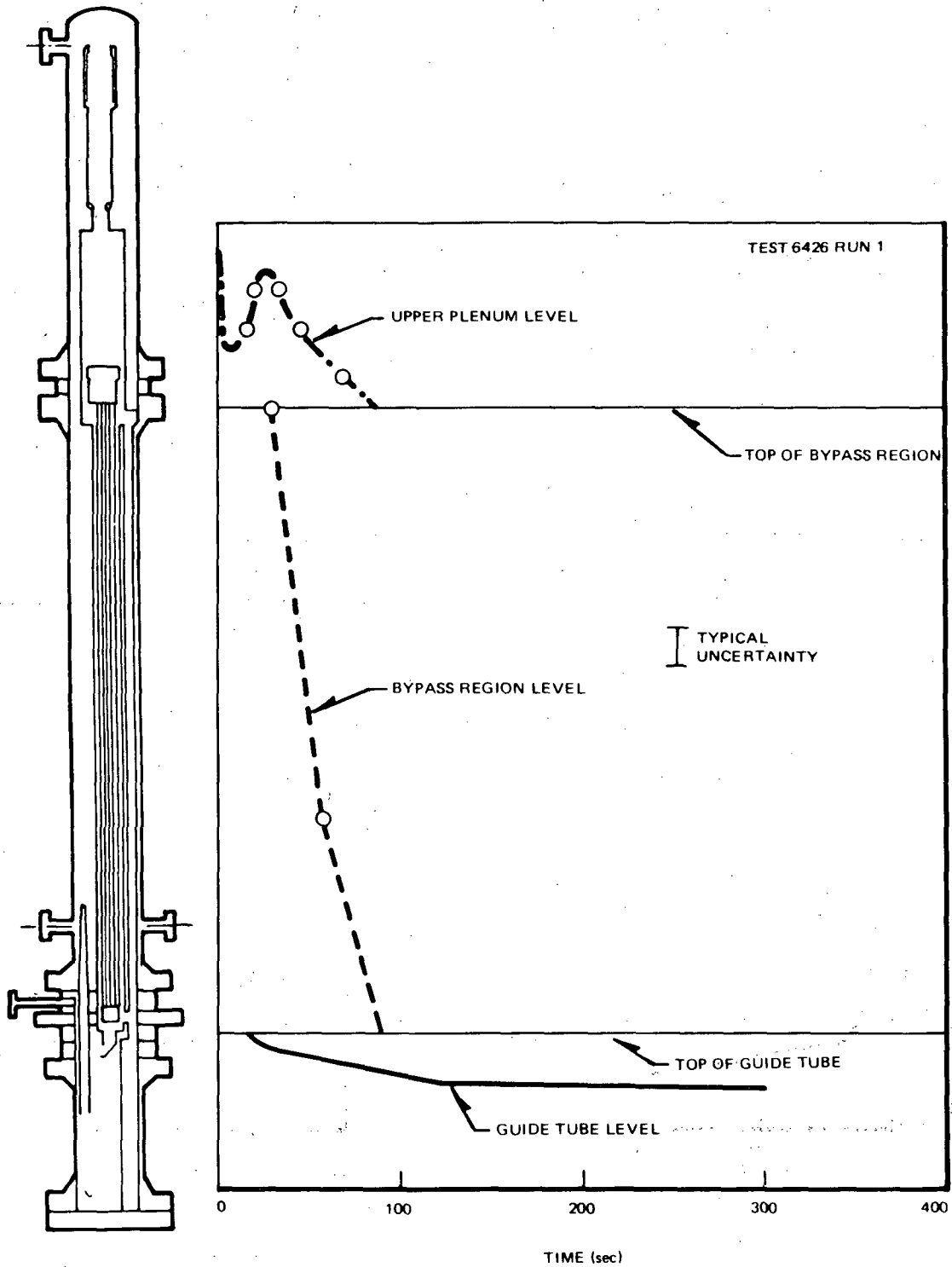


Figure 3-26b. Two-Phase Mixture Level Response along Bypass Path for Test 6426 Run 1 (Avg. Power, No ECC)

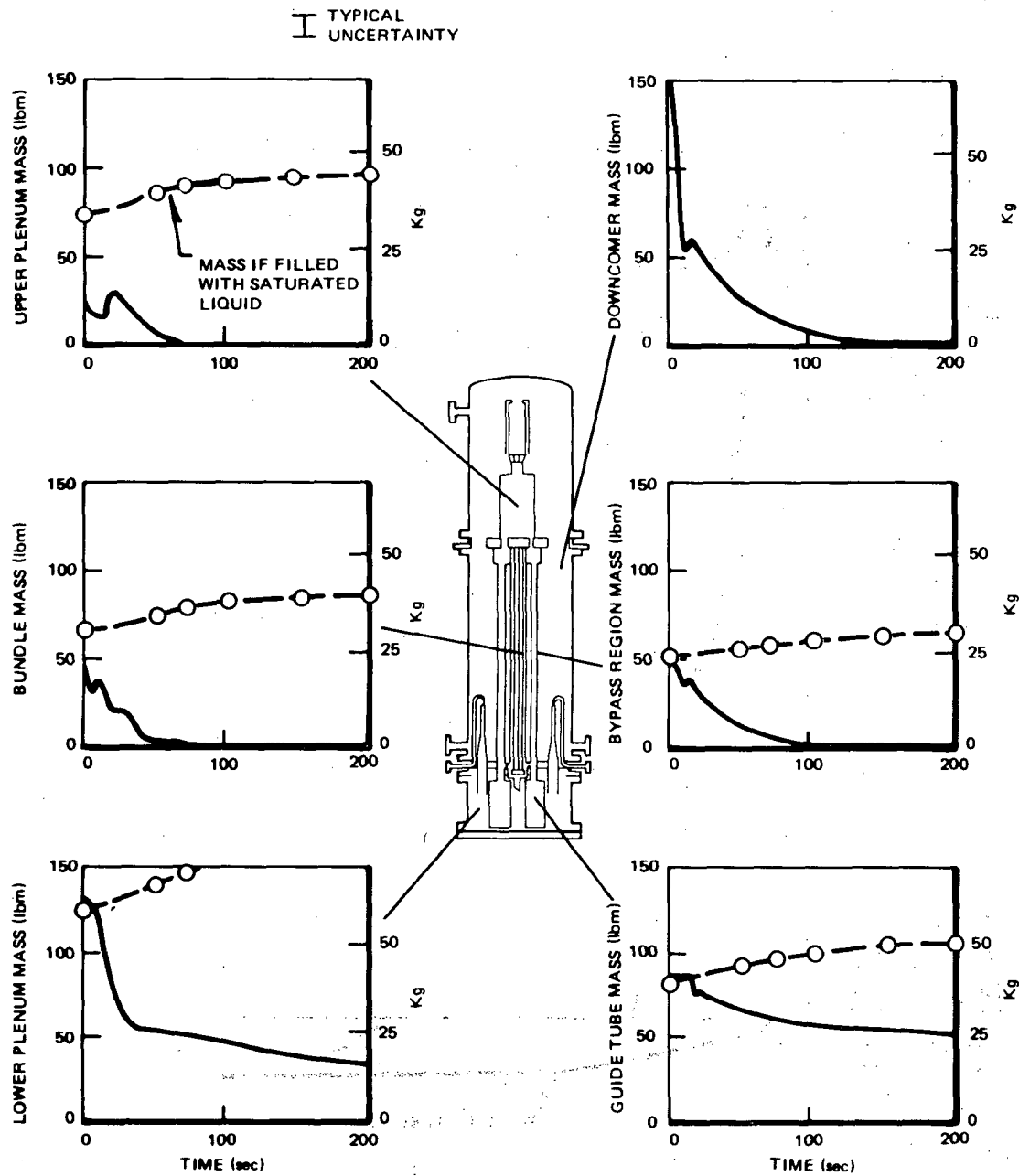


Figure 3-27. Mass Inventory Responses at Various Regions for Test 6426 Run 1 (Avg. Power, No ECC/Valve Failure)

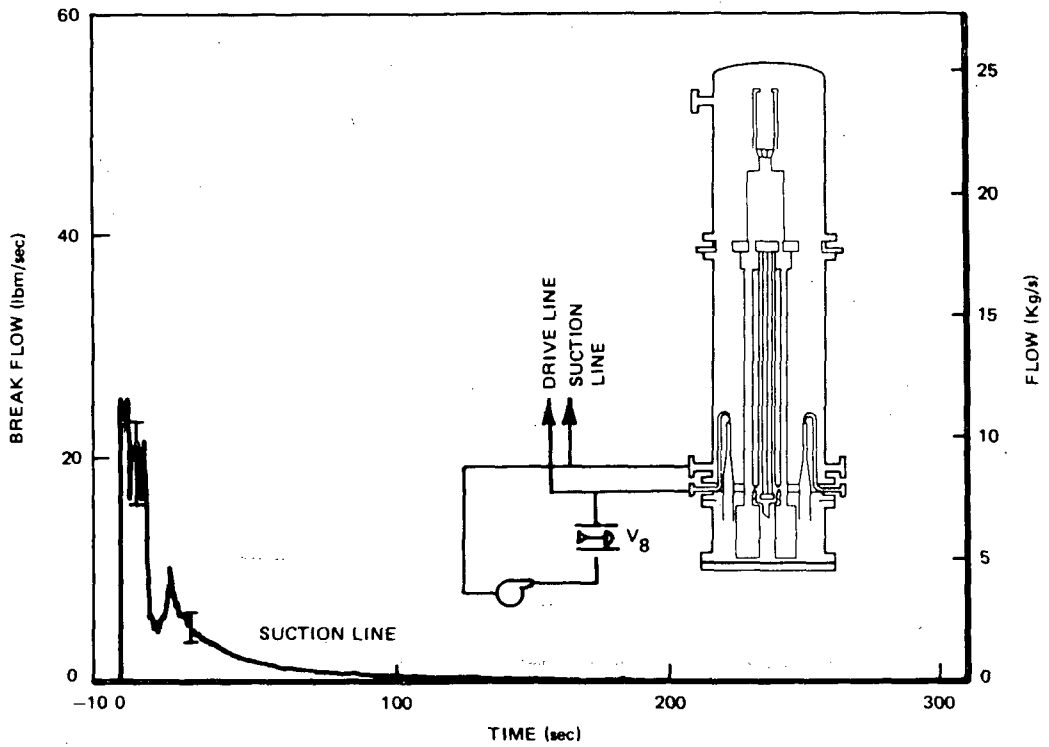
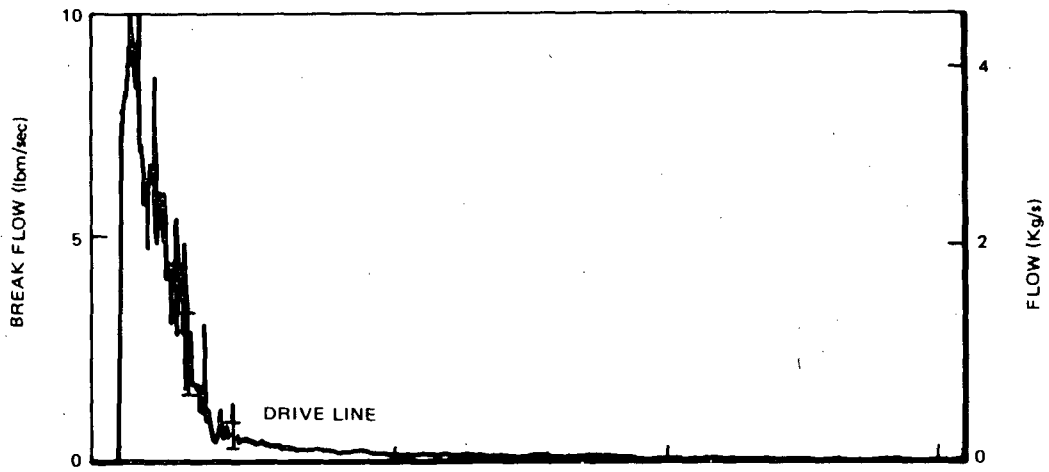


Figure 3-28. Break Flows from Turbine Meter and Drag Disc Measurements for Test 6426 Run 1 (Avg. Power, No ECC, Valve Failure)

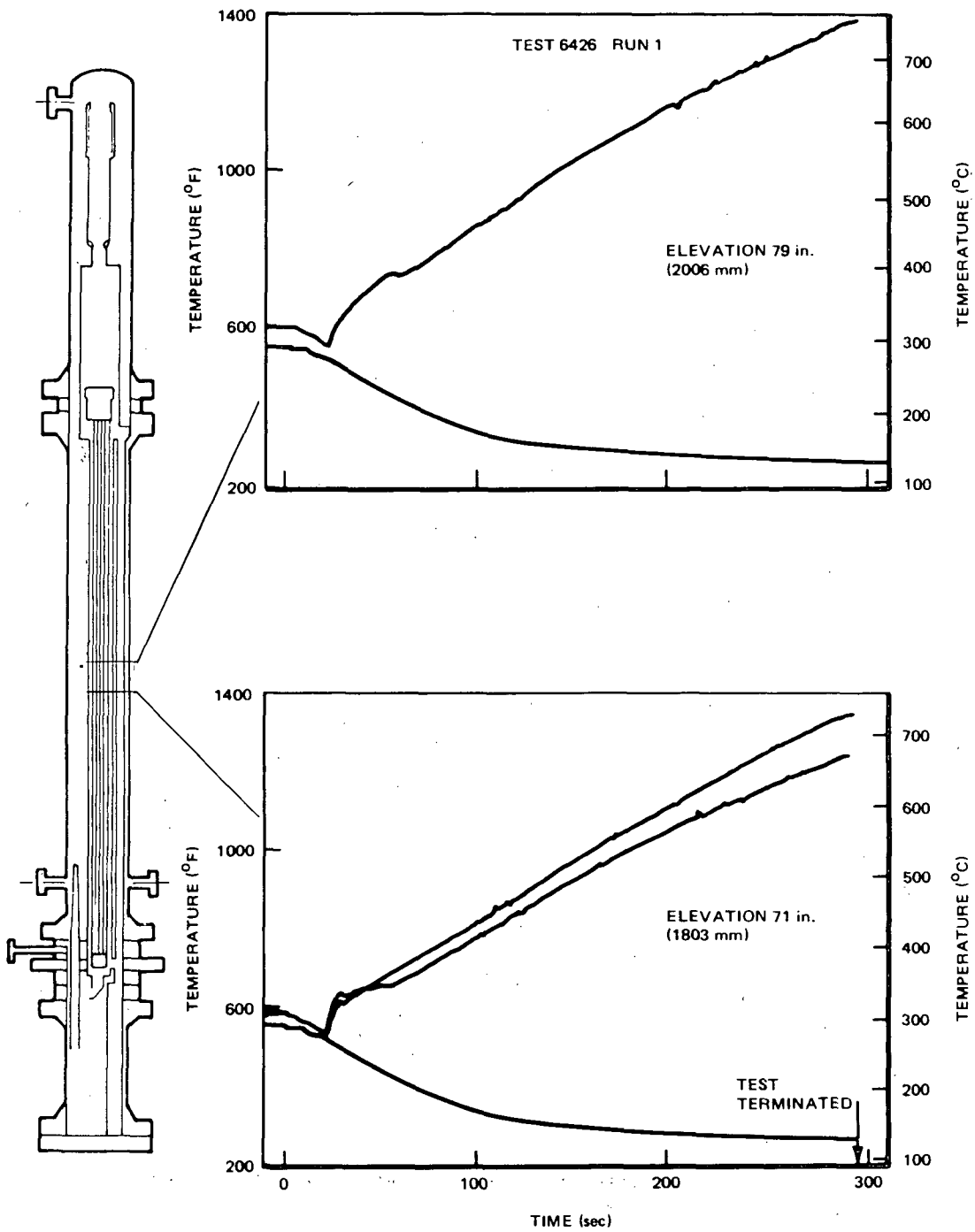


Figure 3-29. Bundle Temperature Response at Peak Power Regions for Test 6426 Run 1 (Avg. Power, No ECC, Valve Failure)

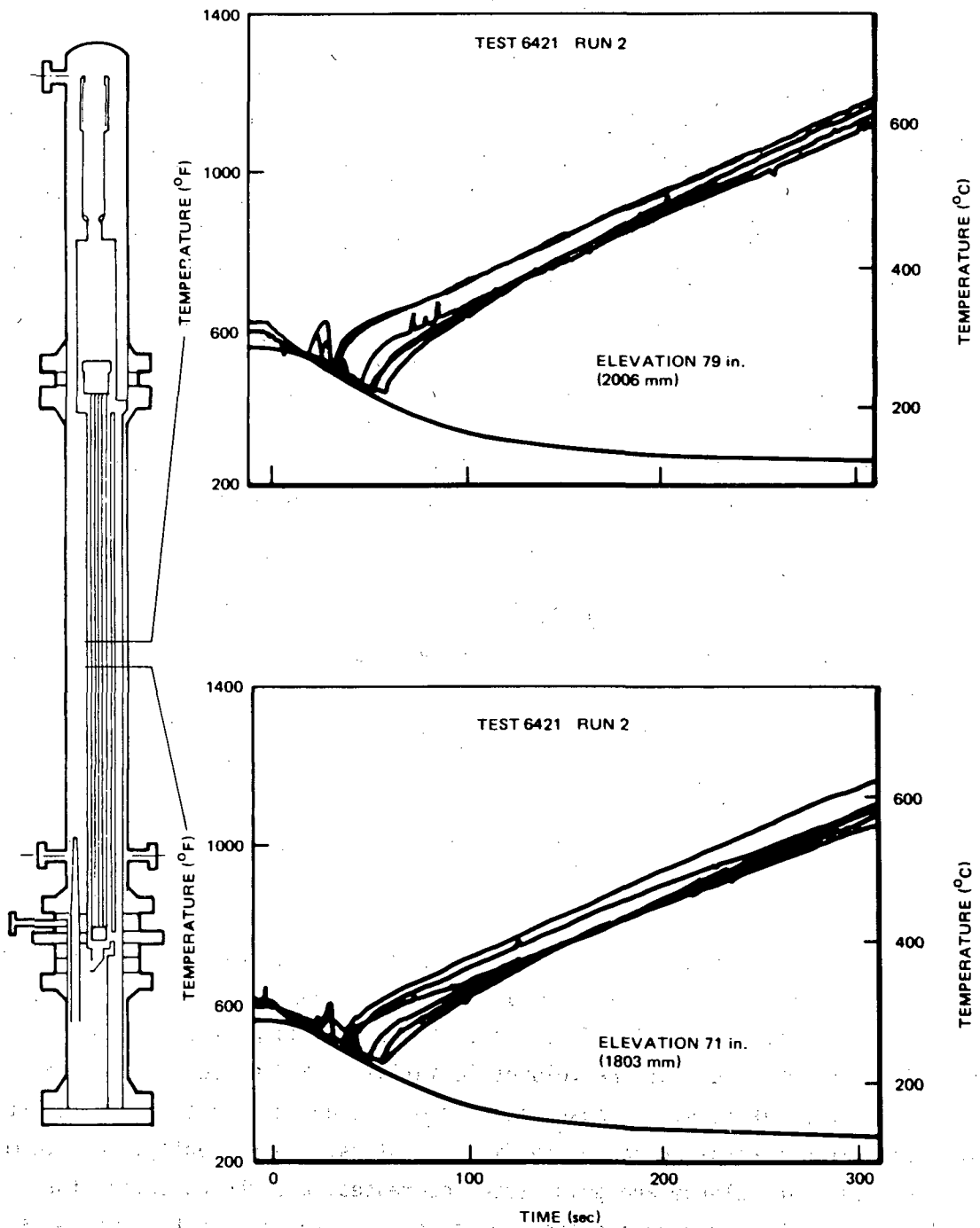


Figure 3-30. Bundle Temperature Response at Peak Power Regions for Test 6421 Run 2 (Avg. Power, No ECC)

include improved break flow measurements are supplemented by those from the comparable test (6421/2) (Appendix L-2).

3.2.2.3 Average Power, Average ECC (6422 Run 3). This test was initially intended to be the reference test. However, owing to improved break flow measurements and the addition of a more representative pressure controller to simulate the early system pressure response, Test 6425 Run 2 has replaced this test as the reference test. The system responses of the two tests are comparable. Detailed discussion on system responses and a complete set of data for this test are included in Appendix M.

3.2.2.4 Peak Power, Low Rate, High Temperature ECC Test (6423 Run 3). Results from this test show that even for this upper bound case of combining a number of unfavorable conditions, the ECC injections were effective in cooling the bundle. The maximum cladding temperature reached, because of boiling transition in the pump coastdown period, is 1020°F (549°C). The maximum cladding temperature because of subsequent dryout is 970°F (521°C).

The low spray rate combined with high ECC water temperature results in system hydraulic responses that are different from those of tests with average ECC rates at nominal temperature. As discussed below, the system pressure levels off at ~85 psia (586 kpa) instead of continuing to decrease, and the bundle refloods only the lower third.

The initial conditions for this test are as depicted in Table 3-9. The sequence of events is presented in Table 3-10.

The system pressure response is shown in Figure 3-31. The system pressure reaches a minimum value of ~75 psia (517 kpa) at ~150 seconds, repressurizes slightly, and levels off at ~85 psia (586 kpa). This repressurization, as discussed later in Subsection 3.4.2, is the result of the volumetric influx of ECC exceeding the volumetric efflux of the break flow. Because the system pressure ceased to decrease after ~150 seconds, steam generation caused by flashing stops. Consequently, the steam updraft from the lower plenum and guide tubes decreases, and the potential for inventory hold-up within the bundle and bypass regions caused by CCFL diminishes.

The mixture level response is shown in Figure 3-32. The bypass region refills first by LPCI in combination with the upper plenum inventory at ~130 seconds (Figure 3-32b). The bundle begins to reflood (Figure 3-32a) as the bypass fluid flows through the leakage path and enters the lower portion of the bundle. The upper plenum empties

Table 3-9

TEST 6423 RUN 3 INITIAL CONDITIONS
(Peak Power, Low Rate/High Temperature ECC)

<u>Initial Conditions</u>	
Bundle power	6.46 ± 0.03 MW
Steam dome pressure	1037 ± 5 psia
Lower plenum pressure	1065 ± 5 psia
Lower plenum enthalpy	518 ± 5 Btu/lbm
Initial water level	123 ± 6 in. El
Feedwater enthalpy	41 ± 2 Btu/lbm
Bundle inlet to outlet DP	16 ± 2 psi
Steam flow	7 ± 1 lbm/sec
Feedwater flow	1.0 ± 0.3 lbm/sec
Drive Pump 1 flow	8.1 ± 1 lbm/sec
Drive Pump 2 flow	8.3 ± 1 lbm/sec
Jet Pump 1 flow	17 ± 2 lbm/sec
Jet Pump 2 flow	19 ± 2 lbm/sec
Bundle inlet flow	33 ± 5 lbm/sec
ECC fluid temperature	200 ± 15°F

All uncertainty bands are judged from the maximum of data fluctuation and/or absolute uncertainties of the measurements.

Table 3-10

SEQUENCE OF EVENTS FOR 6423 RUN 3
(Peak Power, Low Rate/High Temperature ECC)

<u>Event</u>	<u>Time (sec.)</u>
Blowdown valves open	0.0
Bundle power decay initiated	0.5
Feedwater flow stops	0.5
Bypass flow reverses	1.5
Steamline valve completely closed	11.5
Lower plenum bulk flashing	15
Loop 1 isolated	20
HPCS injection begins	27
Lower plenum mixture level reaches jet pump exit plane	39
LPCS, LPCI activated	37
LPCS flow begins	65
LPCI flow begins	72
End of test	400

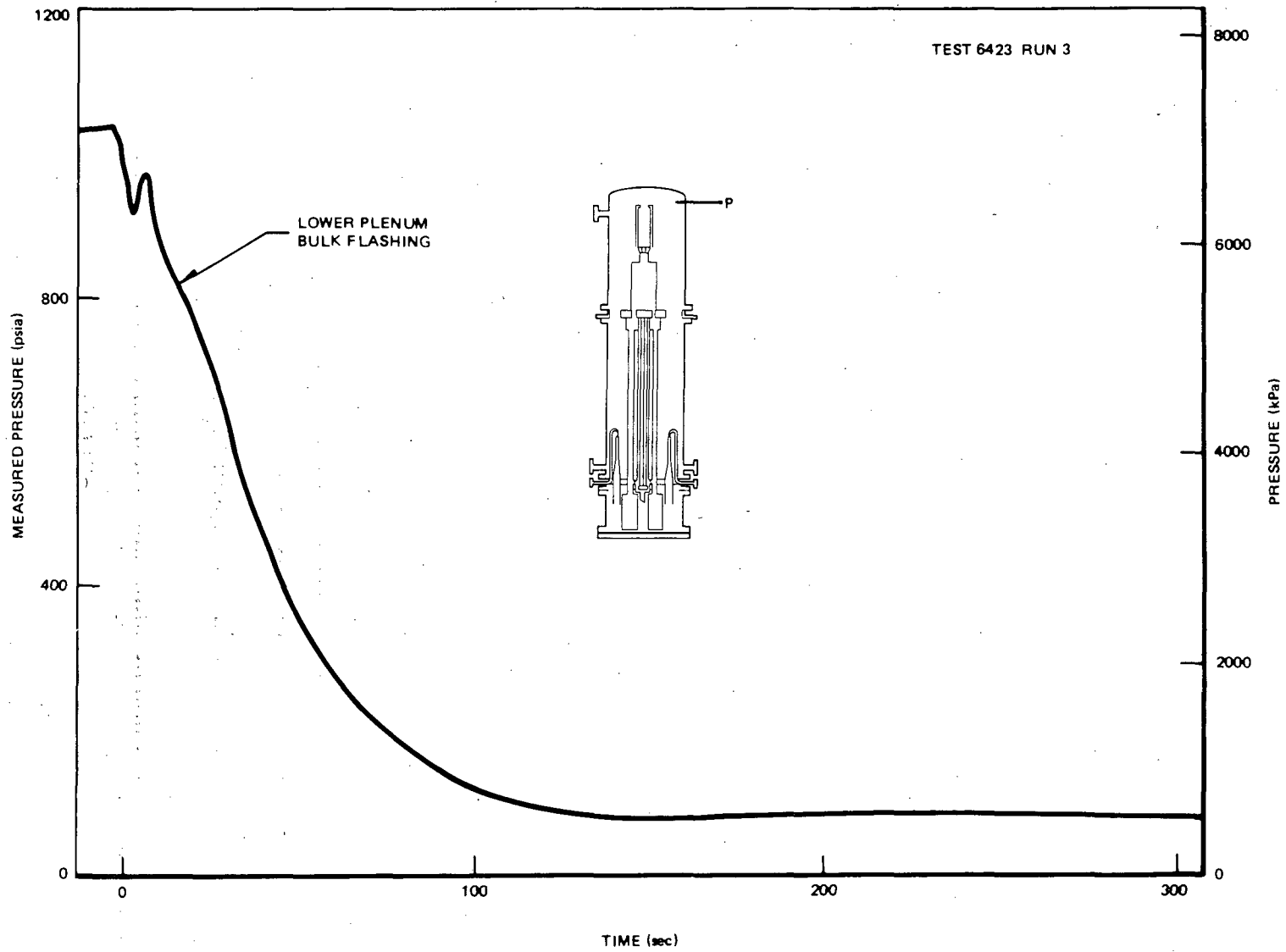


Figure 3-31. System Pressure Response for Test 6423 Run 3 (Peak Power, Low Rate/ High Temperature ECC)

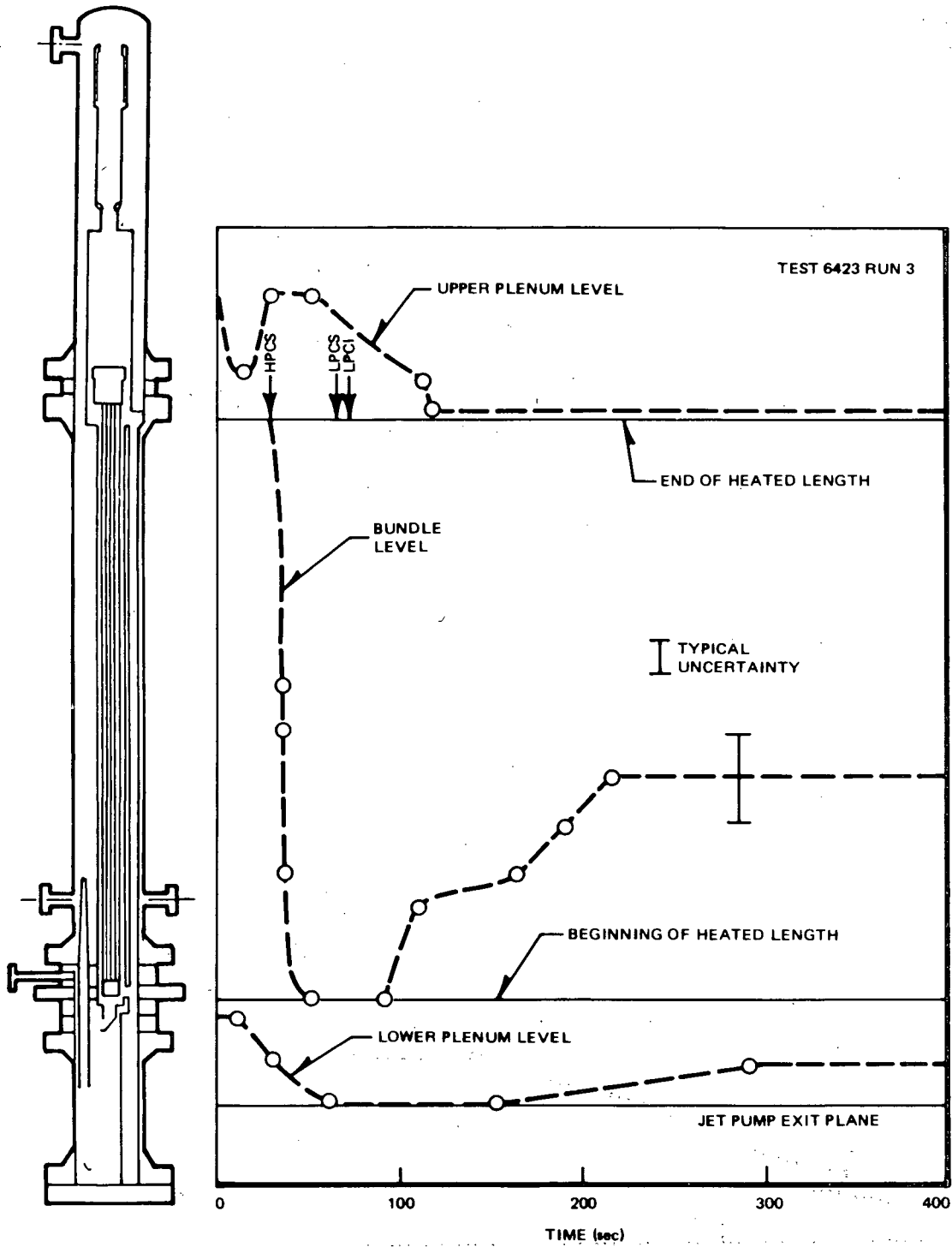


Figure 3-32a. Two-Phase Mixture Level Response along Bundle Path for Test 6423 Run 3 (Peak Power, Low ECC)

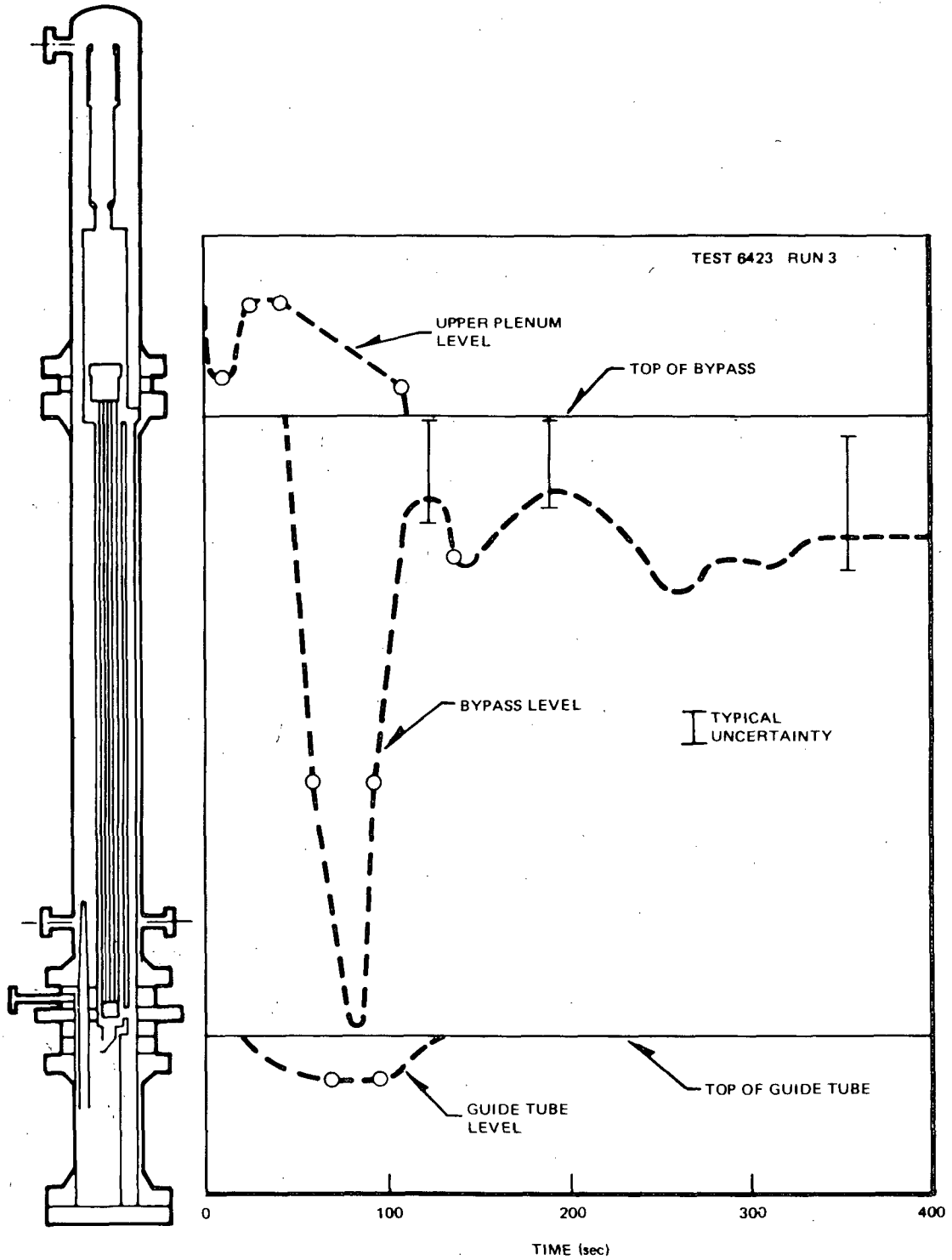


Figure 3-32b. Two-Phase Mixture Level Response along Bypass Path for Test 6423 Run 3 (Peak Power, Low ECC)

as the bypass refills and the bundle refloods. The guide tube region refills from the bypass fluid as with the reference test, but, because the inflow of ECC is lower for this test, the level in the bypass drops momentarily. Once the guide tube is filled the bypass refills again. The net inflow, however, is insufficient to fill the bypass completely.

The bundle refloods only the lower third because of the lower ECC injection and because the CCFL condition at the bundle inlet is less favorable for liquid holdup (due to reduced vapor upflow). As a result there is less pressure difference between the lower plenum and the steam dome as compared to the reference test where the bundle was completely reflooded. This lower pressure difference allows the lower plenum level to rise above the jet pump exit.

Mass inventory transients at various regions are shown in Figure 3-33, and ECC flow rates are in Figure 3-34. The bundle thermal response is represented by the plot of peak cladding temperature in Figure 3-35. A complete set of data for this test is provided in Appendix N.

3.2.2.5 Scoping Series. The Scoping Series of five tests was conducted in TLTA 5. As mentioned in Subsection 2.2, TLTA 5 differs from the later configuration TLTA 5A in two important respects: (a) In TLTA 5 there was no direct leakage path between the bundle and the bypass, and (b) in TLTA 5 the bundle power decay was held constant after 50 seconds because of limitations in the power controller. The effect of this latter limitation was that an atypically high amount of decay power was applied to the bundle during the latter portion of the tests which results in higher cladding temperatures.

A summary of results from the Scoping Series is included in Appendix I.

Significant findings from this series include:

- a. CCFL at bundle inlet side-entry orifice holds up inventory in the bundle and delays bulk heat-up until the lower plenum level reaches the jet pump exit at ~35 seconds, the same as with the later tests in TLTA 5.
- b. ECC injection is beneficial in cooling the bundle. Even without CCFL breakdown at the bundle outlet, drainage into the bundle rewets the dried-out rods and contributes to bundle cooling. Also, under average conditions (as exemplified by Test 6406 Run 1), a period of sustained dryout is followed by a period during which numerous rewettings occur. Consequently, the heat-up within the bundle is mitigated.

I TYPICAL
UNCERTAINTY

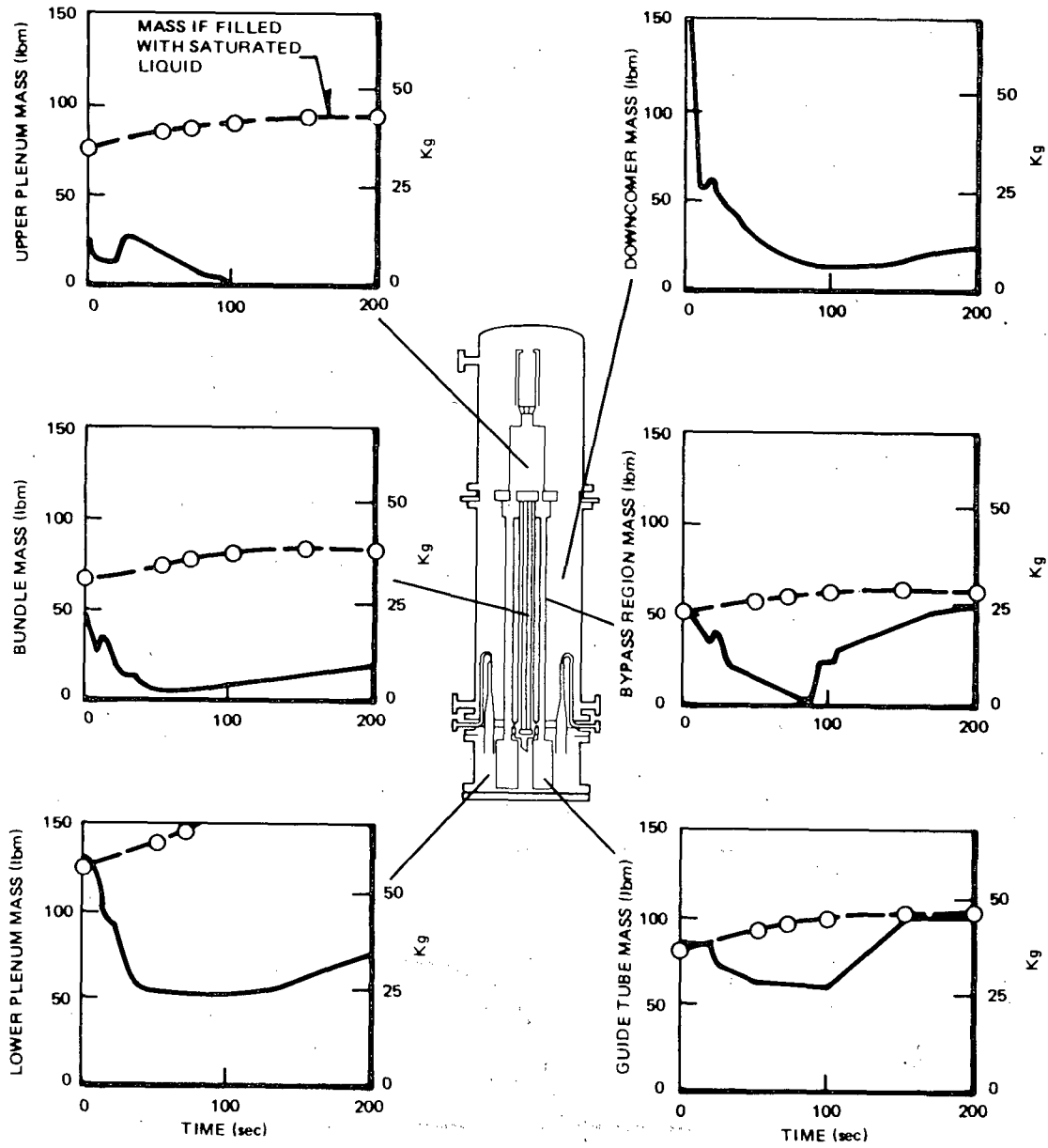


Figure 3-33. Regional Mass Responses for Test 6423 Run 3 (Peak Power, Low Rate/High Temperature ECC)

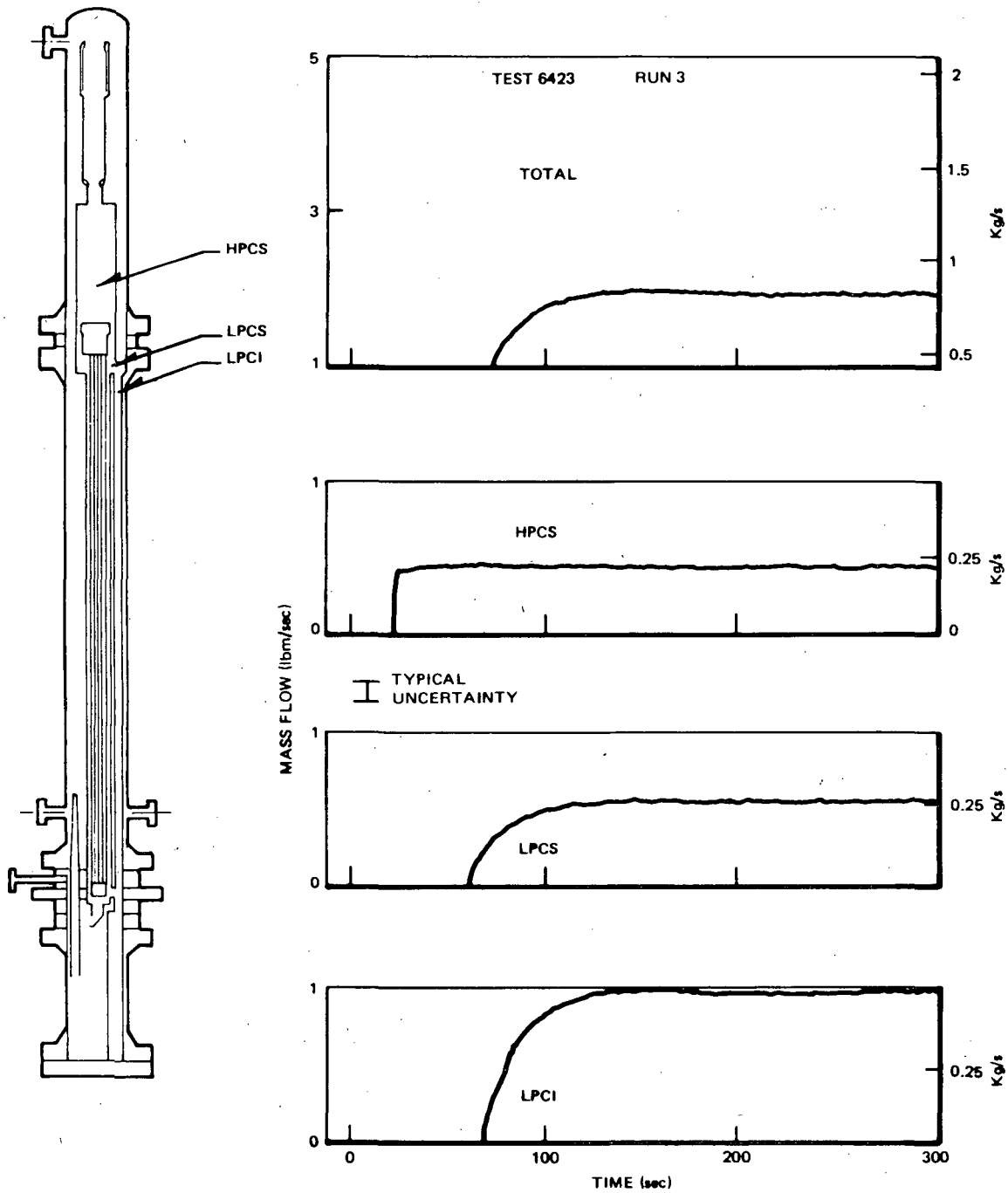


Figure 3-34. ECC Injection Rates for Test 6423 Run 3 (Peak Power, Low Rate/High Temperature ECC)

3-60

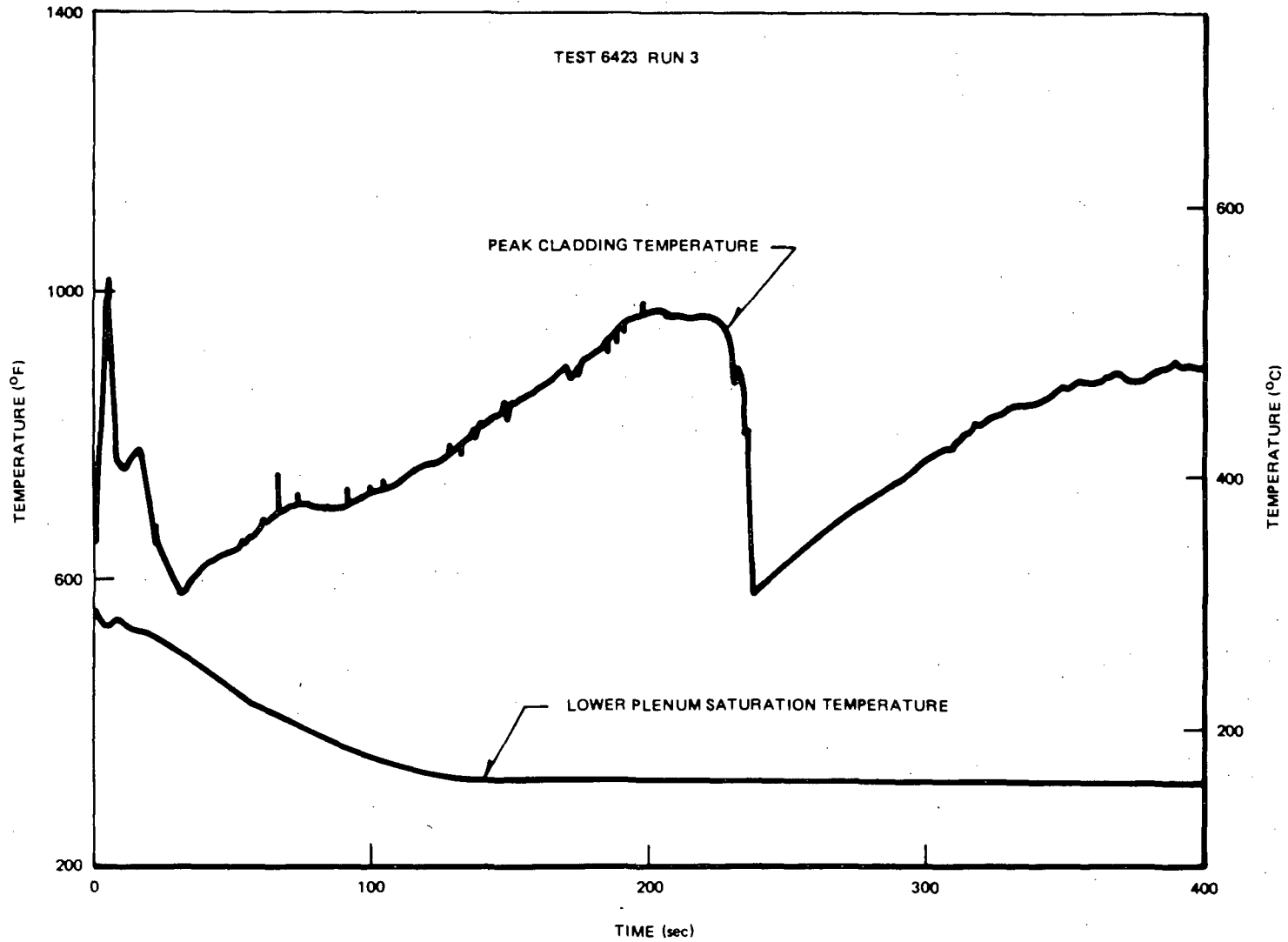


Figure 3-35. Peak Cladding Temperature Response for Test 6423 Run 3 (Peak Power, Low Rate/High Temperature ECC)

- c. The bundle refloods to the equivalent height of the jet pump. (This is significantly different from the TLTA 5A reference test, which refloods completely, because of the difference in leakage path simulation.)
- d. System depressurization for the tests with ECC is affected slightly after ~65 seconds. The cause for the difference is the higher fluid density upstream of the break. The same effect was observed in TLTA 5A.

Highlights from this test series are shown in Figures 3-36 through 3-40. Shown in Figure 3-36 are the system pressure responses for tests with and without ECC. The difference in the system pressure is seen to be discernible at ~65 seconds. The level responses are shown in Figure 3-37. The mass inventories are included in Figure 3-38. The temperature responses are shown in Figure 3-39.

Figure 3-40 presents a comparison of peak power elevation cladding temperatures for the tests in the scoping series. Bundle heat-up is seen to be delayed until 35 seconds because of CCFL at the SEO. Also evident is the benefit of ECC injections in mitigating the bundle heat-up.

A comprehensive set of data for the Reference Test of the Scoping Series (6406 Run 1) is included in Appendix I-3. Data for a comparable test without ECC can be found in Reference 2.

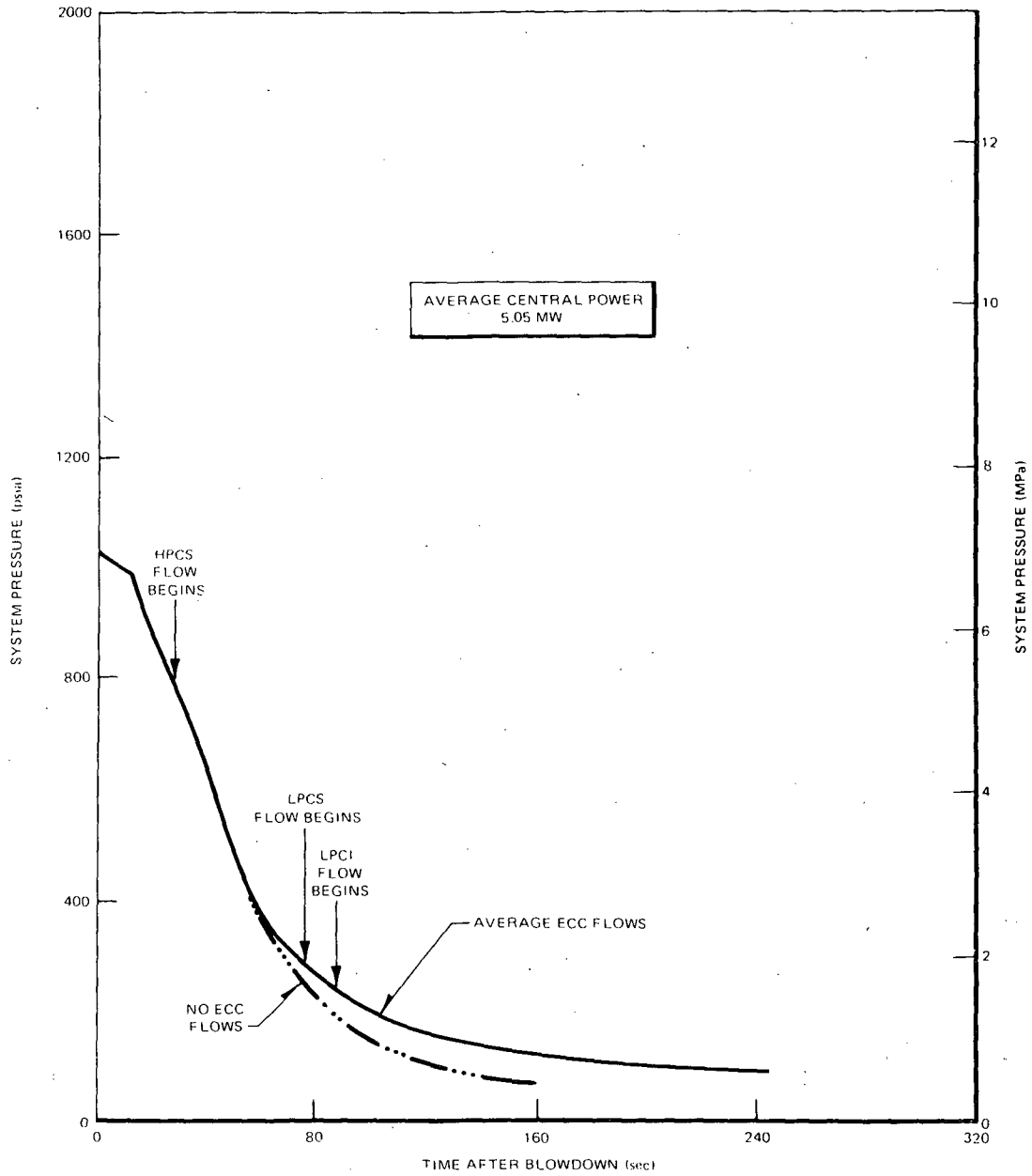
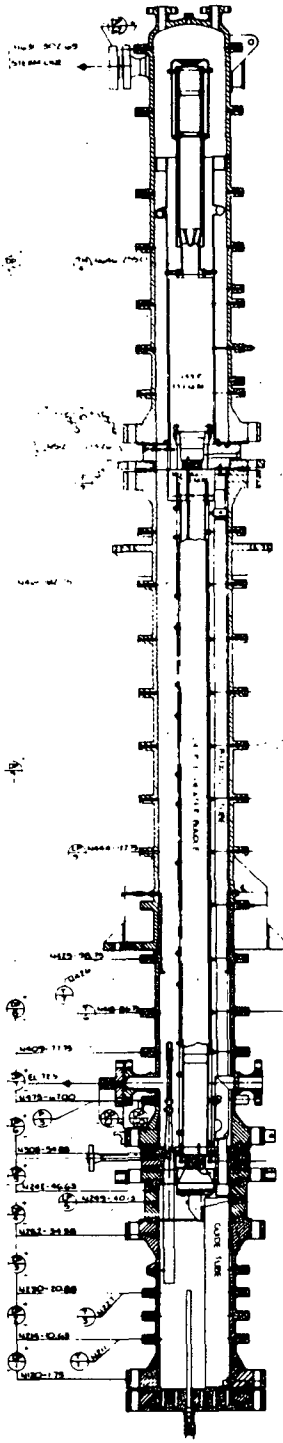


Figure 3-36. System Pressure Responses for Scoping Series Tests 6406 Run 1 and 6406 Run 3 (Avg. Power, with and without ECC)



..... AVERAGE ECC
 ——— NO ECC

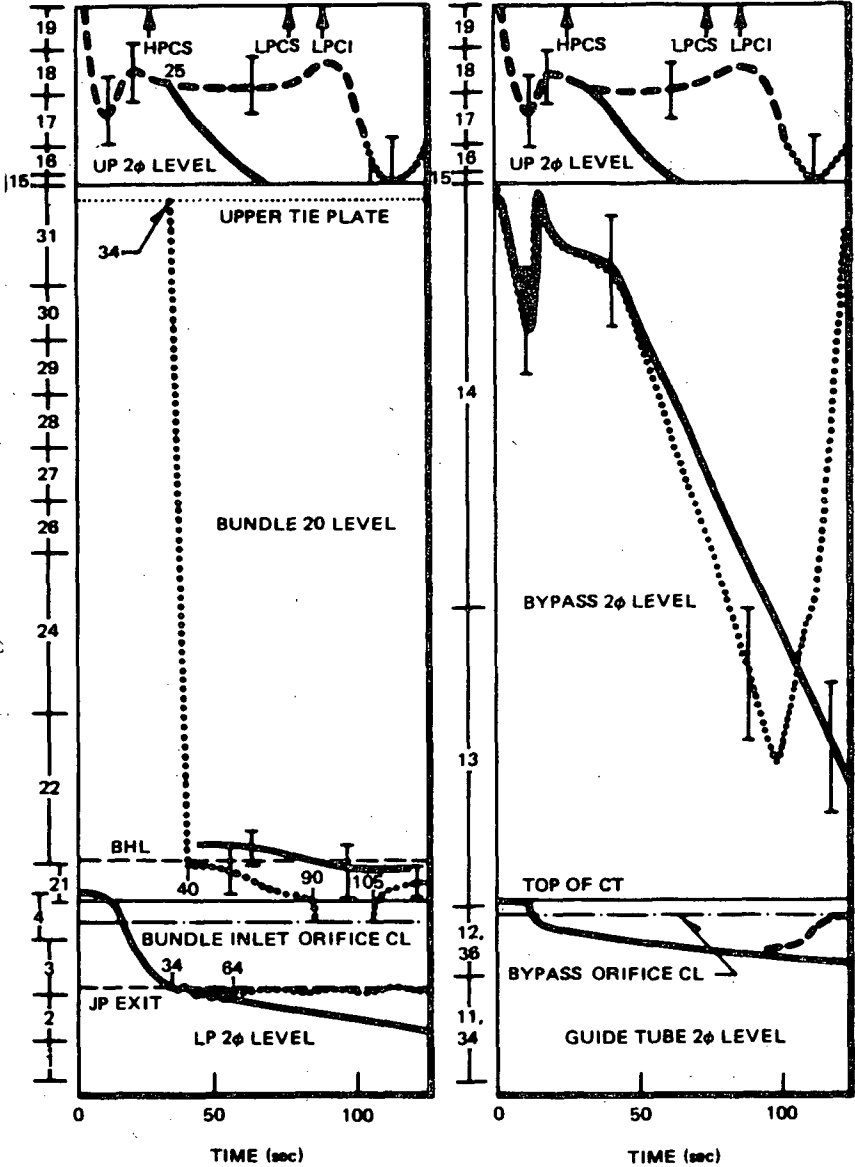


Figure 3-37. Mixture Level Responses for Average Power Tests with and without ECC of Scoping Series

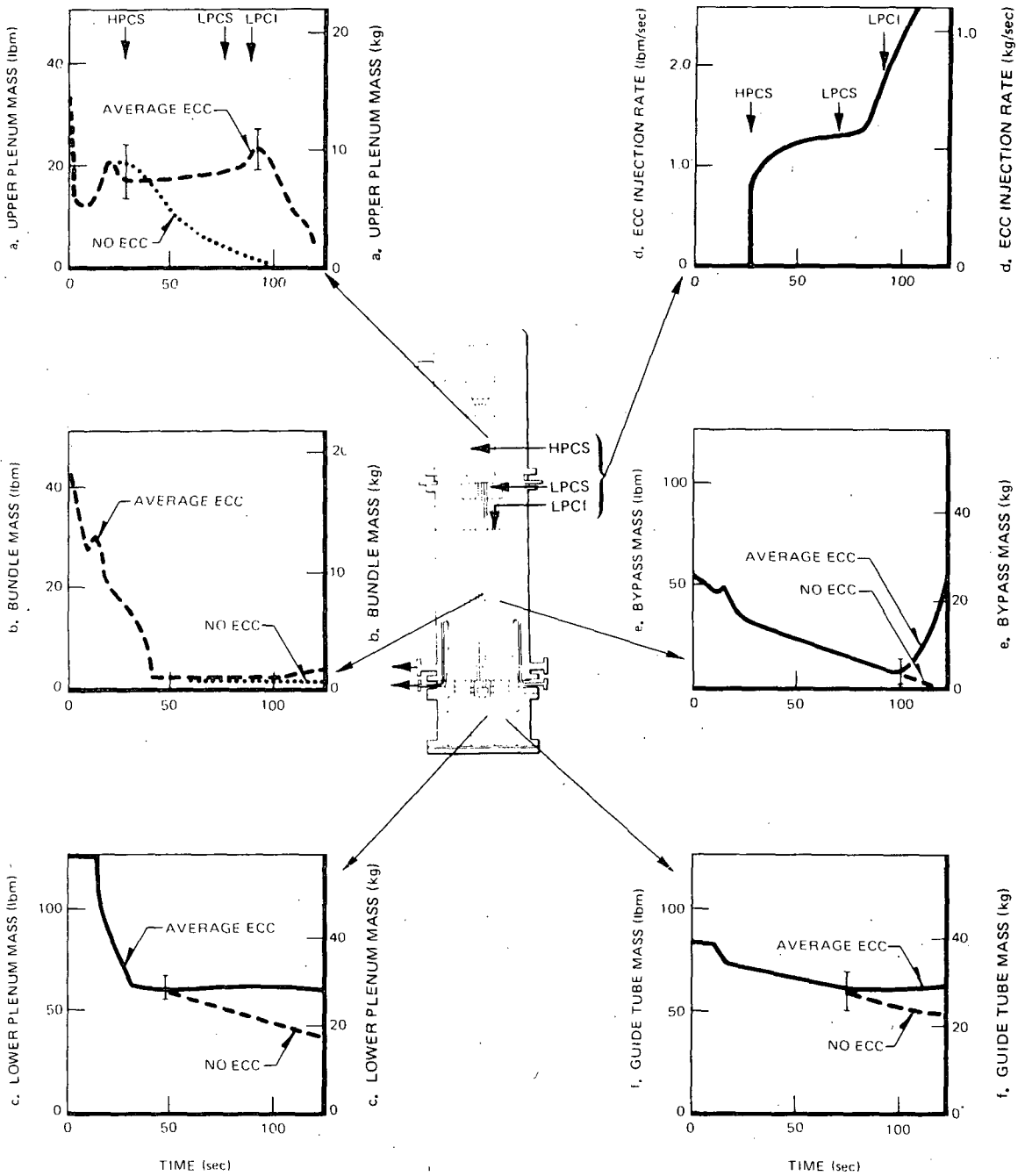


Figure 3-38. Mass Inventory Responses for Average Power Tests with and without ECC of Scoping Series

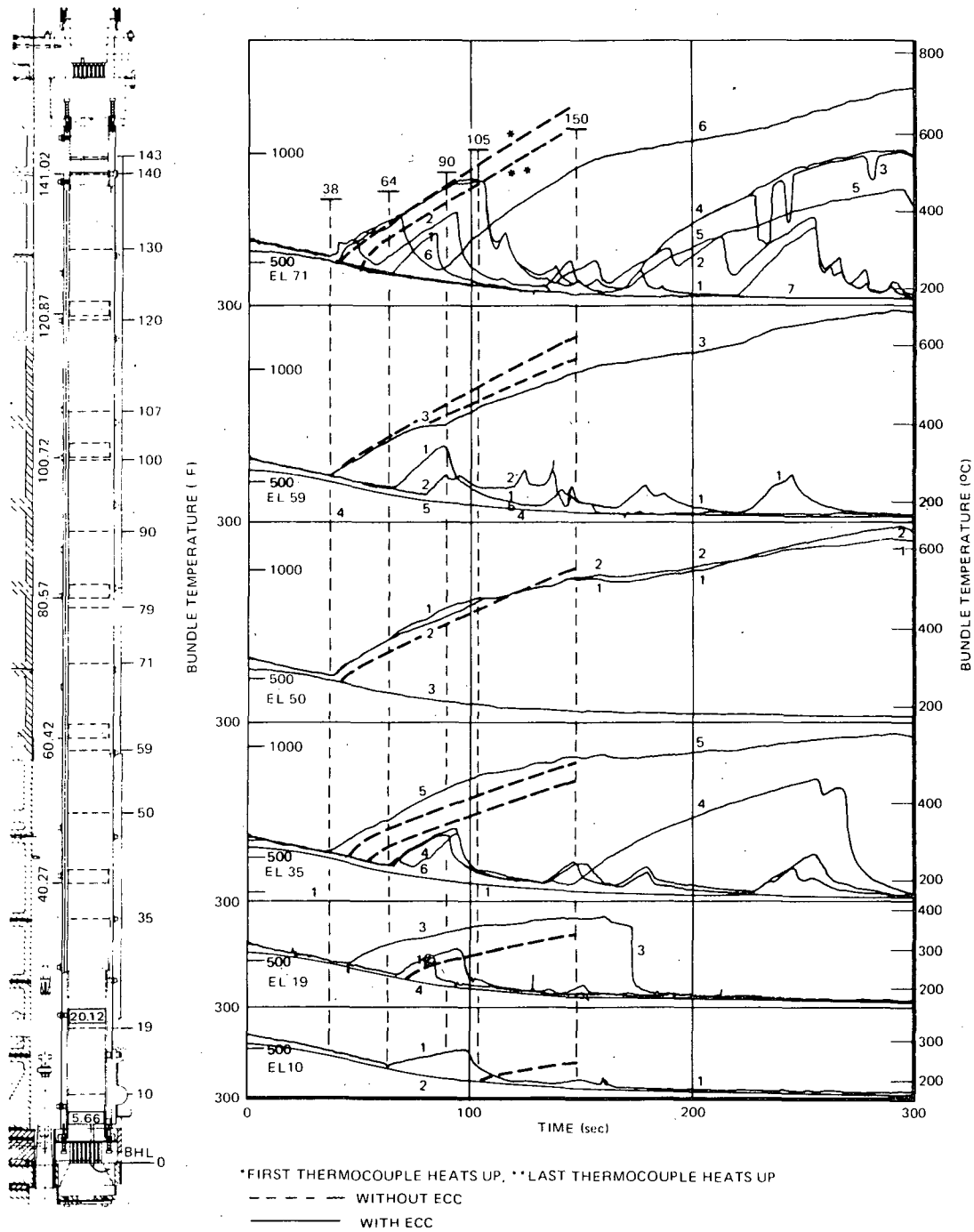


Figure 3-39a. Temperature Responses in Lower Half of Bundle for Average Power Tests with and without ECC of Scoping Series

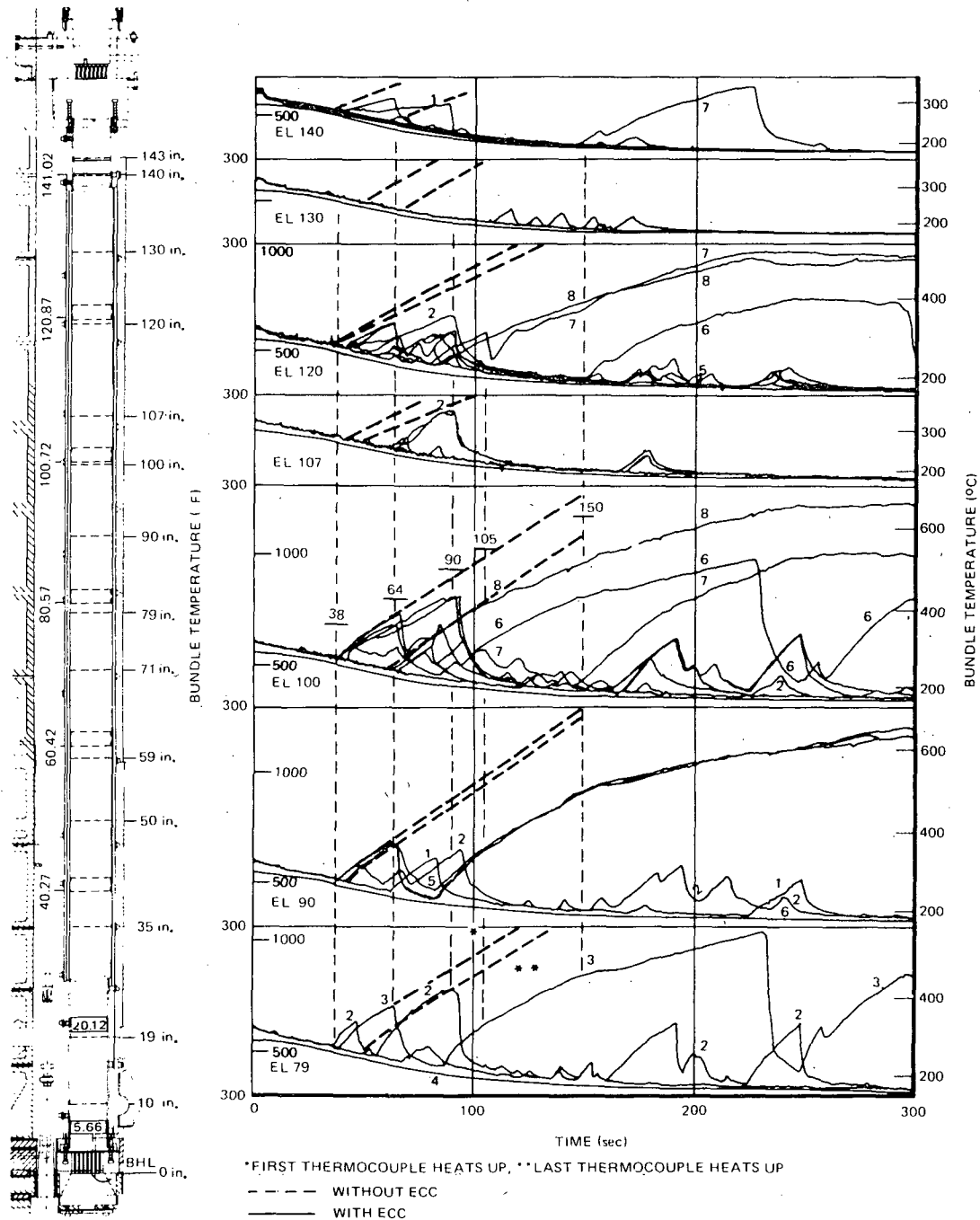


Figure 3-39b. Temperature Responses in Upper Half of Bundle for Average Power Tests with and without ECC of Scoping Series

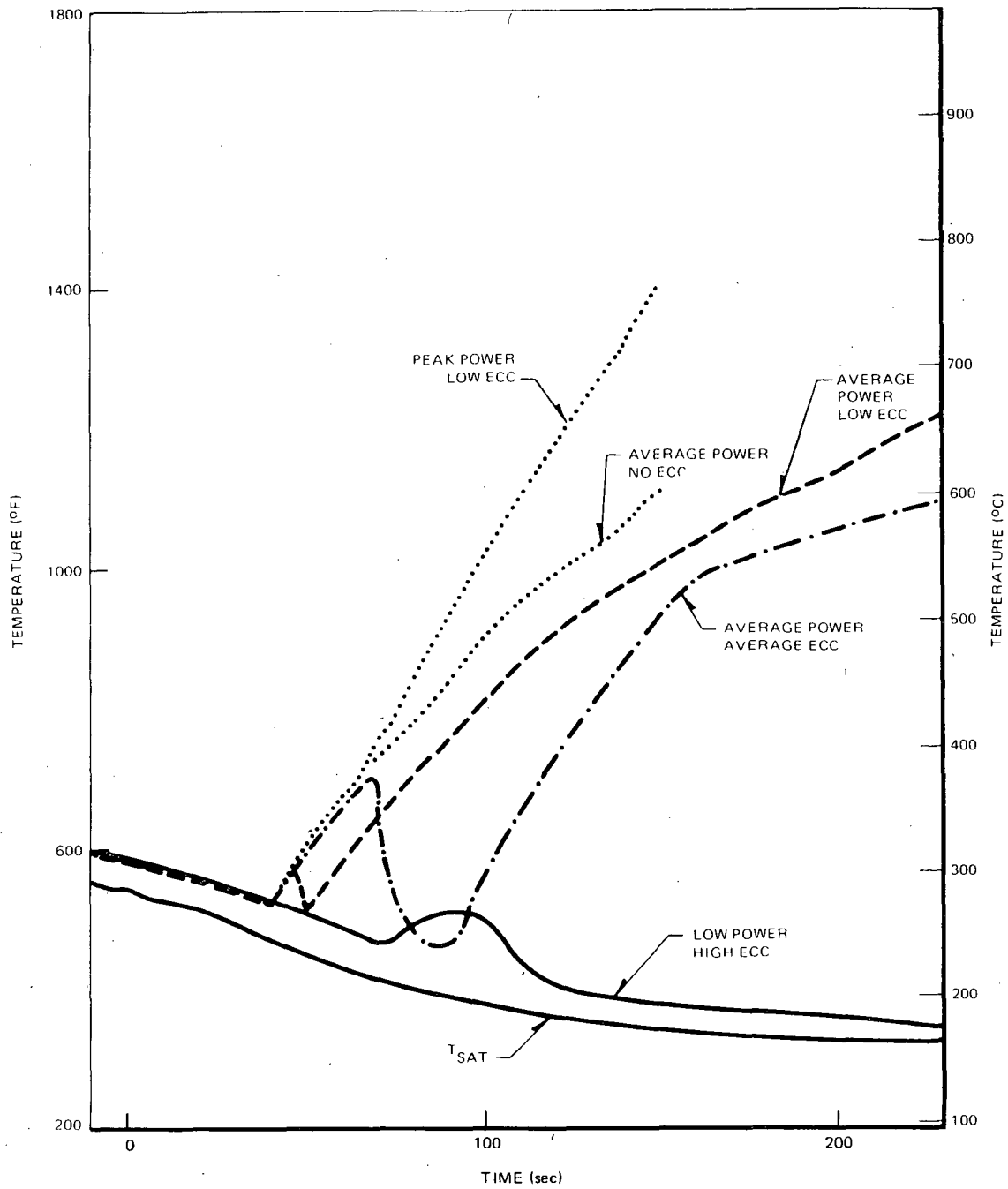


Figure 3-40. Cladding Temperatures at Peak-Power Elevation (71 in.) for Scoping Series Tests

3.3 SYSTEM SIMULATION EFFECTS

The effects of test parameters on the system response are discussed in this subsection. The purpose of this discussion is to examine the significance of these parameters and thereby attain some insights into the typicality of the TLTA data. The effects are assessed phenomenologically by comparing test results. The test parameters assessed for their effects include: bundle power, ECC injection, and system geometry.

3.3.1 Effect of Bundle Power

The bundle power variation has negligible effect on the system response of tests with average ECCS spray rates. The bundle refloods at about the same time (~ 130 seconds) for those tests simulating either the average power or the peak power bundle. The maximum cladding temperature is, as expected, slightly higher for the peak power test.

The system pressure response for the peak power test with average ECC (6424 Run 1) is compared in Figure 3-41 with that for the average power test with average ECC (reference test, 6425 Run 2). The system pressures are approximately the same after LPF and are identical after the bypass region refills (~ 90 seconds). The difference early in the transient (< 20 sec) is due to the response of the pressure control system, not to power. The pressure control system was changed after Test 6424.

A summary comparison of system responses for the two tests is presented in Figure 3-42. The inventory responses at different regions show the similarity in response for the two tests. Some differences in detail are noted for the responses at the time of lower plenum flashing (LPF). The differences are negligible, however, in the post-LPF period. The bundle reflood as reflected by the system inventory differs only in detail between the two tests.

A comparison of pressure drops across the bundle provides additional evidence in illustrating the negligible effect of bundle power variation. Figure 3-43 shows that the bundle pressure drops are nearly identical except for a brief period of from ~ 90 to 130 seconds. The difference during this period is the result of earlier reflood of the lower part of the bundle having the peak power. This earlier reflood for the peak power test can also be seen from Figure 3-44. The earlier reflood of the bundle for the peak power test is probably caused by the slightly higher rate of HPCS injection (Figure 3-45). However, as will be discussed in Subsection 3.3.4, some differences in detailed response are seen in repeating the same test.

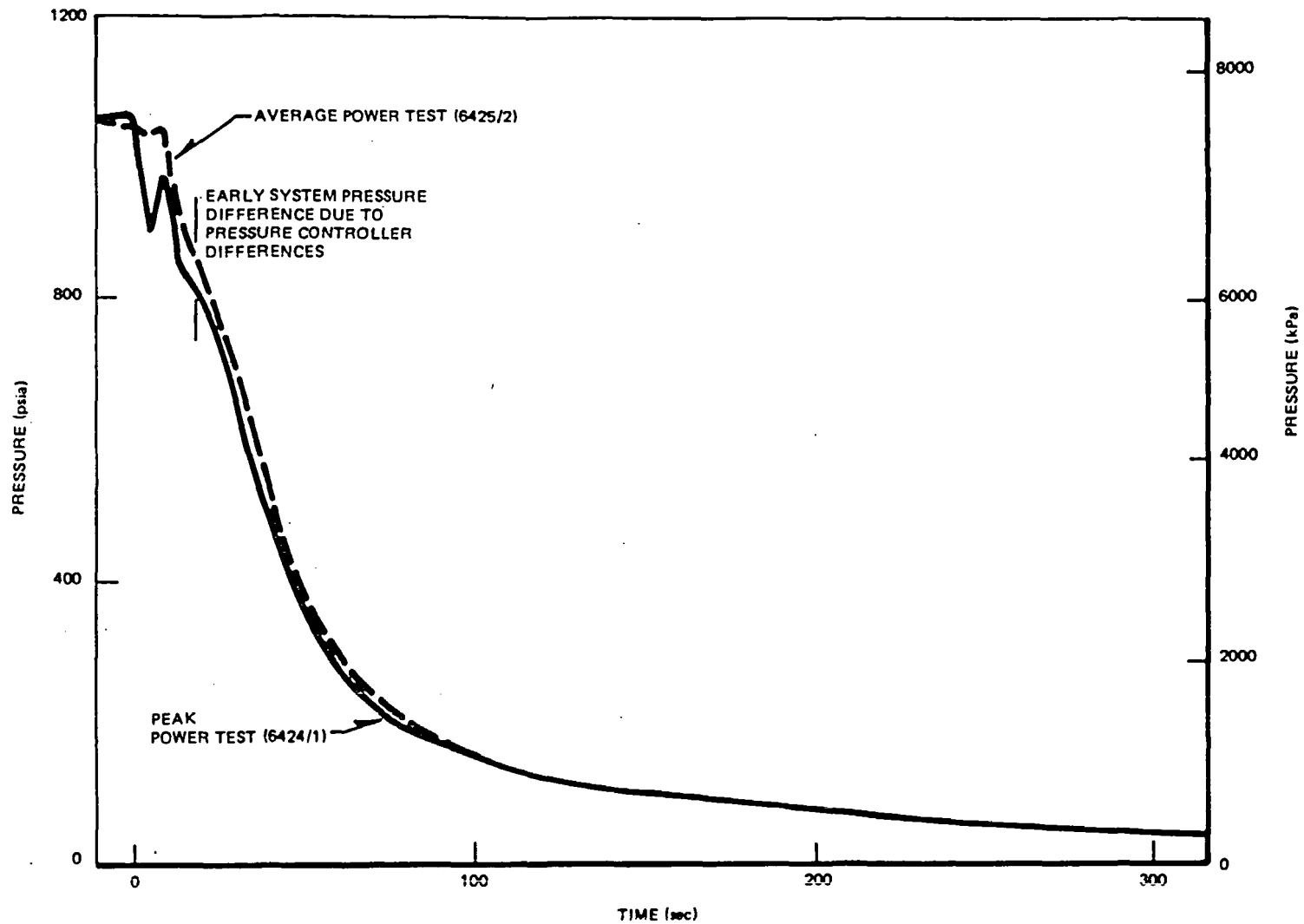


Figure 3-41. Comparison of System Pressure Responses for Average ECC Tests with Average Power (6425/2) and Peak Power (6424/1)

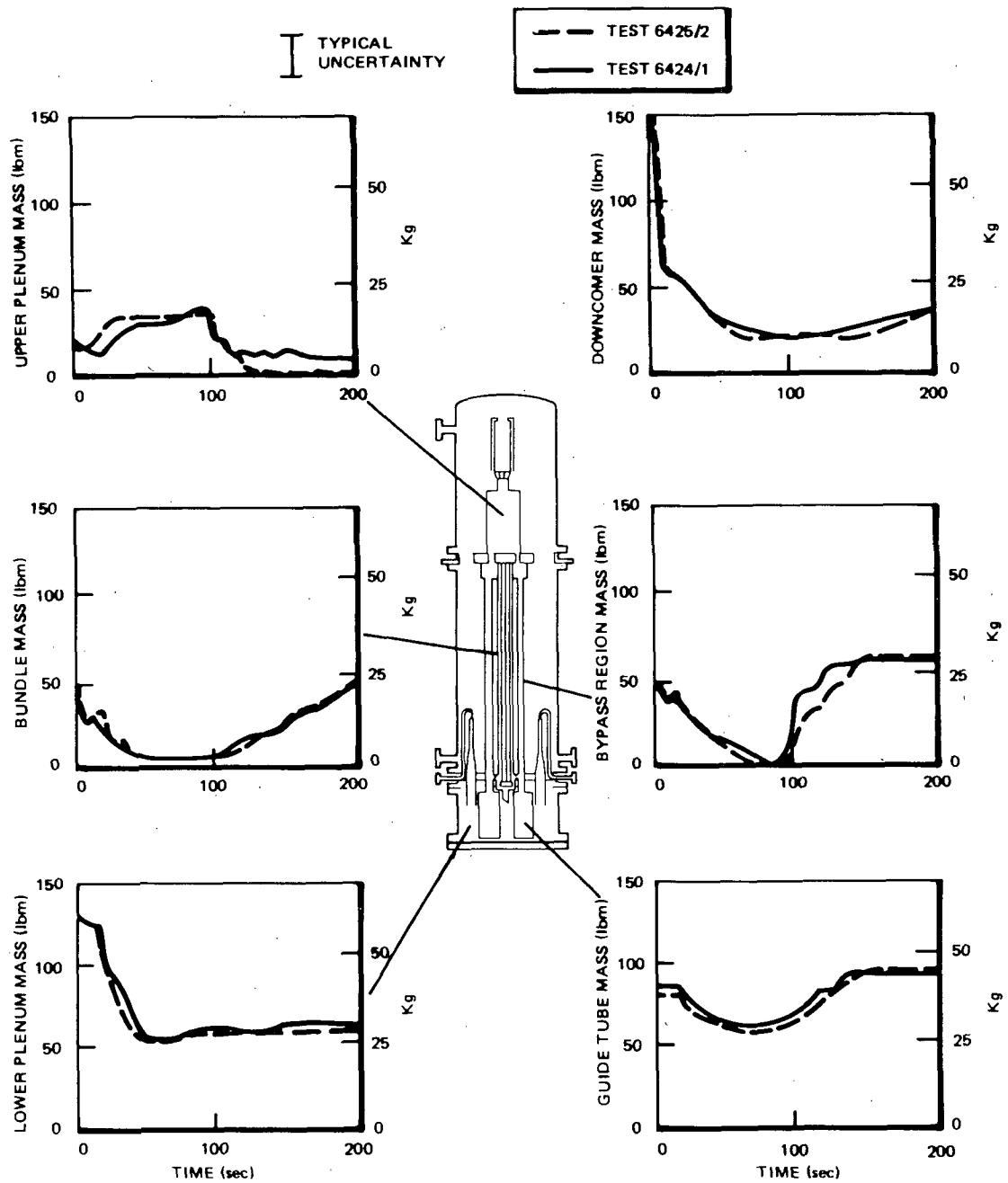


Figure 3-42. Comparison of Regional Inventory Responses for Average ECC Tests with Average Power (6425/2) and Peak Power (6424/1)

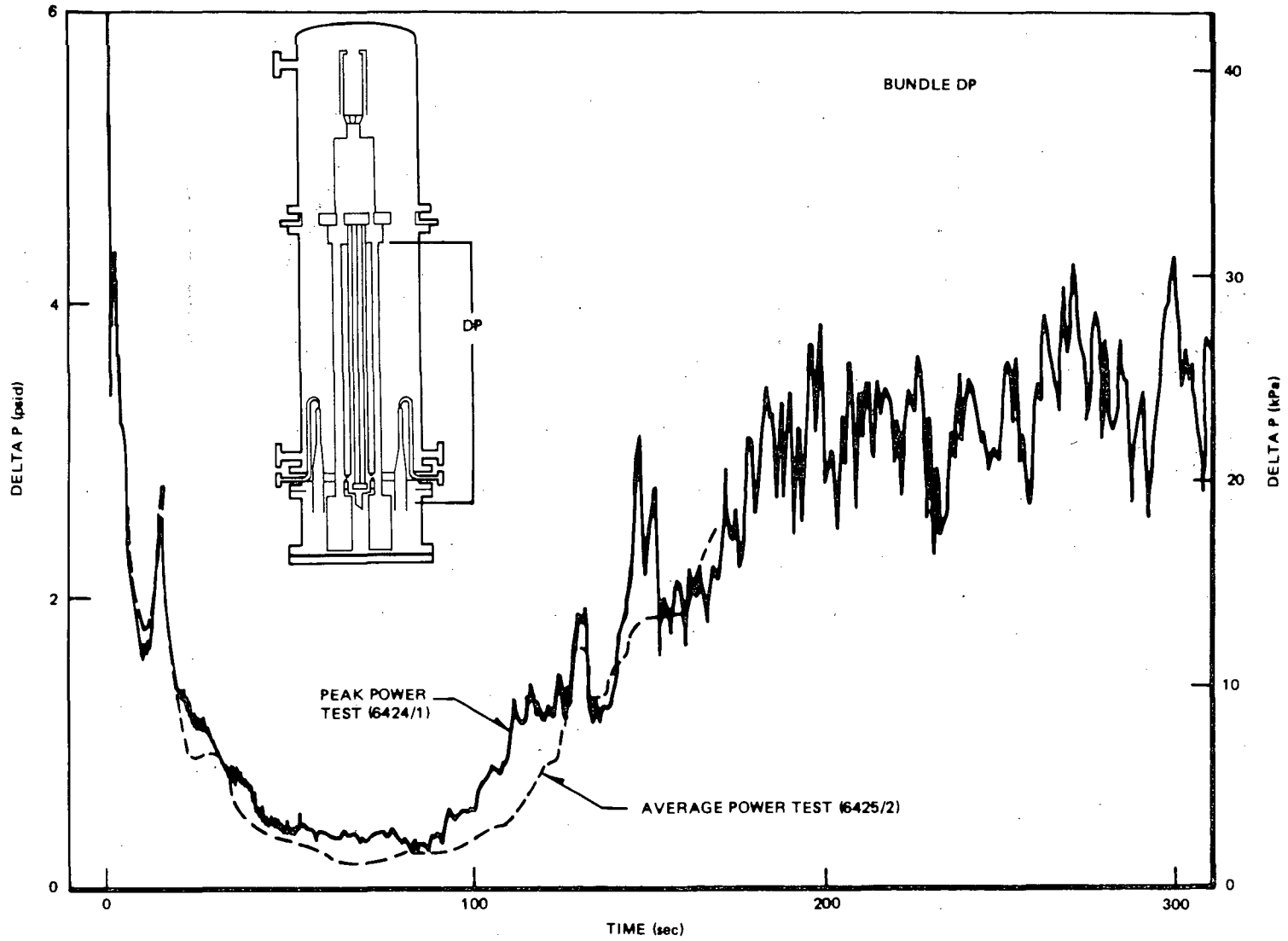


Figure 3-43. Comparison of Pressure Difference across the Bundle for Average ECC Tests with Average Power (6425/2) and Peak Power (6424/1)

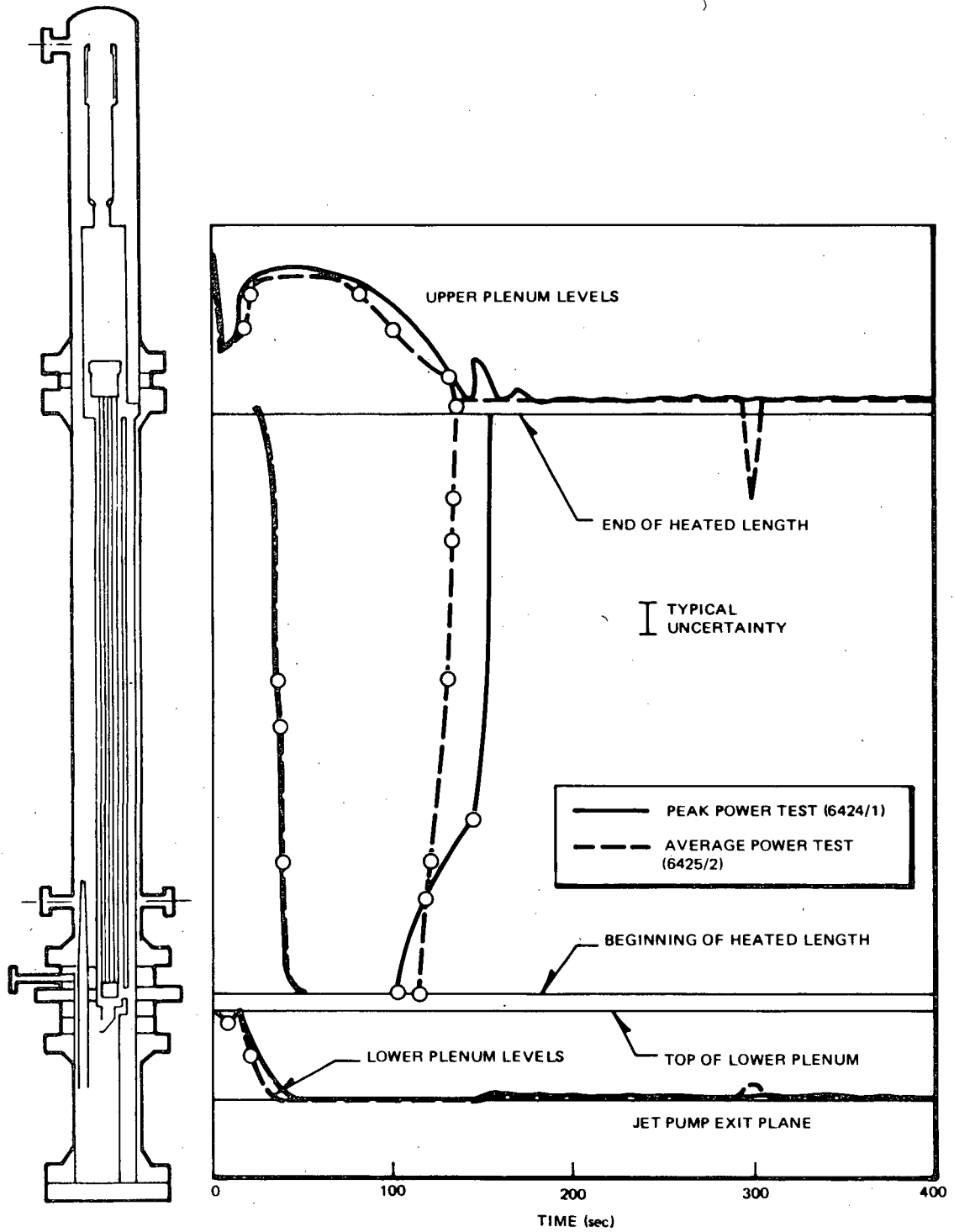


Figure 3-44. Comparison of Mixture Level Response along the Bundle Path for Average ECC Test with Average Power (6425/2) and Peak Power (6424/1)

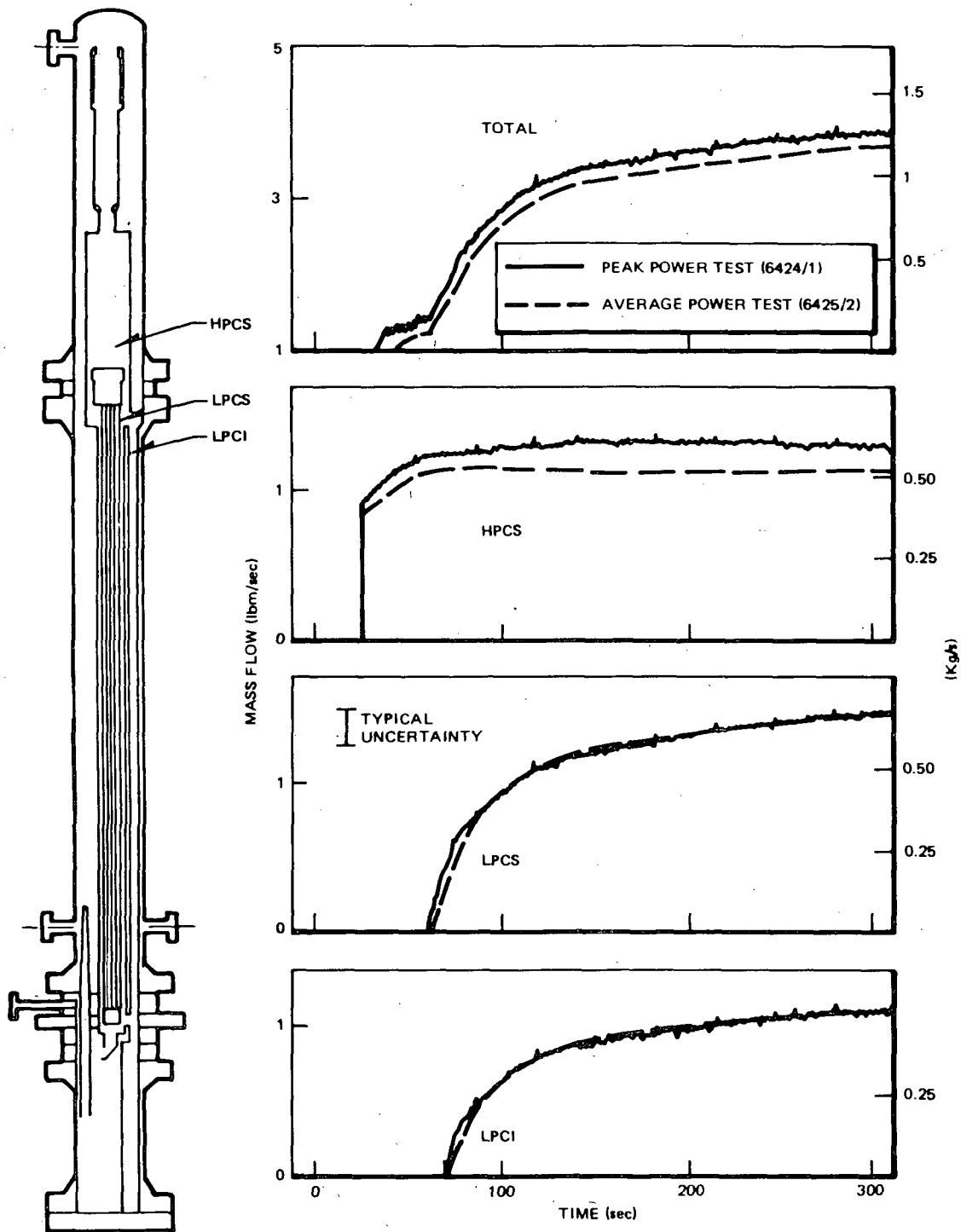


Figure 3-45. Comparison of ECC Injection Rates for Average ECC Tests with Average Power (6425/2) and Peak Power (6424/1)

The peak cladding temperatures are compared in Figure 3-46. These temperatures approach the saturation temperature at ~130 seconds as the bundle refloods in both tests. The temperature responses before that time are different in detail as expected. The maximum temperature resulting from bulk heat-up after uncover is ~810°F (432°C) for the peak power test and ~700°F (371°C) for the average power test. These temperatures occur just prior to the beginning of low-pressure core injection (~75 seconds). The ensuing temperature response shows substantial reduction of cladding temperature in the average power bundle caused by an increase in liquid downflow to the bundle. This response is expected, as the volumetric vapor generation is less for the average power bundle and therefore allows more liquid to drain from the upper plenum.

3.3.2 ECC Injection Effects

To determine effects of ECC injection on system response is one of the principal objectives for the BD/ECC 1A Test Program. The effects of ECC injection on the overall system response are determined by comparing results from the average power tests with and without ECC. The effectiveness of ECC injection on mitigating the consequence of a postulated LOCA is assessed by comparing results from tests with peak bundle power. Results so determined are summarized below.

- ECC injection effects are highly favorable. The cladding temperature is kept below 700°F (371°C) for the central average bundle receiving an average amount of core spray. The bundle is quenched after ~150 seconds, following complete reflood.
- ECC injection slightly reduces the rate of system depressurization after 65 seconds because of collection of ECC liquid in the vicinity of the break. This effect in system pressure is relatively insignificant, however, in light of the low maximum cladding temperature (700°F, or 371°C) and the reflooding of the bundle.
- ECC injection is effective in mitigating the maximum cladding temperature in a LOCA. The cladding heat-up is kept below 1000°F (538°C) even for the upper bound test in which only a minimal amount of core spray fluid at high temperature is assumed available for the peak power bundle.

3.3.2.1 Effects of ECC Injection (Comparison of Average Power Tests). The effects of ECC injection on system responses are evaluated by comparing responses from average power, average ECC test (6425/2), with those from average power, no ECC test (6426/1).

The beneficial effects of ECC injection can be seen in Figure 3-47. The maximum cladding temperature for the test with average core spray (Test 6425 Run 2) is

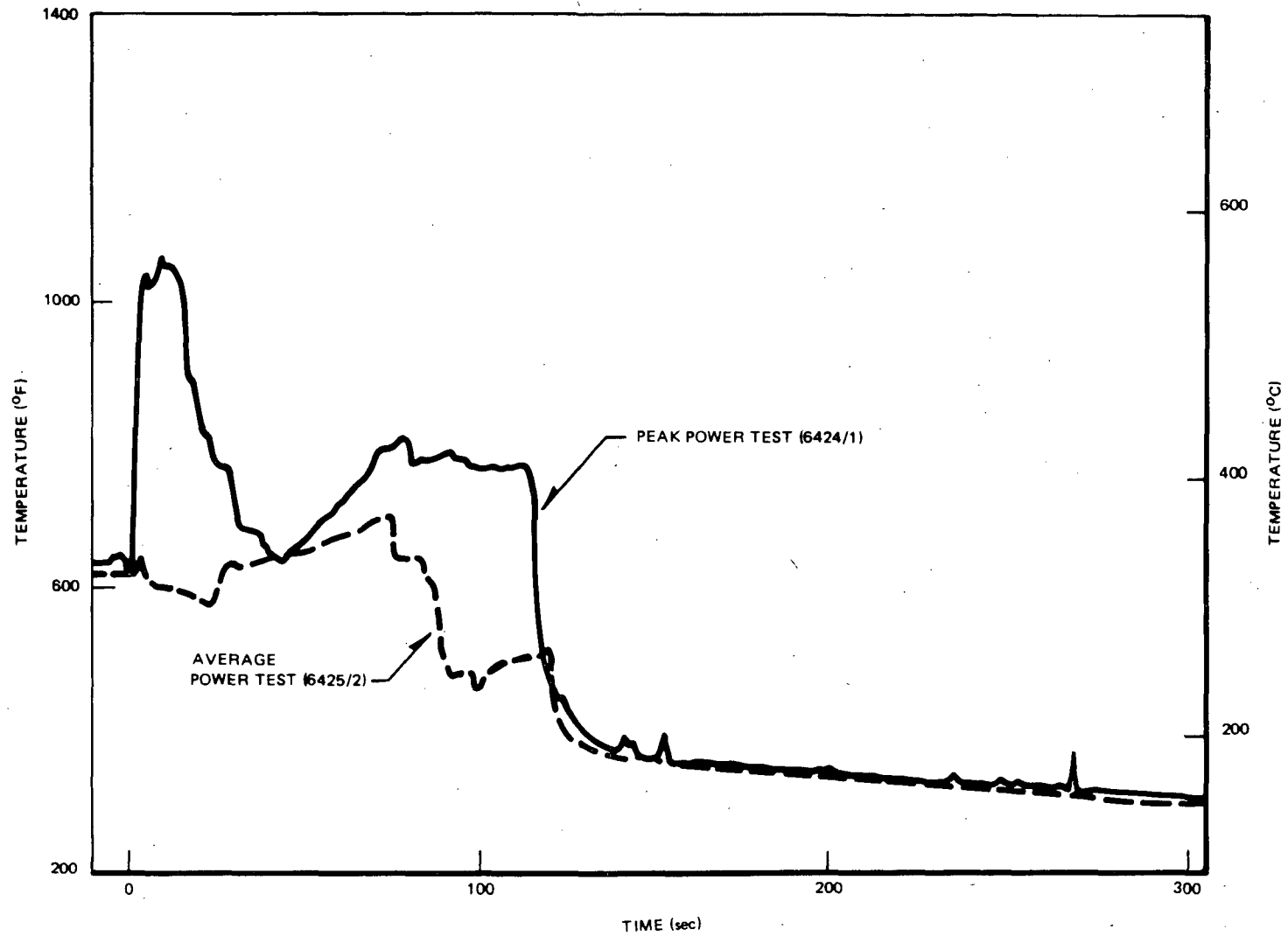


Figure 3-46. Comparison of Peak Cladding Temperature Responses for Average ECC Tests with Average Power (6425/2) and with Peak Power (6424/1)

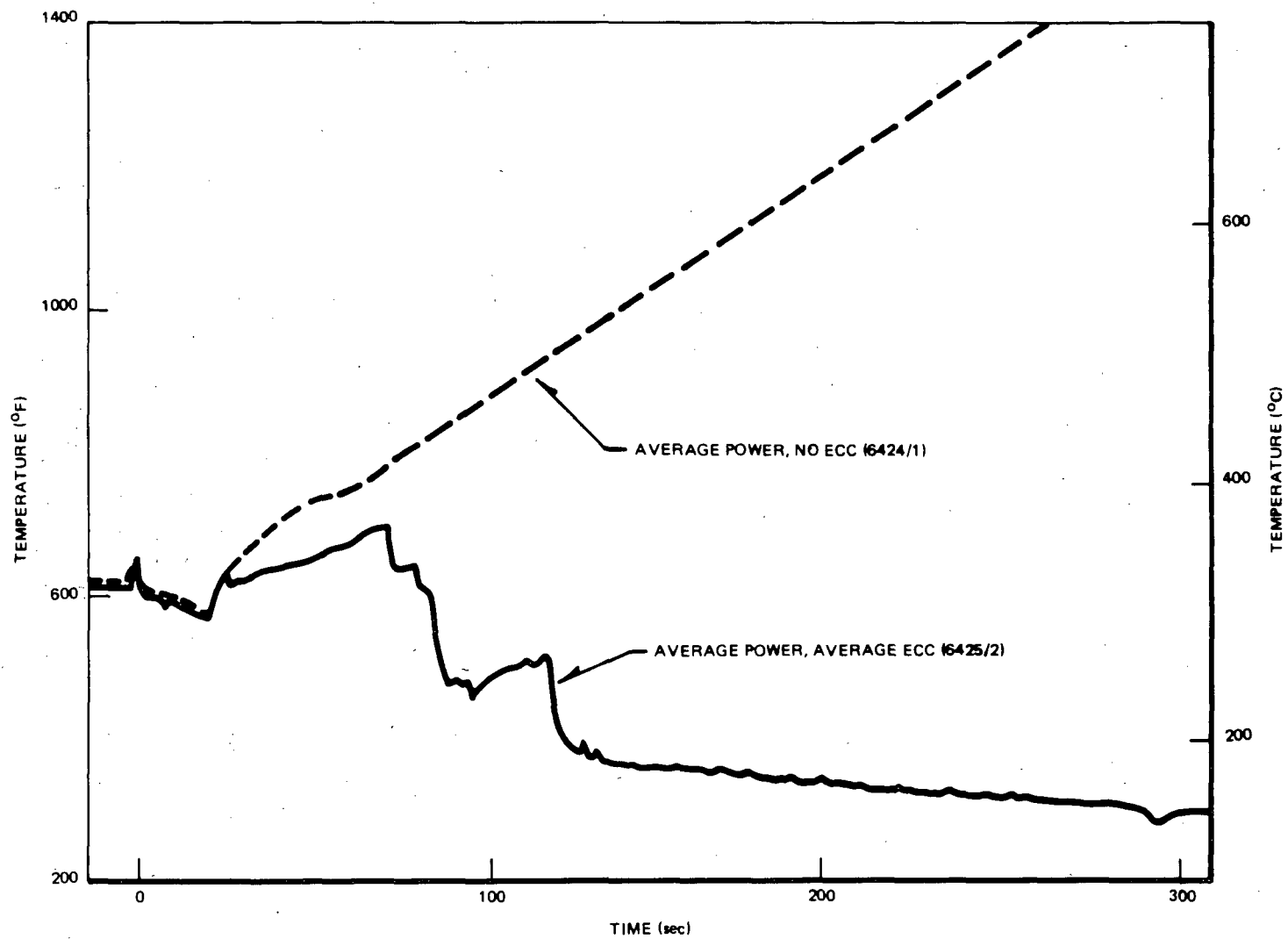


Figure 3-47. Comparison of Peak Cladding Temperatures for Tests with and without ECC

below 700°F (371°C). The peak cladding temperature for this test approaches the saturation temperature at ~130 seconds. On the other hand, the peak cladding temperature for the test without ECC continues to increase, as expected, until test termination.

The system response for the test with ECC has been described in Subsection 3.2.1 and that for the test without ECC in Subsection 3.2.2.2. The most significant effects of injection are in maintaining low cladding temperature and in contributing to reflooding the bundle. The comparison of mass inventory responses in Figure 3-48 illustrates these effects. Refilling of the bypass and other regions occurred in the test with ECC. As expected, the system inventory for the test without ECC depletes continuously.

The effect of ECC injection on the system pressure response is shown in Figure 3-49. The system pressure for the test with ECC injection decreases more slowly from ~65 seconds. This difference in pressure response was first observed in the scoping series tests (Figure 3-36). The inference from available measurements of that series was that the difference resulted from a reduced volumetric break flow through the drive line and suction line breaks, as the fluid upstream of the break had a higher liquid fraction (12).

The same difference in system pressure response for tests with and without ECC is observed for the later test series in TLTA 5A, as shown in Figure 3-49. The previous inference is reaffirmed by results of improved break flow measurements as discussed in Subsection 3.4.3 and Appendix D.

The two curves in Figure 3-49 remain nearly identical up to ~65 seconds, before the ECC effect begins to appear. HPCS is initiated at about 27 seconds into the transient. Its immediate effect is evident in increasing the upper plenum mass and in contributing to the lower cladding temperatures as shown in Figure 3-47. The difference between the upper plenum masses in Tests 6425 Run 2 and 6426 Run 1 are shown in Figure 3-48. The figure indicates that nearly the entire HPCS flow is initially maintained in the upper plenum by CCFL at the upper tieplate and the bypass outlet. Hence, during this period there is no significant global difference in the system responses of tests with and without ECC. (Additional details are provided in the expanded plots of Figures 3-50 through 3-55.)

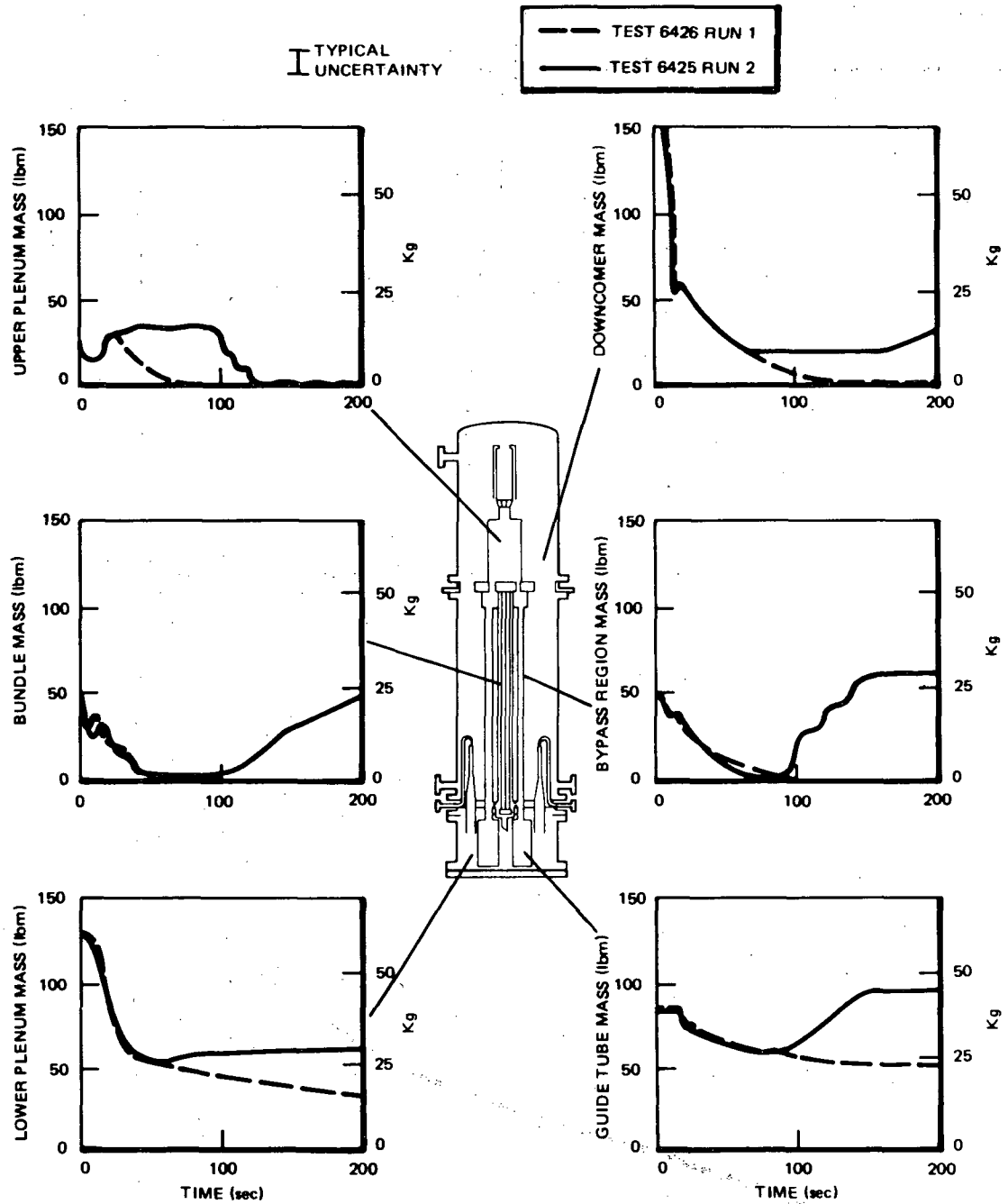


Figure 3-48. Comparison of Regional Masses for Tests 6425/2 (Average Power, Average ECC) and 6426/1 (Average Power, No ECC)

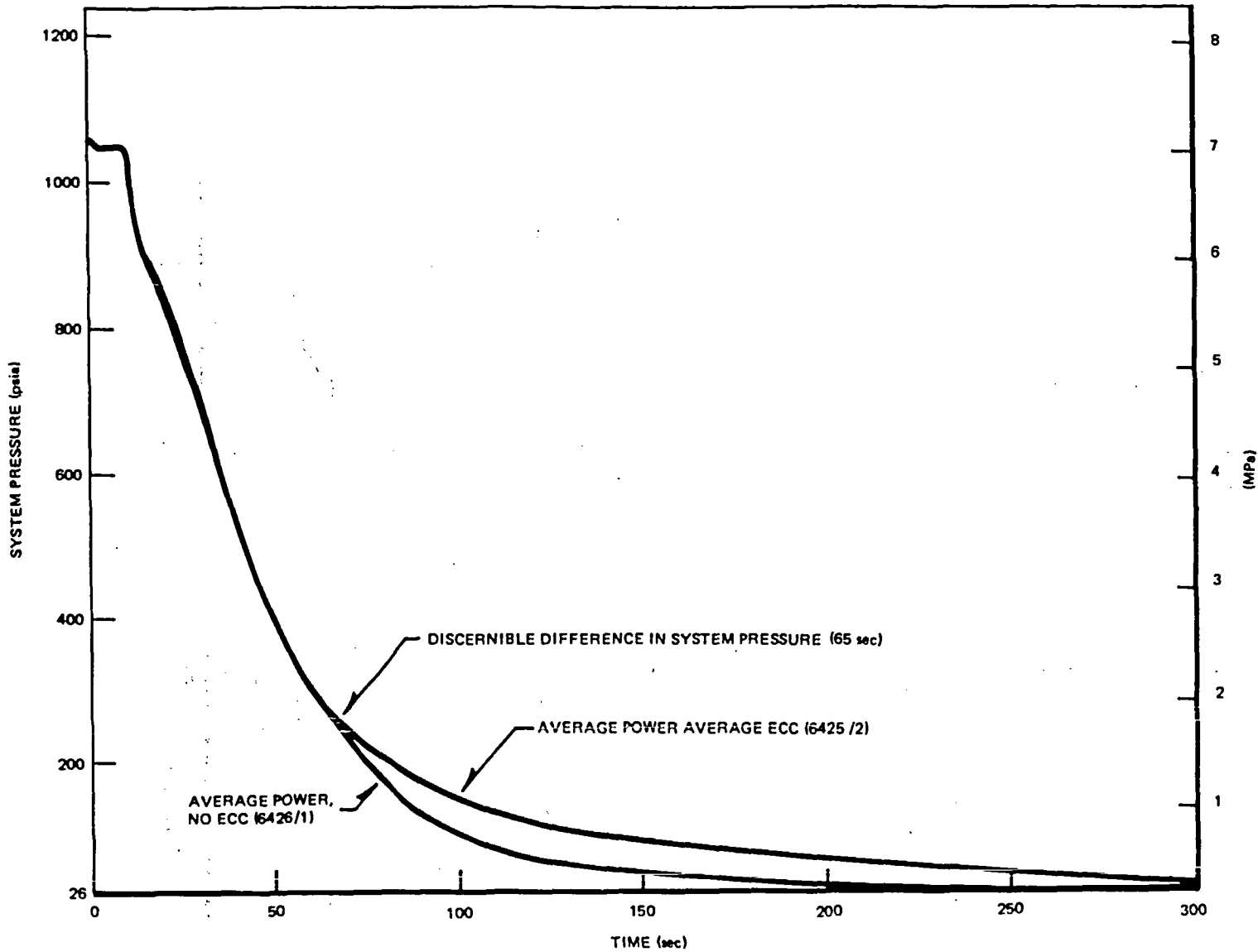


Figure 3-49. Comparison of System Pressures for Average Power Tests with and without ECC

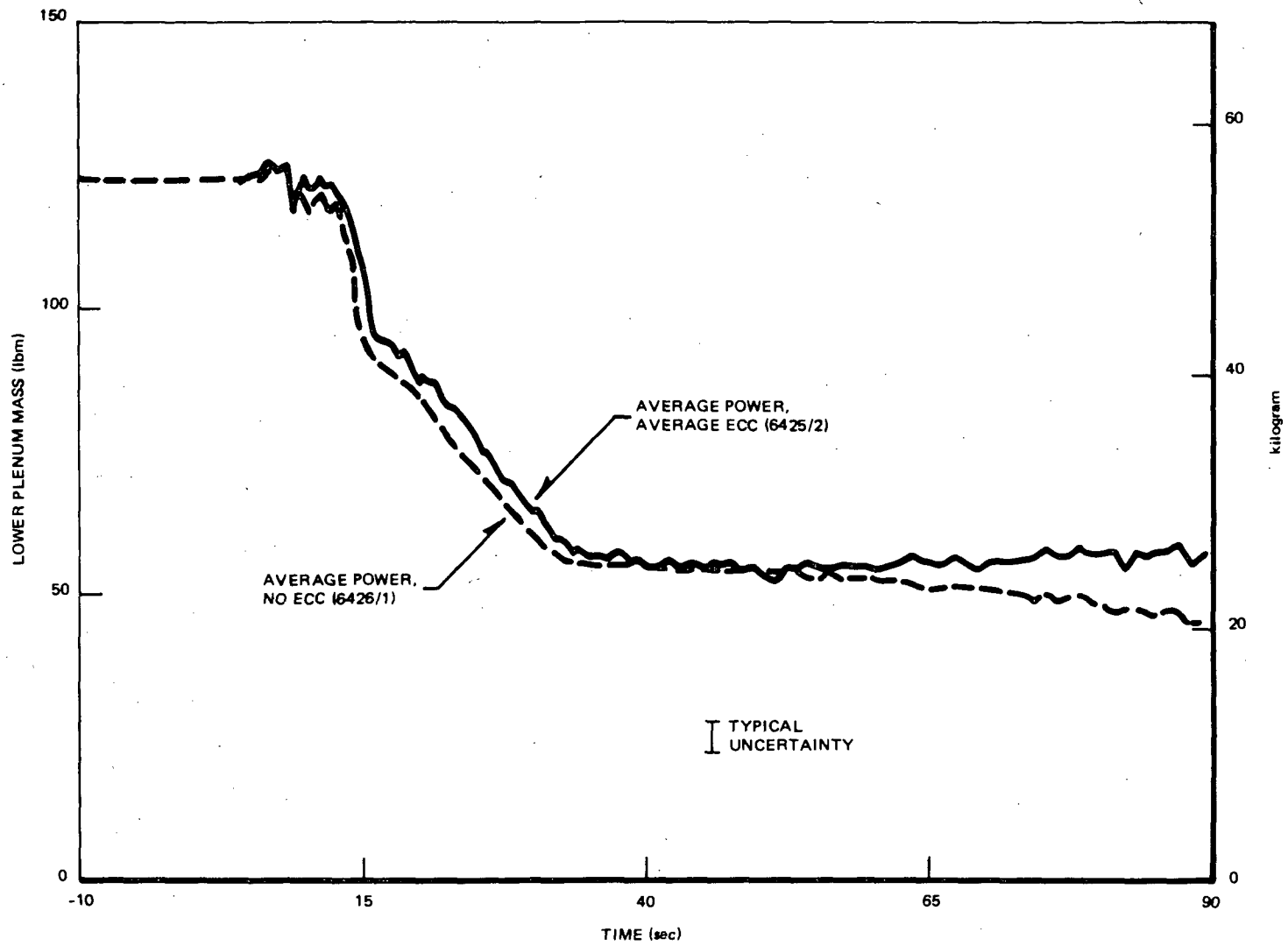


Figure 3-50. Comparison of Lower Plenum Mass Inventories for Average Power Tests with and without ECC

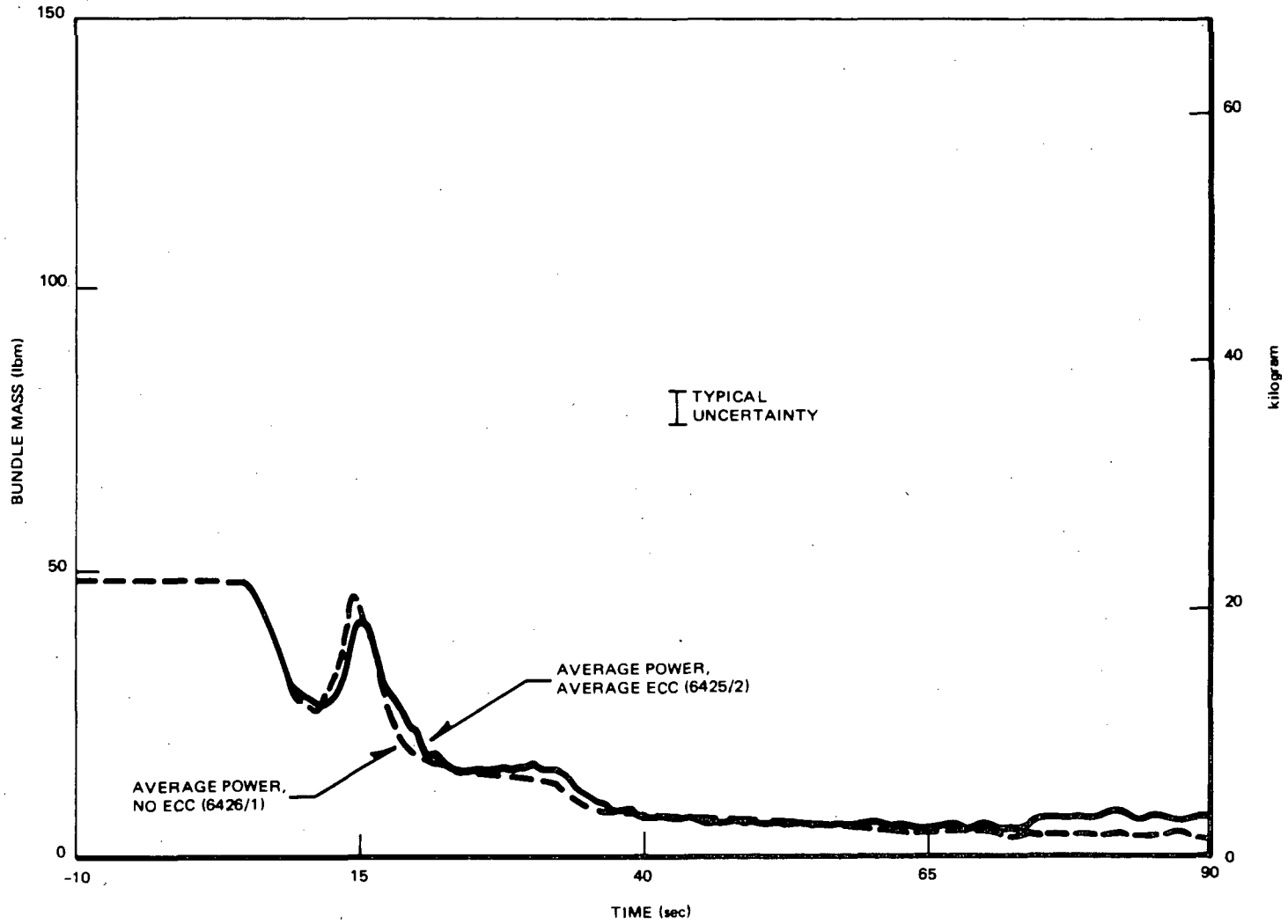


Figure 3-51. Comparison of Bundle Mass Inventories for Average Power Tests with and without ECC

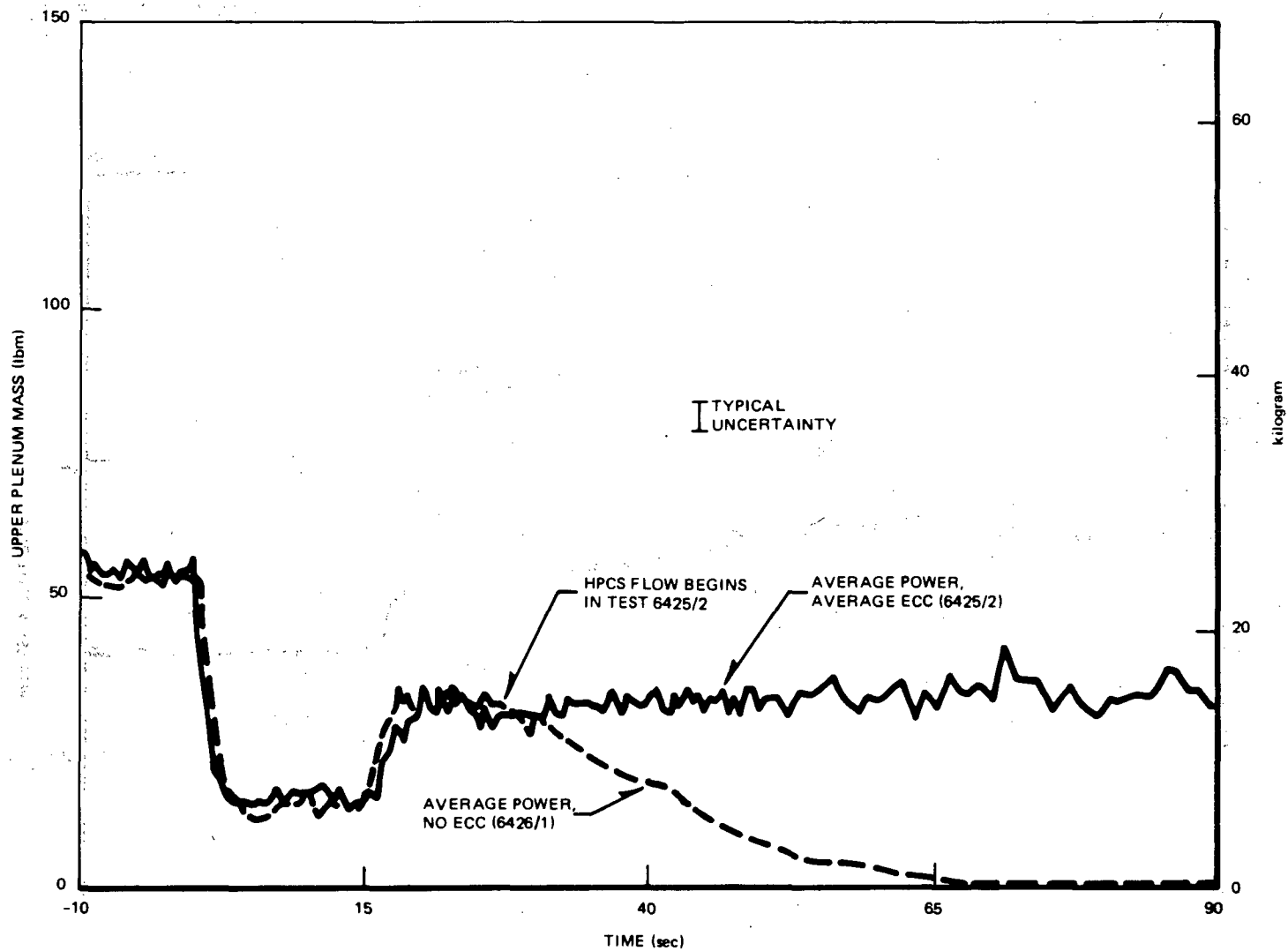


Figure 3-52. Comparison of Upper Plenum Mass Inventories for Average Power Tests with and without ECC

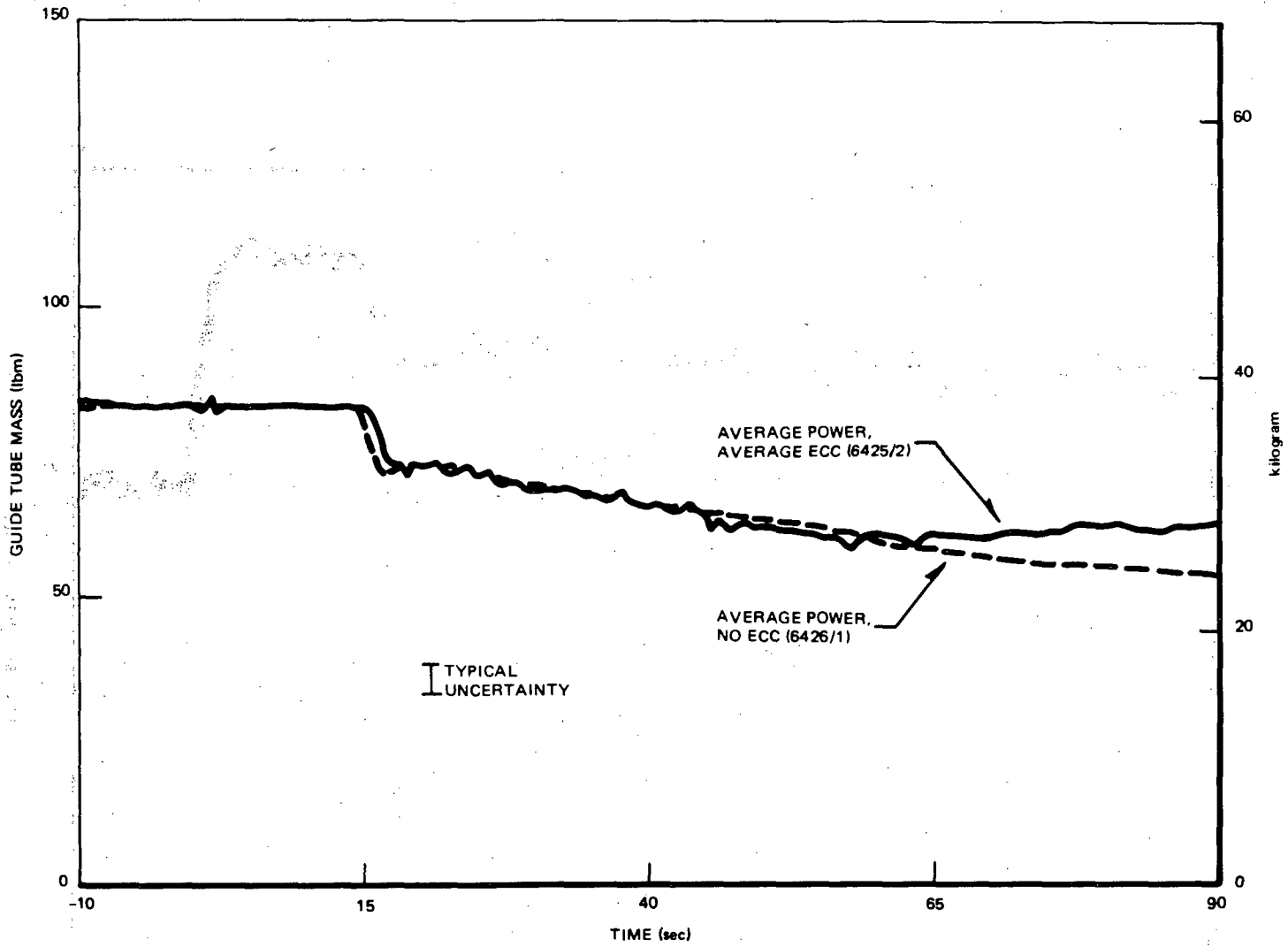


Figure 3-53. Comparison of Guide Tube Mass Inventories for Average Power Tests with and without ECC

3-84

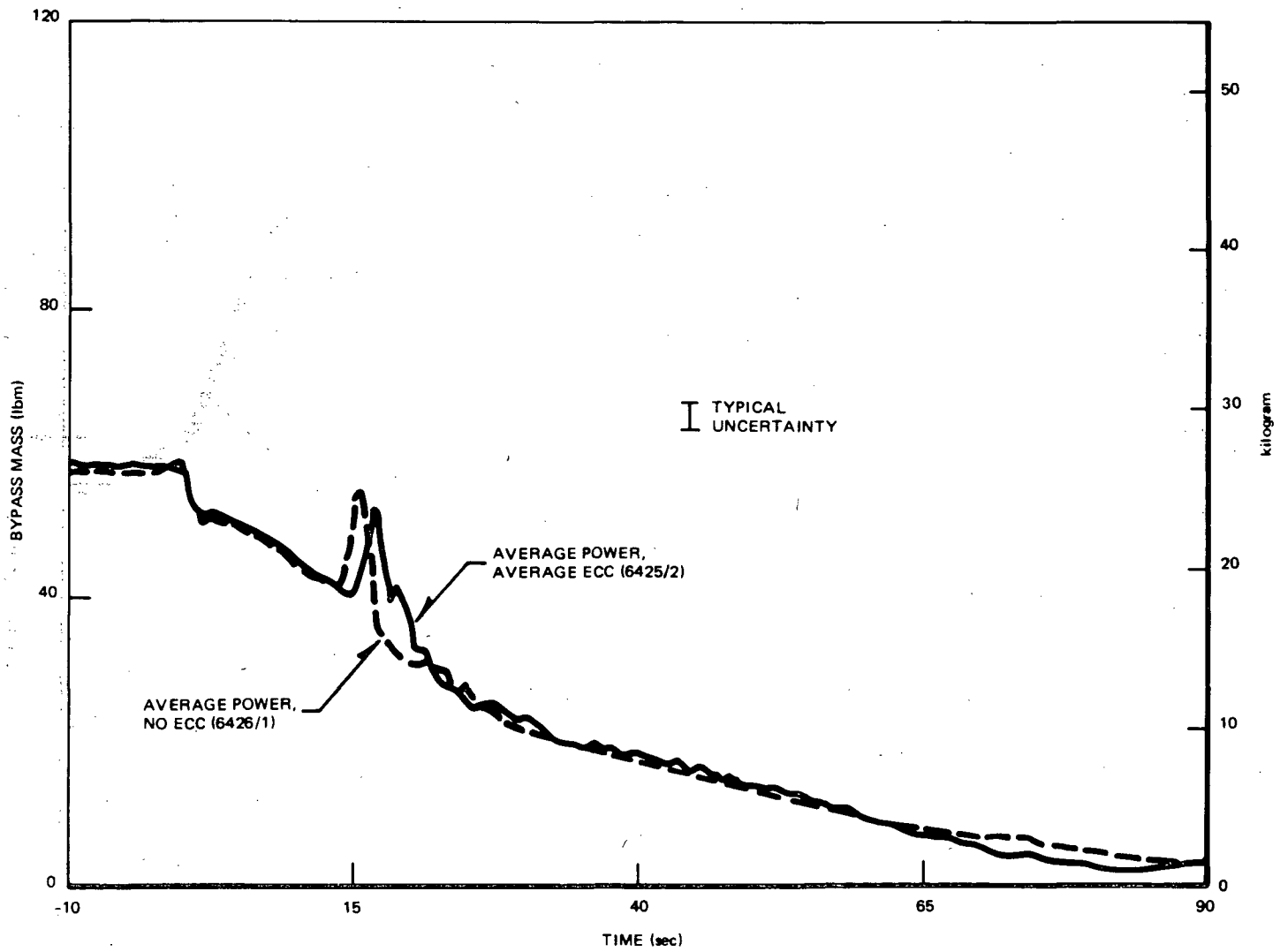


Figure 3-54. Comparison of Bypass Region Mass Inventories for Average Power Tests with and without ECC

3-85

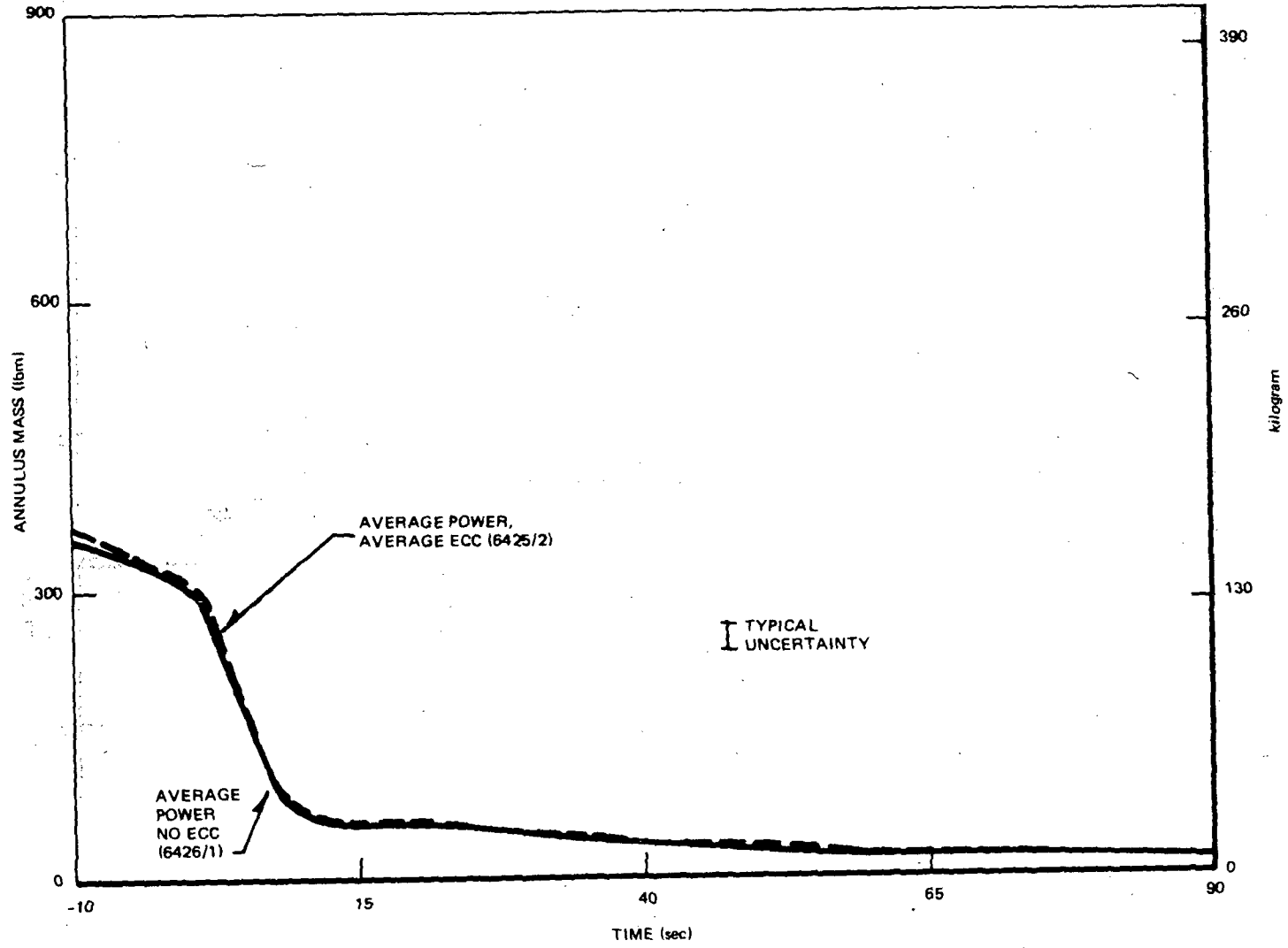


Figure 3-55. Comparison of Annulus Region Mass Inventories for Average Power Tests with and without ECC

The ECC effect on the system pressure becomes apparent as soon as partial drainage of the ECC fluid from the upper plenum begins to influence the lower plenum mass. This drainage also affects the density of the fluid discharging through the jet pump. This in turn increases the discharge fluid density (shown in Figure 3-56) and results in higher mass but lower volumetric blowdown flow. The higher volumetric flows for the case with no ECC are clearly evident from ~60 seconds (see turbine meter measurements in Figures 3-57 and 3-58).*

The reduced volumetric flow discharge from the vessel resulting from the higher pressure drop when some of the ECC fluid is carried out the break decreases the system depressurization rate beyond ~65 seconds. The partial vapor condensation within the system (Figure 3-12) by the subcooled ECC liquid does not totally offset the effect of reduced volumetric discharge. As a result, system pressure in the test with ECC remains slightly higher for the balance of the transient.

3.3.2.2 Effectiveness of ECC Injection (Comparison of Peak Power Tests). The effectiveness of the ECC injection can be appraised by comparing the responses from the peak power tests: one with average ECC (Test 6424 Run 1), the other with low ECC at high temperature (Test 6423 Run 3). The system pressures are compared in Figure 3-59. It is seen that system depressurization is slower for the average ECC test at 80 seconds because of higher density fluid at the break. However, the condensation effect of the subcooled ECC in Test 6424 Run 1 renders the system pressure lower later in the transient. The difference in ECC injection rates are shown in Figure 3-60, and the bundle level responses are shown in Figure 3-61. The upper plenum level, as expected, is higher for the test with average ECC. The bundle level responses indicate that the test with low ECC could reflood only partially, and the lower plenum level responses suggest that the ECC fluid fills the lower plenum in the low ECC test instead of reflooding the bundle from ~150 seconds onward. This is the result of the system depressurization being terminated by the higher volumetric flowrate of the ECC fluid compared to that of the break flow, while the depressurization caused by condensation is insufficient (because of the combined effect of low rate and high temperature) to compensate for the net volumetric influx. Consequently, lower plenum flashing diminishes, and the CCFL condition at the bundle inlet can no longer hold the inventory within the bundle.

*The discrepancies in these figures between the two tests early in the transient were due to an equipment problem which, as explained in Appendix D, has only negligible effect after ~25 seconds.

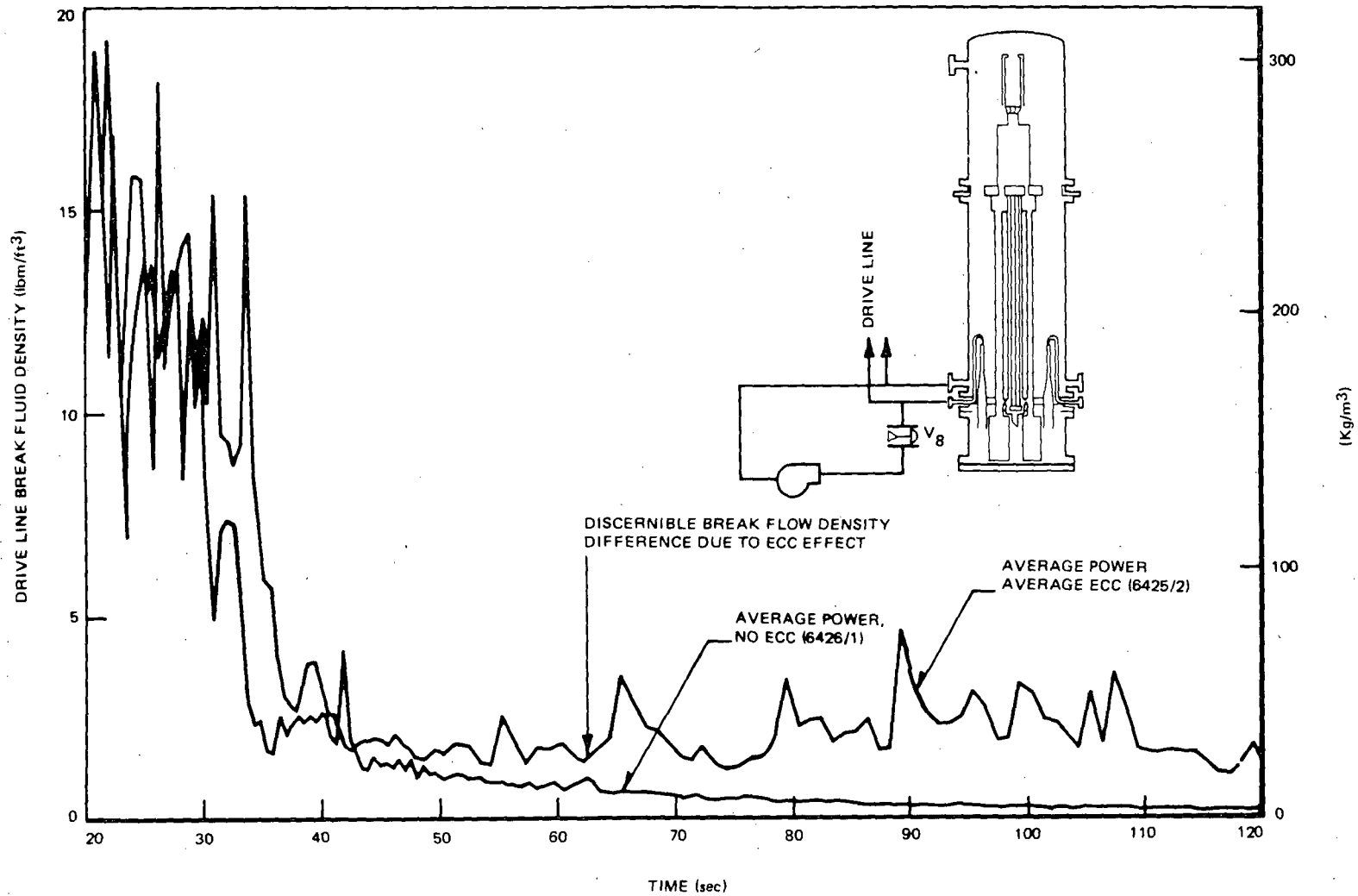


Figure 3-56. Comparison of Calculated Fluid Densities (Based on Turbine Meter and Drag Disc Measurements) at the Drive Line Break Tests with and without ECC

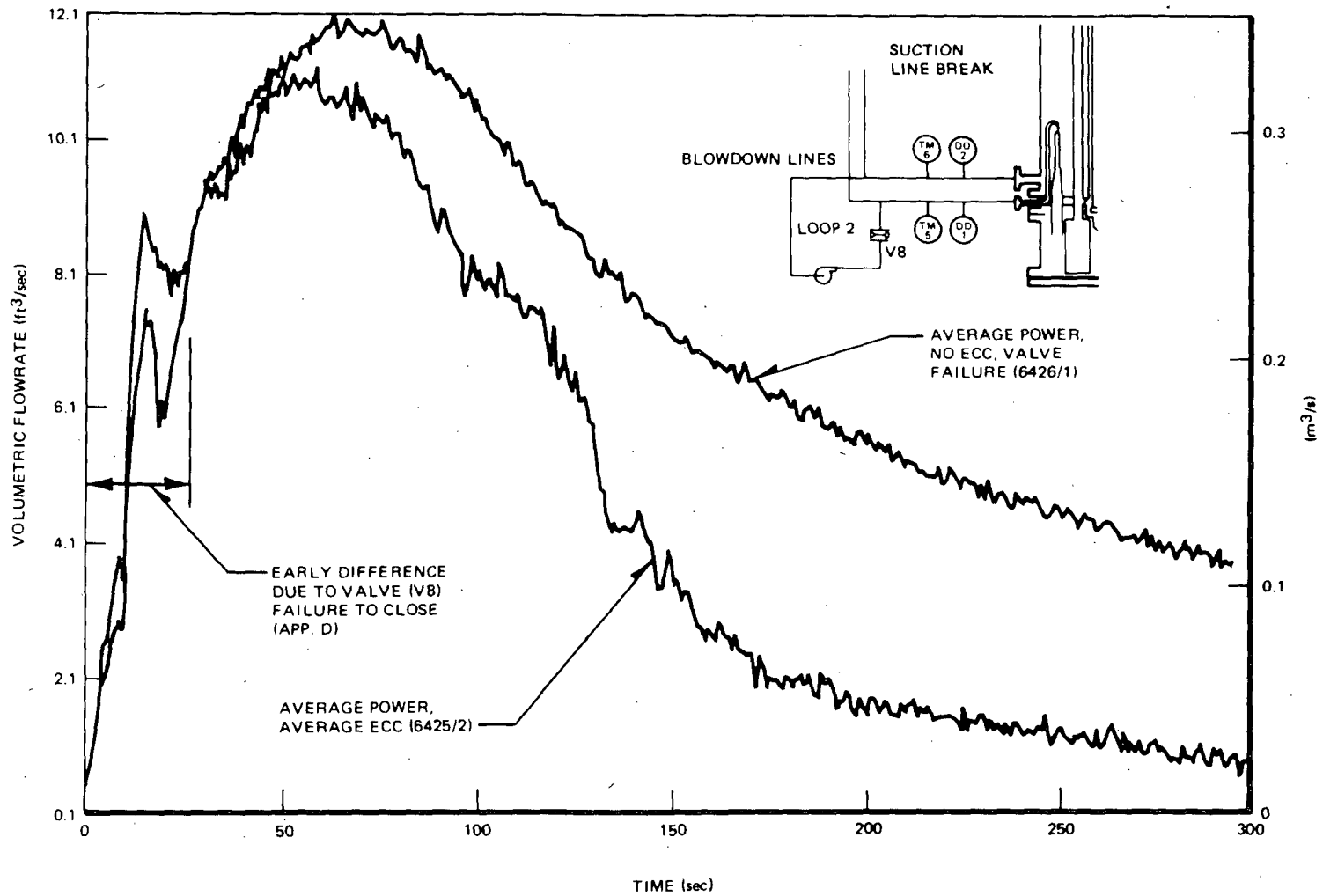


Figure 3-57. Comparison of Volumetric Flowrates through the Suction Line Break for Average Power Tests with and without ECC

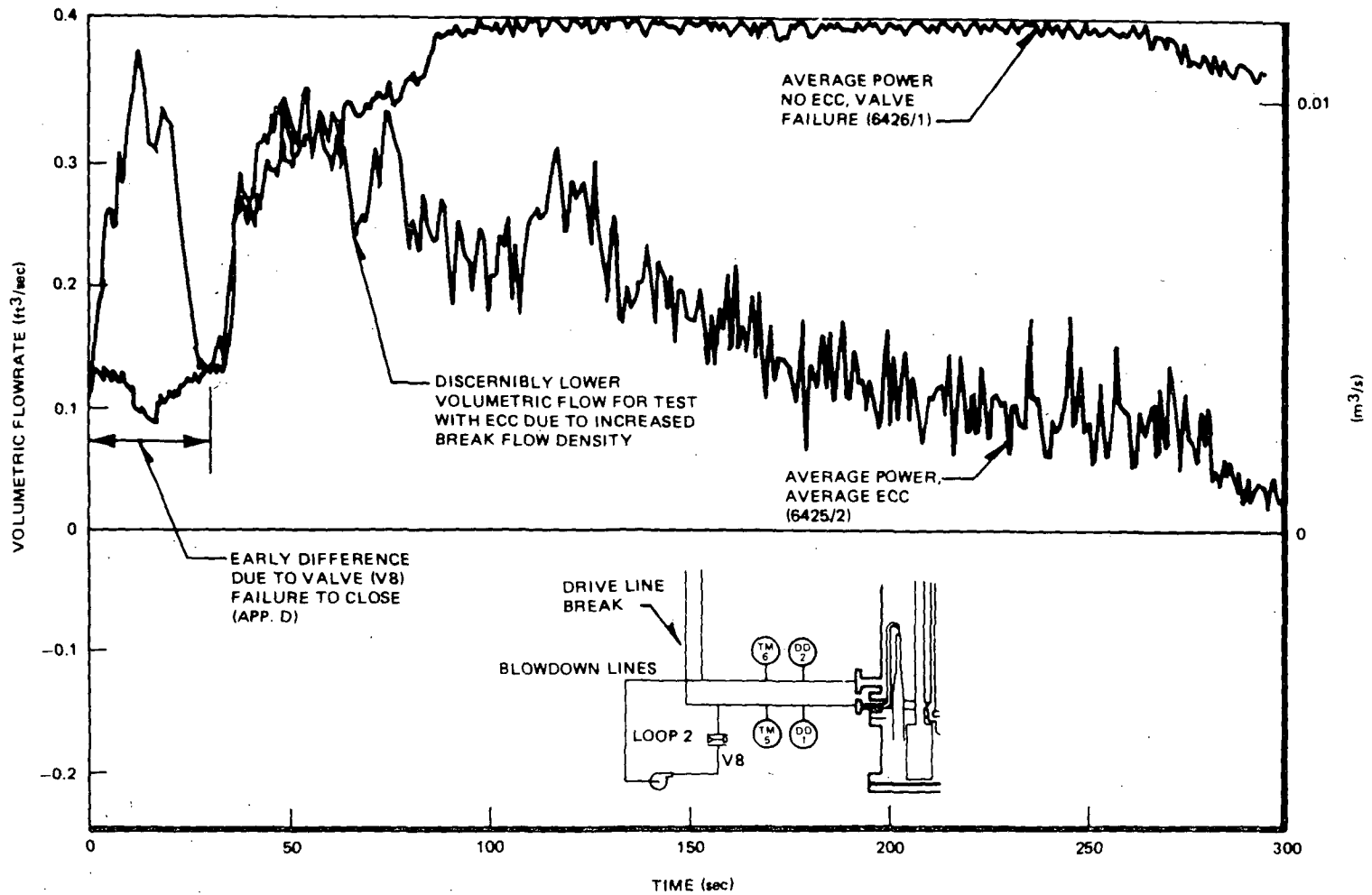


Figure 3-58. Comparison of Volumetric Flowrates through the Drive Line Break for Average Power Tests with and without ECC

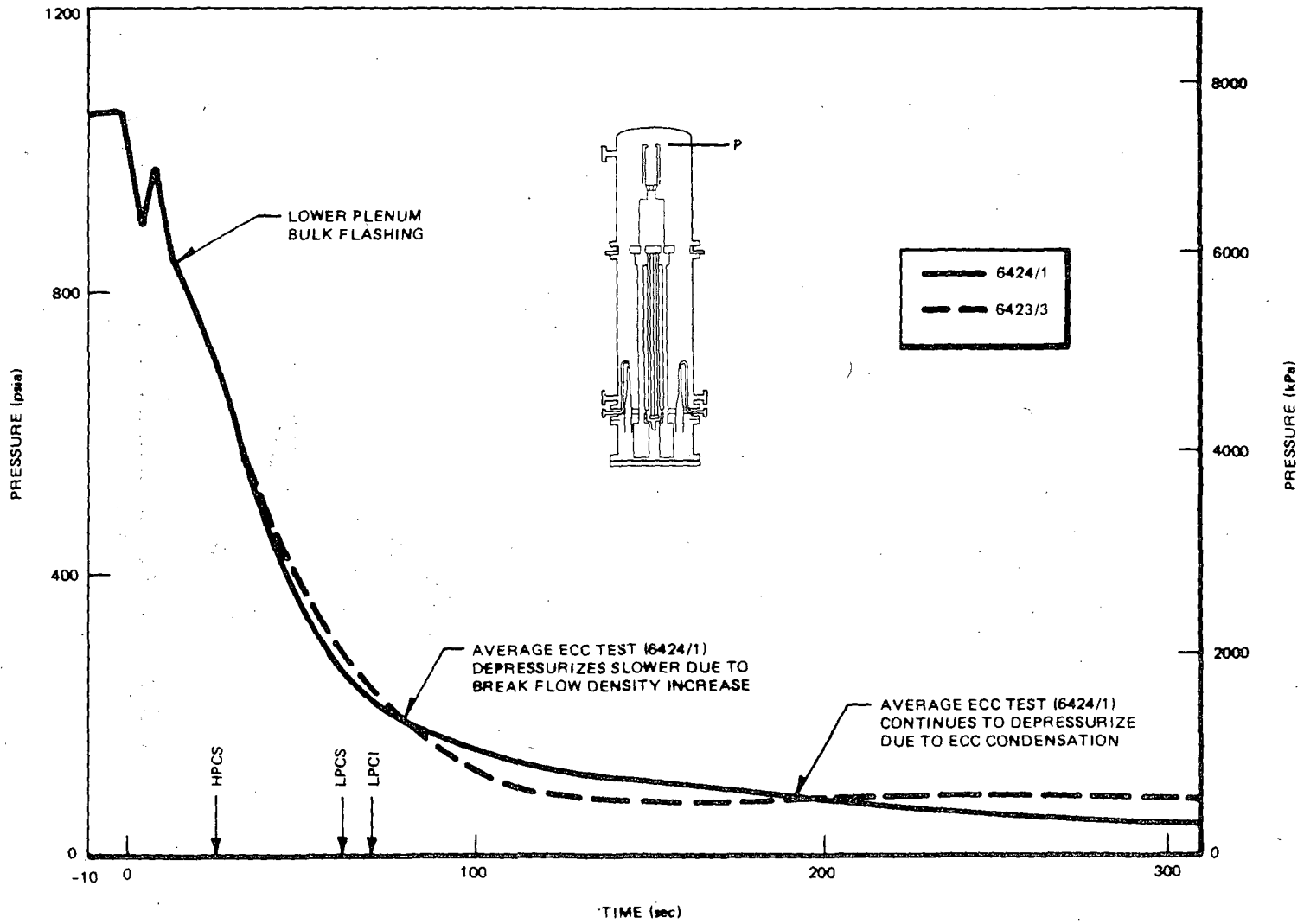


Figure 3-59. Comparison of System Pressure Responses for Peak Power Tests with Average ECC (6424/1) and Low Rate/High Temperature ECC (6423/3)

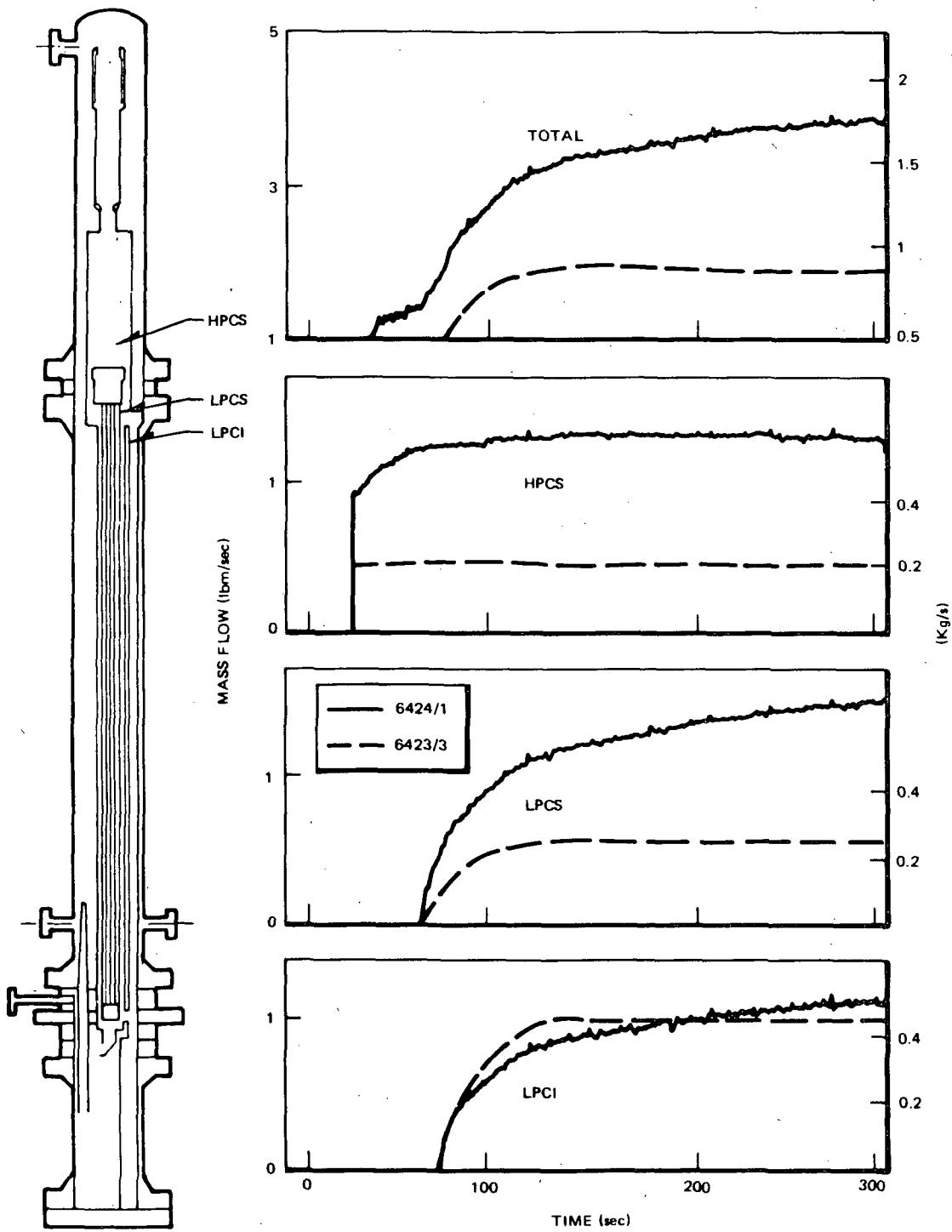


Figure 3-60. Comparison of ECC Injection Rates for Peak Power Tests with Average ECC (6424/1) and Low Rate/High Temperature ECC (6423/3)

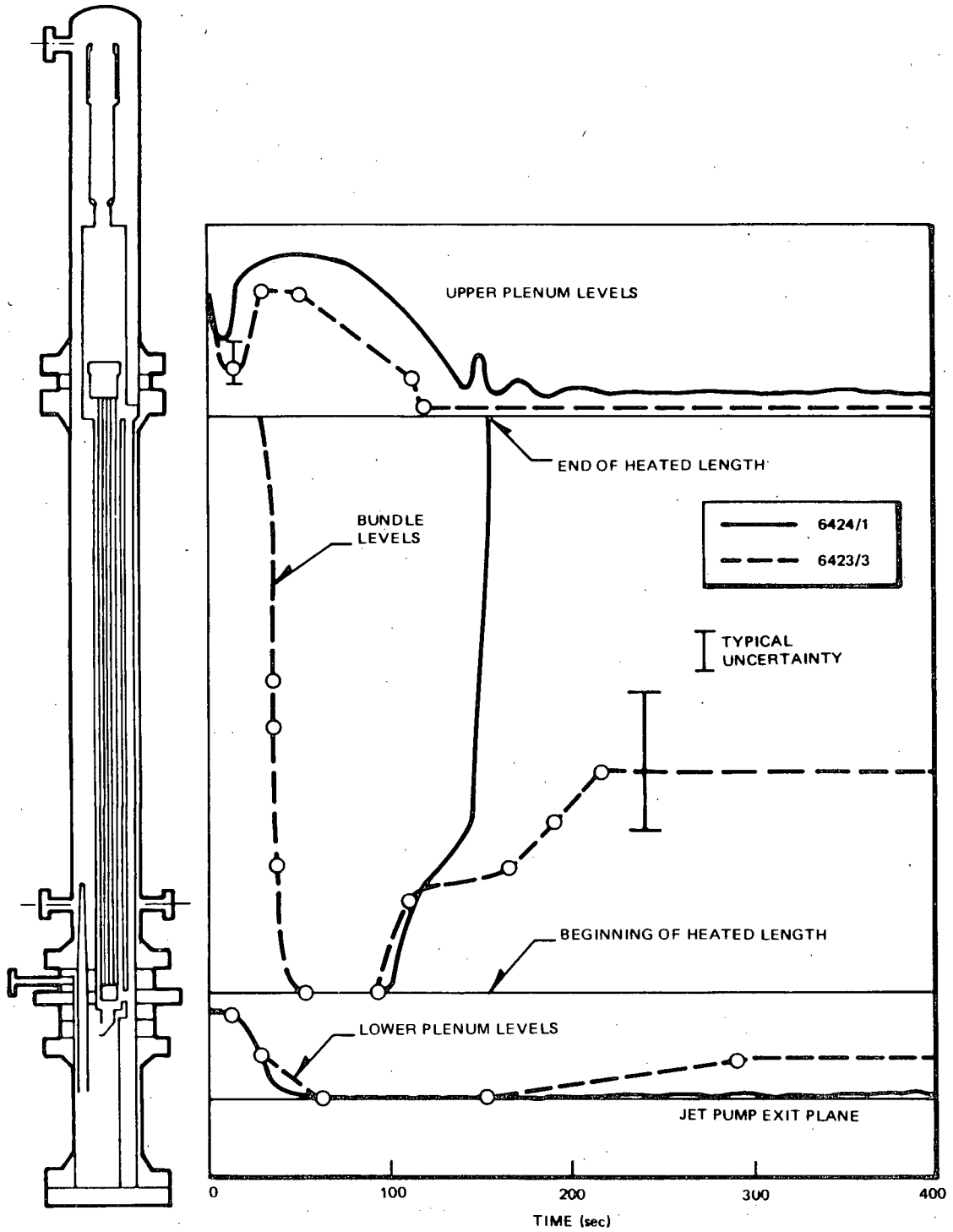


Figure 3-61. Comparison of Two-Phase Levels along the Bundle Path for Peak Power Tests with Average ECC (6424/1) and Low Rate/High Temperature ECC (6423/2)

The peak cladding temperatures for the two peak power tests are compared in Figure 3-62. Whereas the bundle in the test with average ECC completely refloods and becomes well cooled at ~150 seconds, the bundle in the test with low ECC at high temperature only partially refloods. In spite of the fact that the bundle does not completely reflood for the low ECC flow test, the maximum cladding temperature for this test is below ~1000°F (538°C).

3.3.3 Geometric Effects

The most significant geometric difference between Configurations 5A and 5 of TLTA is the leakage path in TLTA 5A. In TLTA 5 the simulation of the BWR leakage path between the bypass and bundles was not present. Instead this leakage path was lumped into the leakage simulation between the guide tube and lower plenum. In TLTA 5A the addition of the leakage flow path results in improved simulation, making it more typical of a BWR (as mentioned in Subsection 2.2.1). The effects of this geometric difference are significant: the bundle refloods from the bypass through the leakage path first; then CCFL breaks down at the upper tieplate and refloods the bundle completely.

The effects of this more representative flow path on the system response can be gleaned from the mixture level response as shown in Figure 3-63. The mixture levels along the bundle path are compared for two average power tests having average ECC injections (Tests 6425 Run 2 and 6406 Run 1). The mixture level for the Test 6425 Run 2 rises as the bundle refloods when the bypass fluid flows into the bundle and is prevented from completely draining into the lower plenum by the CCFL condition at the bundle inlet SEO. The bundle level for Test 6406 Run 1 rises to the height of the jet pump and no further. The reason for this response is that the bypass fluid in Test 6406 Run 1 drains directly into the lower plenum. The only fluid available for the bundle reflood is that allowed by the CCFL condition at the upper tieplate. Consequently, the available fluid was insufficient to completely reflood the bundle. On the other hand, with the leakage path simulated in TLTA 5A, the fluid from the bypass flows directly into the bundle and contributes to reflooding the bundle.

Detailed discussions of the system response for the Reference Test, 6425 Run 2, have been presented in Subsection 3.2.1 and those for Test 6406 Run 1 in Appendix I.

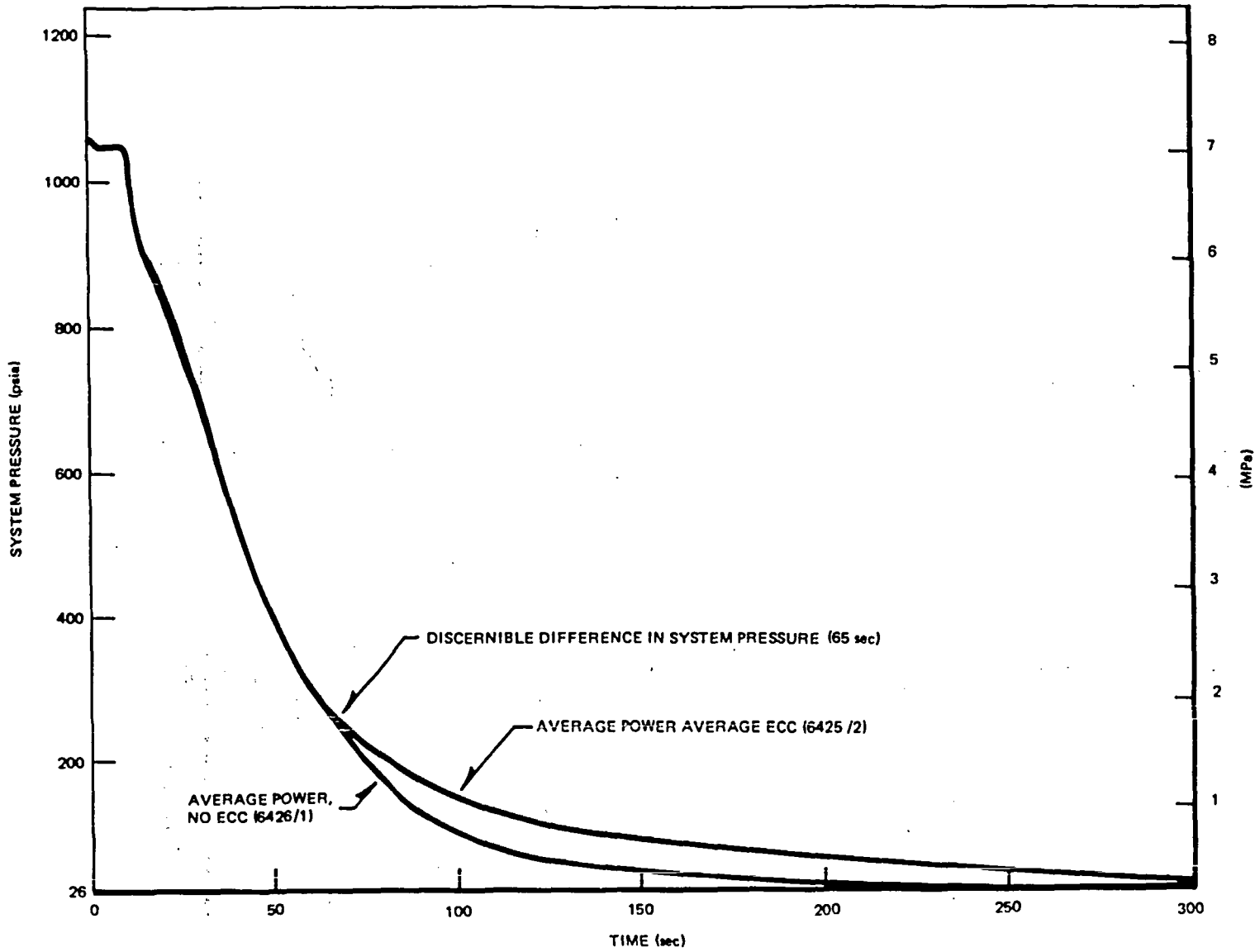


Figure 3-49. Comparison of System Pressures for Average Power Tests with and without ECC

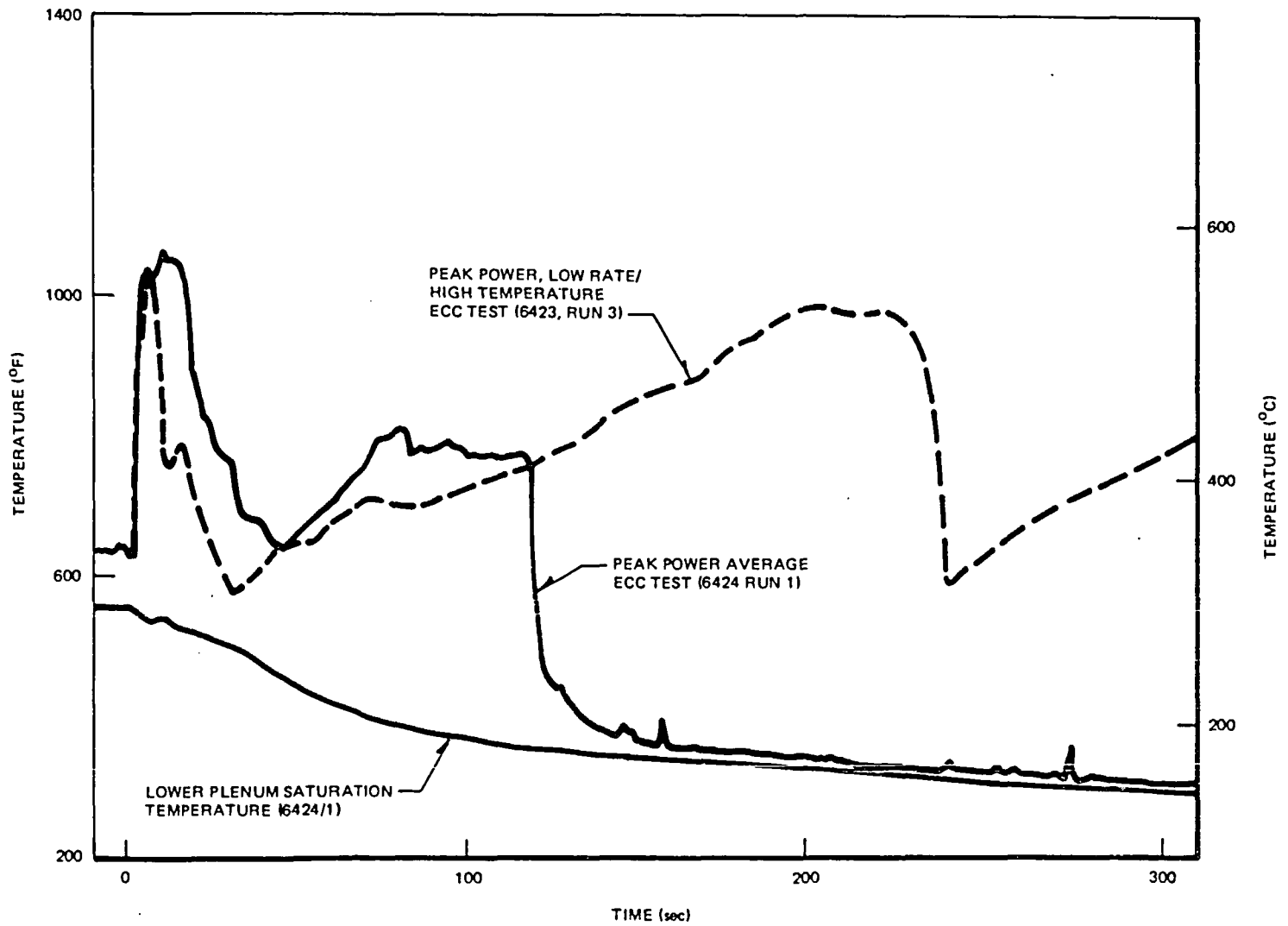


Figure 3-62. Comparison of Peak Cladding Temperatures for Peak Power Tests with Average (6424/1) and Low (6423/3) ECC

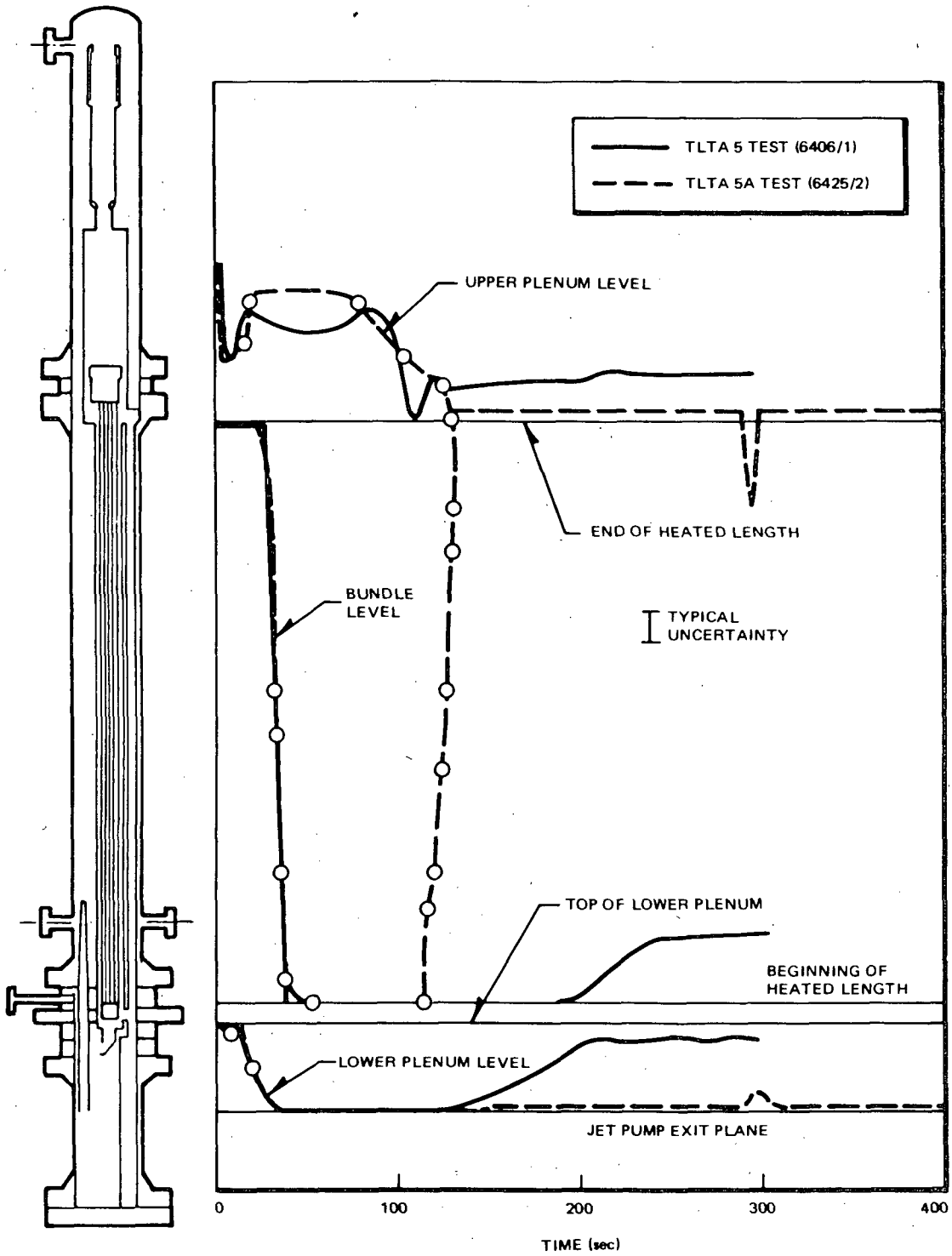


Figure 3-63. Comparison of Mixture Level Responses for Average Power, Average ECC Tests in TLTA 5 and TLTA 5A

Other geometric differences between TLTA 5 and 5A are the removal of the steam separator liquid reservoir and the isolation of the excess fluid volume in Recirculation Loop 1 after 20 seconds in TLTA 5A. The effect of these geometric changes is a slightly faster system pressure decrease for TLTA 5A tests, caused mainly by the isolation of the excess fluid volume in Loop 1. Figure 3-64 shows this effect with the comparison of system pressure responses for Tests 6421 Run 2 and 6406 Run 3. Test conditions for the two tests were comparable: average power with no ECC. The test conducted in TLTA 5A (Test 6421 Run 2) is seen to depressurize faster at 20 seconds. The effect of excess mass on system depressurization will be analyzed in Subsection 3.4.2 below. While the system response was somewhat different, these simple geometry differences should provide an excellent challenge for comparative analyses in assessing best estimate models.

3.3.4 Miscellaneous Effects

In addition to the major systems and parametric effects discussed above, there are other deviations that could affect the system response. Included in this category of miscellaneous effects are break size, vessel heat addition, and test repeatability.

3.3.4.1 Small Break. Detailed description of the responses from the small break tests are presented in a separate topical report. Two small break* tests were conducted, as indicated in Table 3-2. The first test (6431/1) was conducted under the assumption of complete availability of all ECC systems. The second test (6432/1) was conducted under degraded ECC conditions in which the high pressure core spray system was assumed to be inoperative. The results show that, when compared to the global response from the large break LOCA, there were no new phenomena observed in the BWR small break tests. The major effect of the smaller break size was that the timing of key events was extended.

The response of the first small break test was rather uneventful. The high pressure ECC injection alone was capable of supplying more fluid than was lost through the break. The system was refilled and the core region never uncovered. Consequently there was no bundle heat-up.

*NOTE: The break was a 0.125" diameter orifice in TLTA, representing a 0.05 ft² BWR break.

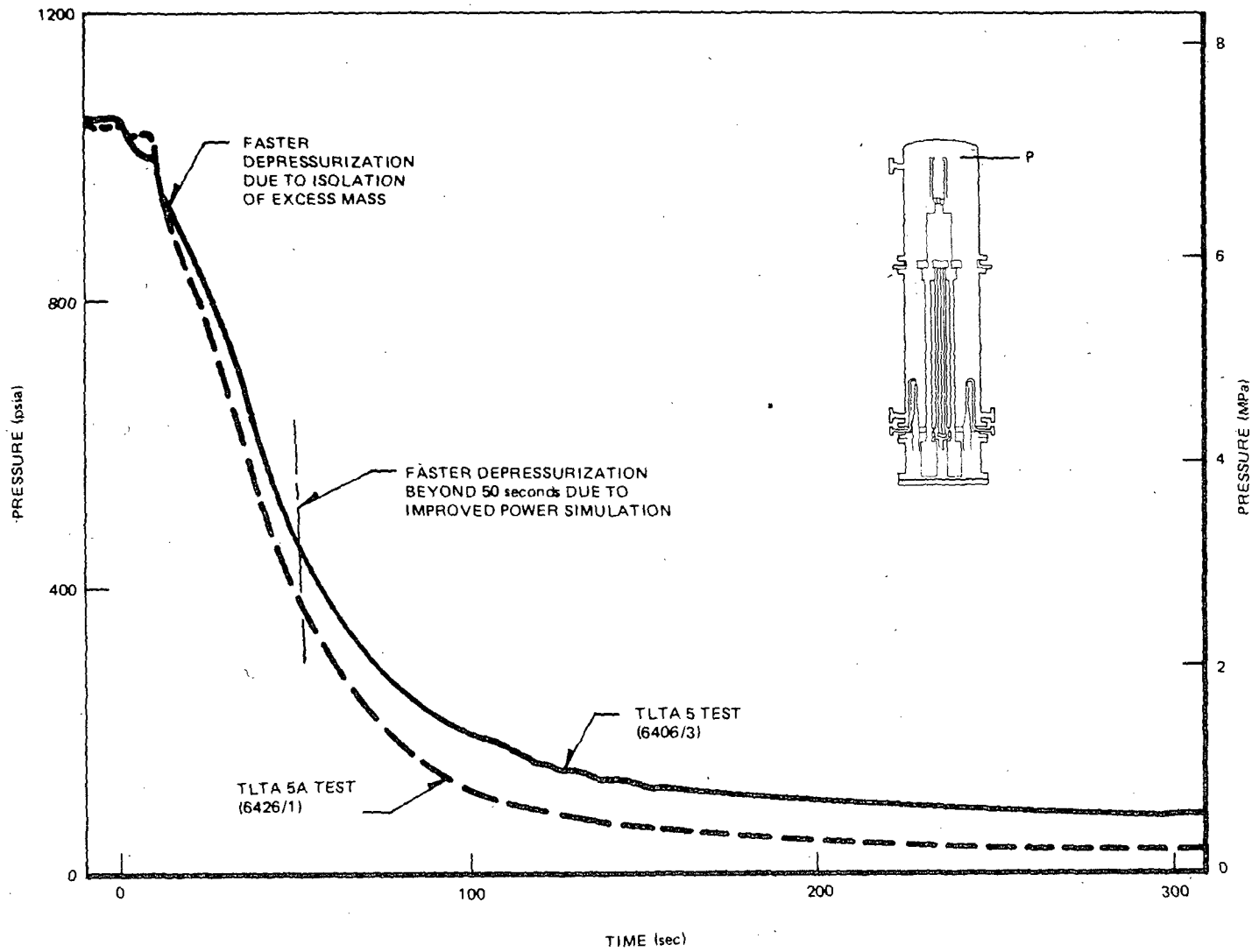


Figure 3-64. Comparison of System Pressure Responses for Average Power, No ECC Tests in TLTA 5 and 5A

In the second small break test, the downcomer inventory and water level continued to decrease as HPCS was assumed to be unavailable. This level drops to the equivalent of Level 1 in a BWR and then, after a delay of 120 seconds, leads to ADS opening. As the vapor discharges through the ADS, the system pressure decreases rapidly (Figure 3-65). This response is similar to the response of a DBA large break (Subsection 3.2.1.1) in which rapid system depressurization follows the recirculation suction uncovering allowing vapor to discharge through the break. In both cases, bulk flashing and subsequent redistribution of the system fluid occur. CCFL condition is observed at the bundle inlet in both large and small break tests.

The system pressure responses for the degraded ECC small break (6432/1) and the large break reference test (6425/2) are compared in Figure 3-65a for detail. The early system depressurization is almost the same for the two tests. Later the system depressurization becomes slower for the small break test because the system inventory at the outset of the rapid depressurization was larger for that test. Another contributing factor for the slower depressurization was that the ADS discharge area of the small break (0.36 sq. in.) was smaller than the suction line discharge area for the large break (0.43 sq. in.). The combined effects of higher system inventory and smaller discharge area lead to the slightly slower depressurization.

The mixture level responses along the bundle path are compared in Figure 3-66. The important phenomenon of the CCFL condition at the bundle inlet is seen in both the large and small break tests. Whereas this CCFL condition delayed heat-up and contributed to bundle reflood in the large break test, it prevented the bundle inventory from emptying into the lower plenum in the small break test. As a result, the level remained above the core region and maintained the bundle well cooled. A cladding temperature comparison shown in Figure 3-67 indicates no heat-up for the small break test. Toward the later period of the small break test, the effects of the subcooled ECCS injection refilling the system and bundle are seen (Figure 3-67) as the measured cladding temperature drops below the system saturation temperature.

3.3.4.2 Vessel Heat Addition. The addition of heat from the vessel to the lower plenum fluid had been anticipated (5); that was why an insulating liner was installed. However, the effectiveness of the insulation has been difficult to ascertain. In general, however, one would expect the heat transfer to increase with time in a transient because of the increase of temperature difference between the vessel wall and the saturated fluid. The mass depletion rate of the lower plenum as compared with that of the guide tube from Test 6426 Run 1, which was run at average

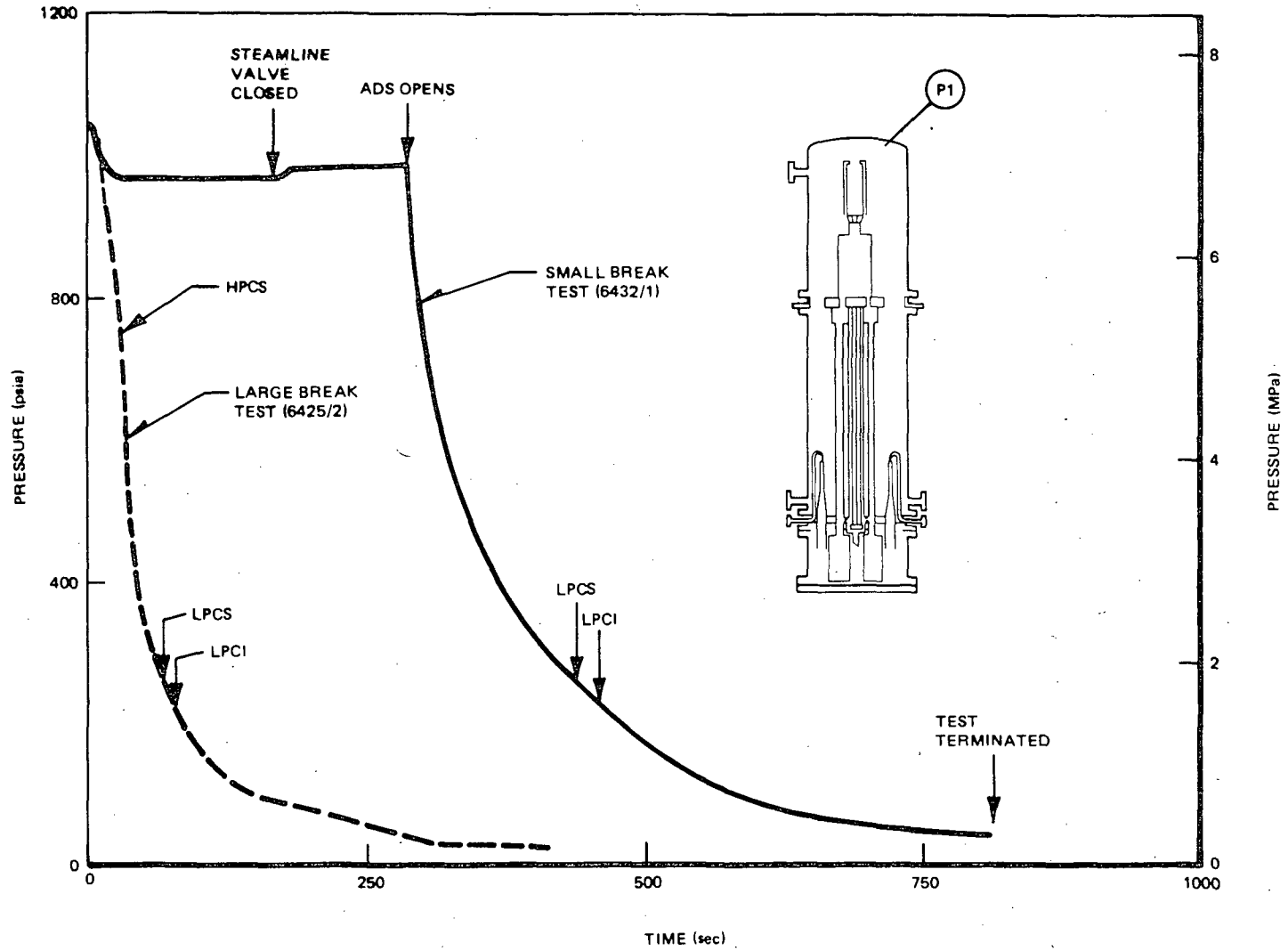


Figure 3-65. Comparison of System Pressure Responses for Large and Small Break Tests

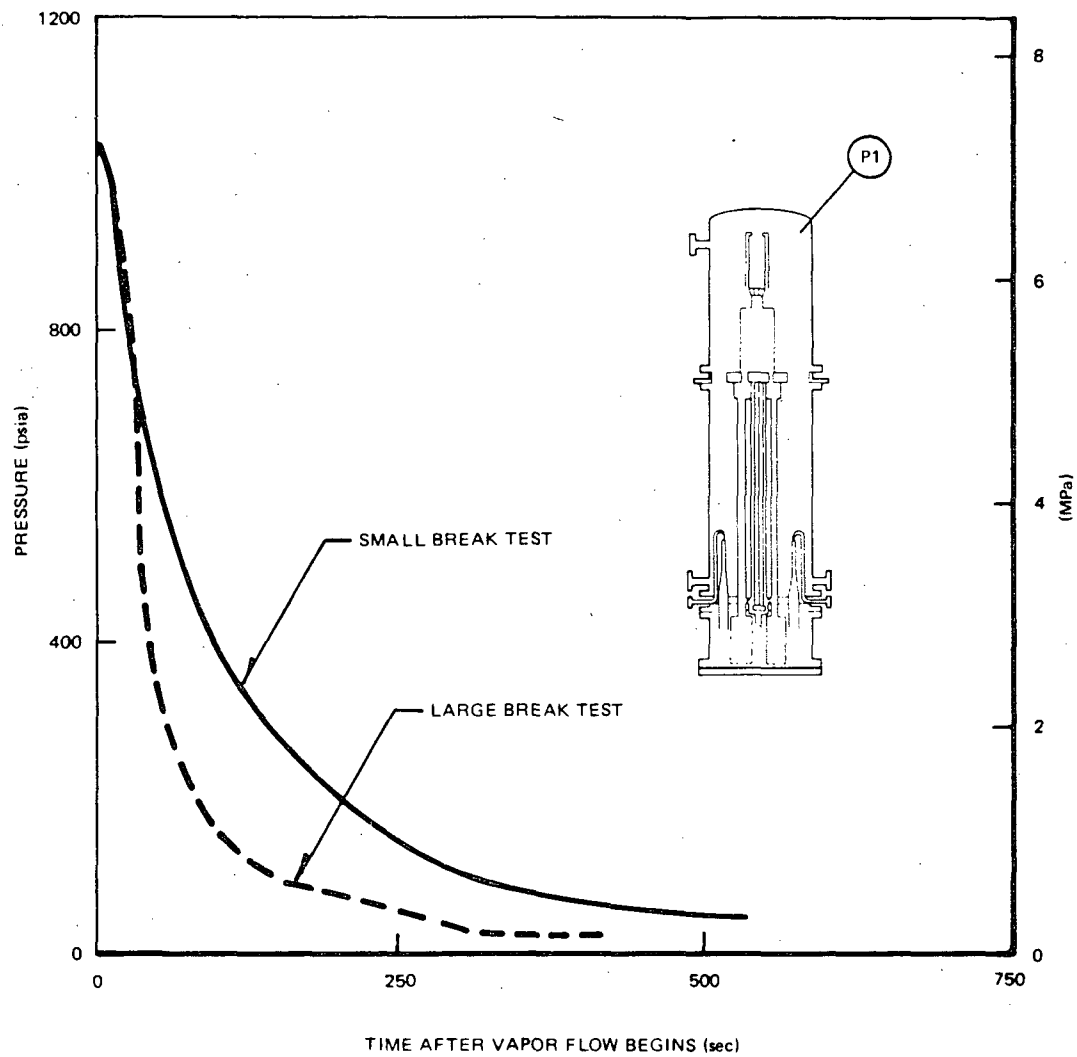


Figure 3-65a. Comparison of System Pressure Responses Following Vapor Flow Initiation

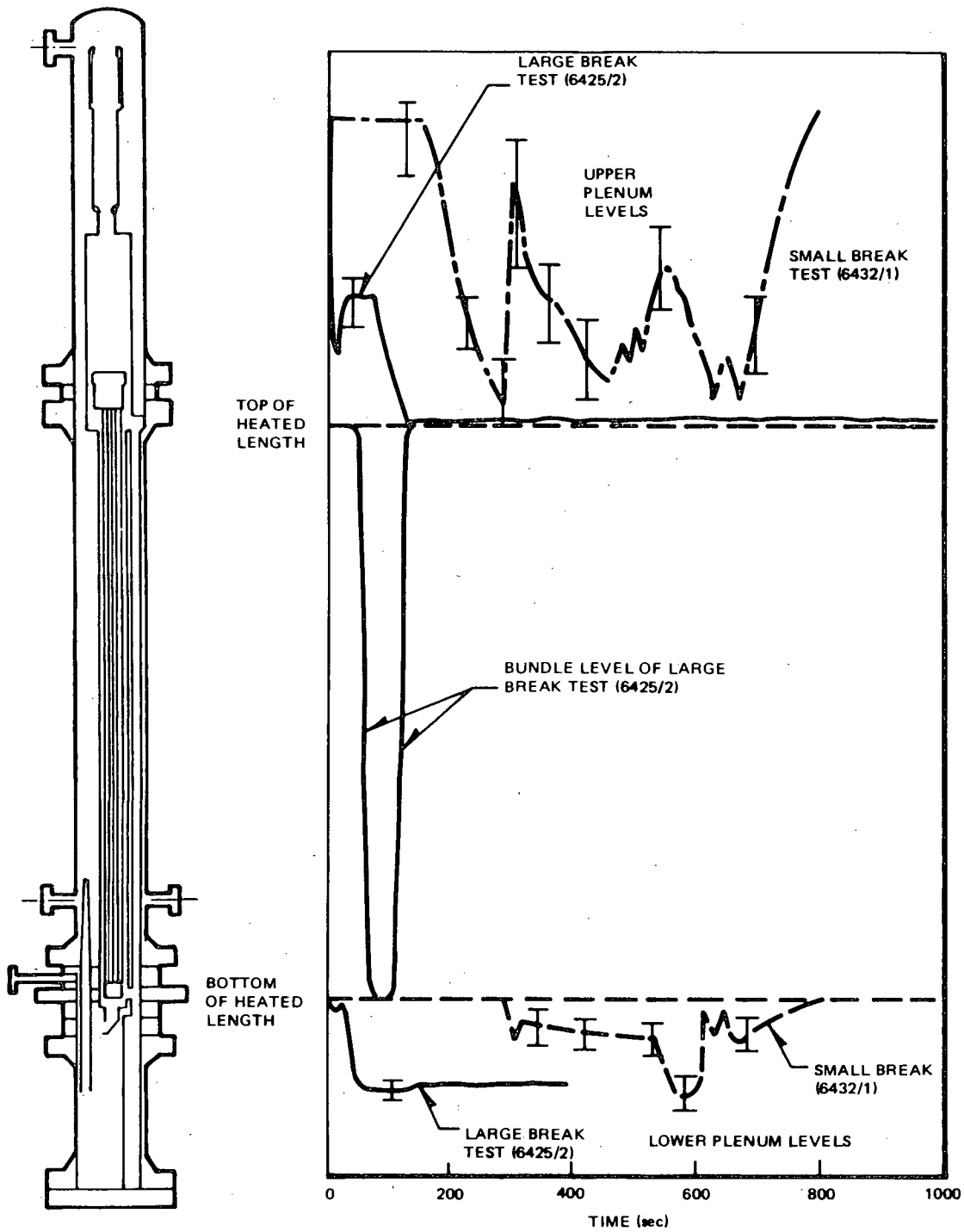


Figure 3-66. Comparison of Mixture Level Responses along the Bundle Path for Large and Small Break Tests

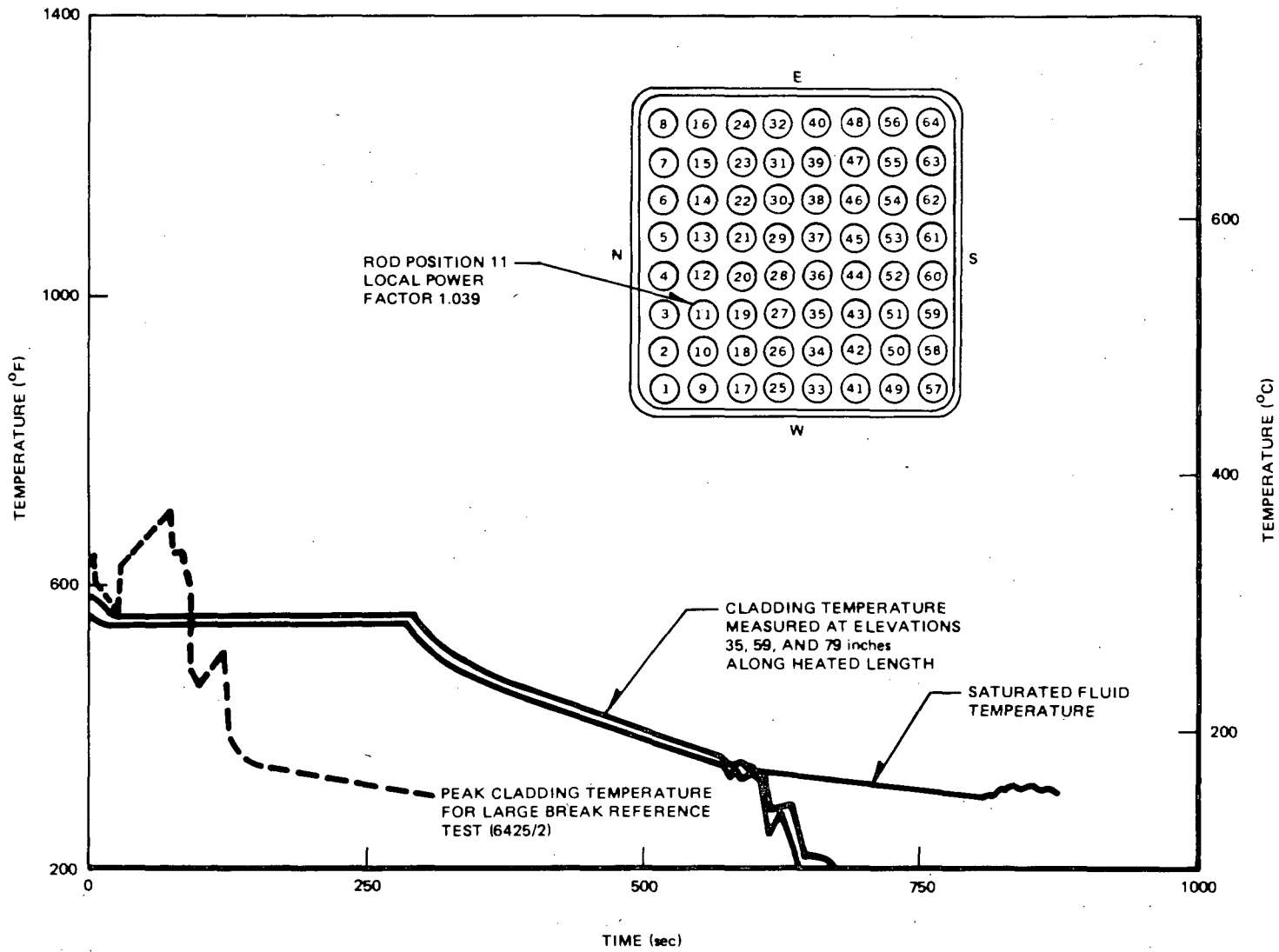


Figure 3-67. Typical Cladding Temperature Response at Selected Elevations for Second Small Break Test (6432) with Degraded ECCS

power with no ECCS, offers a means of estimating the magnitude of heat addition. The heat addition is estimated to be ~60 Btu/sec (63 kW), as discussed below.

Evidence of heat addition can be inferred from Figure 3-68, which shows a faster mass depletion rate for the lower plenum inventory than for the guide tube. Because both these regions are exposed to the same system pressure, the flashing rate is the same for both regions, and therefore the depletion rate caused by flashing should be about the same. The faster depletion rate of lower plenum fluid can be attributed to vapor generation caused by heat addition, as the lower plenum fluid is in direct contact with a thick vessel wall that has a substantial amount of stored energy. The guide tube fluid, on the other hand, is contained in thin wall tubes which have a smaller amount of stored energy. Additionally, the outside of the guide tube is surrounded by the lower plenum fluid so that any stored energy in the guide tube would be shared by the fluid in the two regions. Figure 3-68 shows that, from ~120 seconds and beyond, the effect of heat addition in the lower plenum becomes more evident as the rate of inventory depletion in the two regions becomes discernible.

The magnitude of heat addition after 120 seconds can be evaluated as shown below. The inventory depletion caused by flashing for these two regions can be approximated by the following equations derived from an energy balance in the lower plenum and guide tube (see Appendix E for details).

$$(W_{fg})_{LP} \approx \frac{1}{h_{fg}} \left[\dot{Q}_{LP} - M_{LP} \left(\frac{dh}{dp} \right) \dot{p} \right] \approx -\dot{M}_{LP} \quad (3-1)$$

$$(W_{fg})_{GT} \approx \frac{1}{h_{fg}} \left[-M_{GT} \left(\frac{dh}{dp} \right) \dot{p} \right] \approx -\dot{M}_{GT} \quad (3-2)$$

The heat addition to the lower plenum, as determined from these equations together with test data, is shown in Figure 3-69. It is seen that this heat addition after 120 seconds is ~60 Btu/sec (63 kW). This represents approximately 30 percent of the heat generated in the bundle during this period. However, its effect on the overall system pressure response is small. The main reason for this small effect is that the system energy loss through the break is ~1500 Btu/sec. This energy loss thus overwhelms the effect of bundle power (~200 Btu/sec) and lower plenum heat addition (~60 Btu/sec). That is why the bundle power variations between peak (6.5 MW) and average central power (5.05 MW) show only a negligible effect on the overall system pressure response (Subsection 3.3.1). Locally, in the lower plenum,

3-104

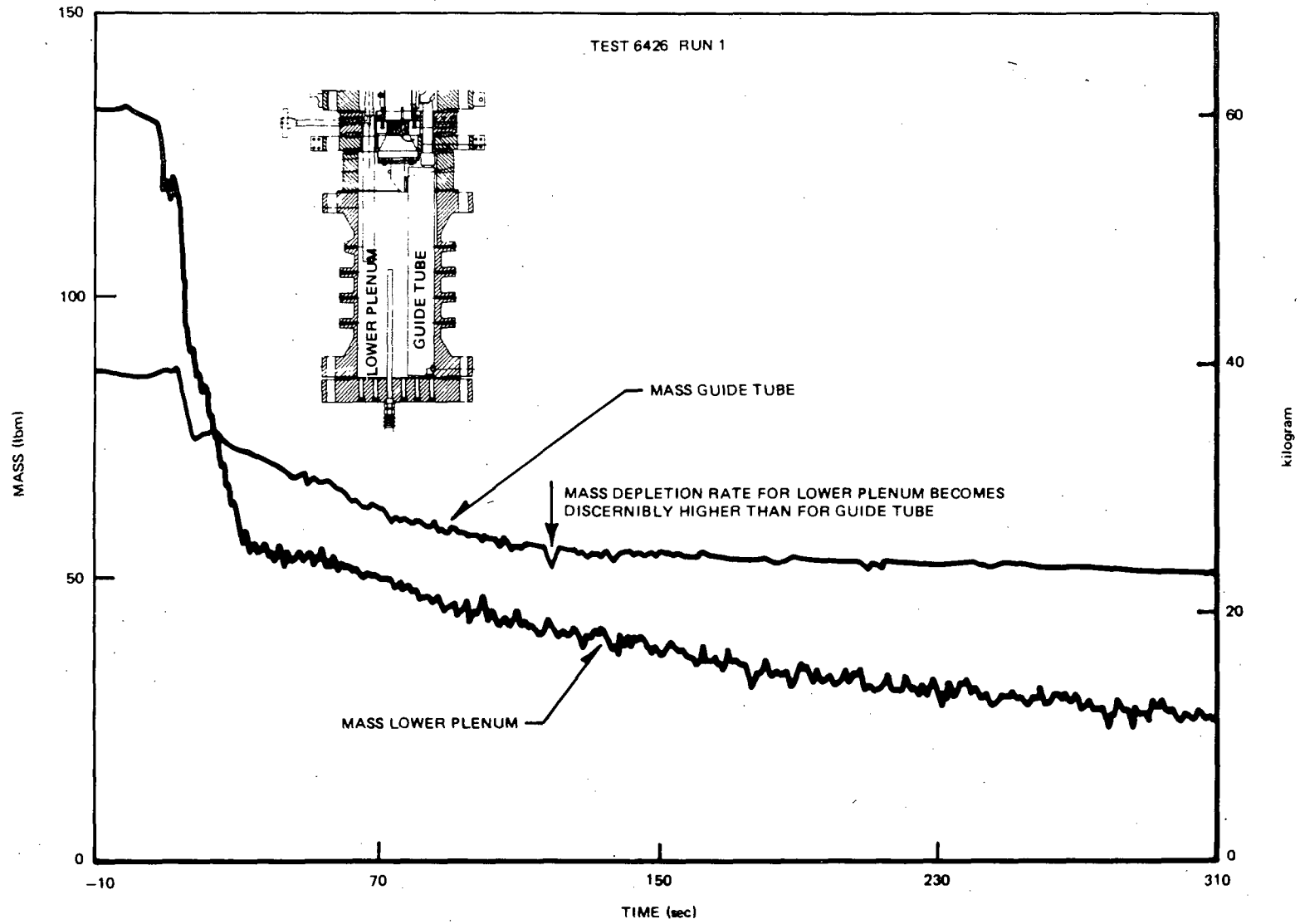


Figure 3-68. Comparison of Mass Depletion Showing Faster Mass Depletion Rate in LP

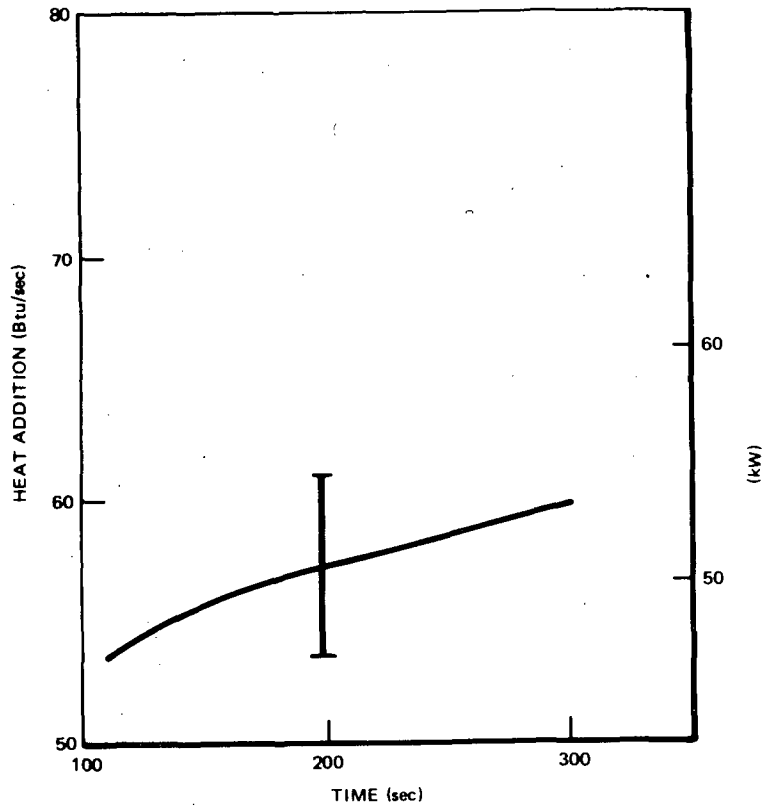


Figure 3-69. Estimated Heat Addition from Vessel to Fluid Based on Figure 3-68

however, this added heat can affect the net steam updraft to the bundle and hence the CCFL conditions at the bundle inlet. Responses of all tests are affected to approximately the same extent.

3.3.4.3 Test Repeatability. Repeatability of tests can be evaluated by comparing results of the two average power, average ECC tests (6422/3 and 6425/2). Test 6422 Run 3 was intended to be the reference test of the test series but was replaced by Test 6425 Run 2 because the latter had an improved pressure controller simulation and improved break flow measurements. Test 6425 Run 2 was a repeat of Test 6422 Run 3, although the objective was not for evaluating test repeatability. Comparison of results shows that the global responses are similar and the controlling phenomena are the same; differences are in detail only.

The initial conditions and timing of events for the two tests are compared in Tables 3-11 and 3-12. Minor differences in initial conditions are noted. The system pressures are presented in Figure 3-70. The difference in the early response is due mainly to the operation of the pressure controller; smaller differences are due to variations in the initial conditions. The pressure responses are nevertheless nearly identical after ~30 seconds. The level responses and the regional masses are presented in Figures 3-71 and 3-72, respectively. The bundle refloods in both cases (Figure 3-71), but in Test 6422 Run 3 the bundle refloods with a denser fluid in a longer time period. The differences noted between these two tests gives an indication or measure of the repeatability that can be achieved in the operation or conduct of these integral system tests.

3.3.4.4 Single Bundle/Bundle Exit. The bundle exit beyond the upper tieplate is rather restrictive in the TLTA because of the extension of the rods to the upper electrode. This, in addition to the absence of multichannels at the bundle exit plane, renders a rather poor simulation of core spray injection distribution. However, the effect of the restrictive geometry appears insignificant in light of the test results discussed in Subsection 3.2.1. It was pointed out that CCFL broke down after the LPCI had refilled the bypass region and the subcooled fluid overflowed onto the top of the bundle. This subcooled fluid augmented the local subcooling and contributed directly, or in combination with the core spray fluid, to break down CCFL at the bundle exit. The effect of single channel versus multi-channel is being evaluated in other programs (13).

Table 3-11

COMPARISON OF INITIAL CONDITIONS FOR AVERAGE POWER, AVERAGE ECC TESTS

<u>Initial Conditions</u>	<u>6422 Run 3</u>	<u>6425 Run 2</u>
Bundle power	5.05 ± 0.03 MW	5.05 ± 0.03 MW
Steam dome pressure	1035 ± 5 psia	1044 ± 5 psia
Lower plenum pressure	1062 ± 5 psia	1071 ± 5 psia
Lower plenum enthalpy	524 ± 5 Btu/lbm	528 ± 5 Btu/lb
Initial water level*	74 ± 6	73 ± 6 in.
Feedwater enthalpy	41 ± 2 Btu/lbm	41 ± 2 Btu/lbm
Bundle inlet to outlet DP	17 ± 2 psi	17 ± 2 psia
Steam flow	6 ± 1 lbm/sec	6 ± 1 lbm/sec
Feedwater flow	1.6 ± 0.3 lbm/sec	1.4 ± 0.3 lbm/sec
Drive Pump 1 flow	8.7 ± 1 lbm/sec	9.1 ± 1 lbm/sec
Drive Pump 2 flow	8.5 ± 1 lbm/sec	8.4 ± 1 lbm/sec
Jet Pump 1 flow	20 ± 2 lbm/sec	22 ± 2 lbm/sec
Jet Pump 2 flow	21 ± 2 lbm/sec	20 ± 2 lbm/sec
Bundle inlet flow	35 ± 5 lbm/sec	39 ± 5 lbm/sec
ECC fluid temperature	120 ± 15°F	120 ± 15°F

All uncertainty bands are judged from the maximum of data fluctuation and/or absolute uncertainties of the measurements.

*Water level reference to jet pump support plate.

Table 3-12
COMPARISON OF TIMING OF EVENTS FOR AVERAGE POWER, AVERAGE ECC TESTS

Events	Time (sec)	
	(6422/3)	(6425/2)
Blowdown valves open	0.0	0.0
Bundle power decay initiated	0.4	0.5
Blowdown loop jet pump flow reverses	0.5	0.5
Feedwater flow stops	0.5	0.5
Bypass flow reverses	3.8	1.7
Jet pump suction uncovers	8.0	6.7
Steamline valve completely closed	14.0	9.0
Recirc. suction line begins to uncover	11.0	9.5
Lower plenum bulk flashing	12.5	11.0
Guide tube flashing	13.7	11.2
Core inlet uncovers (SEO center line)	20	20
Loop 1 isolated	20	20
HPCS injection begins	27	27
Lower plenum mixture level reaches jet pump exit plane	34	35
LPCS LPCI activated	37	37
LPCS flow begins	63	64
LPCI flow begins	71	75
Bypass/guide tube region begins to refill	78	85
CCFL breaks down at bypass outlet	91	95
Bundle begins to refill	95	114
Bypass region refilled	100	125
Bundle reflood with two-phase mixture	150	130
CCFL breaks down at upper tieplate	140	125
Bundle quenched	150	150
End of test	328	400

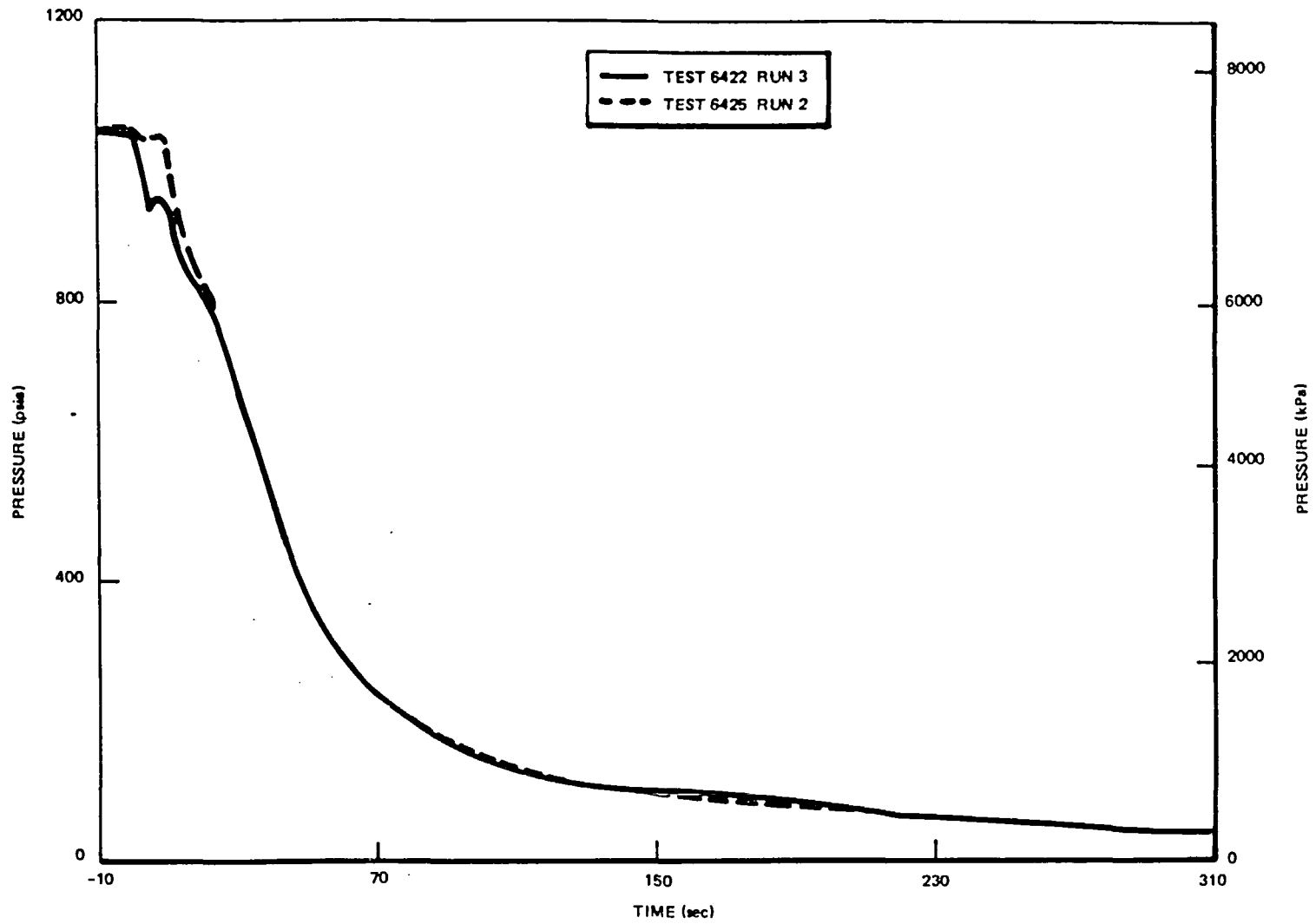


Figure 3-70. Comparison of System Pressure Responses for Average Power, Average ECC Tests

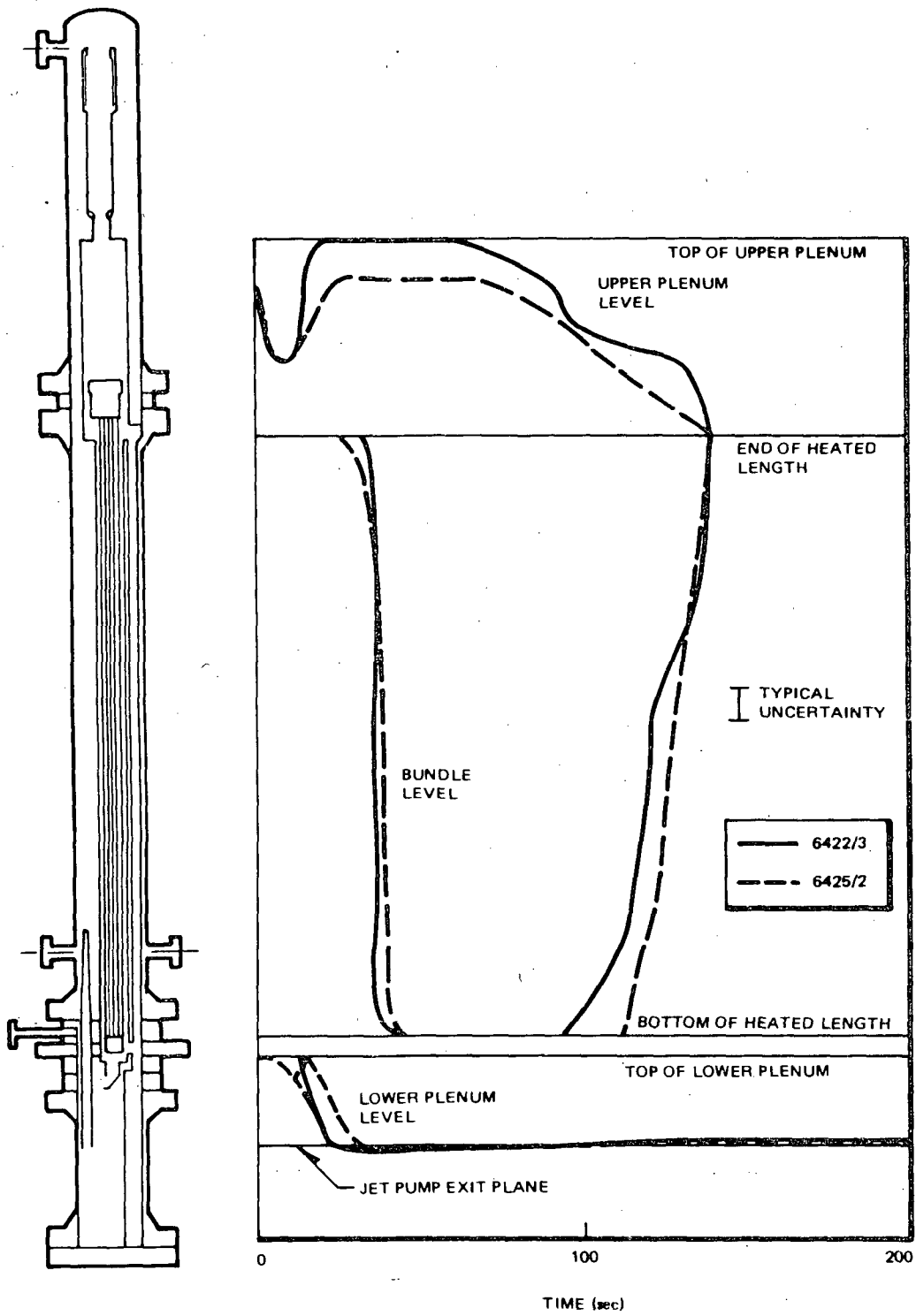


Figure 3-71. Comparison of Level Response along Bundle Path for Average Power, Average ECC Tests

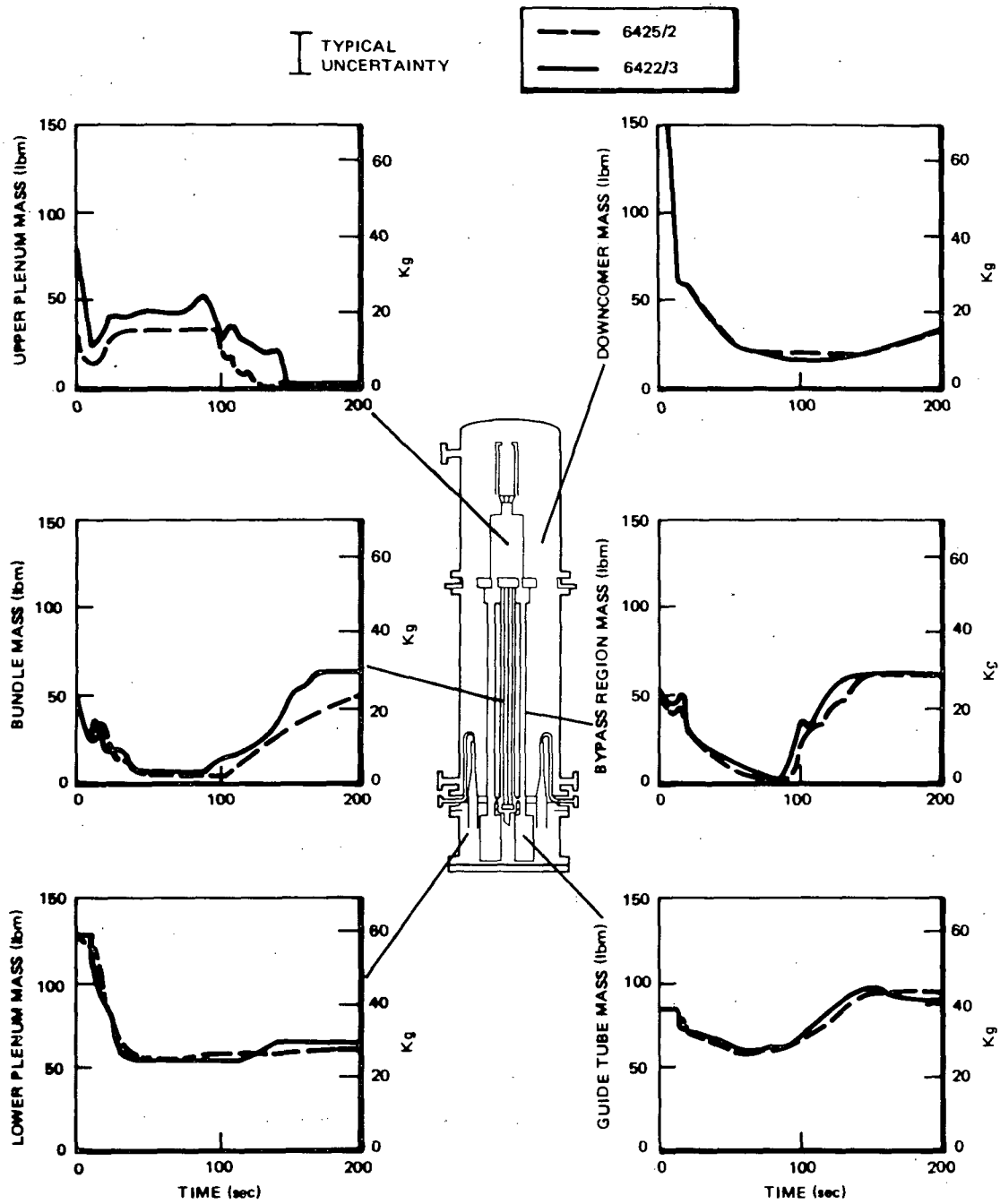


Figure 3-72. Comparison of Regional Mass Responses for Average Power, Average ECC Tests

3.4 ANALYSIS AND EVALUATION

The phenomenological interpretation of results, discussed in the preceding sections, is supplemented by analyses and evaluations presented below. The CCFL phenomenon is evaluated by applying correlations and considerations of condensation. The system depressurization and the effects of parameters are discussed. The break flows, which are important quantities for determining system responses, are evaluated. The bundle heat transfer response is characterized by determining the heat transfer coefficients. Additional characterization of the bundle heat transfer is provided by evaluating the local conditions within the bundle. Finally, heat transfer coefficients determined from test data are compared with those from BWR evaluation models.

3.4.1 CCFL Characteristics

Counter current flow limiting (CCFL) conditions at geometrically restrictive locations, such as bundle inlet and outlet and bypass region outlet, were observed in TLTA tests to have a significant effect on the system response. As discussed in Subsection 3.2.1, CCFL at bundle inlet holds up inventory early in the transient and delays dryout. Later in the transient, CCFL breaks down at the bypass outlet because of LPCI condensation, and the bypass region is refilled with dense fluid. As some of this fluid drains into the lower plenum to hinder the vapor discharge through the jet pump, the CCFL condition again exists at the bundle inlet and contributes to bundle reflood. The CCFL conditions at the bundle inlet SEO, bundle outlet UTP, and the bypass outlet are discussed below. Details of analysis are included in Appendix F.

In the following, a clarification of the term CCFL is first provided. This is followed by results and discussions of: (a) the limiting vapor flow determined for the three locations, (b) a comparison of the limiting vapor flow with vapor generation from flashing, and (c) the operating CCFL conditions at the bundle inlet and outlet.

3.4.1.1 Definitions of CCFL Conditions. Counter current flow limiting (CCFL) condition refers to the flow condition at which the volumetric flux of vapor updraft limits the volumetric flux of liquid downflow. The relationship between the steam upflow and water downflow at the two critical locations across the core region, the bundle inlet (10) SEO and bundle outlet UTP (14), are shown in Figure 3-73. It is seen from this figure that the SEO is considerably more restrictive in limiting water downflow than the UTP.

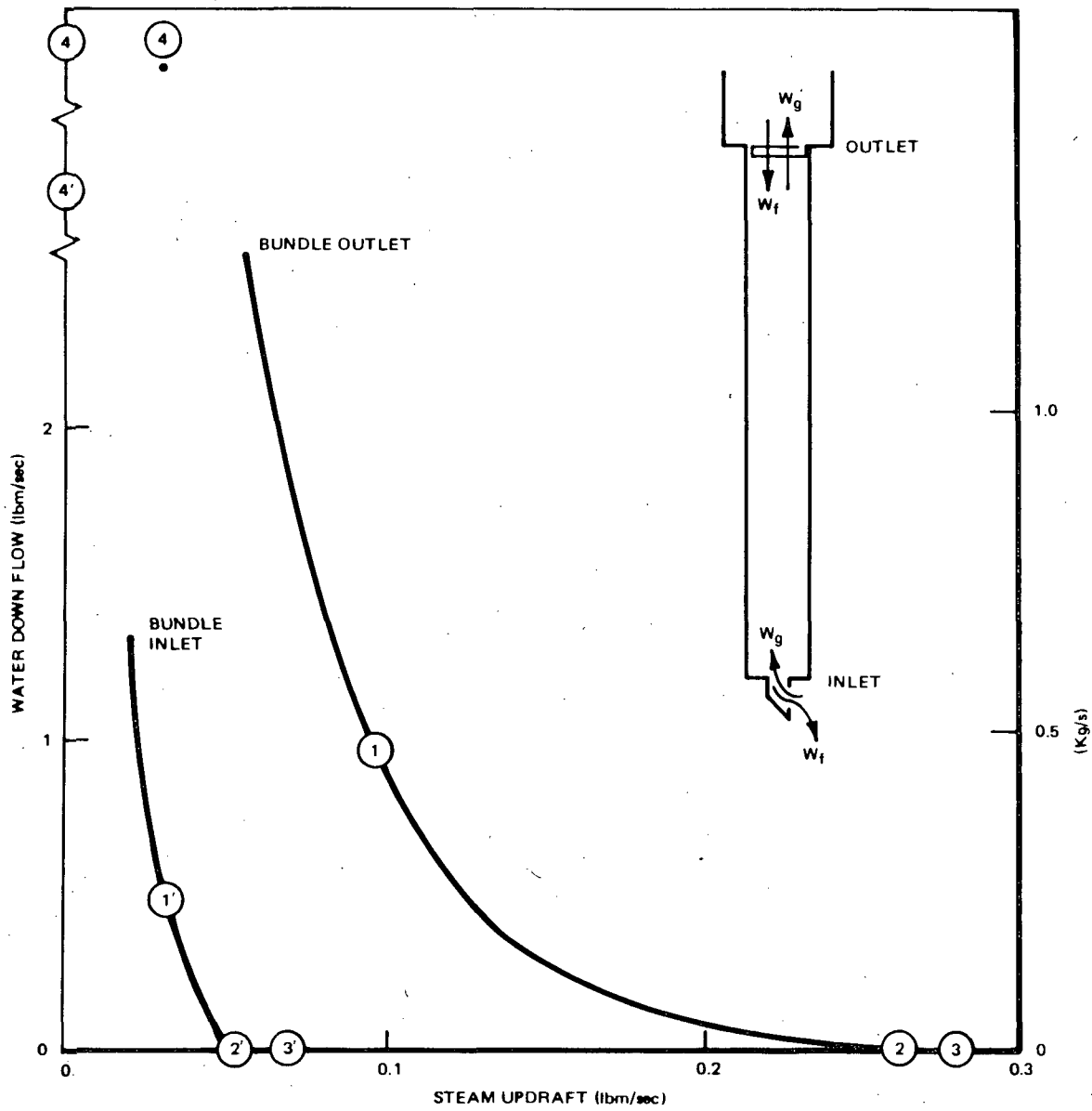


Figure 3-73. Counter Current Flow Limiting Conditions at Inlet and Outlet of Bundle Measured at Atmospheric Pressure

Under counter current flow limiting conditions, the liquid downflow is governed by the steam upflow (Point 1 or 1' in Figure 3-73). If the steam flow increases, the liquid flow decreases correspondingly until complete shutoff of liquid downflow is reached (Point 2 or 2' in Figure 3-73). Further increase in the steam flow leads to continuing shutoff of liquid downflow (Point 3 or 3' in the figure). If the liquid that is about to drain past the restriction is subcooled, it will condense some of the steam as it drains. In addition, if the operating CCFL condition is a point such as 1 or 1' along the CCFL characteristic relationship, the operating condition will quickly shift toward the left (Point 4 or 4') until the liquid downflow is no longer limited by the steam upflow. This condition is referred to as CCFL breakdown. The liquid can then drain freely and is governed only by the hydraulic resistance at the restriction. This free drain condition also exists when there is no net steam updraft.

3.4.1.2 Limiting Vapor Flows. The limiting vapor flows (which stop liquid downflow) for three key locations in the TLTA (bundle inlet orifice, outlet upper tieplate, and bypass outlet) are determined for the reference test (6425/2). Figure 3-74 shows the limiting vapor flows (a CCFL condition analogous to Points 2' and 2 in Figure 3-73) at the bundle inlet and outlet and the bypass outlet. The limiting vapor flow at the bundle inlet SEO is a factor of ~ 5 smaller than the flow at the UTP. This result suggests that conditions could easily exist whereby the vapor flow from the lower plenum is large enough to limit the liquid draining at the SEO, but the combined flow (LP vapor flow plus bundle vaporization) at the UTP is insufficient to stop liquid from draining into the bundle from the upper plenum. Conditions such as these were seen in the reference test during the early blowdown period. As a result, the bulk dryout within the bundle was delayed until ~ 35 seconds.

3.4.1.3 Comparison of Vapor Generation with Limiting Vapor Flow. Vapor generation in different regions of the system can be determined from consideration of the first law of thermodynamics, as shown in Appendix E. Using the relationship in conjunction with measurements from the reference test, the vapor generated from system depressurization (flashing) was estimated for the lower plenum and the guide tube/bypass region. The vapor generation caused by vessel wall heat addition is neglected because heat addition during the early part of the transient is small.

The vapor generated in the lower plenum because of flashing is compared, in Figure 3-75, with the limiting vapor flow at the bundle inlet SEO. The total vapor generated in the lower plenum is seen to be insufficient to completely limit the

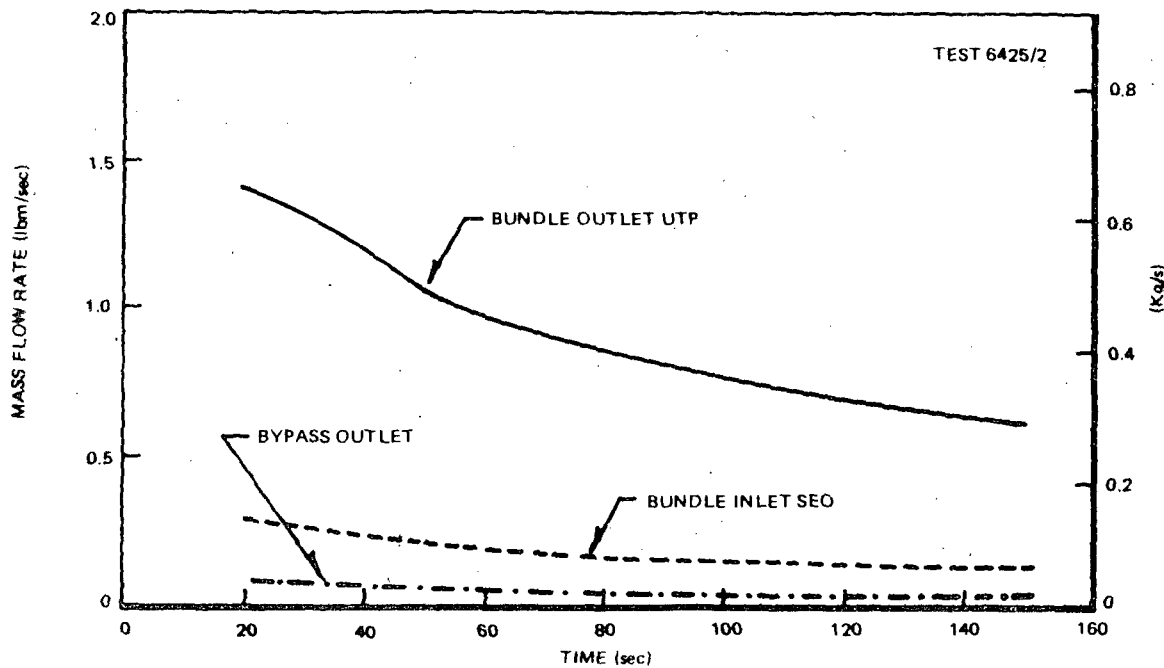


Figure 3-74. Limiting Vapor Flows at CCFL Locations

liquid downflow through the SEO after ~50 seconds. Because a portion of the lower plenum vapor has begun to discharge through the jet pump path after ~35 seconds (when the two-phase level in the lower plenum drops to the jet pump exit plane) the vapor flow through the SEO becomes less than the vapor generated in the lower plenum from that time on. It is likely that liquid begins draining at 35 seconds as the vapor flow through the SEO becomes less than the limiting vapor flow. This result supports the phenomenological inference (Subsection 3.2.1) that the liquid draining from the bundle for the later blowdown period maintains lower plenum inventory so that the mixture level remains at the jet pump exit plane.

The vapor generated in the guide tube/bypass region is compared in Figure 3-76 with the limiting vapor flow at the bypass outlet. The vapor generation was determined from flashing and was adjusted for the condensation effect of the subcooled LPCI. The figure shows that the total vapor generated in the guide tube/bypass region is substantially above the limiting vapor flow. This figure also shows that because of subcooled LPCI condensation, the net vapor generated in the bypass region rapidly approaches zero at ~85 seconds. This result is consistent with the observation (Subsection 3.2.1) that the CCFL breakdown occurred at the bypass outlet at ~85 seconds.

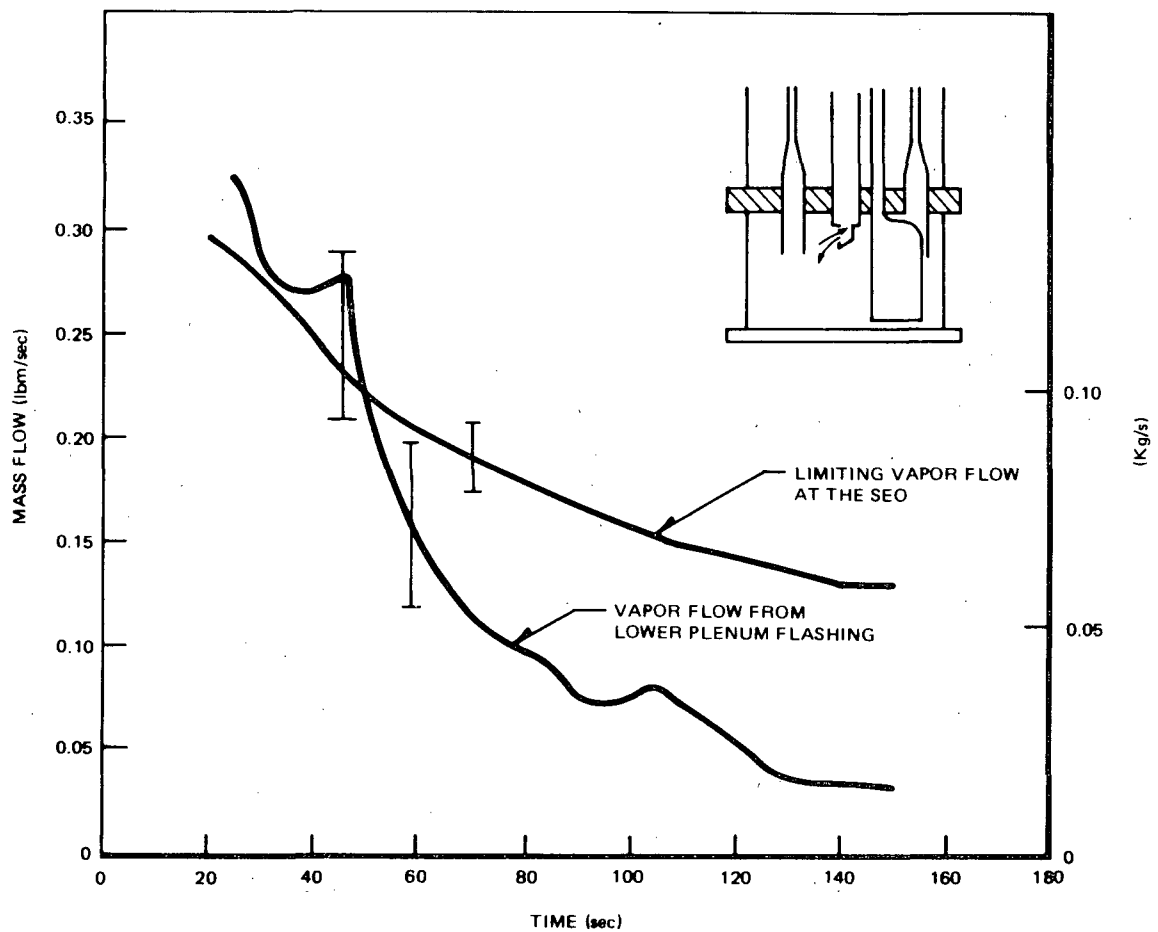


Figure 3-75. Comparison of Lower Plenum Vaporization with Limiting Vapor Flow at SEO for Test 6425 Run 2

3.4.1.4 CCFL Operating Conditions. The operating conditions (e.g., location of Point 1 in Figure 3-73) for the three CCFL locations are evaluated below for the reference test (6425/2). The CCFL operating conditions are defined by the vapor upflow and the liquid downflow. The liquid downflows are determined from test measurements by considering mass conservation in adjacent regions (details are shown in Appendix F). The vapor upflow that corresponds to the liquid downflow was estimated from the various CCFL correlations which are shown in Appendix F. The vapor flows are also compared with the limiting vapor flow discussed in Subsection 3.4.1.2.

3.4.1.4.1 Conditions at bundle inlet. The estimated liquid drainage at the bundle inlet SEO is shown in Figure 3-77a, and the corresponding vapor flow is compared with the limiting vapor flow in Figure 3-77b. These figures show that before the lower plenum mixture level falls below the jet pump exit plane at ~35 seconds, little liquid drains through the SEO because the vapor flow is

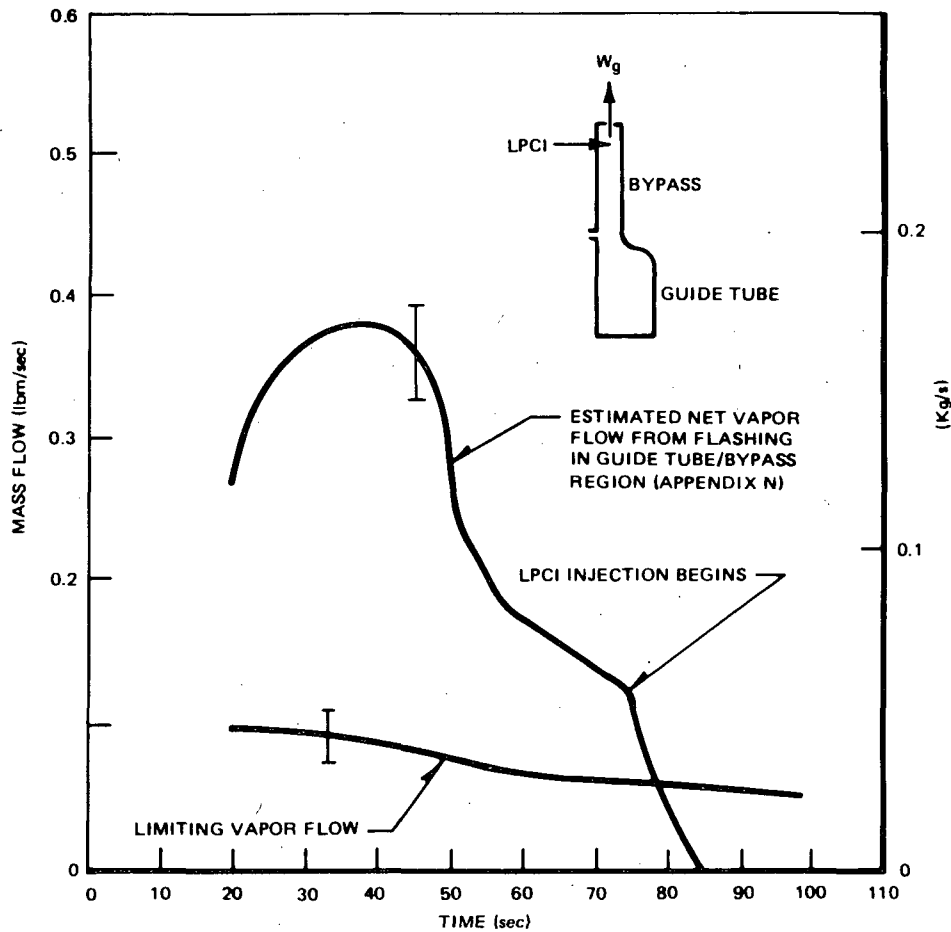


Figure 3-76. Comparison of Guide Tube/Bypass Vapor Generation with Limiting Vapor Flow at Bypass Outlet for Test 6425 Run 2

above the limiting flowrate (i.e., operating point equivalent to Point 3 in Figure 3-73). After the lower plenum level falls to the vicinity of the jet pump exit plane, significant liquid downflow occurs because a large proportion of lower plenum vapor discharges through the jet pump flow path. The vapor upflow remains below the limiting flow rate as liquid continues to drain through the SEO. This liquid drainage increases at ~130 seconds following the complete bundle reflood as CCFL at the bundle outlet breaks down.

3.4.1.4.2 Conditions at bundle outlet UTP. The liquid downflow at the bundle outlet UTP and the corresponding vapor flow are shown in Figure 3-78a and 3-78b. The vapor flow is also compared with the limiting vapor flow and the vapor generation caused by bundle power (i.e., decay heat). The liquid downflow confirms the observed liquid drainage into the bundle and substantiates the inference that many rods rewet prior to complete reflooding of the bundle (Subsection 3.2.1).

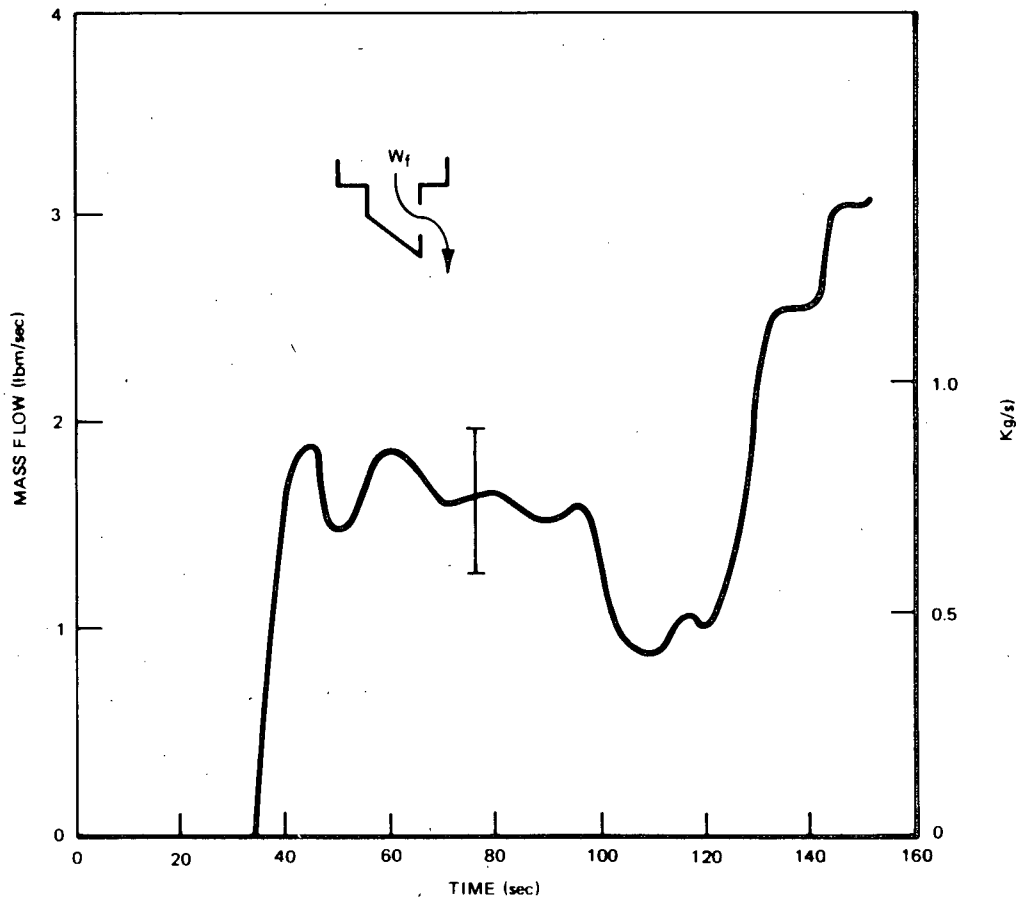


Figure 3-77a. Estimated Liquid Downflow at the Bundle Inlet SEO for Test 6425 Run 2 (Avg. Power, Avg. ECC)

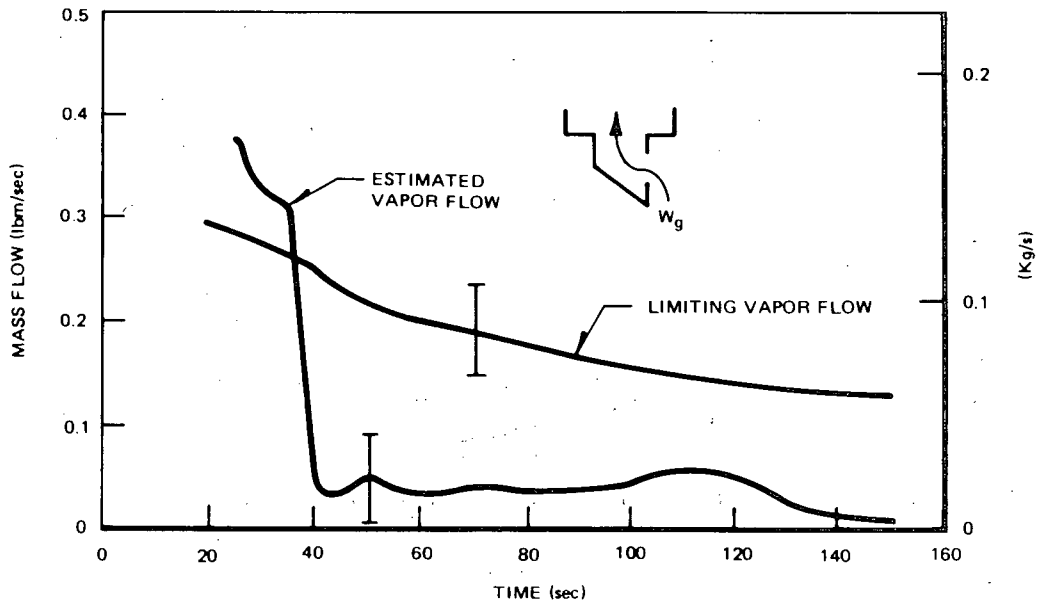


Figure 3-77b. Estimated Vapor Flow Corresponding to the Liquid Flow at the SEO for Test 6425 Run 2. (Avg. Power; Avg. ECC)

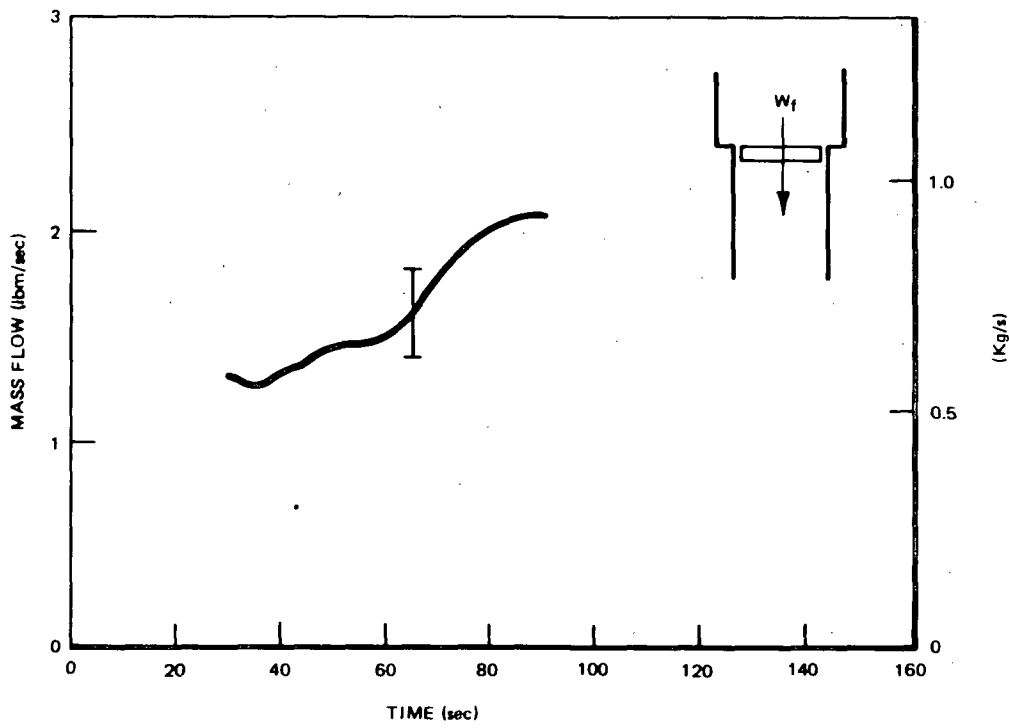


Figure 3-78a. Estimated Liquid Downflow into Bundle through UTP for Test 6425 Run 2

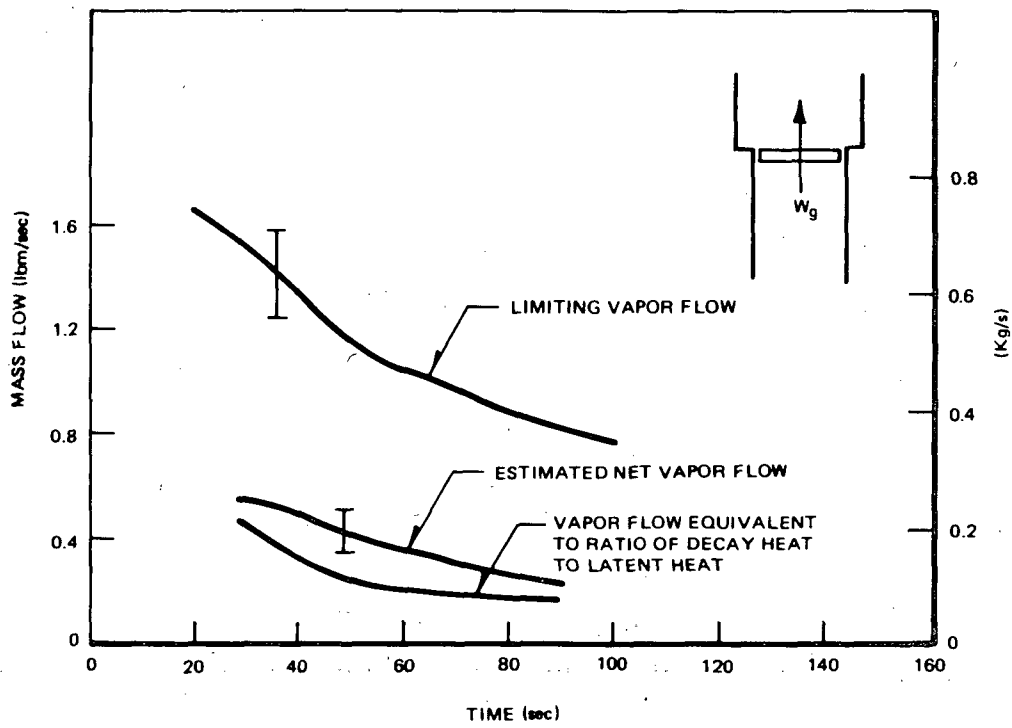


Figure 3-78b. Estimated Vapor Flow Corresponding to Liquid Flow at UTP for Test 6425 Run 2

3.4.1.4.3 Summary remarks on CCFL and condensation. Evaluation of the CCFL conditions confirms the phenomenological observations stated in Subsection 3.2.1. In addition, the CCFL condition at the SEO is more restrictive than that at the UTP. In both these locations, the limiting condition of no liquid downflow does not persist after ~35 seconds. The condensation effect of the LPCI is seen to cause CCFL breakdown at the bypass outlet.

The results show that the condensing capability of only one LPCI system was sufficient to condense all the vapor generated in the guide tube/bypass region and cause CCFL breakdown at the bypass outlet. Following CCFL breakdown at the outlet, the bypass region was refilled with fluid from the upper plenum in combination with that from LPCI. As the fluid draining from the bypass region is less than one LPCI, the subcooled LPCI fluid spills into the upper plenum and augments the condensation capability of the core spray ECC. Consequently, CCFL breaks down at the top of the bundle. The results of bundle UTP CCFL breakdown were observed for both the average and peak power tests with average ECCS injection. The CCFL condition at the bundle inlet is rather restrictive so that the liquid drainage through the SEO is reduced by the steam generated from continuing lower plenum flashing. The CCFL condition at this location contributes to a rapid reflooding of the bundle as it holds up the inventory in the bundle.

In addition, the combined condensing capacity of the three ECC systems (one HPCS, one LPCS, and one LPCI) is sufficient to condense all the updrafting vapor from the core region (bypass and bundle) into the upper plenum. Evidence of this can be found in measurements which show: (a) subcooled temperature of the bypass region (see plot of T25, T26, App. J), (b) subcooled fluid temperature in the upper plenum (Figure 3-6), (c) subcooled temperature measurements of rod cladding (Figure 3-8), and (d) reverse steam flow through the separator indicating that steam was drawn into the upper plenum from the steam dome (Figure 3-12).

3.4.2 System Depressurization

The system pressure is evaluated below in light of some of the effects of thermal-hydraulic quantities discussed previously (Subsections 3.2.2.4, 3.3.2.1, and 3.3.3). The evaluation uses the depressurization equation which is derived from consideration of mass and energy conservations as detailed in Appendix G. Effects evaluated are: (a) mass/energy influx, (b) system mass inventory, and (c) discharge fluid quality.

The system depressurization equation is given by:

$$-\frac{dp}{dt} = \frac{(v_g W_g + v_f W_f) - v_e W_e + v_{fg} W_e (h_f - h_e)/h_{fg} + \dot{q} v_{fg}/h_{fg}}{-\left[\frac{v_{fg}}{h_{fg}} \left(m_f \frac{dh_f}{dp} + m_g \frac{dh_g}{dp} - v \frac{144}{J} \right) - m_f \frac{dv_f}{dp} - m_g \frac{dv_g}{dp} \right]}$$

$$\equiv \frac{\left(\text{volumetric flow out the break} \right) - \left(\text{volumetric flow from ECC} \right) + \left(\text{volume of fluid condensed} \right) + \left(\text{heat addition} \right)}{f \left(\text{fluid mass, system pressure} \right)}$$

where:

- v_g = vapor specific volume [ft³/lb]
- v_f = liquid specific volume [ft³/lb]
- m_f = mass of liquid [lbm]
- m_g = mass of vapor [lbm]
- W_g = vapor flow outbreak [lb/sec]
- W_f = liquid flow outbreak [lb/sec]
- v_e = ECC specific volume [ft³/lb]
- W_e = ECC flow rate [lb/sec]
- h_f = enthalpy of saturated liquid [Btu/lb]
- h_e = ECC enthalpy [Btu/lb]
- $v_{fg} = v_g - v_f$ [ft³/lb]
- h_{fg} = latent heat of vaporization [Btu/lb]
- \dot{q} = heat addition [Btu/sec]
- h_g = enthalpy of saturated vapor [Btu/lb]
- P = pressure [lbf/in²]
- V = system volume [ft³]

J = Conversion factor [Btu/ft-lb]

144 = Conversion factor [in^2/ft^2]

The equation shows that if the volumetric flow rate of the influx of ECC ($v_e W_e$) is larger than the discharge through the break ($v_g W_g + v_f W_f$) plus the fluid volume decrease caused by condensation, then the system pressure will increase instead of decrease. Such a system pressure increase was observed in Test 6423 Run 3 (peak power, low rate/high temperature ECC) (Subsection 3.2.2.4).

The effect of system mass on depressurization was discussed in Subsection 3.3.3. It was pointed out that the system pressure decreased faster in TLTA 5A after the excess mass in the intact loop was isolated. This effect can be approximated, as shown in Appendix G, by the following ratio,

$$\frac{(dP/dt)_{\text{TLTA 5A}}}{(dp/dt)_{\text{TLTA 5}}} \sim \frac{(M_f)_{\text{TLTA 5}}}{(M_f)_{\text{TLTA 5A}}}$$

which shows that $dP/dt \sim 1/M_f$. Because the liquid mass in TLTA 5A was less after the intact loop was isolated, the depressurization rate was higher.

The depressurization equation was used for a sensitivity study. Differential coefficients, as shown in Appendix G, were used to assess the effect of break area, heat addition to coolant, ECC enthalpy, ECC flow rate, and fluid quality at the break. Results, summarized in Table 3-13, indicate that the two predominant variables affecting system depressurization are the fluid quality within the system and local quality at the break. These results support the inference discussed in Subsection 3.3.2.1 that the ECC fluid retards the system depressurization somewhat as it decreases the steam quality of the fluid inside the vessel as well as at the break.

3.4.3 TLTA Break Flow Evaluation

The break flows are evaluated in this section for the average power tests with and without ECC. The break flows are determined from four methods that are based on different measurements. Details of break flow determination are shown in Appendix H. Presented below are: summary of the methods, summary of the results, and an evaluation of the uncertainties.

Table 3-13

SENSITIVITY OF SYSTEM DEPRESSURIZATION* TO VARIATION OF SYSTEM PARAMETERS

<u>System Fluid Quality</u>	<u>Break Flow Quality</u>	<u>Heat Addition (Btu/sec)</u>	<u>Depressurization Rate (psi/sec)</u>
0.082	1.0	0.25	-23
0.082	1.0	125	-21
0.063	1.0	0.25	-20
0.063	1.0	125	-19
0.063	0.8	0.25	-18
0.063	0.8	125	-17

*NOTE: Based on measured system conditions from Test 6406 Run 1 at 65 seconds.

The methods utilized were: (a) system inventory based on nodal DPs, (b) volumetric and momentum flows based on turbine meters and drag discs, (c) mass discharge based on DP measurement of suction line nozzle, and (d) suppression tank mass increase based on DP measurements. Measurements, other than the nodal DPs, that are used for break flow determination are shown in Figure 3-79.

The vessel inventory method is considered the reference method, as it is based on proven techniques. Applying this method, the total break flows for the average power tests with and without ECC are presented in Figure 3-80. The uncertainties associated with the determined values are included in the figure. In general, these uncertainties are smaller during the period of the transient when the flow pressure drops are negligible.

The break flows determined from the combined turbine meter/drag disc measurements are presented in Figure 3-81a for the suction line and Figure 3-81b for the drive line. In addition to the mass flows, these measurements provide information on the density of the discharging fluid, as is discussed in Appendix H. This information is useful for explaining the break flow difference for the tests with and without ECC. The mass flow for the test with ECC is higher, as seen in Figure 3-81. However, the volumetric flow for the test with ECC is lower (see Appendix H) because the density of the test with ECC is higher (see Figure 3-56). While the measurements

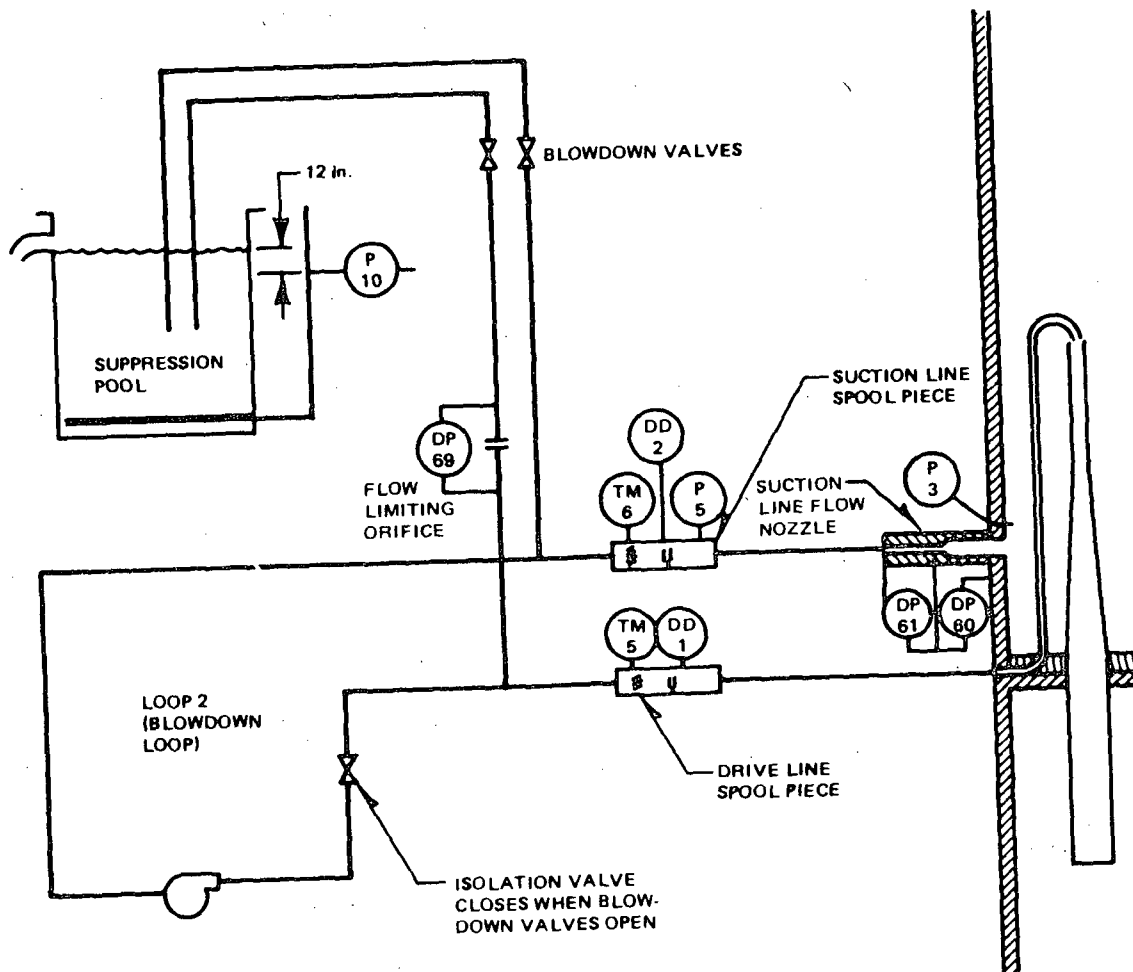


Figure 3-79. Blowdown Loop Break Flow Measurement Locations in TLTA 5A

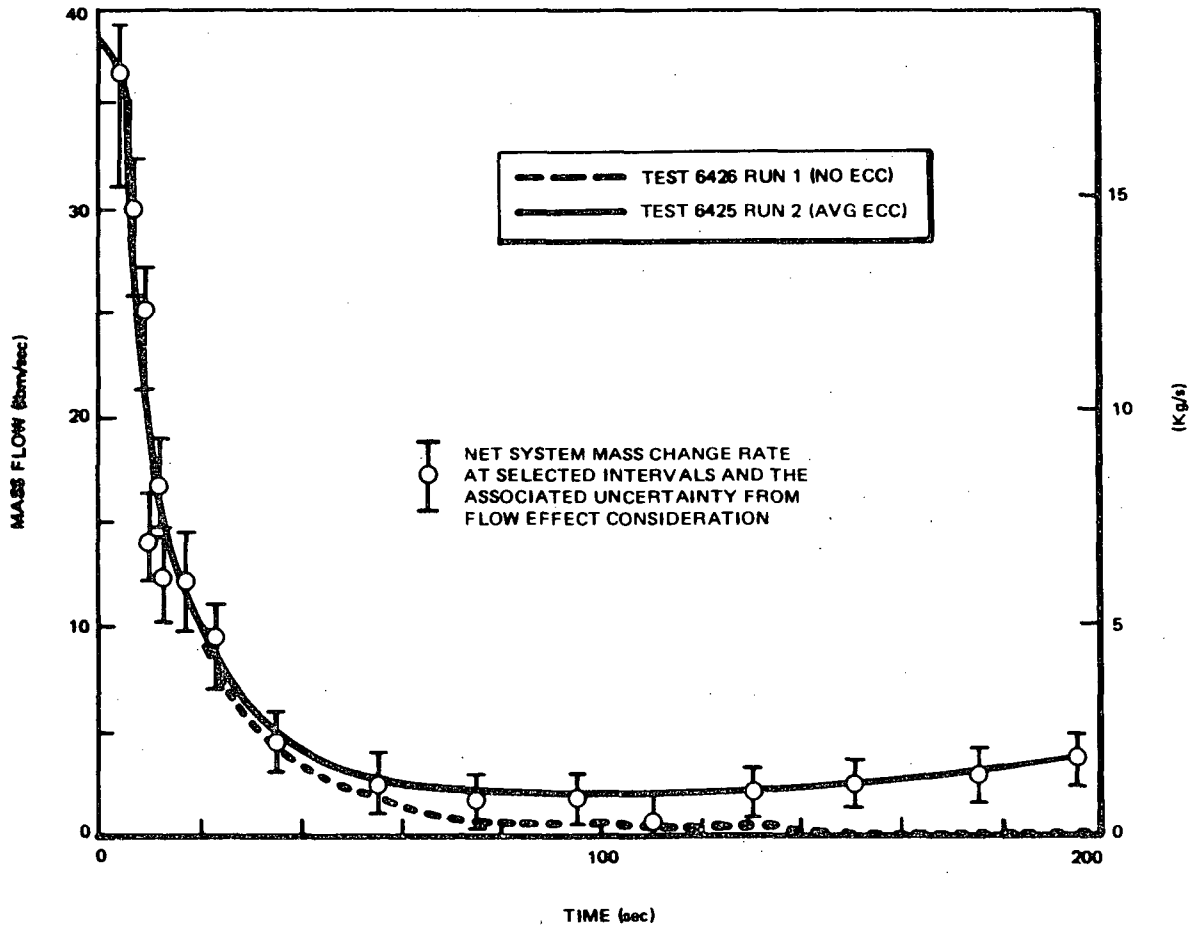


Figure 3-80. Total Break Flow Determined from Inventory Method for Average Power Tests with (6425/1) and without (6426/1) ECC

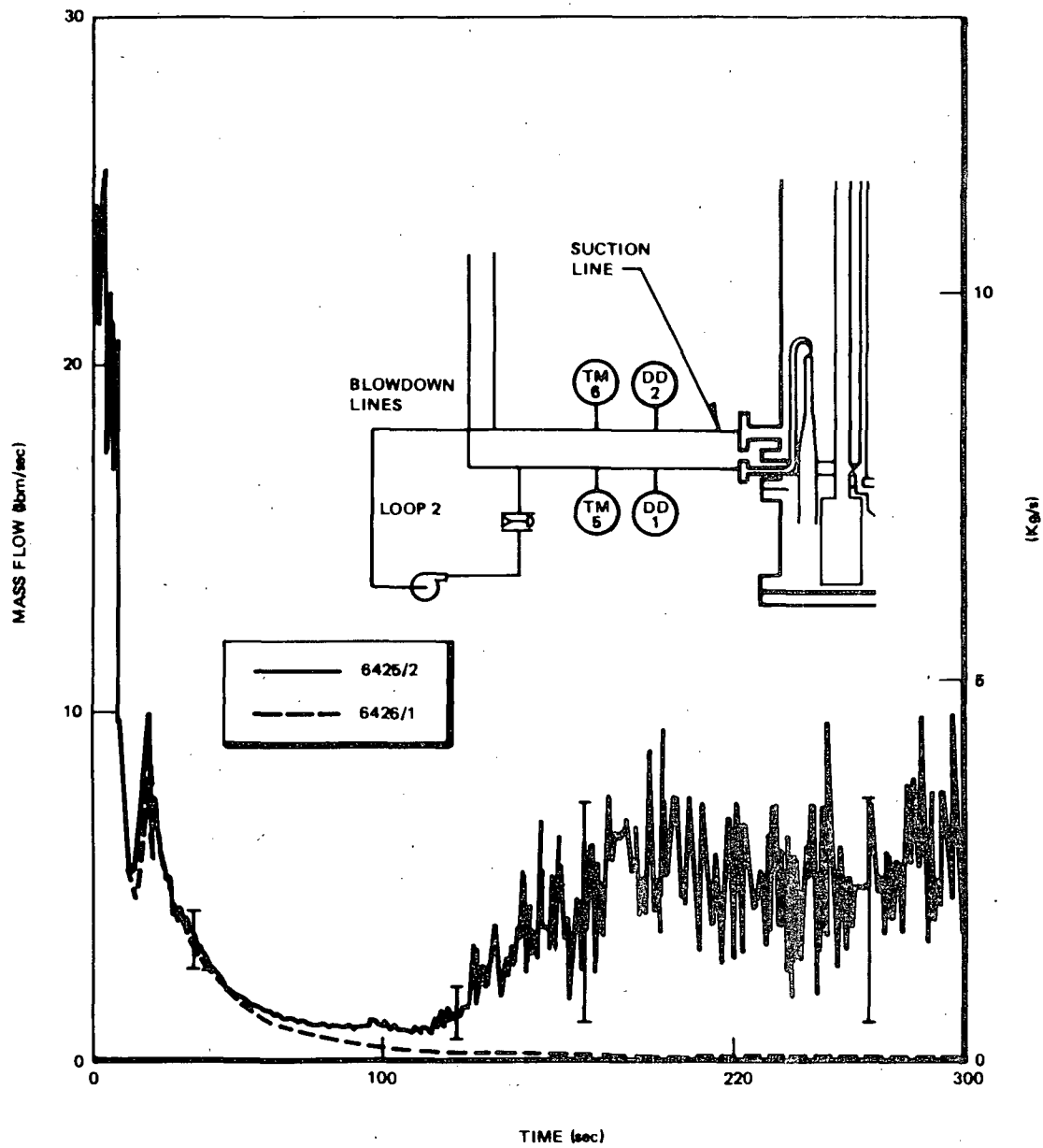


Figure 3-81a. Suction Line Break Flow from TM/DD Measurements for Average Power Tests with (6425/2) and without (6426/1) ECC

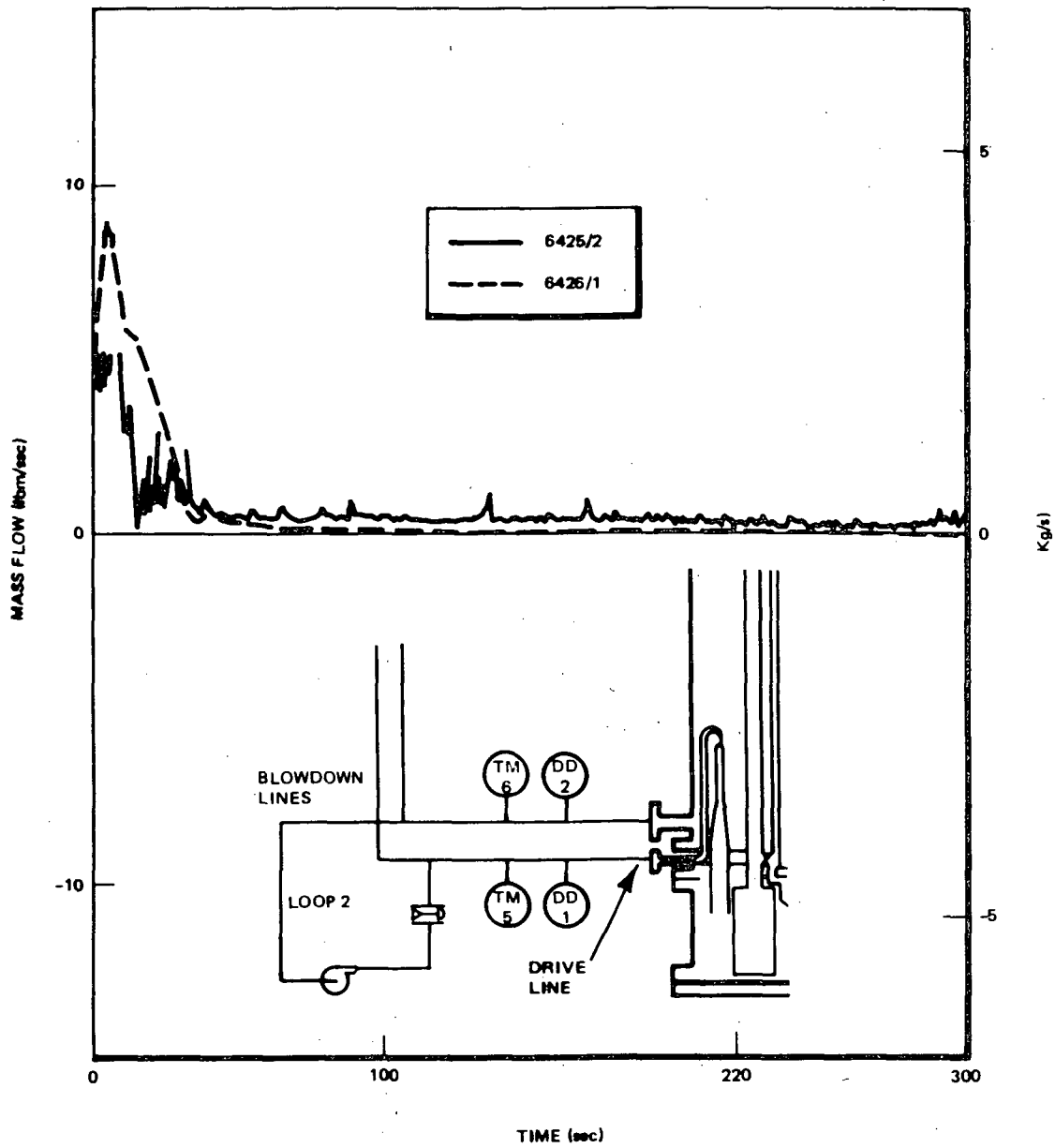


Figure 3-81b. Drive Line Break Flow from TM/DD Measurements for Average Power Tests with (6425/2) and without (6426/1) ECC

used in this method are informative, the mass flow rate determined from this method is seen to be higher than those shown in Figure 3-80 after 120 seconds. This is consistent with expectations because the accuracy of this method is influenced by the assumption of homogeneous flow for that period (Appendix H).

The blowdown nozzle method offers an additional means of determining the break flow through the suction line. The flows determined for the two tests are shown in Figure 3-82. The results are consistent with those found by other methods. The accuracy of this method also depends on the assumptions that are necessary for the calculation. One major assumption is that the flow through the nozzle is homogeneous equilibrium flow.

The suppression pool collection method was used to check its feasibility. Results are shown in Table H-2 of Appendix H. It is concluded that this method appears promising but could be improved by optimizing the instrumentation.

In summary, the system inventory method provides a reliable means of determining the system blowdown flow. The disadvantage of this method is that it entails considerable effort, and its accuracy is somewhat impaired when rapid mass flow occurs in the system. The combined turbine meter and drag disc measurements are informative and provide an excellent supplement to the system inventory method. These measurements were improved for the last three tests in TLTA 5A (Tests 6424, 6425, and 6426) by a careful selection of components. The results showed that these measurements can be improved to provide qualitative transient response of local break flow conditions. The blowdown nozzle method appears to be an excellent supplement to the turbinometer drag disc combination for the suction line. The advantage of this method is that the measurements are at the flow-limiting nozzle. The spool piece for the turbinometer and drag disc, on the other hand, is located in a large diameter* pipe downstream of the break. Consequently, the break flow through the suction line flashes and expands upstream of the spool piece and could affect the accuracy of the measurement.

*The inside diameter of the pipe is 2.88 inches (73.2mm). This is in contrast to the flow nozzle diameter of 0.743 inch (18.6mm).

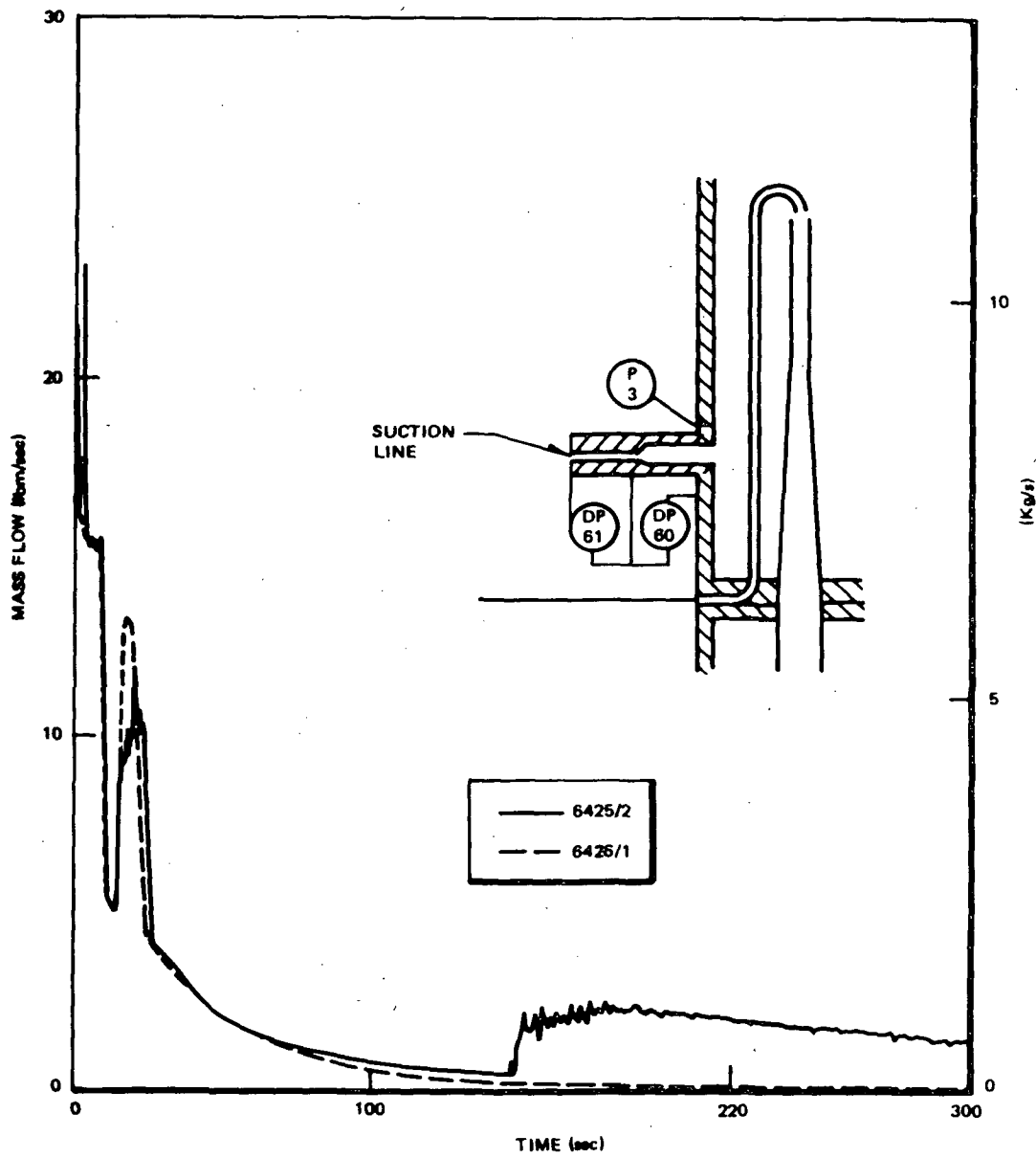


Figure 3-82. Suction Line Break Flow from Blowdown Nozzle DP Measurements for Average Power Test with (6425/2) and without (6426/1) ECC

3.4.4 Heat Transfer Coefficient

Heat transfer coefficients at three bundle locations have been determined for three tests in TLTA 5A. The heat transfer coefficients (HTC) were determined from the inverse heat conduction solution applied to the heater rods with HCODE (15). Thermocouple measurements and power supplied to the bundle were input to the program. Heat transfer coefficients were evaluated for the following three tests: average power, no ECC (Test 6421); average power, average ECC (Test 6422); and peak power, low ECC (Test 6423). Three bundle locations were evaluated, as shown in Figure 3-83. These are peak power locations, and the thermocouples chosen were among the ones showing the highest temperature responses.

The measured cladding temperatures and the heat transfer coefficients at the three locations for the test with average power and no ECC (Test 6421) are shown in Figure 3-84. At the early part of the transient, the bundle is well cooled, and the heat transfer coefficients range from 5600 to 8600 Btu/hr ft² °F, which are typical of nucleate boiling. As the bundle inventory decreases following the jet pump exit uncovering at ~35 seconds, the heat transfer coefficient drops sharply after the rods dry out and the bundle heats up. The heat transfer coefficient drops to the range of 20 to 50 Btu/hr ft² °F, then declines gradually for the remainder of the test. The bundle is cooled by steam updraft after ~60 seconds, so the heat transfer coefficient decreases as the flashing rate in the lower plenum decreases.

The temperatures and heat transfer coefficients for the test with average power, average ECC (Test 6422), are shown in Figure 3-85. The bundle is well cooled with heat transfer coefficients in the range of 8000 to 10,600 Btu/hr ft² °F until ~20 seconds when local dryout occurs. This local dryout, as pointed out in Subsection 3.2, rewets because of fluid redistribution within the bundle. The bundle heat-up begins at ~35 seconds when the vapor flow at the bundle inlet decreases and the bundle loses inventory. The minimum heat transfer coefficient reached is ~20 Btu/hr ft² °F. The heat transfer coefficients return to the order of 1000 Btu/hr ft² °F following ECC fluid injection when the bundle begins to re-flood and the rods rewet. The bundle becomes well cooled after reflooding completely at ~130 seconds (not shown in figure).

The measured temperatures and calculated heat transfer coefficients for the limiting test, peak power and low ECC at high temperature (Test 6423), are shown in Figure 3-86. The initial heat transfer coefficients are in the order of

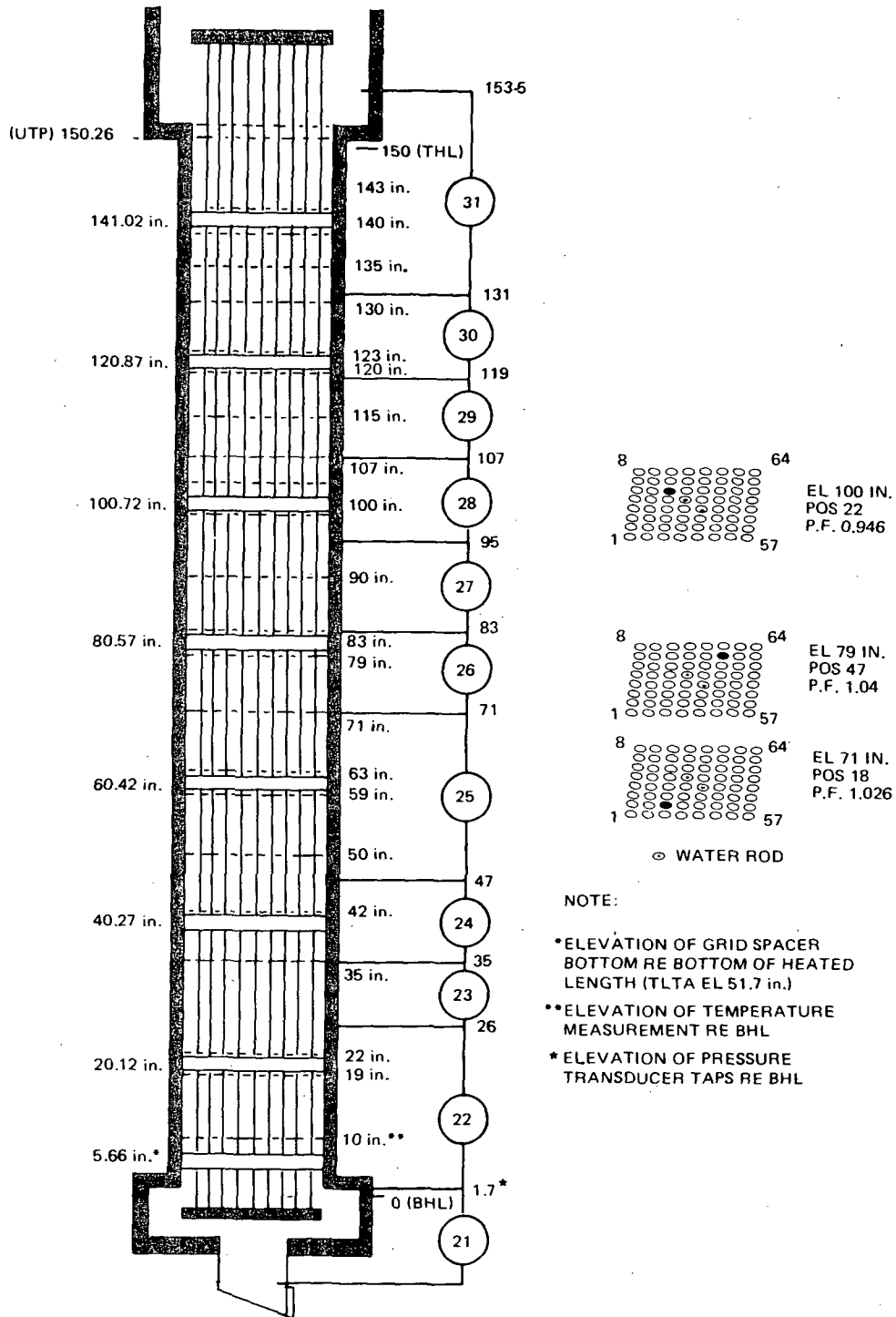
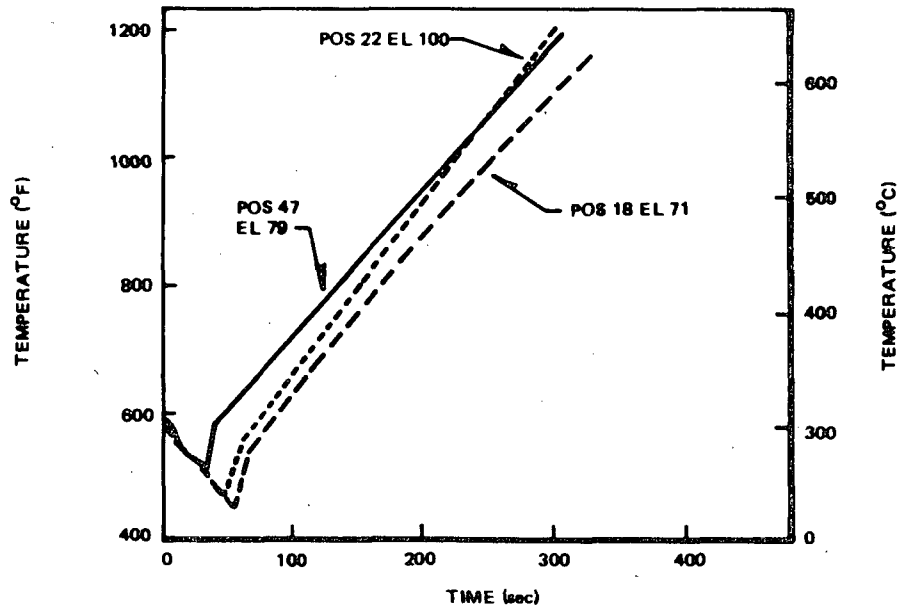
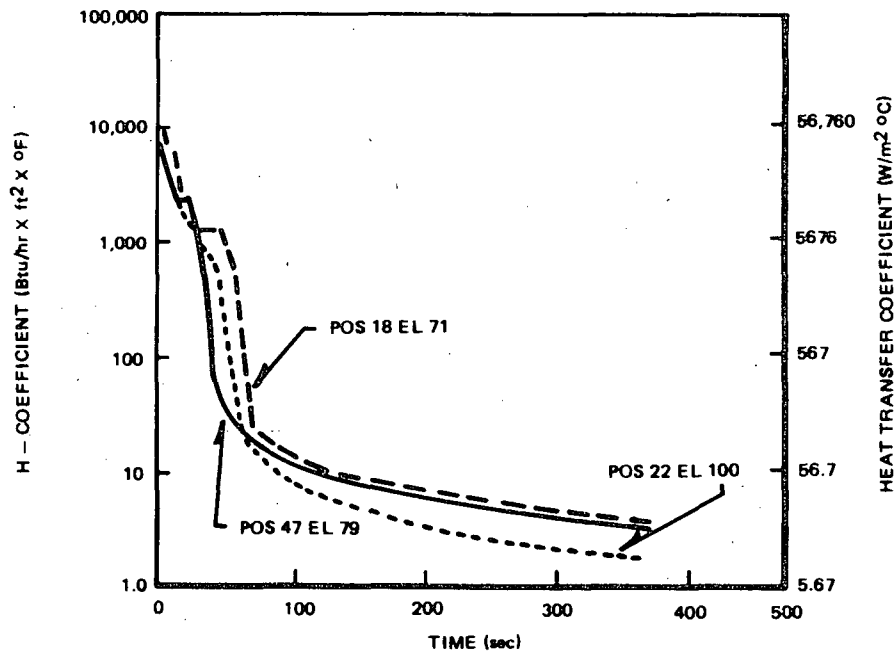


Figure 3-83. Selected Bundle Locations for Heat Transfer Coefficient Evaluation for TLTA 5A Tests

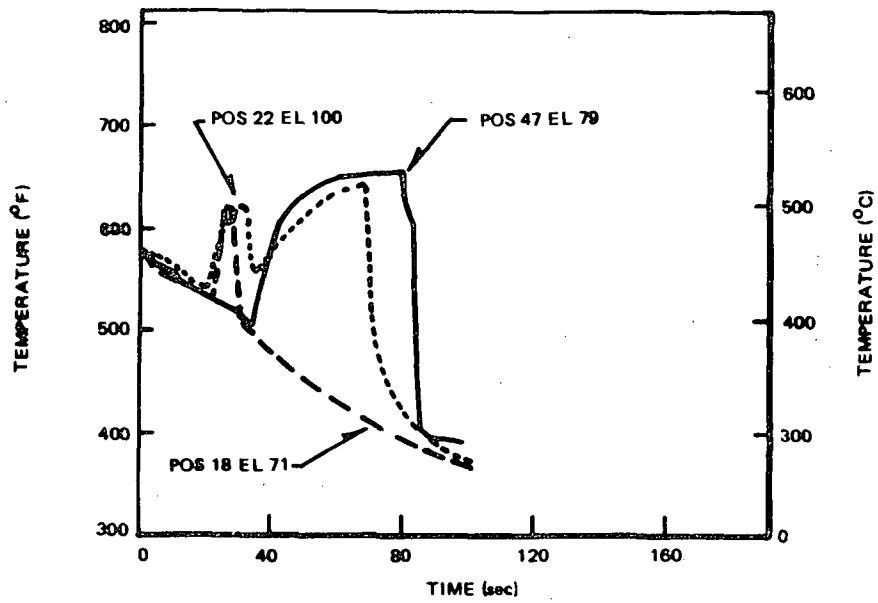


(a) CLADDING TEMPERATURE

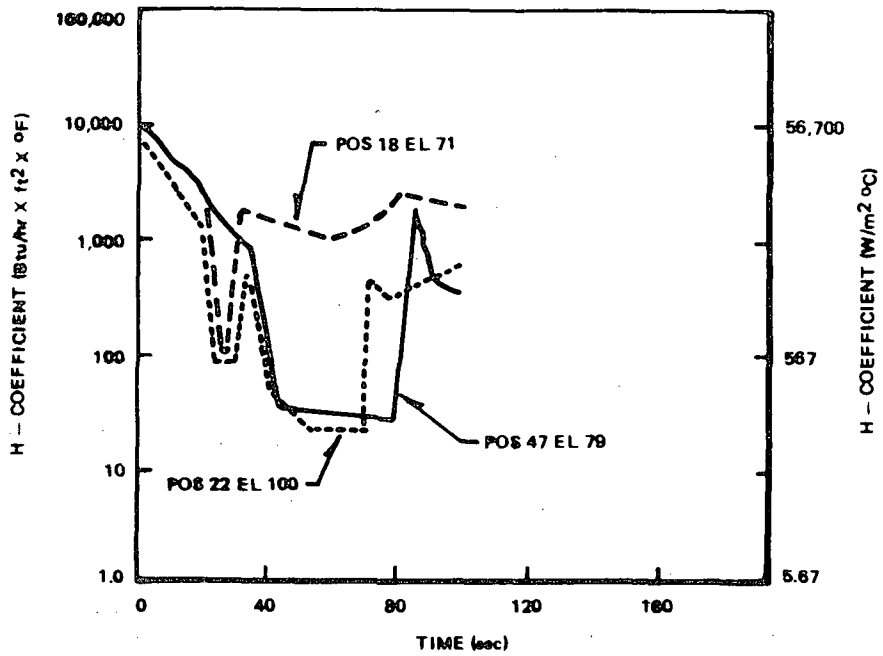


(b) HEAT TRANSFER COEFFICIENT

Figure 3-84. Measured Temperatures and Calculated Heat Transfer Coefficients for Test 6421 Run 2 (Avg. Power, No ECC)



(a) CLADDING TEMPERATURE



(b) HEAT TRANSFER COEFFICIENT

Figure 3-85. Measured Temperature and Calculated Heat Transfer Coefficient for Test 6422 Run 3 (Avg. Power, Avg. ECC)

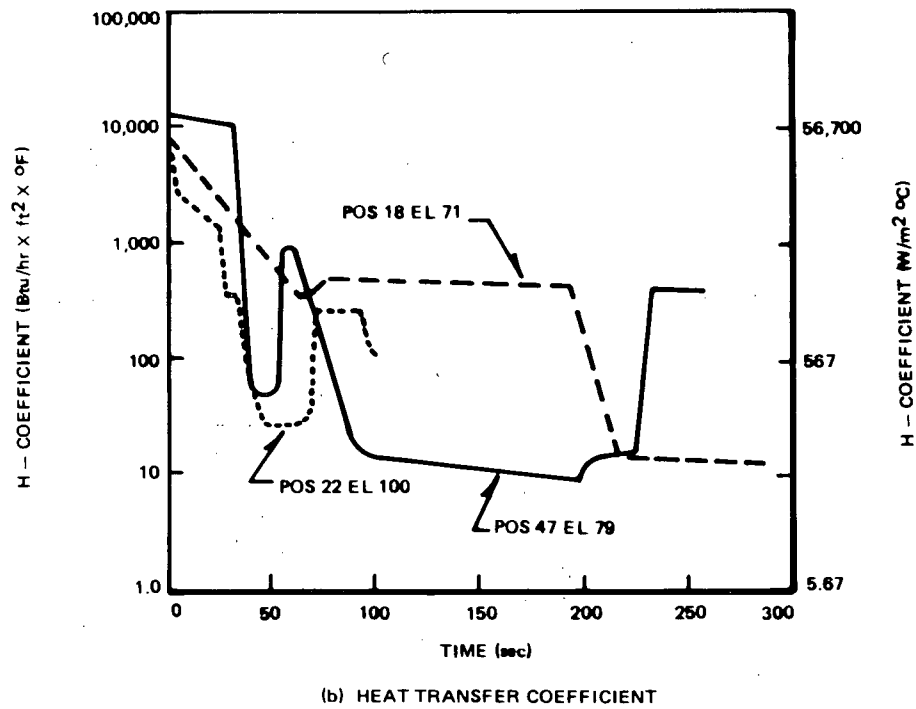
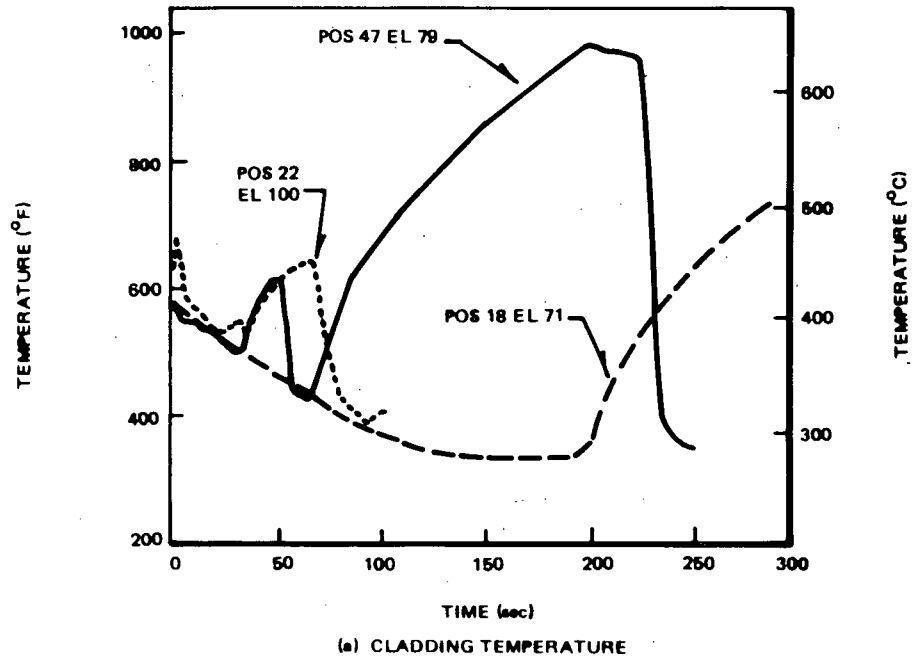


Figure 3-86. Measured Temperature and Calculated Heat Transfer Coefficient for Test 6423 Run 3 (Peak Power, Low Rate/High Temperature ECC)

10,000 Btu/hr ft² °F. Early boiling transition and rewet, as well as local dry-outs and rewet, are seen with the corresponding drops of the heat transfer coefficients. The effectiveness of the ECC injection in mitigating the bundle heat-up is evident from the plots of temperature and heat transfer coefficient. Sharp drops of temperature which are accompanied by sharp rises in heat transfer coefficient occur because of ECC fluid draining from the upper plenum into the bundle. The minimum heat transfer coefficient found in Figure 3-86b is 9 Btu/hr ft² °F. This value is higher than that found in the average power test with no ECC at a comparable time.

3.4.5 Comparison of Heat Transfer Coefficients

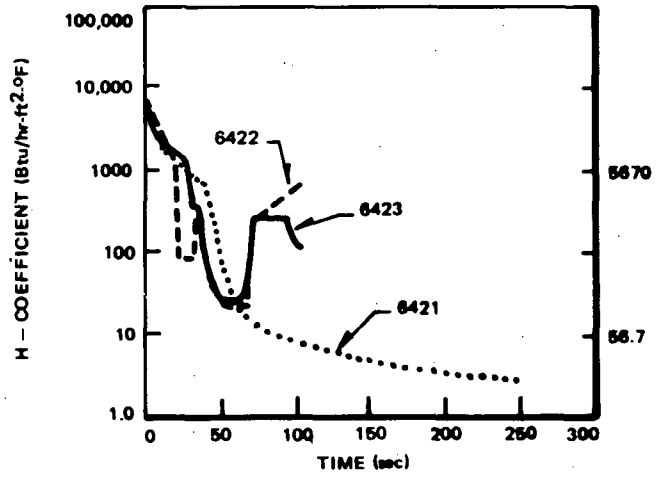
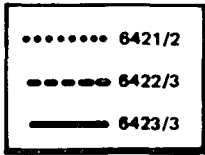
The heat transfer coefficients for each of the three locations and each of the three tests are compared in Figure 3-87. The heat transfer coefficient at 100 inches elevation (Figure 3-87c) are lower for the test with average ECC from ~30 to ~65 seconds because the bundle inventory is lower. As indicated in Subsection 3.3.1, the upper plenum inventory is higher for the test with ECC; therefore, the bundle level is lower so that the total head across the bundle/U.P. path is balanced by that across the jet pump path.

Results compared at other locations show the expected trend of generally better heat transfer with ECC injections. The effectiveness of ECC in mitigating bundle thermal response can be seen from Figures 3-87b and c in which the heat transfer coefficient of the limiting cases is higher than for the test having no ECC.

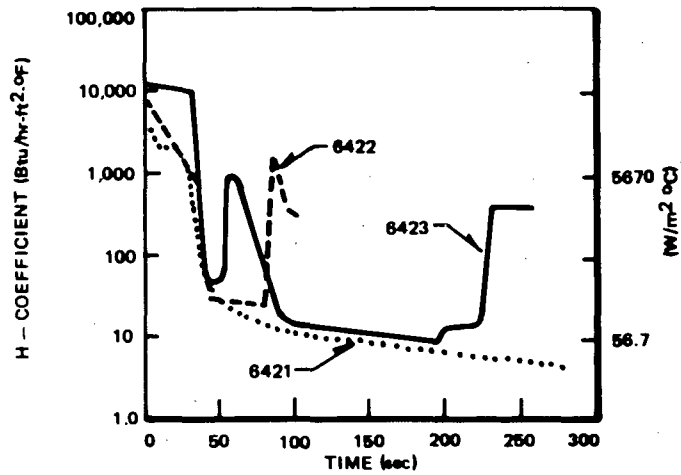
The preceding evaluations bring into focus the important observation that heat transfer during the early blowdown phase is sufficient to remove the stored energy of the bundle.* Even for peak power bundle, the early boiling transitions were quickly rewetted as the fluid redistributed inside the system and within the bundle. Other than the localized boiling transition in the peak power bundle, the majority of the rods in the bundle was kept well cooled following lower plenum flashing until jet pump exit exposure at ~35 seconds. These results of well cooled bundles are observed in the tests with and without ECC, as well as those in the scoping series and the 8 x 8 BDHT tests (2). Hence the observation that the bundle heat transfer was sufficient to remove the stored energy is consistent with the results presented in Subsection 3.3.1, which show that the system response was insensitive to bundle power.

*NOTE: The direct heaters used in TLTA are capable of accurately simulating both the stored energy and decay heat in the BWR fuel rod counterpart (8).

a. ELEVATION 100 in.
POSITION 22



b. ELEVATION 79 in.
POSITION 47



c. ELEVATION 71 in.
POSITION 18

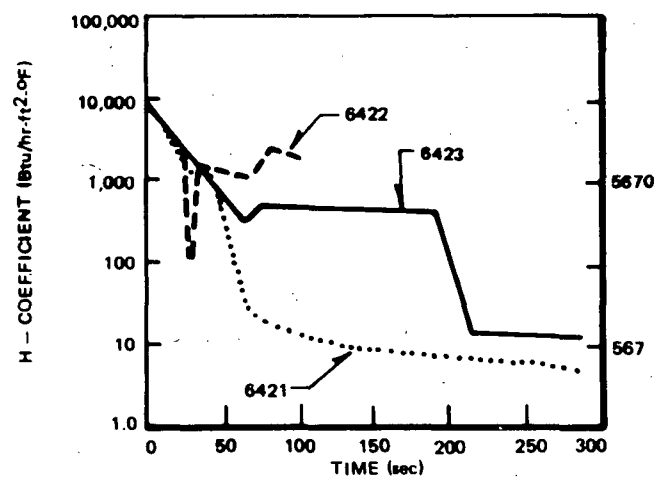


Figure 3-87. Comparison of Heat Transfer Coefficients for Tests 6421 Run 2 (Avg. Power, No ECC), 6422 Run 3 (Avg. Power, Avg. ECC), 6423 Run 3 (Peak Power, Low Rate/High Temperature ECC)

3.4.6 Local Flow Conditions

Local flow conditions for the peak power, low-flow/high-temperature ECC test (6423/3) were evaluated using MAYU04 (16). MAYU04 is a computer code for one-dimensional, single-channel analysis. It calculates hydraulic conditions along the length of the bundle and provides heat transfer information at various elevations for each rod group. In this study, the rods were grouped together by common peaking factors, and an average local peaking factor was found for each rod group.

Inputs into MAYU04 consisted of geometric information describing the core region, power characteristics, material properties, core inlet flow, core inlet enthalpy or void fraction, system pressure, and bundle power. The core inlet mass flux is shown in Figure 3-88. The core inlet flow which determines the inlet mass flux consists of the SEO flow from the lower plenum and the flow from the bypass leakage. The bypass flow was determined from DP measurements. The SEO flow was found by using the method described in Appendix C-4 for the first 8 seconds. During the window period (from jet pump suction uncover to lower plenum flashing), the SEO flow is assumed negligible; the net core inlet flow is due solely to the bypass leakage flow. During lower plenum flashing, the SEO flow was found from DP40 measurements. The SEO flow is again assumed negligible in the post-lower plenum flashing period.

The inlet enthalpy for the first 13 seconds was determined from the lower plenum pressure and temperature measurements. During lower plenum flashing, the void fraction of Node 3 in the lower plenum is input. After lower plenum flashing, the void fraction of the bottom bypass node is input for determining the inlet enthalpy.

The system pressure was found by taking the average of the lower plenum pressure minus the core inlet pressure drop and the upper plenum pressure. The bundle power was input directly from data.

The local void fraction and mass flux based on MAYU04 for the first 30 seconds of the test are shown in Figures 3-89 and 3-90 for three elevations. It is seen that the mass fluxes at the three elevations decrease in the early part of the window period. When the two-phase level drops below the 100-in. elevation, the local mass flux reaches a slightly negative value for downward liquid flow (counter current flow) but then quickly reverts to cocurrent upward flow with a highly-voided mixture. The local mass fluxes at the other two elevations

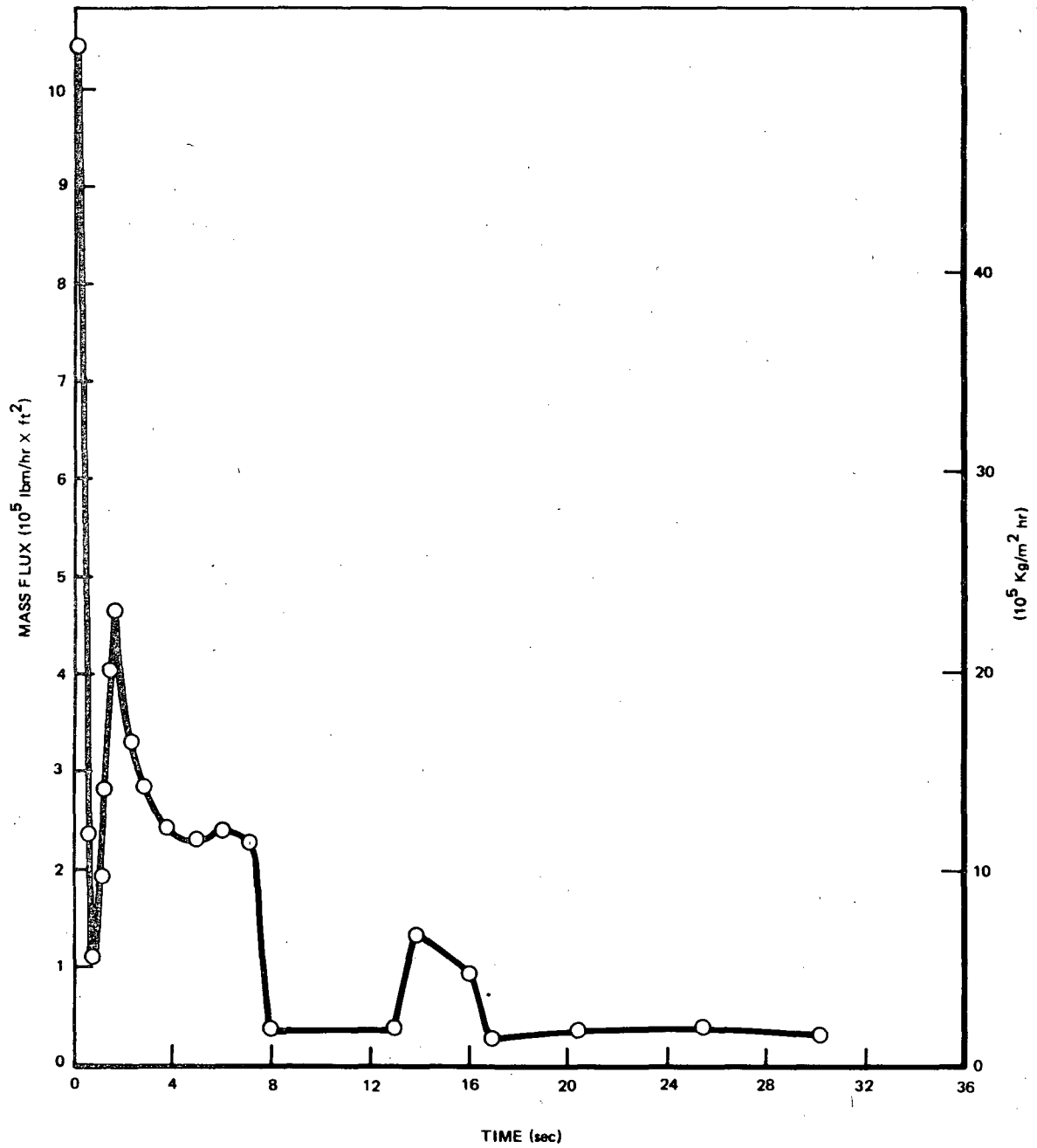


Figure 3-88. Core Inlet Mass Flux Used for MAYU Calculation of Test 6423 Run 3 Local Conditions

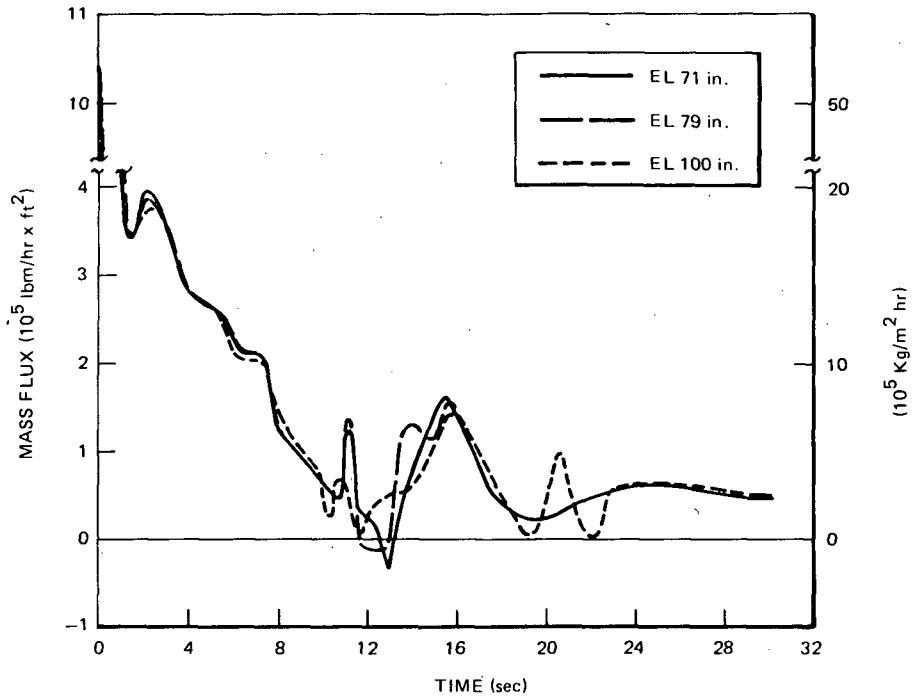


Figure 3-89. Local Mass Flux Determined by MAYU for Selected Elevations of Peak Power Low ECC Test (6423/3)

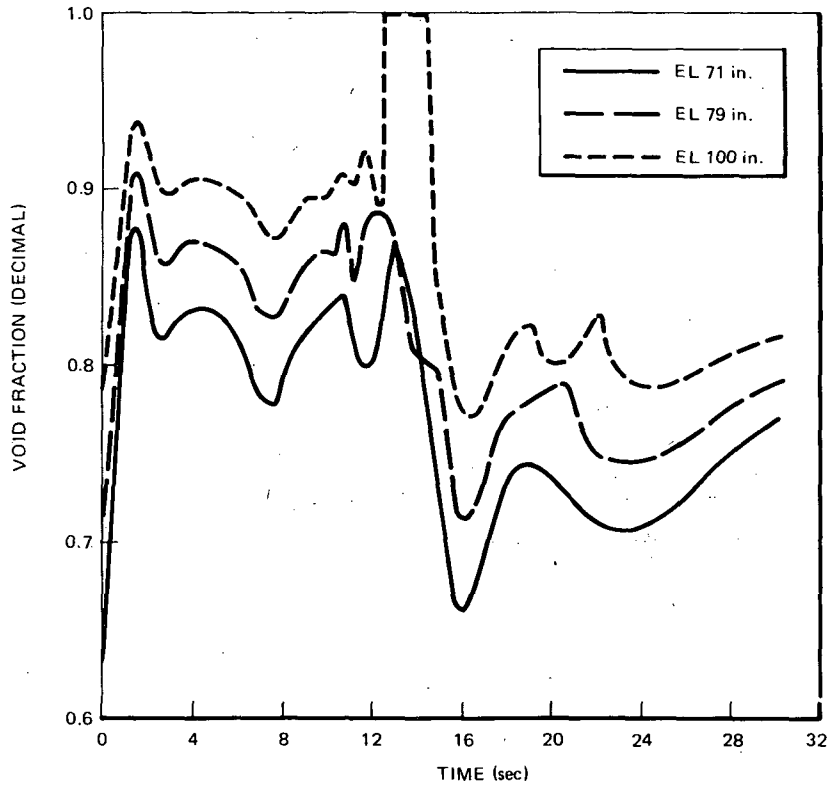


Figure 3-90. Local Void Fraction Determined by MAYU at Selected Elevations for Peak Power Low ECC Test (6423/3)

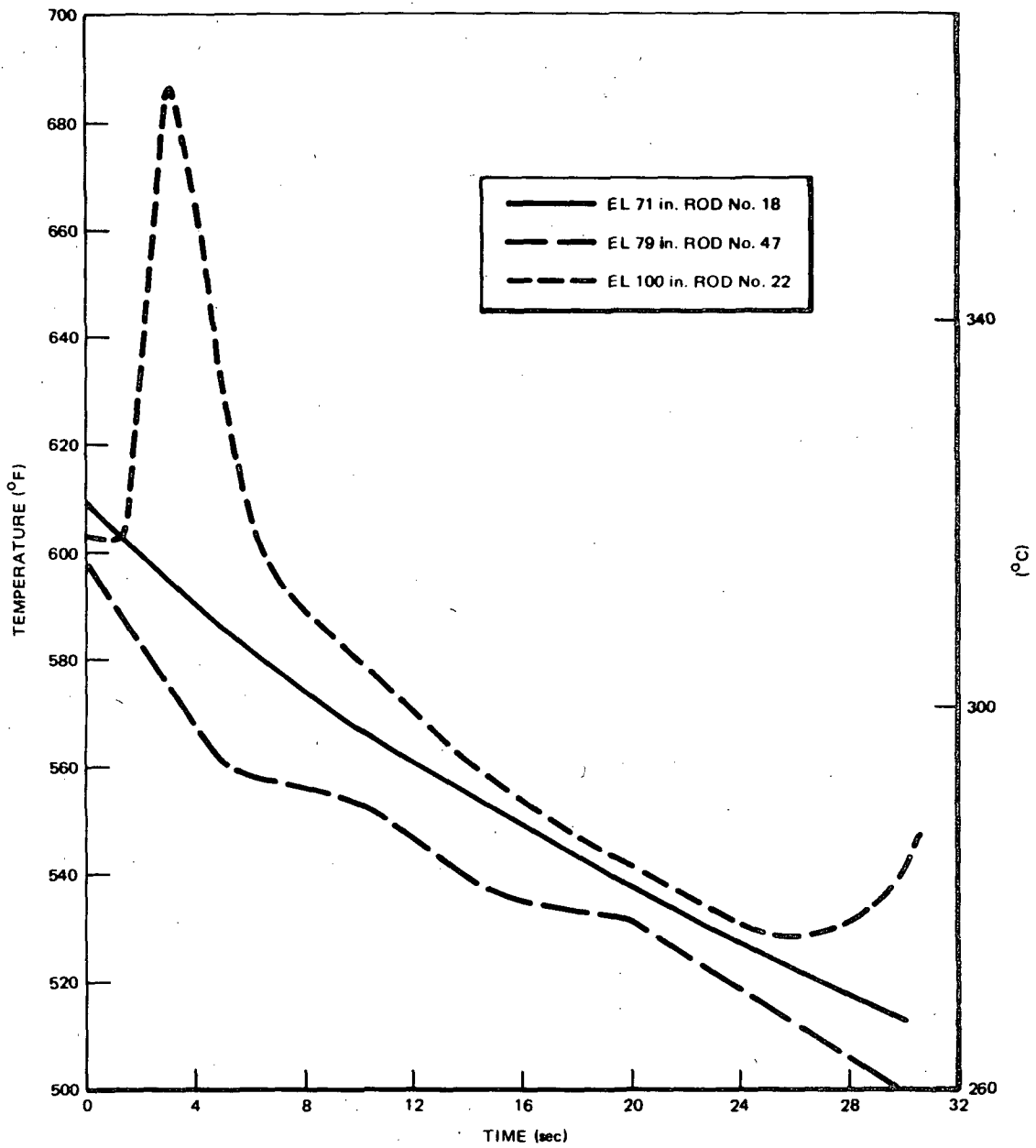


Figure 3-91. Measured Inside Cladding Temperatures at Selected Elevations for Peak Power, Low ECC Test (6423/3)

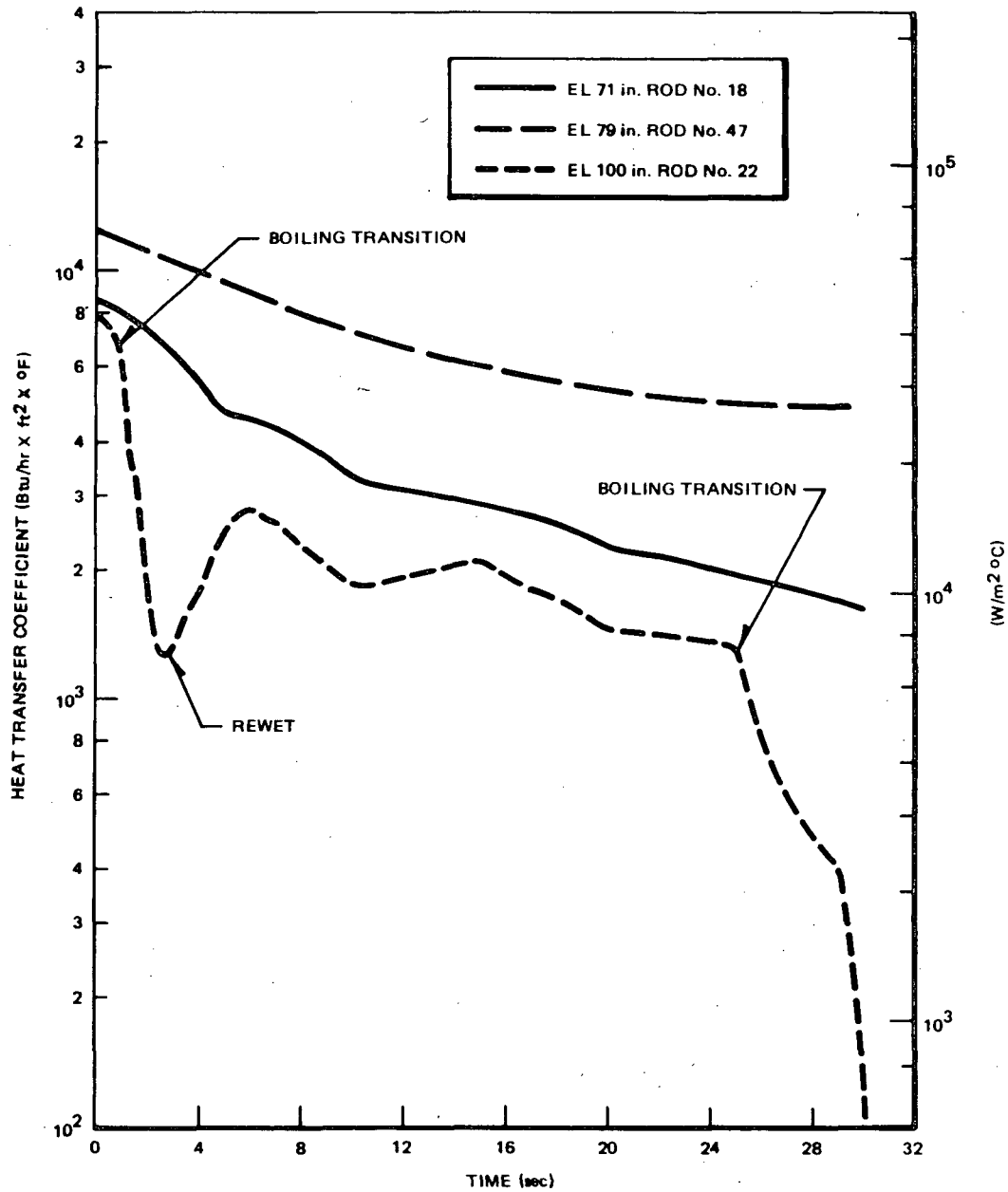


Figure 3-92. HCODE Determined Heat Transfer Coefficients at Selected Elevations for Peak Power, Low ECC Test (6423/3)

(71 and 79 inches) continue to show liquid down flow until lower plenum flashing. The mass flux at each elevation remains in cocurrent upflow after lower plenum flashing because the bundle is fed by fluid from the bypass region and by continued flashing within the bundle.

The void fraction at each elevation is shown in Figure 3-90. The void fraction derived in MAYU04 is based on the work of G.E. Dix (17). The distribution coefficient and drift velocity assumed are: $C_o = 1$, $V_{gj} = 1$ ft/sec. The void fraction at the 100-in elevation reaches unity as the mixture level drops below this elevation at ~12 seconds.

The inside cladding temperatures and the heat transfer coefficients for these three elevations are shown in Figures 3-91 and 3-92 in the same time scale for easy comparison with the hydraulic conditions. The longer time plots for these values have been presented in the preceding section.

3.4.7 Comparison of Heat Transfer Coefficients (Prediction vs. Data)

Current BWR/LOCA Elevation Models (EM) had been used to predict TLTA results of the BDHT program, and the comparison between the calculated values and data was reported (18). The EM was found to contain a number of heat transfer modeling assumptions that could be improved upon in light of test data. Among the significant ones that could be improved upon are: instantaneous transition from nucleate boiling to film boiling, forced boiling transition during the window period, and the omission of rewet and steam cooling heat transfer. As a result of these assumptions (which could be improved for more realistic modeling), the predicted cladding temperatures are substantially (over 1000°F [538°C]) higher than measured temperatures. The difference in temperatures is attributable to the lower heat transfer coefficients determined by the EM.

The heat transfer coefficients at 100 inches (2538 mm) for the three tests are compared with those determined with the EM for the average power, average ECC test. These HTC's were derived from measured boundary conditions across the bundle, including system pressure, inlet flow and enthalpy, and bundle two-phase mixture level. Timing of the events that trigger the application of a prescribed correlation or value in the EM are determined from the test results. The correspondence of events and values are as follows:

- Initial nucleate boiling; HTC from Jens-Lottes correlation.
- Boiling Transition; HTC from Dougall-Roshenow film boiling correlation.

- Window period (JP suction uncover + 1.0 second); HTC from Ellion pool boiling correlation.
- Lower plenum flashing; Dougall-Roshenow film boiling correlation.
- Post-lower plenum flashing dryout; HTC = 0
- Low-pressure ECCS reaches rated flow (system pressure ~127 psia); heat transfer coefficient between 1.5 and 3.5 Btu/hr-ft² depending on rod position.
- Bundle reflood (in EM/licensing calculation timing determined, assuming lower plenum refills first); HTC = 25 Btu/Hr-ft² °F.

The timing of the above events as determined from the data of Test 6422 Run 3 are:

Nucleate boiling assumed until jet pump suction uncover (8.0 sec).
 Lower plenum flashing at 13.7 sec.
 Bundle dryout at 100 inches EL at 34 sec.
 System pressure of 127 psia at 112 sec.
 Bundle reflood (without completely refilling lower plenum) at 138 sec.

Figure 3-93 shows a comparison between HTCs determined from the methodology used in the EM and those from data.* The comparison shows that the HTCs that are determined from data remain substantially higher than those from the EM, even for the test without the benefit of ECC.

*NOTE: The HTCs from data are shown up to only 100 seconds because, in tests with ECC injection, the HTC reached the minimum value and increased rapidly after ~100 seconds.

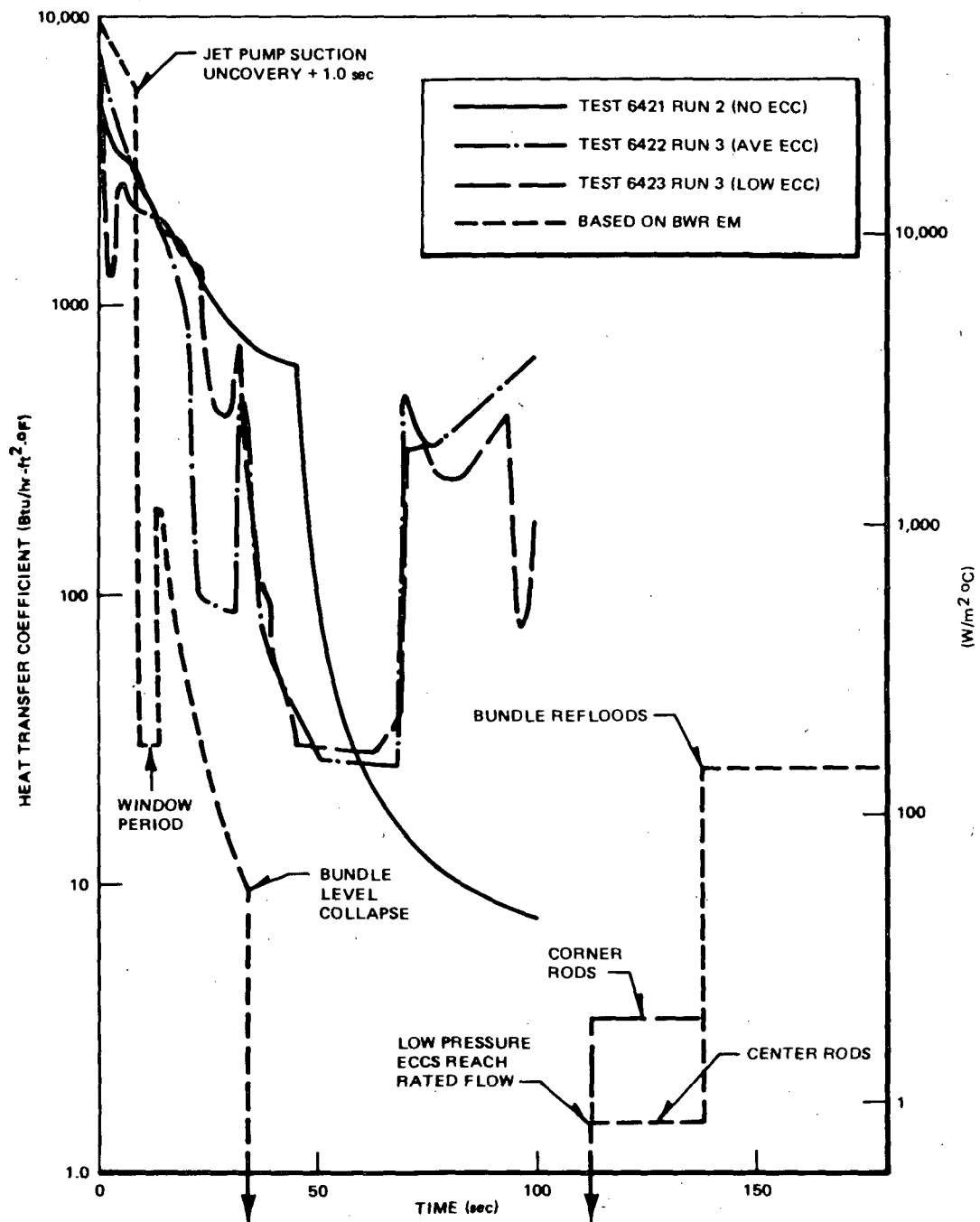


Figure 3-93. Comparison of Heat Transfer Coefficients between Those Determined from Data and Those from EM Methodology

Section 4
UTILIZATION OF RESULTS

The results obtained from the BD/ECC 1A Program have been described and evaluated. These results contribute to the understanding of the important phenomena occurring in a BWR system during a design basis loss-of-coolant accident. This understanding contributes to defining the large safety margin in current design models and to guiding the development of the best-estimate models. Ultimately, these results will be used to assess the best-estimate BWR-TRAC model. The work will be conducted as part of the BWR Refill/Reflood Program (19). Because the results were obtained from an integral system whose thermal hydraulic performance was designed to represent a BWR, these data comparisons with the best-estimate models will enhance confidence for their application to a BWR system.

Section 5

SUMMARY AND CONCLUSIONS

Test results from the BD/ECC 1A program enable the effects of subcooled ECC fluid injection on integral system response to be defined. Significant results are summarized below. Also included below are conclusions drawn from evaluation and interpretation of results from this program.

- a. The bundle inventory (liquid mass) is prevented from completely draining early in the transient by counter-current flow limiting condition at the inlet. This CCFL condition prevails until the lower plenum mixture level drops to the jet pump exit at ~35 seconds. Before that time, steam generated from lower plenum flashing maintains the CCFL condition at the bundle inlet and holds up the inventory.
- b. Because of inventory retention of up to 35 seconds, the rods are maintained well cooled during this period, and the bundle dissipates almost all the stored energy. A few rods in the peak power bundle that enter into film boiling are quickly rewetted by the redistribution of inventory within the system following lower plenum flashing.
- c. The subcooled ECC injections (based on the nominal system performance and the limiting single failure criterion availability assumption) have sufficient capacity to condense all the steam generated within the core region (bundle, bypass, guide tube, and lower plenum) and to break down CCFL at the top of the bundle.
- d. The bypass region refills rapidly as the subcooled ECC fluid condenses the steam upflow, breaks down CCFL at the bypass outlet, and thereby allows parts of the upper plenum inventory to drain into the region.
- e. The bundle refloods following bypass region refill. The bundle initially refloods from below as fluid from the bypass is available to begin reflooding the bundle through the leakage holes. Later, CCFL breaks down at the upper tie plate to quicken the process and leads to rapid quenching of the bundle.
- f. CCFL at the bundle inlet contributes to rapid bundle reflood prior to complete refilling of lower plenum.
- g. The upper plenum remains empty after CCFL breakdown, with the bulk of the ECC injection passing through the bundle and bypass regions.
- h. The ECCS is effective in mitigating the cladding heatup even before the bundle refloods, as the steam volumetric flow at the bundle outlet is not high enough (in relation to CCFL characteristics) to prevent ECC water from draining into the bundle.

- i. The heatup response of the bundle is rather mild. The maximum cladding temperature for the central average power bundle receiving an average amount of core spray is less than 700°F (310°C). The maximum for a comparable peak power bundle is less than 1000°F (538°C). The low temperatures are attributable to: (1) dry-out delay caused by CCFL conditions at bundle inlet early in the transient; (2) rewetting of dried-out rods and enhanced cooling caused by core spray, and (3) complete quenching of bundle because of early reflood.
- j. The bundle power variation shows negligible effect on the system response for tests with average ECC spray rates. The bundles reflood at about the same time (~130 seconds). The maximum cladding temperature, however, is slightly higher for the peak power test, as expected.
- k. The improved simulation of the bypass leakage path in the TLTA 5A configuration has significant effects on the system response. The leakage path allows the bypass inventory to reflood the bundle from below as the CCFL condition at the bundle inlet restricts the drainage of fluid into the lower plenum.
- l. The injection of ECC fluid contributes to decreasing the depressurization within the system because of drainage of ECC fluid through the core region, into the lower plenum, and out through the break. The combination of injected fluid and lower volumetric discharge (caused by higher fluid density) retards the depressurization rate.
- m. The effectiveness of the ECC injection in mitigating the thermal transient is demonstrated by the maximum cladding temperature for the test with peak power but minimum core spray flow injected at high temperature. This temperature is less than 1000°F (538°C), for a transient of 400 seconds. Without ECC injection, the average power test reaches a temperature of ~1400°F (760°C) when the power was terminated at 294 seconds.
- n. Results from the small break tests indicate that the system response and governing phenomena are similar to those observed from the large break tests, except that the timing of key events are stretched out in time.
- o. Test results from this program provide a physical understanding of the LOCA phenomena in the BWR system simulator. This understanding, along with the data, is useful in assessing advanced best-estimate codes for BWR systems.

Section 6

REFERENCES

1. R. Muralidharan, BWR Blowdown Heat Transfer Final Report, General Electric Company, February 1976 (GEAP-21214).
2. W. S. Hwang and B. S. Schneidman, BWR Blowdown/Emergency Core Cooling Program - 64-Rod Bundle Blowdown Heat Transfer (8x8 BDHT), Final Report, General Electric Company, September 1978 (GEAP-NUREG-23977) (EPRI NP-1720).
3. W. S. Hwang, BWR Small Break Simulation Tests With and Without Degraded ECC Systems - BWR Blowdown/Emergency Core Cooling Program, General Electric Company, February 1981 (GEAP-24963, NUREG/CR-2230, EPRI-NP-1782).
4. D. S. Seely and R. Muralidharan, BWR Low Flow Bundle Uncovery Tests and Analysis - BWR Blowdown/Emergency Core Cooling Program, General Electric Company, February 1981 (GEAP-24964, NUREG/CR-2231, EPRI-NP-1781).
5. W. J. Letzring, BWR Blowdown/Emergency Core Cooling Program, Preliminary Facility Description Report for the BD/ECC 1A Test Phase, General Electric Company, December 1977 (GEAP-23592).
6. C. G. Hayes, ECC System Calibration and Performance Verification, General Electric Company, July 1978 (NEDG-21956).
7. BWR Blowdown/Emergency Core Cooling 14th Quarterly Progress Report, General Electric Company, Vol. 1, No. 1, August 1979 (GEAP-21304-14).
8. R. J. Muzzy et al., Task B Topical Report: Evaluation of Direct Heaters and Hydrodynamic Measurement Techniques under Simulated LOCA Conditions in a Single Loop Test Apparatus, General Electric Company, June 1974 (GEAP-20512).
9. BWR BDHT 11th Quarterly Progress Report, January 1 - March 31, 1975, General Electric Company, April 1975 (GEAP-13317-11).
10. D. D. Jones, Test Report, TLTA Components CCFL Tests, General Electric Company, December 1977 (NEDG-23732).
11. J. C. Wood and A. F. Morrison, BWR Blowdown/Emergency Core Cooling Program - 64-Rod Bundle Core Spray Interaction (BD/ECC 1A) Test Plan, General Electric Company, February 1978 (GEAP-21638).
12. BWR Blowdown/Emergency Core Cooling, 15th Quarterly Progress Report, General Electric Company, February 1980 (GEAP-21304-15).
13. D. G. Schumacher, BWR Refill - Reflood Program Task 4.4 - CCFL/Refill System Effects Tests (30° Sector) Experimental Task Plan, General Electric Company, April 1981 (GEAP-24893).

14. D. D. Jones, Subcooled Counter-Current Flow Limitation Characteristics of the Upper Region of a BWR Fuel Bundle, General Electric Company, July 1977 (NEDG-23549).
15. R. J. Muzzy, J. H. Avila, and D. E. Root, Topical Report: Determination of Transient Heat Transfer Coefficients and the Resulting Surface Heat Flux from Internal Temperature Measurements, January 1975 (GEAP-20731).
16. W. C. Punches, MAYU04: A Method to Evaluate Transient Thermal Hydraulic Conditions in Rod Bundles, General Electric Company, March 1977 (GEAP-23517).
17. G. E. Dix, Vapor Void Fraction for Forced Convection with Subcooled Boiling at Low Flow Rates, General Electric Company, November 1971 (NEDO-10491).
18. L. S. Lee, G. W. Burnette, R. Muralidharan, and B. Schneidman, Comparison of LOCA Evaluation Models Predicted with Blowdown Heat Results, General Electric Company, March 1978 (NEDO-21836).
19. J. A. Findlay and G. L. Sozzi, BWR Refill-Reflood Program Task 4.8 - Model Qualification Task Plan, General Electric Company, January 1981 (GEAP-24898).

Appendix A

WORK SCOPE FOR BD/ECC PROGRAM - CONTRACT NO. NRC-04-76-215

A-1. OVERALL PURPOSE

The purposes of the EPRI/NRC/GE Integral Blowdown/Emergency Core Cooling, BD/ECC, test program are to:

- a. obtain and evaluate basic BD/ECC data from test system configurations which have calculated performance characteristics similar to a BWR with 8x8 fuel bundles during a hypothetical LOCA; and
- b. determine the degree to which models for BWR system and fuel bundles describe the observed phenomena, and, as necessary, develop improved models which are generally useful in improved LOCA analysis methods.

A-2. SPECIFIC OBJECTIVES

The specific objectives of the integral BD/ECC interaction test program are:

- a. Scaling Analysis: evaluate and document the scaling basis of the TLTA in the configurations selected for BD/ECC interaction tests as compared to reference BWR designs.
- b. 7x7 Counter-Current-Flow-Limited (CCFL) Flooding Characteristics: conduct CCFL flooding characteristic tests of the present TLTA bundle geometry to establish the need, or lack thereof, to modify the present test apparatus design for the initial BD/ECC interaction experiments.
- c. 8x8 Blowdown Heat Transfer Tests: conduct 8x8 BDHT tests for comparison with 7x7 BDHT data and to serve as a BDHT baseline for BD/ECC interaction experiments.
- d. BD/ECC Interaction Tests: evaluate system response and heat transfer; evaluate effectiveness of ECC during the blowdown period and the period extending well beyond the initial flow coastdown and lower plenum "flashing" periods of the calculated BWR-LOCA in one or more system configurations.
- e. Alternate Power Shape BD/ECC: determine the effects of axial power shape on the system response and bundle heat transfer behavior during the calculated BWR LOCA.
- f. Non-Jet Pump Plant BD/ECC: investigate the ECC interaction with the system during blowdown in a representative non-jet pump test system configuration.

- g. Reporting of Data: report all data (including pertinent error bands) in conventional parametric form suitable for correlation by others.
- h. Model Development: develop, verify, and document an improved bundle thermal-hydraulic model that can be incorporated into analyses of BWR LOCAs.
- i. Application of Data: specify how General Electric intends to use the data to qualify the degree of conservativeness of BWR LOCA evaluation models.

A-3. SCOPE

A-3.1 Task AA - Program Planning and Administration

1. General Electric will prepare a preliminary BD/ECC Program plan that elaborates on the means for meeting the program objectives. The program plan will include, but not be limited to: (a) BWR configurations and LOCA conditions to be tested; (b) test parameters and their ranges; (c) updated conceptual designs and testing strategies; (d) an outline of model development and verification activities; and (e) the method of relating previous 7x7 rod bundle data to the 8x8 rod bundle data. Sufficient discussion of the above items will be included to substantiate the basis for the preliminary program plan. The program plan will also include an updated schedule, a proposed data verification and reporting plan, and the planned utilization of data by General Electric to assess current BWR LOCA evaluation methods.

The preliminary program plan will be provided for EPRI and NRC review, comment, and approval on an agreed-upon time schedule. If comments are not supplied to General Electric by NRC or EPRI within the agreed schedule, General Electric may proceed as proposed.

2. Following mutual agreement on the results from Task AA-1 and on the appropriate phase of Tasks BB and CC-1, General Electric will prepare a detailed test plan for each major testing phase. Each detailed test plan will include the test objectives, test phase description, test matrices, parameter ranges and reasons for selection, test execution plan, planned utilization of the data, and the planned schedule for completing that phase.

The preliminary test plans will be provided for EPRI and NRC review, comment, and approval on an agreed-upon time schedule. If comments are not supplied to General Electric by EPRI or NRC within the agreed schedule, General Electric may proceed as proposed.

A-3.2 Task BB - Heater Evaluation

1. Perform appropriate analysis relating electrical heater performance to predicted nuclear fuel rod temperature performance during an ECC transient. This analysis will describe the method of programming initial and decaying electrical power to produce representative BWR LOCA thermal response and will describe how differences in thermal properties are accounted for in the electrical simulations.

2. Evaluate the need for tests to demonstrate the validity of the above analyses. The heater evaluation, including documentation of the above item, will be provided by EPRI and NRC review, comment, and approval on an agreed-upon time schedule. If comments are not supplied to General Electric by EPRI or NRC within the agreed schedule, General Electric may proceed as proposed.

A-3.3 Task CC - Test Facility Design and Fabrication

1. Scaling and design analyses to define each system configuration will be performed and documented. Particular attention will be given to attaining a real-time simulation of calculated BWR system and fuel bundle thermal-hydraulic LOCA response.

Design trade-off and scaling compromise studies will be performed to establish the final scaling basis to be used for design and operation of each configuration. Appropriate analytical methods including, but not necessarily limited to, those used for BWR performance analyses will be applied to obtain best-estimate performance predictions of the BWR reference plants and the test system configurations. These pretest predictions will include time-to-boiling transition (BT), lower plenum flashing effects, post-BT heat transfer, and response to ECCS operation. Differences in anticipated dynamic response of the test apparatus as compared to a BWR will be identified by appropriate analysis. Measurement requirements to obtain program objectives, including type, number, location, and accuracy of instruments will be specified, and an instrumentation plan to meet these requirements will be developed. A preliminary facility description including documentation of the above items, presenting the technical basis for the preliminary design, will be provided for EPRI and NRC review; comment, and approval on an agreed-upon time schedule. If comments are not supplied to General Electric by EPRI or NRC within the agreed schedule, General Electric may proceed as proposed.

2. Upon resolution of comments, if any, the contractor will provide a revised facility description as necessary.

The final design and procurement of necessary material for each configuration will be completed, and the system will be prepared for calibration testing.

A-3.4 Task DD - Test Section Design and Fabrication

Upon completion of Task BB and an evaluation of the BDHT test section counter-current-flow-limiting (CCFL) characteristics, General Electric will complete the design, procurement, and assembly of the 8x8 rod test sections for BD/ECC testing. The test section designs will be documented in the appropriate facility description reports.

A-3.5 Task EE - System Startup Tests

Upon assembly of each configuration, conduct performance and flow calibration tests. Perform hydrostatic, hydrodynamic, and transient startup tests for each configuration to establish system operational characteristics including adequacy of heater and instrumentation response. Conduct steady-state and/or transient separate effects tests necessary to provide the basis for interpretation of BD/ECC experimental results.

A-3.6 Task FF - BD/ECC Interaction Tests

For each configuration, perform tests as detailed in Tasks AA-2 and CC-2.

A-3.7 Task GG - Data Evaluation and Model Development

1. Analyze and document the as-built system performance characteristics based on system startup tests. Evaluate the test apparatus design for meeting program objectives on the basis of system startup performance tests. Determine what, if any, minor modification and/or adjustments should be made on the test facility, and update the predictions of system response as appropriate.
2. Upon completion of a specified test series, reduce, evaluate, and report the experimental data. Provide the experimental basis for confirming or modifying the assumptions and models used in LOCA evaluations such as the onset of boiling transition (BT), the subsequent heat transfer rates, effects of lower plenum flashing on core thermal response, and the effects of ECC on core and system response. Document the data obtained, the storage format, and how they can be accessed by others.
3. As appropriate, develop and document improved analytical models, which can be incorporated into best-estimate analyses of BWR LOCAs. This will include, but not be limited to, the development of a self-standing transient thermal-hydraulic model for the prediction of local thermodynamic parameters in rod bundles during LOCAs. These local parameters are necessary for the phenomenological understanding and correlation of local heat transfer coefficients. Values for local heat transfer coefficients are desired which may be expressed as a function of local conditions such as temperature differences, flow rates, pressure, and quality.
4. Indicate how the data obtained can be used to assess current BWR LOCA evaluation models, including a quantitative determination of safety margins.

Appendix B
BD/ECC PROGRAM
LIST OF REPORTS

BD/ECC PROGRAM REPORTS

LIST OF REPORTS PREPARED AS PART OF BWR BD/ECC PROGRAM DOCUMENTATION

<u>Report No./Type</u>	<u>Title/Author(s)</u>	<u>Principal Contents</u>
GEAP-21207 Informal	BWR 8x8 Fuel Rod Simulation Using Electrical Heaters J. P. Dougherty, R. J. Muzzy, March 1976.	Analysis of electrical heaters to simulate nuclear fuel rods.
GEAP-21304-1 Quarterly	BWR Blowdown/Emergency Core Cooling First Quarterly Progress Report January 1-March 31, 1976.	
GEAP-21255 Topical Report	Preliminary BWR Blowdown/ Emergency Core Cooling Program Plan R. J. Muzzy, June 1976.	Design consideration leading to various test configurations. Test parameters and ranges. Test strategy.
GEAP-21304-2 Quarterly	BWR Blowdown/Emergency Core Cooling Second Quarterly Progress Report April 1-June 20, 1976.	
GEAP-21333 Topical Report	64-Rod Bundle BDHT Test Plan J. P. Walker, September 1976.	Test matrix and test strategy for 8x8 test plan.
GEAP-21304-3 Quarterly	BWR Blowdown/Emergency Core Cooling Third Quarterly Progress Report July 1-September 30, 1976.	
GEAP-21656 Topical Report	Blowdown Flow in the BWR BDHT Test Apparatus A. F. Morrison, October 1976.	Long nozzle critical flow versus short venturi type nozzle.
GEAP-21304-4 Quarterly	BWR Blowdown/Emergency Core Cooling Fourth Quarterly Progress Report October 1-December 31, 1976	
GEAP-21304-5 Quarterly	BWR Blowdown/Emergency Core Cooling Fifth Quarterly Progress Report January 1-March 31, 1977	
GEAP-23517 Topical Report	MAYU04-A Method to Evaluate Transient Thermal-Hydraulic Conditions in Rod Bundles W. C. Panches, March 1977	

LIST OF REPORTS PREPARED AS PART OF BWR BD/ECC PROGRAM DOCUMENTATION
(Continued)

<u>Report No./Type</u>	<u>Title/Author(s)</u>	<u>Principal Contents</u>
GEAP-21638	64-Rod Bundle Core Spray Interaction (BD/ECC1A) Test Plan A. F. Morrison, June 1977.	Test matrix and strategy for BD/ECC1A test plan.
NEDG-NUREG-23732	TLTA Components CCFL Tests D. D. Jones, December 1977.	Results of CCFL testing of TLTA-1 and -3 core inlets and TLTA jet pump. Results of single phase liquid pressure drops across TLTA-3 core inlet and single phase reverse flow steam pres- sure drops across TLTA jet pumps.
GEAP-23592	BWR Blowdown/Emergency Core Cooling Program Preliminary Facility Description Report for the BD/ECC-1A Test Phase W. J. Letzring, editor, December 1977.	Detailed description of TLTA configuration for BD/ECC-1A.
GEAP-NUREG-21304-8	BD/ECC 8th Quarterly Progress Report October 1-December 31, 1977.	
GEAP-NUREG-21304-9	BD/ECC 9th Quarterly Progress Report January 1-March 30, 1978.	
GEAP-NUREG-21638A	BWR Blowdown/Emergency Core Cooling Program 64-Rod Bundle Core Spray Interaction (BD/ECC1A) Test Plan J. C. Wood and A. F. Morrison, February 1978.	Test matrix and test strategy for BD/ECC1A phase.
GEAP-21304-10 Quarterly	BWR Blowdown/Emergency Core Cooling 10th Quarterly Progress Report April 1-June 30, 1978.	
GEAP-21304-11 Quarterly	BWR Blowdown/Emergency Core Cooling 11th Quarterly Progress Report July 1-September 30, 1978.	

LIST OF REPORTS PREPARED AS PART OF BWR BD/ECC PROGRAM DOCUMENTATION
(Continued)

<u>Report No./Type</u>	<u>Title/Author(s)</u>	<u>Principal Contents</u>
GEAP-NUREG-23977	64-Rod Bundle Blowdown Heat Transfer (8x8) Final Report September, 1978.	Topical report covering blowdown heat transfer without ECC injection.
GEAP-NUREG-21304-12	BWR Blowdown/Emergency Core Cooling 12th Quarterly Progress Report October 1-December 31, 1978.	
GEAP-NUREG-21304-13	BWR Blowdown/Emergency Core Cooling 13th Quarterly Progress Report January 1-March 31, 1979.	
GEAP-21207 Informal	BWR 8x8 Fuel Rod Simulation Using Electrical Heaters, J. P. Dougherty, R. J. Muzzy, March 1976.	Analysis of electrical heaters to simulate nuclear fuel rods
GEAP-21304-1 Quarterly	BWR Blowdown/Emergency Core Cooling First Quarterly Progress Report January 1-March 31, 1976.	
GEAP-21255 Topical Report	Preliminary BWR Blowdown/ Emergency Core Cooling Program Plan R. J. Muzzy, June 1976.	Design consideration leading to various test configurations. Test parameters and ranges. Test strategy.
GEAP-21304-2 Quarterly	BWR Blowdown/Emergency Core Cooling Second Quarterly Progress Report April 1-June 30, 1976.	
GEAP-21333 Topical Report	64-Rod Bundle BDHT Test Plan J. P. Walker, September 1976.	Test matrix and test strategy for 8x8 plan.
GEAP-21304-3 Quarterly	BWR Blowdown/Emergency Core Cooling Third Quarterly Progress Report July 1-September 30, 1976.	
GEAP-21304-4 Quarterly	BWR Blowdown/Emergency Core Cooling Fourth Quarterly Progress Report October 1-December 31, 1976.	

LIST OF REPORTS PREPARED AS PART OF BWR BD/ECC PROGRAM DOCUMENTATION
(Continued)

Report No./Type	Title/Author(s)	Principal Contents
GEAP-21304-5 Quarterly	BWR Blowdown/Emergency Core Cooling Fifth Quarterly Progress Report January 1-March 31, 1977.	
GEAP-2351T Topical Report	MAYU04 - A Method to Evaluate Transient Thermal Hydraulic Conditions in Rod Bundles, W. C. Panches, NRC-2, March 1976.	Describes the technical basis for a one- dimensional, single channel, thermal hydrau- lic computer code.
GEAP-21304-6 Quarterly	BWR Blowdown/Emergency Core Cooling Sixth Quarterly Progress Report April 1-June 30, 1977.	
GEAP-21304-7 Quarterly	BWR Blowdown/Emergency Core Cooling Seventh Quarterly Progress Report July 1-September 30, 1977.	
GEAP-NUREG-21304-14	BWR Blowdown/Emergency Core Cooling 14th Quarterly Progress Report April 1-June 30, 1979.	
GEAP-NUREG-21304-15	BWR Blowdown/Emergency Core Cooling 15th Quarterly Progress Report July 1-September 30, 1979.	
GEAP-NUREG-21304-16	BWR Blowdown/Emergency Core Cooling 16th Quarterly Progress Report October 1-December 31, 1979.	
GEAP-NUREG-21304-17	BWR Blowdown/Emergency Core Cooling 17th Quarterly Progress Report January 1-March 31, 1980.	
GEAP-NUREG-21304-18	BWR Blowdown/Emergency Core Cooling 18th Quarterly Progress Report April 1-June 30, 1980.	
GEAP-NUREG-21304-19	BWR Blowdown/Emergency Core Cooling 19th Quarterly Progress Report July 1-September 30, 1980.	

LIST OF REPORTS PREPARED AS PART OF BWR BD/ECC PROGRAM DOCUMENTATION
(Continued)

<u>Report No./Type</u>	<u>Title/Author(s)</u>	<u>Principal Contents</u>
GEAP-NUREG-21304-20	BWR Blowdown/Emergency Core Cooling 20th Quarterly Progress Report October 1-December 31, 1980.	
GEAP-24962 NUREG/CR-2229 EPRI-NP-1783 DIST. CODE NRC-2 FIN NO. B3014	BWR Large Break Simulation Tests - BWR Blowdown/Emergency Core Cooling Program	Results of large break (DBA) tests conducted in TLTA.
GEAP-24963 NUREG/CR-2230 EPRI-NP-1782 DIST. CODE NRC-2 FIN. NO. B3014	BWR Small Break Simulation Tests with and without Degraded ECC Systems - BWR Blowdown/Emergency Core Cooling Program	Results of two small break tests conducted in TLTA.
GEAP-24964 NUREG/CR-2231 EPRI-NP-1781 DIST. CODE NRC-2 FIN. NO. B3014	BWR Low Flow Bundle Uncovery Test and Analysis - BWR Blowdown/Emergency Core Cooling Program	Results and analyses of the low flow bundle uncovery tests conducted in TLTA.

Appendix C

DATA UNCERTAINTY ANALYSIS

(W. S. Hwang, D. A. Wilhelmson)

C-1. UNCERTAINTIES IN PRIMARY MEASUREMENTS

Table C-1 summarizes the data uncertainties in the bundle power, pressure, differential pressure, and loop and bundle temperature measurements. The uncertainty of each measurement is discussed individually as follows:

C-1.1 Electrical Power to the Bundle

For the steady-state response, systematic errors are judged to be negligible compared to random errors because:

- a. actual calibration data are used in the data reduction, and
- b. zeroes are recorded just prior to the test and automatically subtracted from readings.

The data uncertainty from random errors was estimated by comparing the theoretical uncertainty to the difference between actual power measurements made by two independent, redundant power measurement systems. The theoretical uncertainty was determined based on the published accuracies of the transducers and data acquisition system. Because the difference between the two redundant systems is larger than the theoretical uncertainty, that difference itself is taken as the uncertainty. Extensive analysis of this difference indicates an uncertainty in electrical power of $\pm 0.5\%$ of reading or ± 7 kW.

The transient response is governed by the output filter in the watt transducer, which was specially modified for faster response. The present filter has three stages, each with a 0.035-second time constant. Transient checks have confirmed the expected response. The delay is about 0.1 second on ramp changes in power.

C-1.2 Differential Pressures

For the steady-state response, the systematic errors are judged to be negligible compared to the random errors because:

Table C-1
ESTIMATED DATA UNCERTAINTY

Primary Measurements

Electrical Power to Bundle

Steady State: $\pm 0.5\%$ of Reading, ± 7 kW

Transient: 0.1 sec. time constant

Pressures

Steady-State: ± 6 psi

Transient: Time constant < 0.02 second

Differential Pressures

Steady State:

Core Inlet (DP-40):	± 0.05 psid
Bypass Orifice (DP-41, 42):	± 0.08 psid
Jet Pump Diffuser:	
#1 (DP-43):	± 0.11 psid
#2 (DP-46):	± 0.08 psid
Lower Plenum: (DP-1, 2, 3, 4):	± 0.03 psid
Bundle: (DP-21, 31):	± 0.03 psid
ECCS Flow Orifice:	
HPCS (DP-65)	± 0.17 psid
LPCS (DP-66)	± 0.08 psid
LPCI (DP-63)	± 0.20 psid

Transient: Studies indicate time constants of 0.1 second or less

Loop Temperatures $\pm 4^{\circ}\text{F}$

Bundle Temperatures: $\pm 0.18\%$ of reading.

- a. actual calibration data are used in the data reduction, including quadratic best fits to nonlinearities;
- b. zeroes of the entire measurements systems are recorded just prior to the transient and automatically subtracted from readings; and
- c. zeroes are recorded immediately after the transient to determine zero shift with system pressure, and corrections are interpolated for intermediate pressures during the transient.

Random errors were estimated from two approaches:

- a. published and calculated accuracies of transducers, electronics, data acquisition system, effect of cold leg temperature, etc.; and
- b. repeated in-place measurements of known differential pressures (net cold leg heads) with the vessel full and with the vessel empty.

Because the actual measurement checks showed larger differences, they are used as the basis of estimated uncertainty. This additional uncertainty, in excess of theoretical values, is thought to be due to small gas bubbles remaining in the vertical sections of the pressure-sensing tubing, even after all reasonable measures have been taken to ensure proper fill in the nominally horizontal sections and thorough purging and bleeding of the lines. It may represent gas coming out of solution in the water. Both theory and experience suggest that actual uncertainties during the test are substantially smaller than the listed uncertainty because the higher test pressures tend to collapse these bubbles. Instead of individually analyzing the scatter in all 70 of the differential pressure measurements, the approach used was to experimentally determine what generic tolerance had to be allowed to bring 90 percent of the errors during cold leg test checks within tolerance with a reasonable amount of purging, bleeding, and other fine-tuning. The appropriate generic tolerance proved to be about $\pm 0.6\%$ of transducer full scale rating or ± 0.02 psi. This format is somewhat unusual, having no "percent of reading" term but seems best suited to this application because most of the actual sources of uncertainties tend to be independent of reading. Transducer full-scale rating was used instead of maximum net cold leg because it better reflected the effects, at opposite extremes, of large flow effects and of the limited number of transducers available in the very low ranges. This generic uncertainty is translated as shown in Table C-1 into specific uncertainties for key differential pressures.

Transient uncertainty is much more difficult to characterize. The published values of transducer frequency response and damping are often irrelevant because the overall response is largely determined by the masses, compliances, and restrictions of

the fluids within the connecting tubing. Even these can be theoretically estimated, but they are so subject to unpredictable secondary effects, such as small gas bubbles in the tubing and the interaction between transducers connected to the same lines, that they would have to be confirmed by repeated and costly in-place checks on the actual systems. The limited studies which have been done in this area indicate that the transient response of most of the differential pressure systems can be characterized by a single time constant of the order of 0.1 second or less, providing that no extreme sizes or lengths of tubing are used and that reasonable care has been taken to purge gases from the system. A discussion of transducer/tubing system response tests is included in GEAP-23592 (C-1).

C-1.3 Pressure

The foregoing discussion of systematic and random uncertainties in differential pressure measurements applies to the pressure measurements as well. Comparisons between several pressure measurements at known levels, typical operating pressure levels, and zero flow were used as the independent check. The same $\pm 0.6\%$ of range tolerance proved to be appropriate, indicating an uncertainty of ± 6 psi. Additional uncertainty caused by transients is negligible because time constants are less than 0.02 second.

C-1.4 Loop Temperatures

Comparisons among temperature readings at many locations in the loop and throughout the bundle taken under steady-state, adiabatic conditions show differences which are consistent with the standard, published uncertainty of approximately $\pm 4^{\circ}\text{F}$.

C-1.5 Bundle Temperatures

Agreement with published uncertainties at loop temperatures (see above) supports the assumption that uncertainties at higher temperatures will also be consistent with published values, approximately $\pm 0.8\%$ of reading.

C-2. ESTIMATE OF TLTA SYSTEM MASS

A great number of nodal differential pressures were measured in various regions throughout the system in the TLTA test. The measured nodal differential pressure consists of static head, dynamic pressure change, and pressure loss across the measuring node:

$$DP_{\text{meas.}} = DP_{\text{static head}} + DP_{\text{dynamic change}} + DP_{\text{loss}} \quad (\text{C-1})$$

Shortly after the break initiation, the recirculation pump coastdowns rapidly, and the internal flow throughout the TLTA system becomes small. The contributions from the flow effects (the dynamic pressure change and pressure loss) to the measured differential pressure are small or negligible. The nodal average fluid density can be derived from the measured differential pressure with the following equation:

$$DP_{\text{meas.}} \approx DP_{\text{static head}} = \rho gh \quad (C-2)$$

where

ρ = nodal average fluid density

g = gravity constant

h = nodal height

Furthermore, fluid mass in the measuring node can be obtained:

$$M = \rho V \quad (C-3)$$

where

V = nodal volume.

Strings of differential pressure measurements have been made throughout the TLTA system. The total system mass can be derived by integrating all nodal fluid masses obtained with these nodal differential pressures throughout the system. A typical result derived with this method is shown in Figure C-1.

Fluid mass derived with the above method is valid only when the flow effects on the derived nodal average density are negligible. During the rapid blowdown and recirculation pump coastdown of the initial transient, the lower plenum flashing surge, and the breakdown of counter current flow limiting (CCFL), relatively higher flow changes will result in certain regions. In such case nodal fluid mass derived with the measured differential pressure which includes the flow effect has a relatively large uncertainty and is carefully evaluated and corrected. The uncertainty bands indicate the possible flow effect on the derived mass obtained with the differential pressure measurements during the transient.

C-6

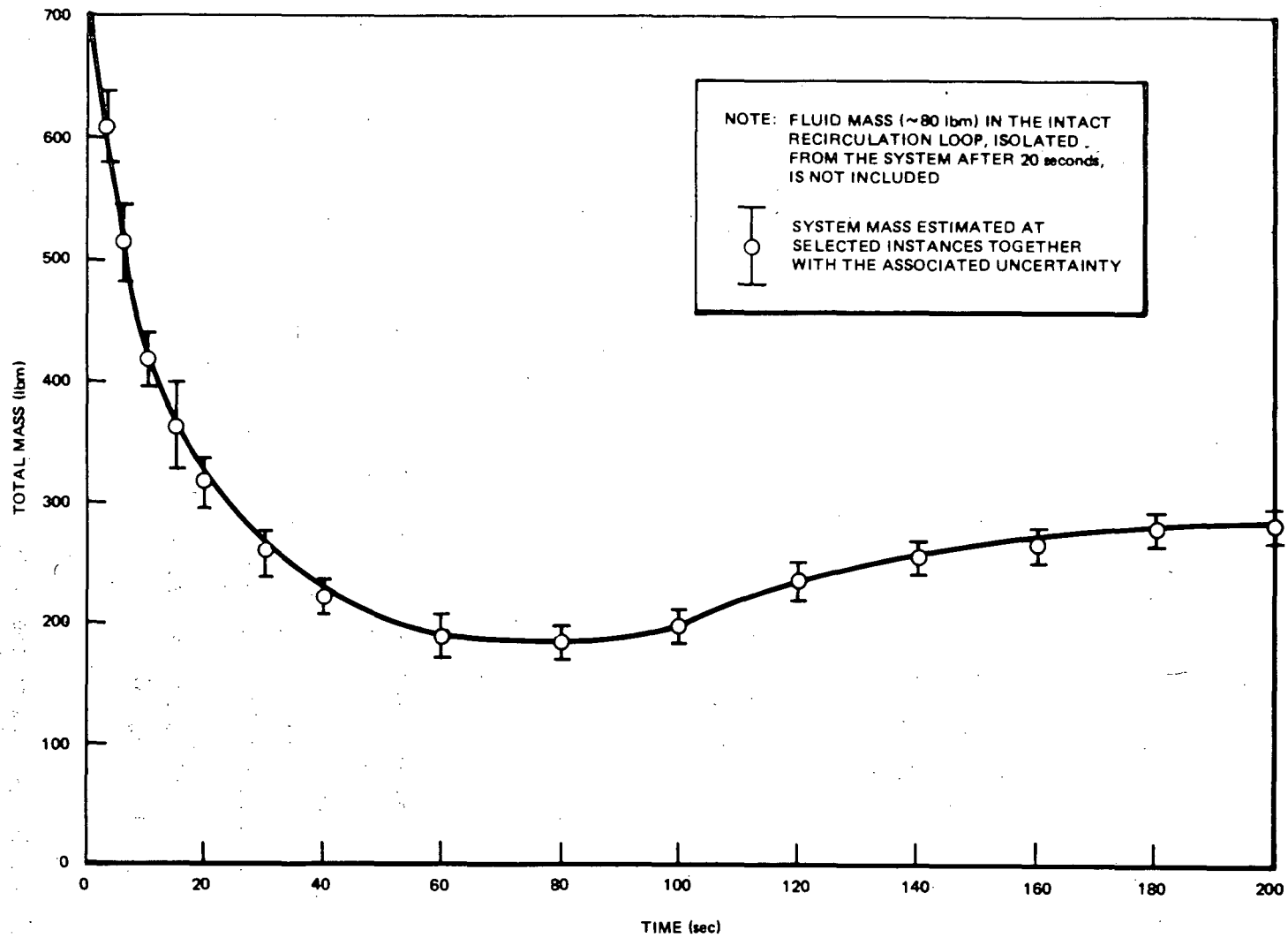


Figure C-1. System Mass Test 6425 R2

C-3. ESTIMATE OF TLTA BREAK FLOW

After the system total mass transient is obtained, the break flow can be estimated by applying the conservation of mass flow to the system:

$$\begin{aligned}\frac{dM_{\text{sys}}}{dt} &= \dot{M}_{\text{In}} - \dot{M}_{\text{Out}} \\ &= (\dot{M}_{\text{FW}} + \dot{M}_{\text{ECC}}) - (\dot{M}_{\text{STM}} + \dot{M}_{\text{BK}})\end{aligned}$$

where

\dot{M}_{In} = Mass flow into the system which is contributed by feedwater and/or ECCS flow

\dot{M}_{Out} = Mass flow out of the system which includes break flow and/or discharge flow through steamline

Figure C-2 shows the estimated break flow from the system mass given in Figure C-1. The uncertainty bands represent the combined effects of the uncertainties in mass as discussed in the previous subsection and the uncertainty in obtaining the derivative in this quantity.

C-4. CORE INLET FLOW MEASUREMENTS IN TLTA

The core inlet flow in the TLTA can be derived from three methods using different measurements during the coastdown and lower plenum flashing period. Comparisons of these measurements are made in this study. Following lower plenum flashing, the core inlet flow rates are very low and counter-current flow limiting conditions are established at the inlet orifice because of continued flashing and vapor updraft from the lower plenum. Because of the CCFL condition at the core inlet, a reliable measurement of the core inlet flow with these methods cannot be obtained. The present study discusses only the measurements shortly after the lower plenum flashing.

Figure C-3 shows locations of the measurements made in the TLTA. Three methods to derive the core inlet flow* are:

*For TLTA5 this is the flow to the heated bundle. For TLTA5 part of this flow is lost through the leakage holes between the bundle and bypass region. Therefore, the net flow to the heated bundle will be slightly less.

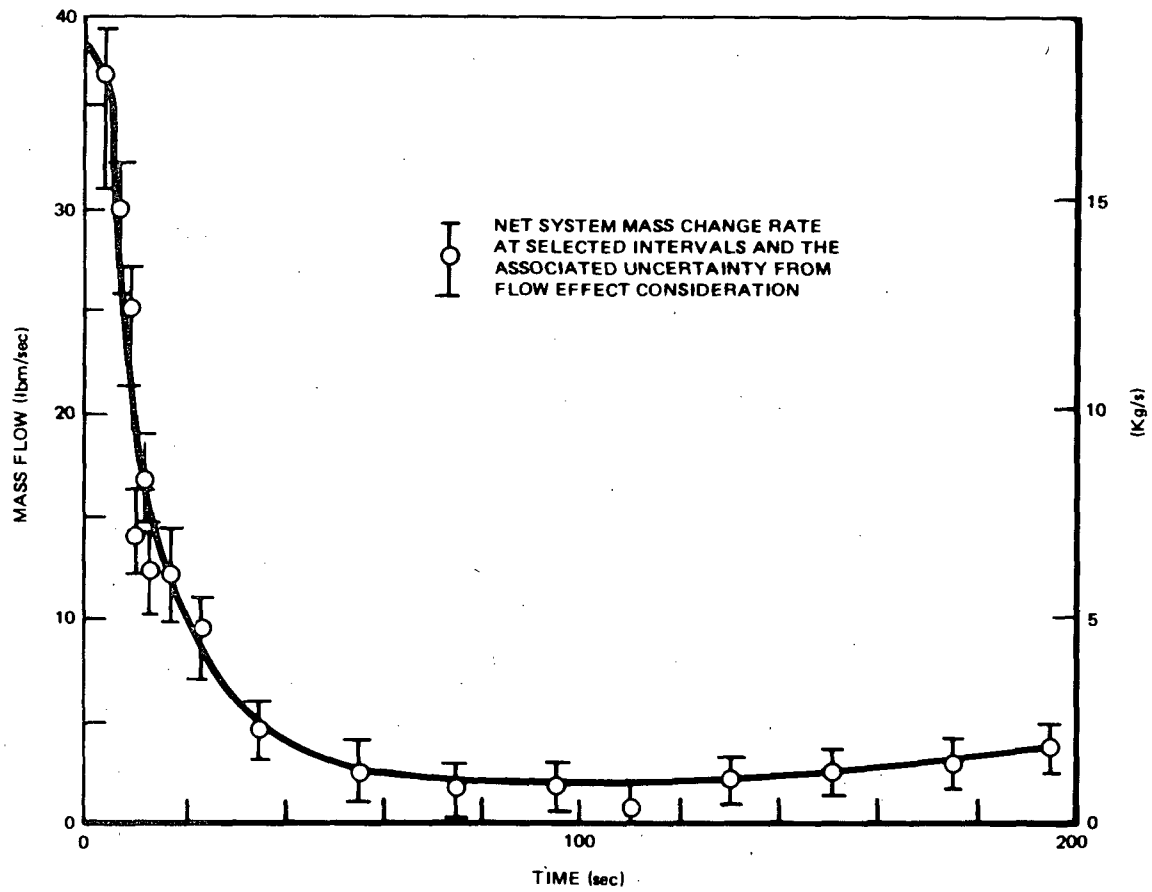


Figure C-2. Total Break Flow Determined from Inventory Method for Average Power, Average ECC Test (6425/2)

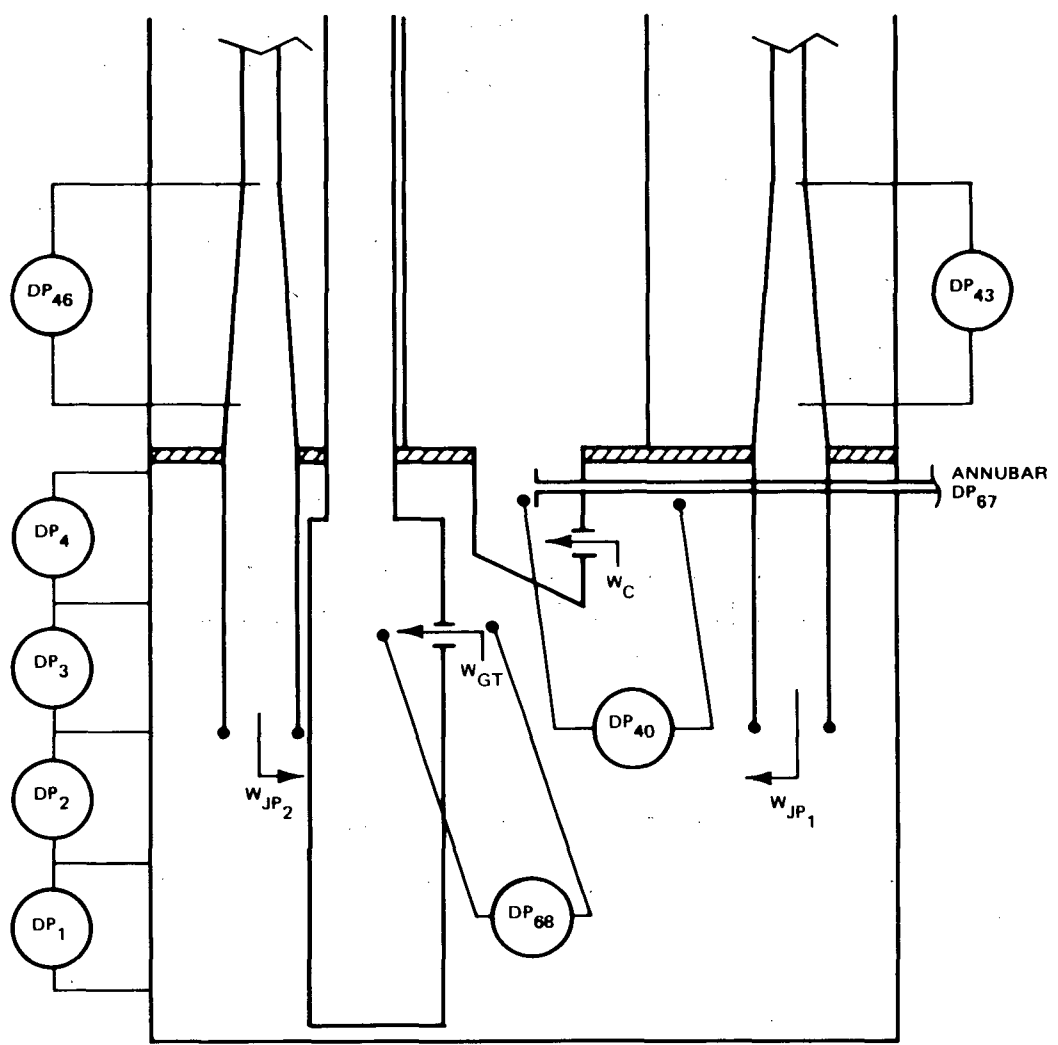


Figure C-3. Core Inlet Flow Measurements.

- a. a direct measurement with the differential pressure across the core inlet orifice, DP₄₀;
- b. an indirect measurement, derived from the flow balance in the lower plenum.

$$W_c = W_{JP1} + W_{JP2} - W_{GT} - \frac{\Delta M_{LP}}{\Delta t}$$

where

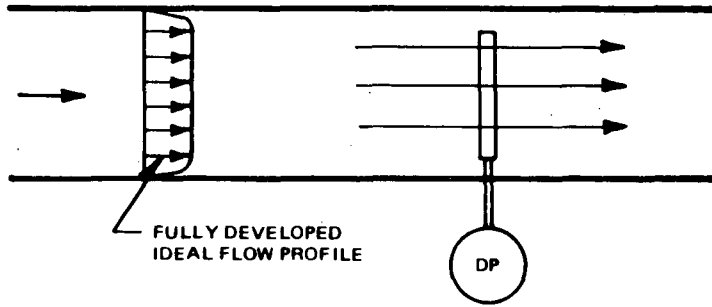
W_{JP1} , W_{JP2} and W_{GT} are measured with the differential pressures, DP₄₃, DP₄₆ and DP₆₈ respectively.

$\frac{\Delta M_{LP}}{\Delta t}$ is the mass change in the lower plenum which can be derived from differential pressures, DP1 - DP4; and

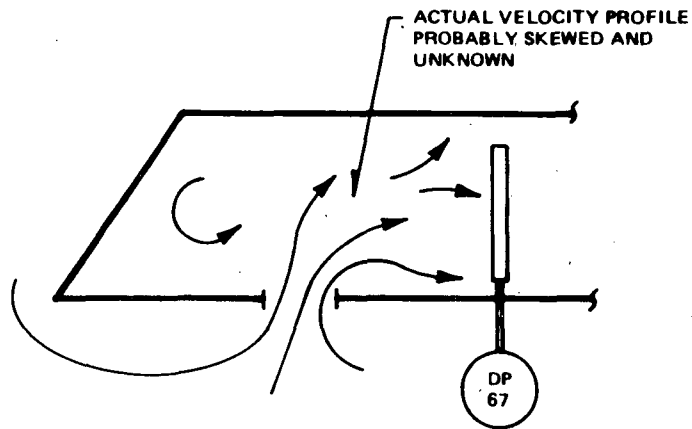
- c. a direct measurement with an annubar installed at the core inlet, DP₆₇.

During the early transient, fluid in the lower plenum and jet pumps is primarily subcooled, and the fluid density is derived from the measurements of the fluid temperature and pressure there. All three methods measure the flow rate with the differential pressures. The flow coefficient used in the first two methods was obtained by an in-place flow calibration. The calibration factor used in the third method was provided by the vendor. This calibration factor was obtained with a fully developed ideal pipe flow condition (Figure C-4a). The geometry of the TLTA core inlet is relatively complicated, and the flow coefficient cannot be evaluated without conducting an in-place calibration. For application in the TLTA the vendor's calibration factor was used, as in-place calibration was not performed.

Typical flow data reduced with these methods are shown in Figures C-5 and C-6. While the measurements with the core inlet orifice and the lower plenum flow balance agree well, particularly prior to the lower plenum flashing, the annubar consistently indicates a higher core inlet flow. Figures C-7 and C-8 show the same data but normalized with their own initial values at t=0 second. The normalized results essentially eliminate the effect of different flow coefficients, which were obtained from different calibrations:



(a) ANNUBAR CALIBRATION BY THE VENDOR



(b) ANNUBAR INSTALLATION IN TLTA

Figure C-4. Annubar Flow Measurement

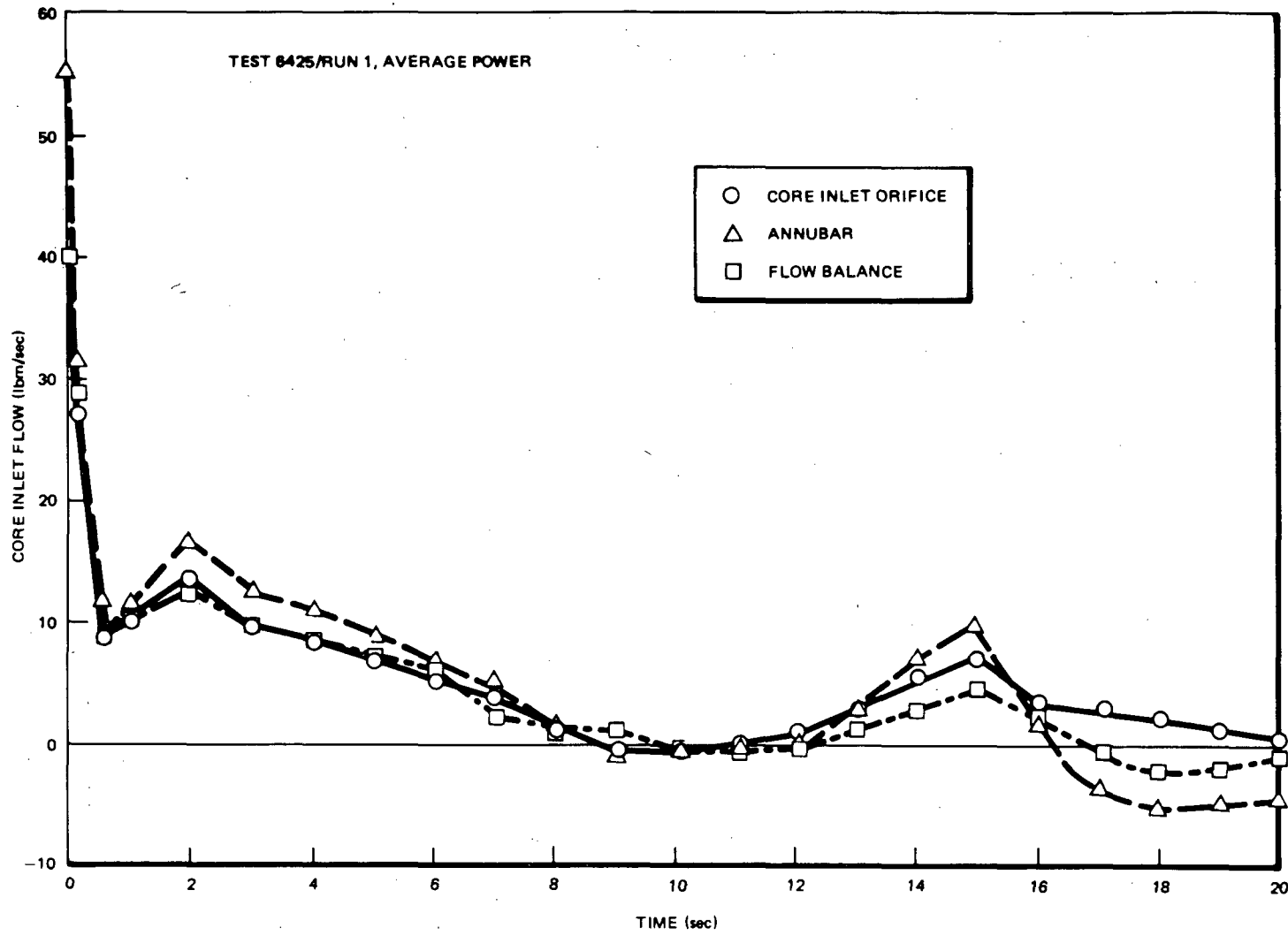


Figure C-5. Core Inlet Flow, Average Power Test.

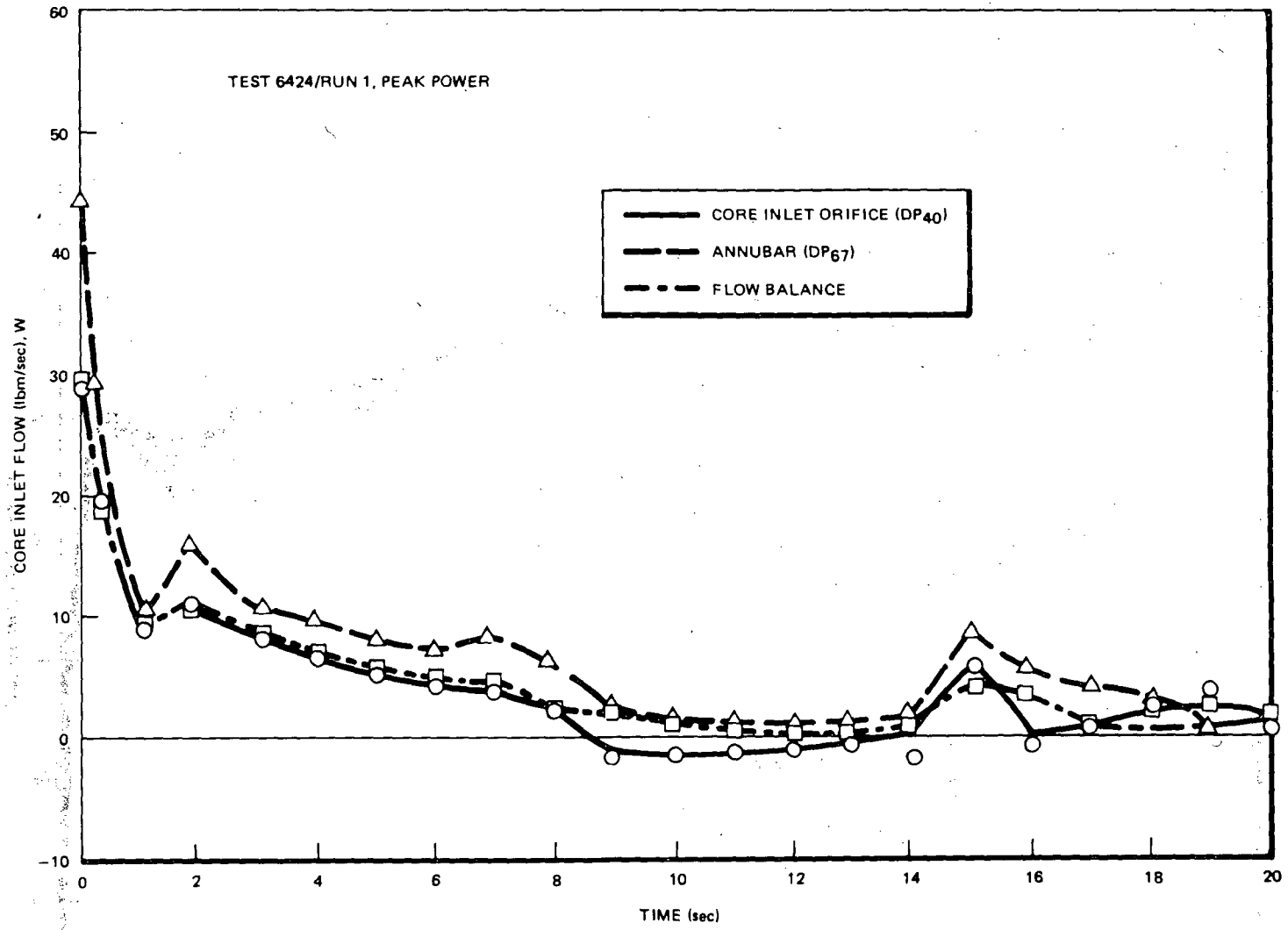


Figure C-6. Core Inlet Flow, Peak Power Test.

C-14

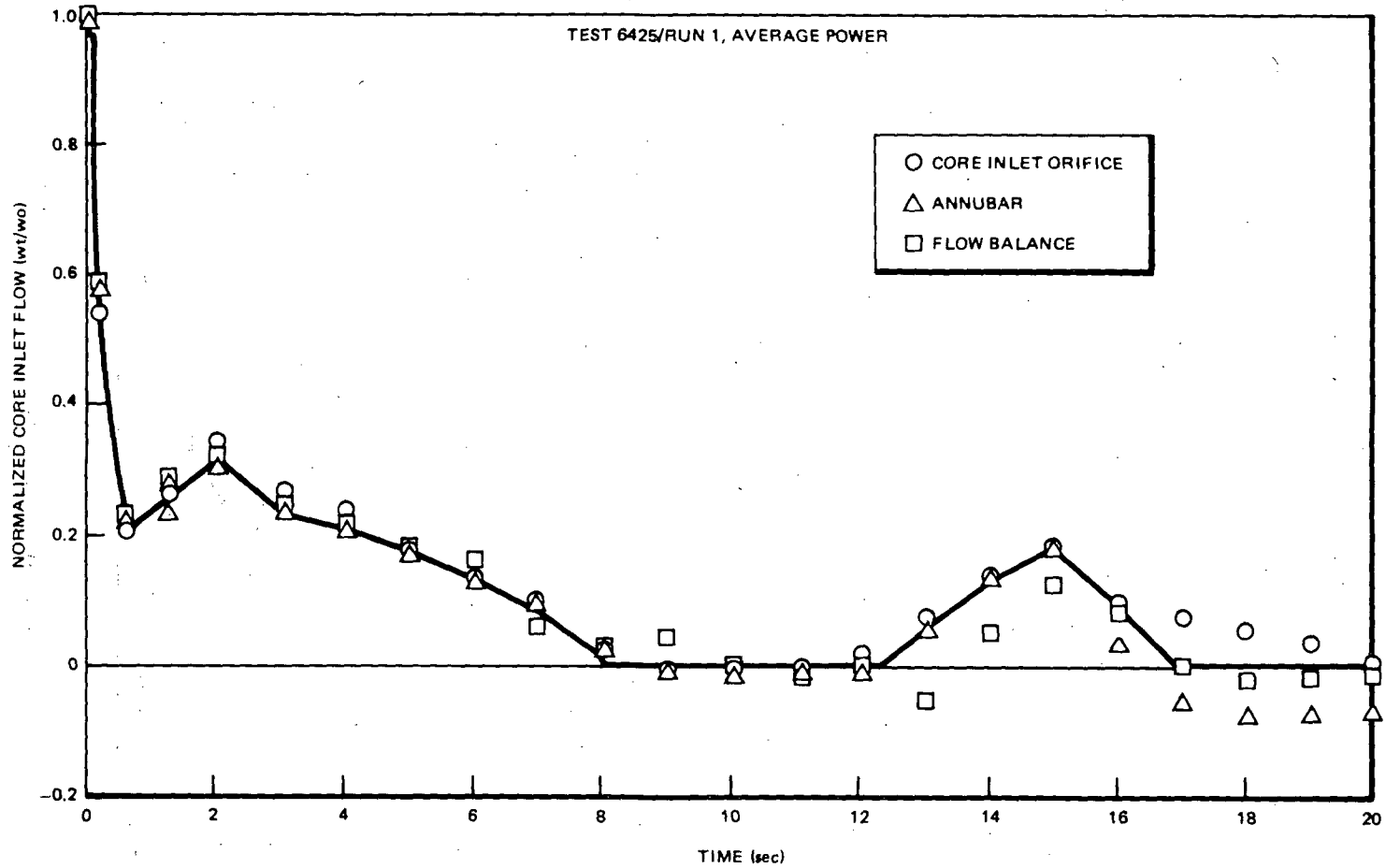


Figure C-7. Normalized Core Inlet Flow, Average Power Test.

C-15

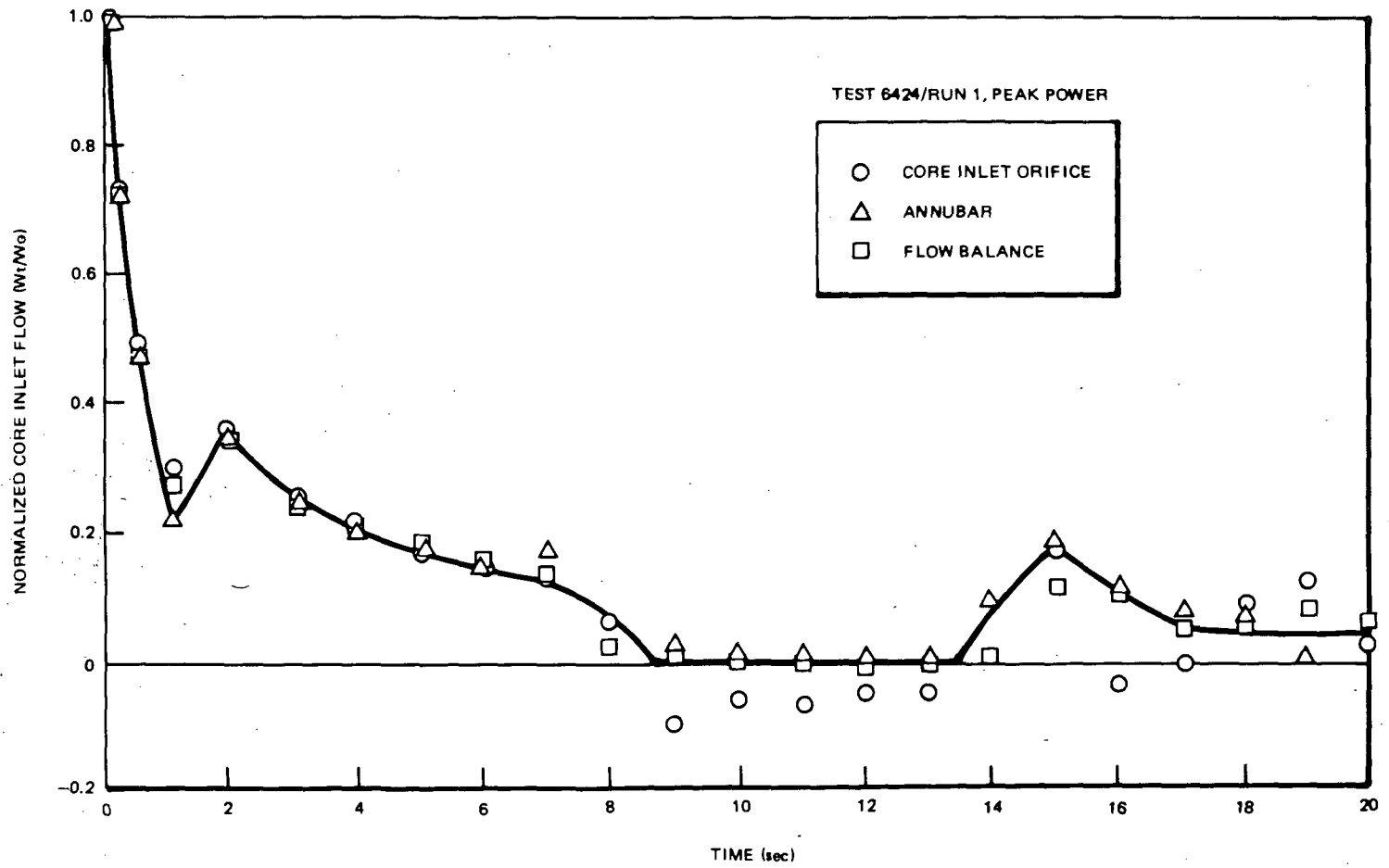


Figure C-8. Normalized Core Inlet Flow, Peak Power Test.

$$\frac{W_t}{W_o} = \frac{C_1 (\rho_t \Delta \rho_t)^{1/2}}{C_1 (\rho_o \Delta \rho_o)^{1/2}} = \left(\frac{\rho_t \Delta \rho_t}{\rho_o \Delta \rho_o} \right)^{1/2}$$

The good agreement between the normalized curves indicates that the differences seen in Figures C-5 and C-6 are mainly attributed to the flow coefficients for the annubar. This result also implies that a reliable core inlet flow measurement can be obtained, provided that an accurate flow coefficient is used.

During and beyond the lower plenum flashing, all measurements are affected by the highly voided and complicated two-phase flow and CCFL conditions at the core inlet. In addition, the third method, flow balance, is also affected by the relatively large uncertainties in the jet pump two-phase flow measurements and net mass change in the lower plenum during this period. (A vapor space begins to form in the upper portion of the lower plenum caused by the continued flashing and vapor generation.) Data shown in Figures C-5 and C-6, after lower plenum flashing (≈ 12 seconds), are obtained using the same flow coefficient without any correction for the two-phase flow effects. Therefore, the measurements with the three methods show a relatively large uncertainty during this period.

As mentioned previously, the flow coefficients used in the core inlet orifice and flow balance method were obtained by an in-place flow calibration, while the annubar method used the coefficient from the manufacturer. Therefore, the magnitude of the flow-rate measurement with the first two methods is judged to be more reliable than that with the annubar method in this study. Detailed discussions and evaluations on the core inlet orifice and flow balance methods are given in GEAP-13317-11 (C-2). The uncertainty of these methods was estimated to be less than $\pm 15\%$.

Although the annubar measurement in this study consistently indicates a higher flow caused by the calibration factor as mentioned above, a new flow factor can be determined by conducting an in-place calibration or by using the core inlet orifice measurement (DP_{40}) at time zero as a reference. It is believed that the annubar method is useful in future TLTA applications because it provides the following advantages:

- a. improved signal response because of its small inertia (this measurement will be more sensitive to flow reversal and low flow conditions than other methods); and
- b. provides a direct, in-line measurement of the true flow ΔP .

C-5. REFERENCES

- C-1. W. J. Letzring, editor, BWR Blowdown/Emergency Core Cooling Program Preliminary Facility Description Report for the BD/ECC1A Test Phase, General Electric Company, December 1977 (GEAP-23592).
- C-2. BWR Blowdown Heat Transfer 11th Quarterly Progress Report, January 1 - March 31 1975, General Electric Company, April 1975 (GEAP-13317-11).

Appendix D

EFFECTS OF VALVE FAILURE IN TEST 6426 RUN 1 (AVG. POWER, NO ECC)

(J. J. Ashjaee, L. S. Lee)

Leaving open the isolation valve (because of controller failure) in the blowdown loop has noticeable effects on the break flows during the early portion of the transient. The effects on the global system response are small, however, after 25 seconds.

The blowdown loop (Loop 2) with break flow measurements is shown in Figure D-1. The isolation valve, V-8, which was on automatic control to close at break initiation, is located downstream of the drive pump. This valve failed to close because of a faulty controller in Test 6426 Run 1. It appears to have closed either actually or effectively after 25 seconds, as is evident from the differential pressure measurement (DP58 in Figure D-2) across the orifice flowmeter upstream of V-8. Flow reversal at the outset of break flow is seen from the plot of DP58 in Figure D-2. During the early stage of the blowdown, additional flow discharge from the drive line finds a path, through the open V-8, to the suction blowdown line (Figure D-1). Because the restrictive part of the break flow path is at the vessel for the suction line and downstream of the measurement spool piece for the drive line, the open valve leads to higher break flow through the drive line. However, there is a limit to the increase because of a rather restrictive inlet to the drive blowdown line. The drive blowdown line inlet opening diameter is 0.453 inch compared to the flow limiting orifice diameter of 0.32 inch.

The added break flow from the drive line to the suction line at the downstream of the restrictive nozzle increases the back pressure in the suction line discharge as shown in Figure D-3 and, therefore, reduces the direct discharge through the suction line. The lower suction-line volumetric flow rate of Test 6426 is seen in Figure D-4 in comparison with Test 6425. The volumetric flow rate for the two tests should be the same except that V-8 failed to close in 6426.

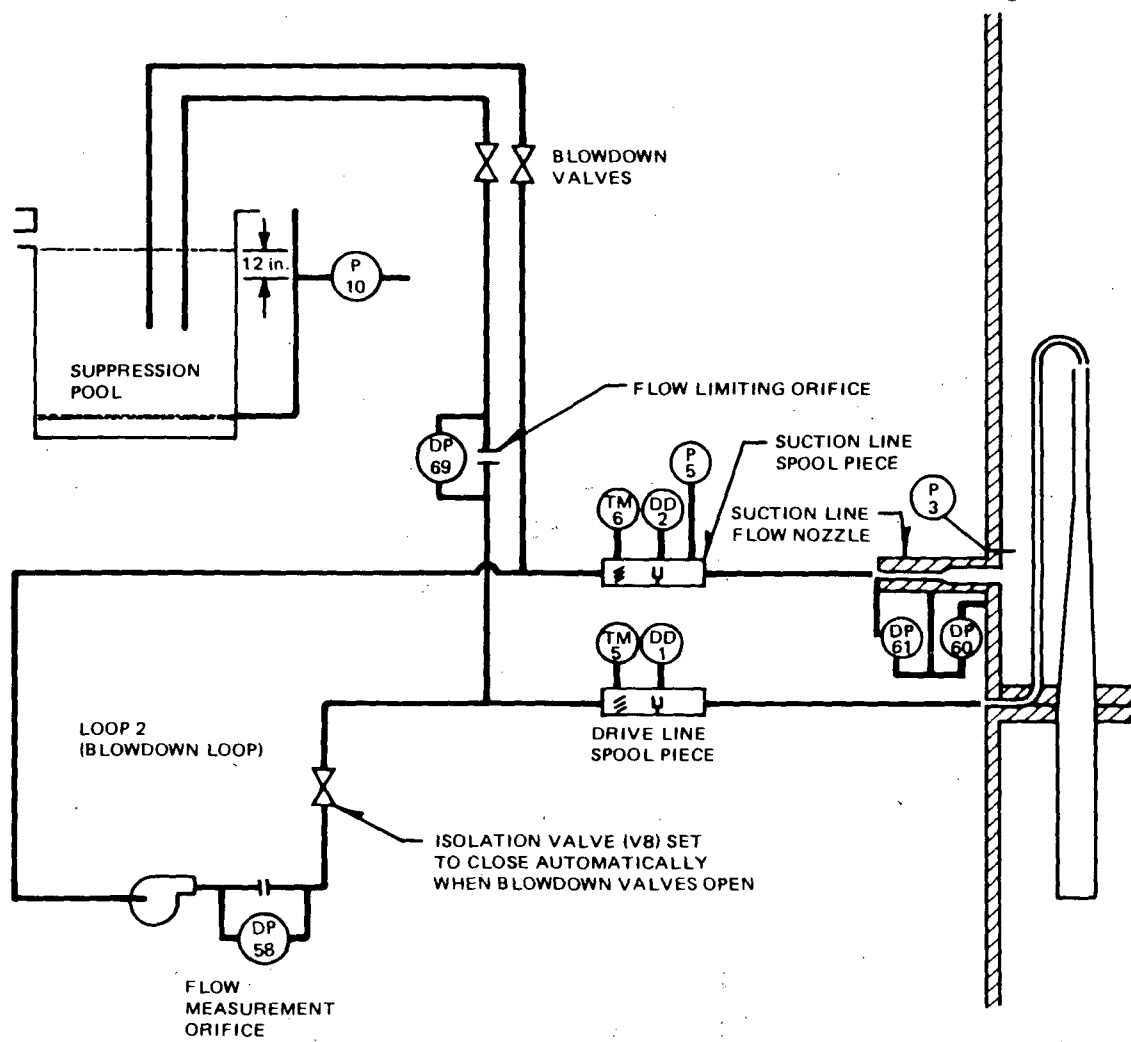


Figure D-1. Blowdown (Broken) Loop Break Flow Paths and Measurement Devices in TLTA 5A

D-3

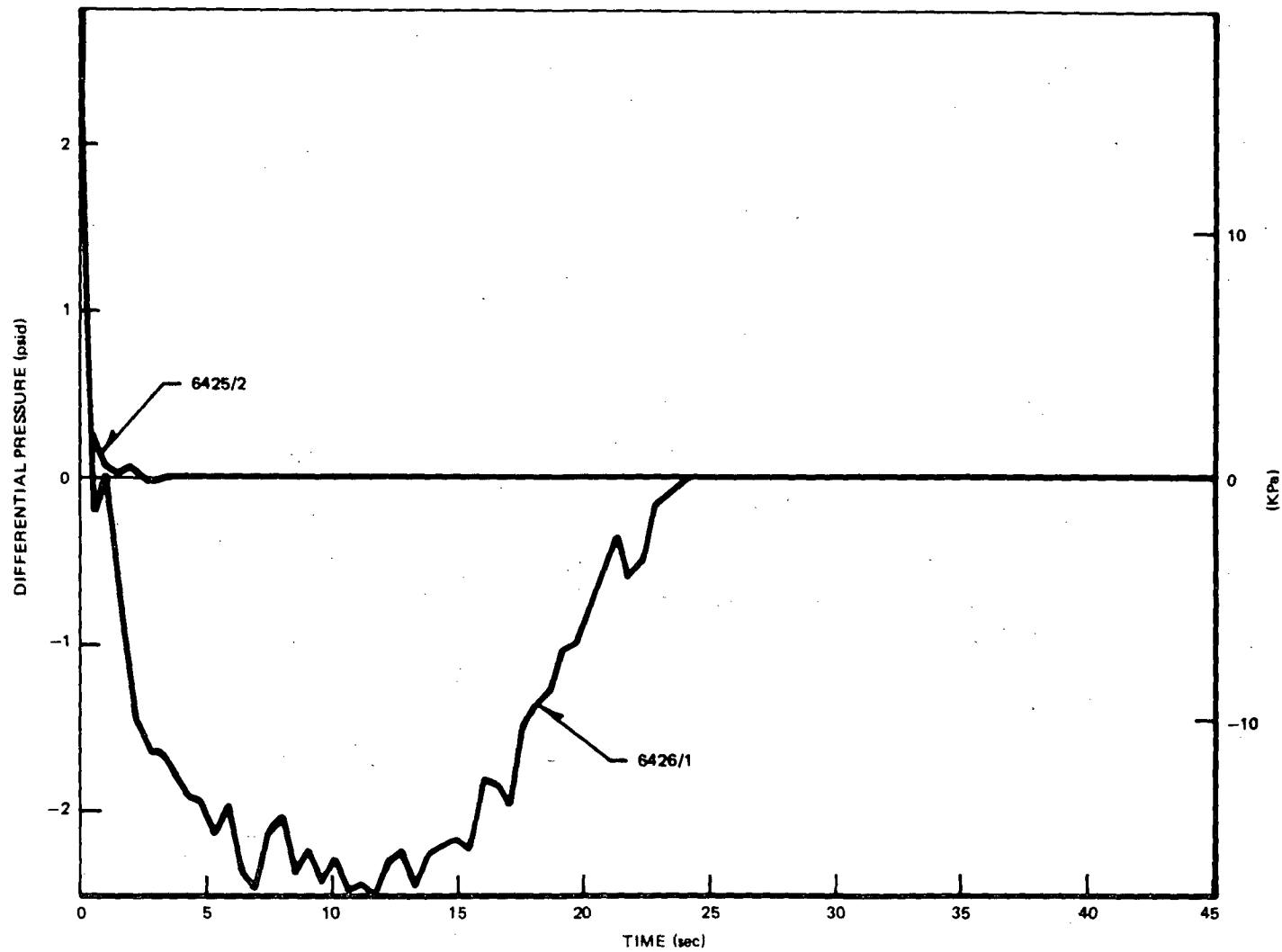


Figure D-2. Comparison of DP Measurements across Flow Orifice (DP58) in Broken Loop Showing Evidence of Valve Failure in Test 6426/1

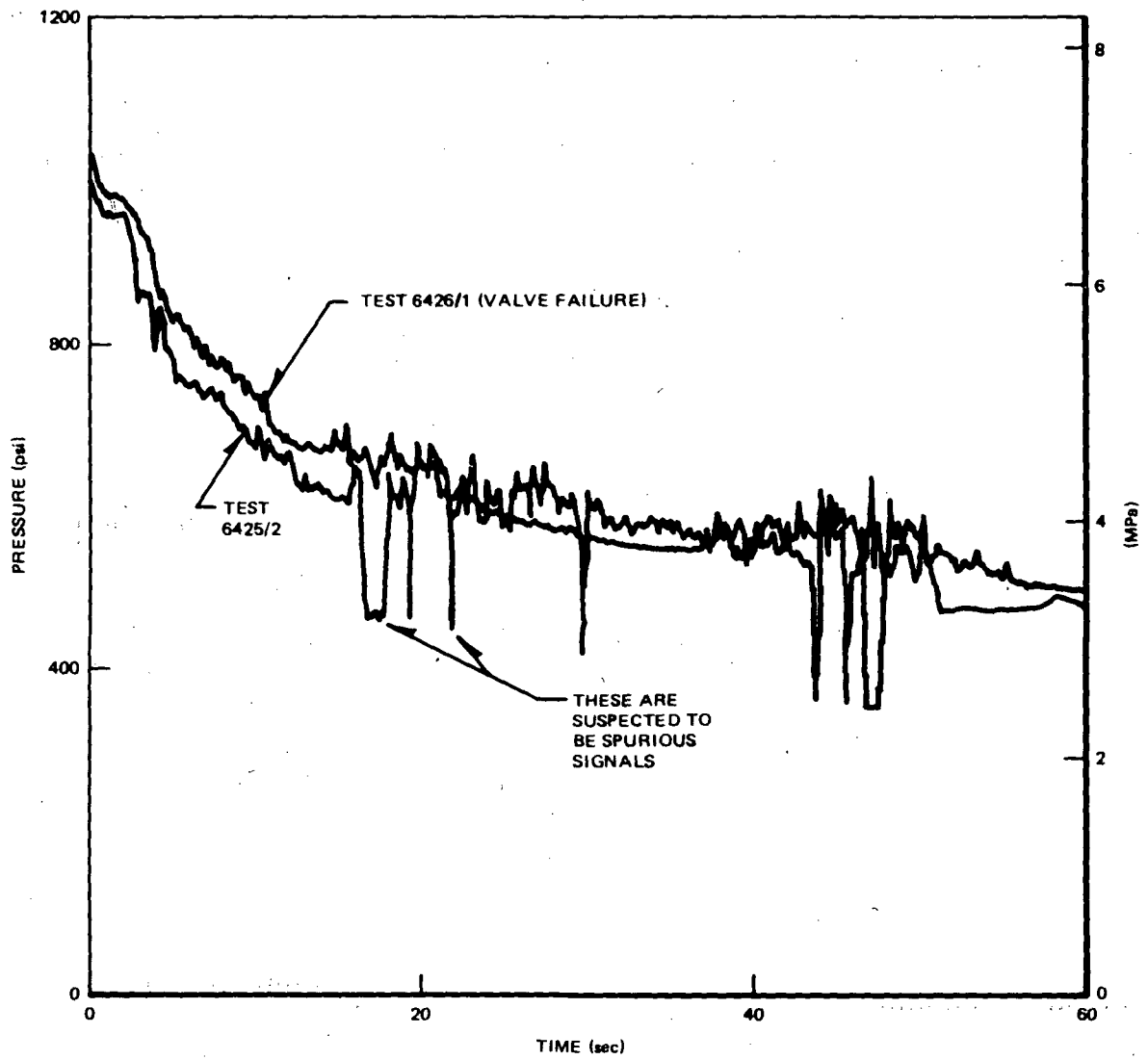


Figure D-3. Comparison of Suction Line Pressures (P5) for Test 6426/1 (Valve Failure) and 6425/2 (Reference Test)

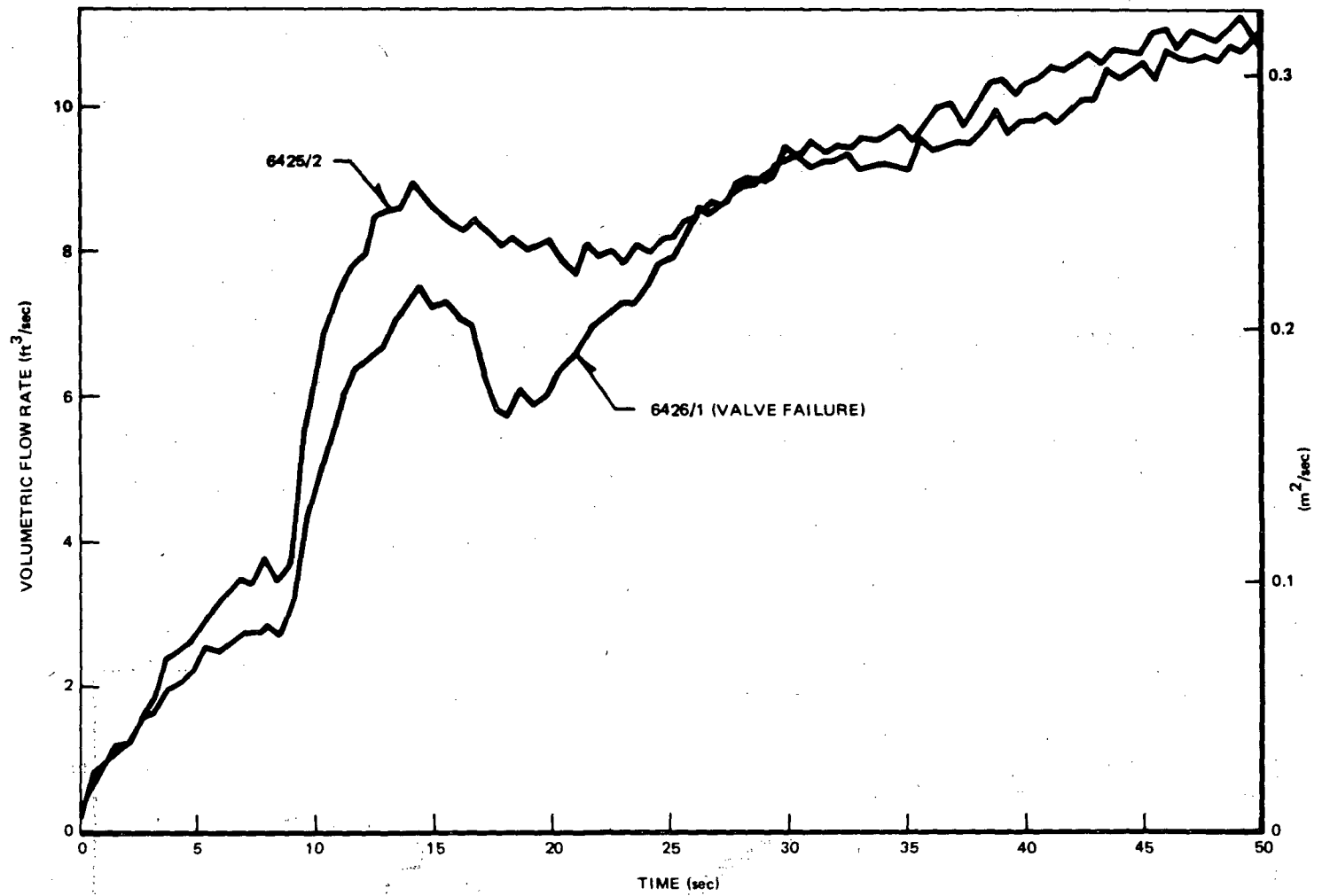


Figure D-4. Comparison of Suction Line Break Flows for Tests 6425/2 and 6426/1 (Valve Failure)

The estimated volumetric flow rate through V-8, based on DP58 measurements and fluid density at the suction inlet, is shown in Figure D-5. The excess flow through the drive line in Test 6426 can be seen in Figure D-6.

The dashed line in Figure D-6 represents the sum of the drive line volumetric flow rate in Test 6425/2 and the estimated volumetric flow rate through V-8 in Test 6426/1 that is shown in Figure D-5. It is seen that, with the adjustment, the volumetric flow rates of the two tests are very close. That the drive line break flow is affected only slightly by the valve failure in Test 6426/1 is reaffirmed by the comparison of pressure drop measurements across the flow-limiting orifice, DP69, as shown in Figure D-7.

The effect of Valve V-8 failure can be seen to diminish after 25 seconds from Figures D-2 through D-7. The volumetric flows through the suction break line in Figure D-4 are nearly identical for the tests with/without ECC from 25 to 50 seconds (before the effects of ECC set in). Similarly, the flows through the drive break line in Figure D-6 show good agreement from 25 seconds on. The differential pressure measurements across the flow-limiting orifice in the break line (DP69, Figure D-7) provide further evidence that the system responses for the two tests are nearly the same after 25 seconds. The differences observed later (~65 seconds) are, therefore, attributable to the ECC injection effects.

The global system responses were examined in Figures 3-50 through 3-55 in Sub-section 3.3.2.1. The effect of valve failure on the global system responses was small after 25 seconds. However, there is some local effect on the bundle response that extends into ~40 seconds. The DPs across the bundle are compared in Figure D-8. The test with valve failure (6426) shows an earlier lower plenum flashing and a lower DP between 17 and 40 seconds. This lower DP, which could be due to lower mass inventory, occurs at the time of bundle fluid redistribution following LPF. This could be the reason that the rods, dried out at ~20 seconds, did not rewet in this test but rewet in all other tests.

D-7

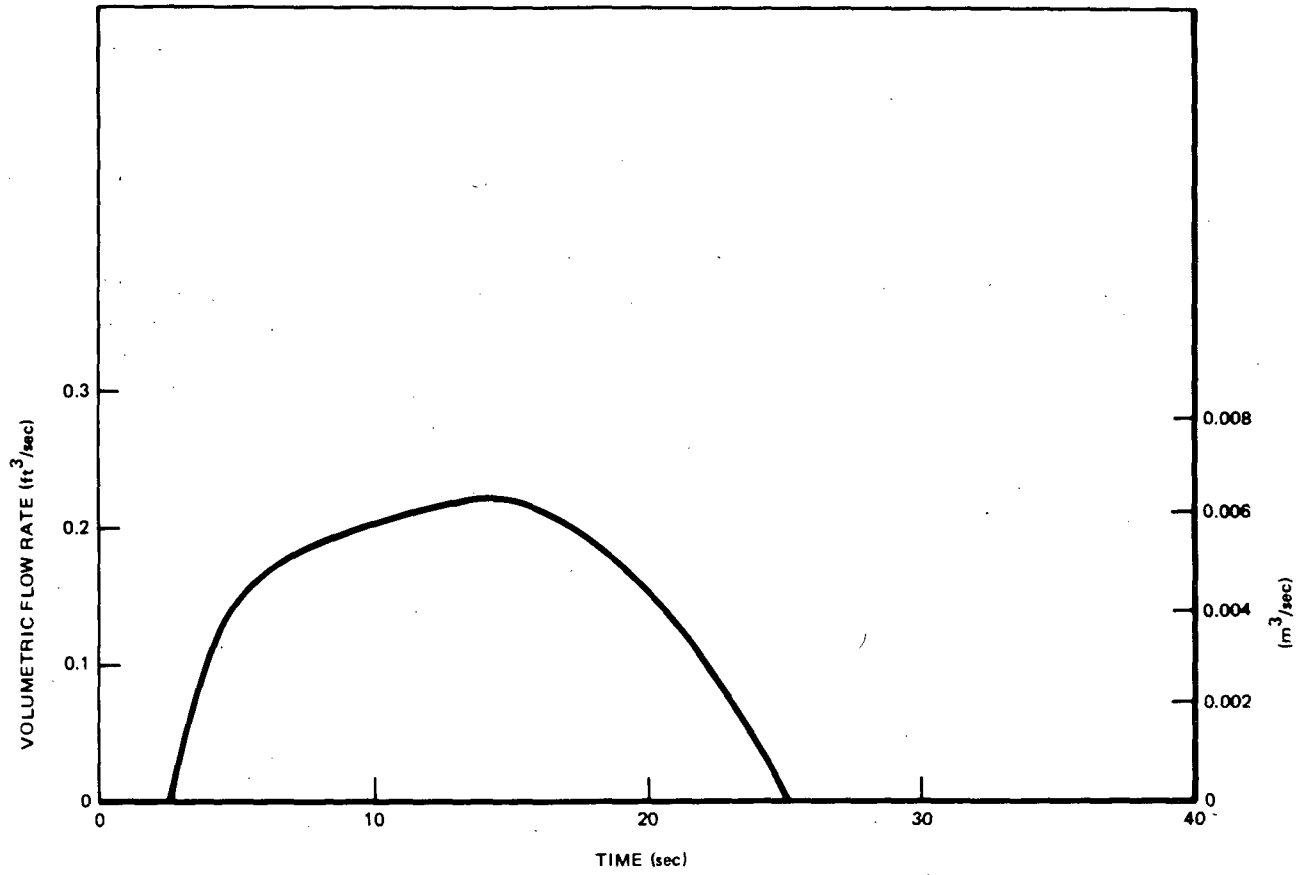


Figure D-5. Estimated Flow Rate through V-8, Test 6426/1.

8-D

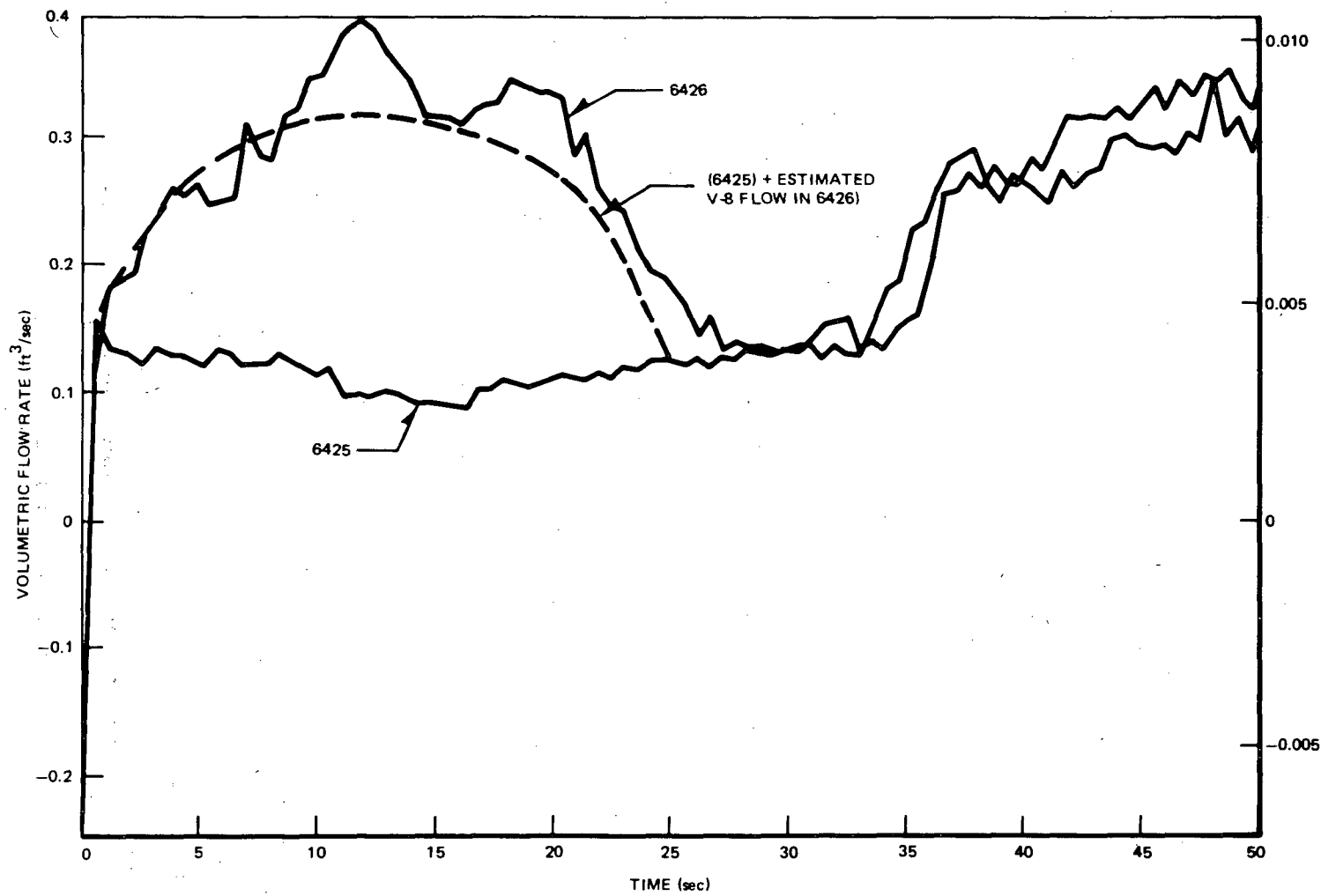


Figure D-6. Comparison of Volumetric Flow Rates through the Drive Line for Tests 6426/1 (Valve Failure) and 6425/2

D-9

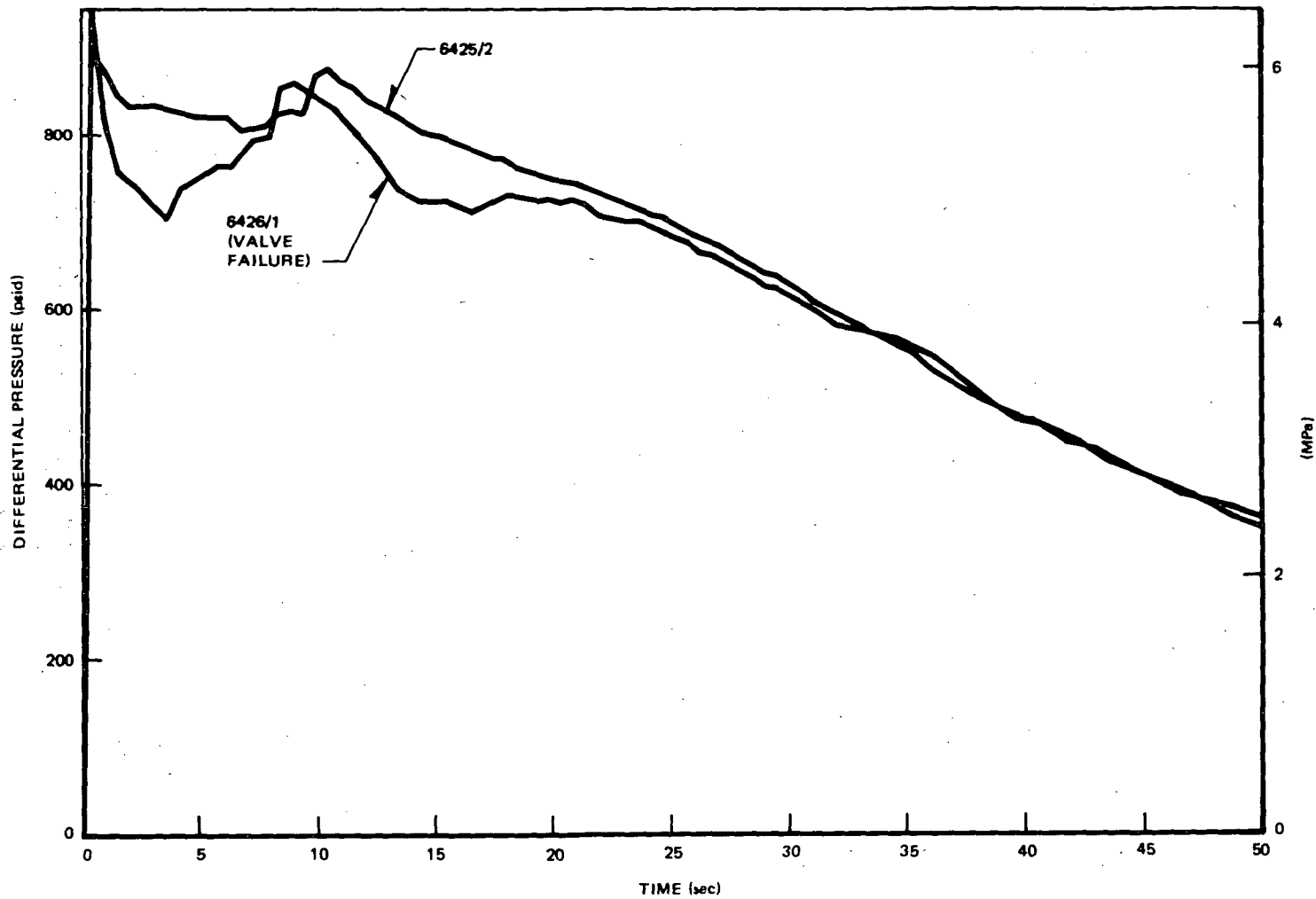


Figure D-7. Comparison of DP Measurements across the Flow-Limiting Orifice in the Drive Line

D-10

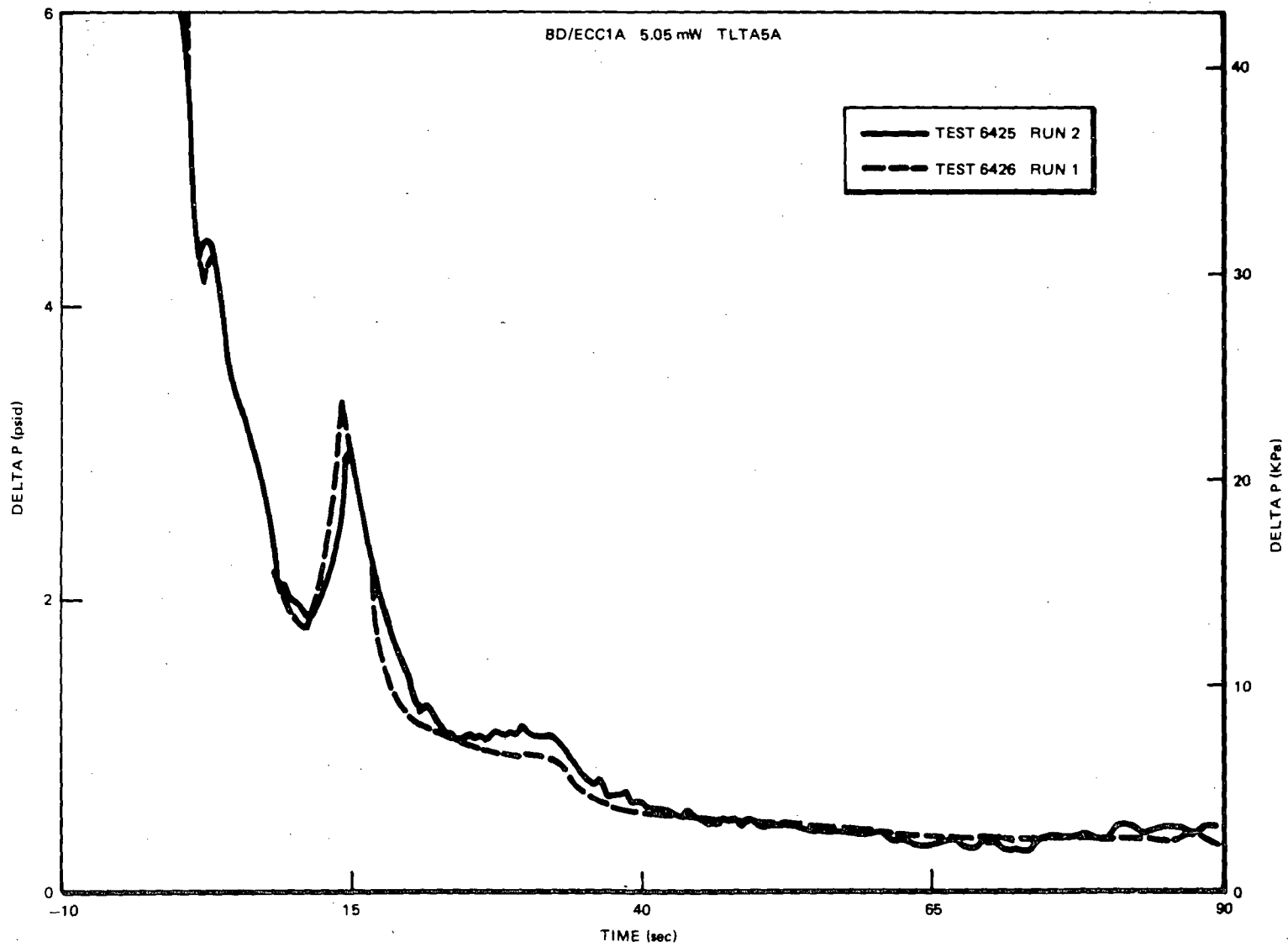


Figure D-8. Comparison of Bundle DPs for Tests 6425/2 and 6426/1

Appendix E

VAPOR GENERATION DUE TO FLASHING

(S. A. Allison)

An expression for the vapor generation rate caused by flashing is determined in Appendix G for an open system using the First Law of Thermodynamics. This equation can be simplified by assuming that the net effect of the flow across the control volume is negligible. Such an assumption is justifiable in cases where the mass in the control volume remains rather constant (as in the case of the lower plenum) and where the mass in the control volume decreases slowly with negligible mass influx (as in the case of the bypass region with CCFL at the outlet). In those cases, the control volume is virtually a closed system.

From Equation G-12 (Appendix G) the vapor generation rate of the no-flow mass in a control volume is given by:

$$W_{fg} = \frac{1}{h_{fg}} \left[\dot{Q} - M_f \frac{dh_f}{dP} \frac{dP}{dt} - M_g \frac{dh_g}{dP} \frac{dP}{dt} + V \frac{dP}{dt} \right] \quad (E-1)$$

where

W_{fg} = vapor generation rate due to flashing (lbm/sec)

M_f = saturated liquid mass (lbm)

M_g = saturated vapor mass (lbm)

V = system volume (ft³)

\dot{Q} = rate of heat addition to system (Btu/sec)

The system volume is defined from the system mass balance as:

$$V = M_f v_f + M_g v_g \quad (E-2)$$

Substituting Equation E-2 into E-1 and rearranging gives:

$$w_{fg} = \frac{1}{h_{fg}} \left[\dot{Q} - M_f \frac{dP}{dt} \left(\frac{dh_f}{dP} - v_f \right) - M_g \frac{dP}{dt} \left(\frac{dh_g}{dP} - v_g \right) \right] \quad (E-3)$$

If it is known that $dh_f/dP \gg v_f$ and that the term $M_g dP/dt (dh_g/dP - v_g)$ is negligible, Equation E-3 is reduced to:

$$w_{fg} = \frac{1}{h_{fg}} \left[\dot{Q} - M_f \frac{dP}{dt} \frac{dh_f}{dP} \right] \quad (E-4)$$

By further assuming that the heat transfer to the system is negligible, the vapor generation rate is reduced to its simplest form:

$$w_{fg} = \frac{1}{h_{fg}} \left(- M_f \frac{dP}{dt} \frac{dh_f}{dP} \right) \quad (E-5)$$

Appendix F
COUNTER-CURRENT FLOW LIMITATION ANALYSIS
(S. A. Allison, L. S. Lee)

Additional details and discussion on the counter-current flow limitation (CCFL) analysis are presented below to supplement the discussion in Subsection 3.4.1. Included in the presentation below are CCFL correlations used for analysis, limiting vapor flows, condensing potentials, and the determination of flow rates from mass balances.

F-1. CCFL CORRELATIONS

A general form of the modified Wallis (F-1) correlation for CCFL is given by:

$$K_g^{1/2} + m K_f^{1/2} = b \quad (F-1)$$

where

$$K_g = (j_g \rho_g^{1/2}) / [gg_c \sigma (\rho_f - \rho_g)]^{1/4} \quad (F-2)$$

$$K_f = (j_f \rho_f^{1/2}) / [gg_c \sigma (\rho_f - \rho_g)]^{1/4} \quad (F-3)$$

$$j = W/\rho A \text{ is the volumetric flux} \quad (F-4)$$

m and b are coefficients determined from experiments. The values of these constants for the three locations are:

- (1) Bundle inlet side entry orifice,

$$m = 0.59 \quad b = 1.53$$

determined from data of Jones (F-2)

(2) Bundle outlet upper tieplate

$$m = 1.0 \quad b = 2.08$$

determined from data of Jones (F-2) and Naitoh (F-3)

(3) Bypass outlet

$$m = 1.0 \quad b = 1.5$$

assumed from the range of values (F-4) for bundle outlet.

A schematic plot of Equation F-1 is shown in Figure F-1. As was pointed out in Subsection 3.4.1.1, the term CCFL has a broad meaning that refers to any point along the line P-Q. The narrow meaning of the term CCFL refers specifically to Point P.

F-2. LIMITING VAPOR FLOW

The CCFL condition of limiting vapor flow occurs at Point P of Figure F-1. This limiting vapor flow condition which prevents the liquid downflow at the three locations is evaluated below with the system conditions.

Because the liquid downflow is zero as a result of limiting vapor flow, the dimensionless liquid volumetric flux, K_f , is set to zero in the CCFL correlation, Equation F-1. A solution for the dimensionless vapor volumetric flux, K_g , is then found using the following equation:

$$K_g = b^2 \tag{F-5}$$

where

b is given in Section F-1 for the three locations.

The corresponding vapor flow is calculated using Equations F-2 and F-4 and assuming that saturated conditions exist. The system pressure needed to find the saturated conditions is taken directly from the steam dome pressure curve in Appendix J. Knowing the system pressure history, the limiting vapor flow throughout the transient at each of the three CCFL locations is easily evaluated.

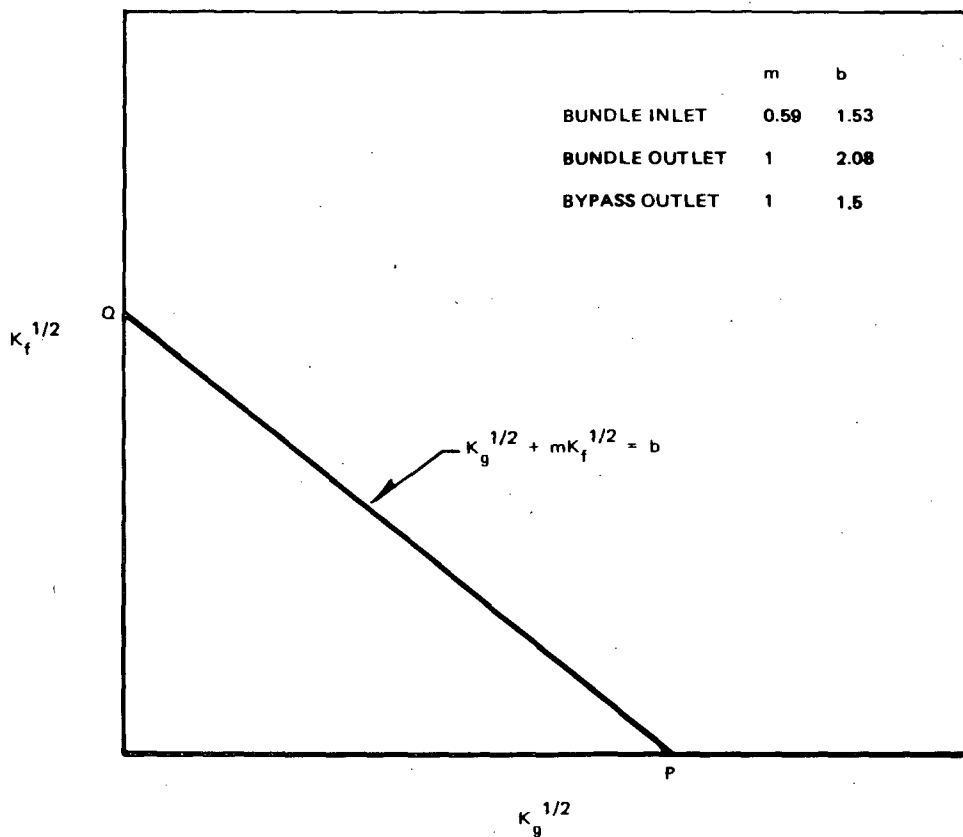


Figure F-1. Schematic Plot of CCFL Correlation Showing Special Cases of Limiting Vapor Flow (P) and CCFL Breakdown (Q). Empirical Coefficients Used in Analysis Are Also Shown

F-3. CONDENSING POTENTIAL

The condensing potential of the subcooled ECC fluid is an indication of the potential for CCFL breakdown at the bypass outlet and upper tieplate. This potential is defined as the amount of vapor which can be condensed if all the ECC fluid is used for condensation purposes, W_{g_c} , divided by the subcooled ECC liquid flow, W_{ECC} . Thus:

$$\text{Condensing Potential} = \frac{W_{g_c}}{W_{ECC}} \quad (\text{F-6})$$

The First Law of Thermodynamics for the condensation process gives:

$$W_{g_c} h_{fg} = W_{ECC} (h_f - h_{sub}) \quad (\text{F-7})$$

h_{sub} = specific enthalpy of the subcooled ECC fluid.

Rearranging Equation F-7 and combining it with Equation F-6, the following expression for the condensing potential is produced:

$$\frac{W_{g_c}}{W_{ECC}} = \frac{h_f - h_{sub}}{h_{fg}} \quad (\text{F-8})$$

F-4. DETERMINATION OF FLOW RATES AT CCFL LOCATIONS USING MASS BALANCES

Regional mass balances in the TLTA are used to estimate the liquid flows through the SEO, after JP exit uncover, and the UTP. Vapor flow through each of these two restrictions is then determined using a modified CCFL correlation with the appropriate coefficients.

Vapor flows through the SEO, prior to JP exit uncover, and the bypass outlet are estimated from vapor mass balances. Liquid flows are then determined from the CCFL correlation, when the vapor flows are less than the limiting vapor flows.

F-4.1 Bundle Inlet SEO Flow Rates

After LP flashing and before JP exit uncover, most of the vapor generated by LP flashing flows through the SEO. Assuming vapor flow through the JPs is negligible,

the expression for SEO vapor flow, $W_{g_{SEO}}$, is derived using the vapor mass balance:

$$W_{g_{SEO}} = W_{fg_{LP}} + W_{GT} \quad (F-9)$$

where

$W_{fg_{LP}}$ = vapor generation from LP flashing

W_{GT} = guide tube flow (assumed to be saturated vapor).

From the First Law of Thermodynamics, W_{fg} is approximated as:

$$W_{fg} = 1/h_{fg} \left[\dot{Q} - M_f \frac{dh_f}{dP} \frac{dP}{dt} \right] \quad (F-10)$$

where

\dot{Q} = heat transfer from the nearby walls and internals (≈ 0)

M_f = total saturated liquid mass

$W_{g_{SEO}}$ is calculated using Equations F-9 and F-10 and numbers derived from the test data in Appendix J. Because $W_{g_{SEO}}$ is much greater than the corresponding limiting vapor flow before JP exit uncover, the SEO liquid flow, $W_{f_{SEO}}$, during this period is 0.

After the JP exit plane is uncovered, a portion of vapor generated within the LP flows through the JPs. A mass conservation equation for the control volume shown in Figure F-2 is derived:

$$W_{f_{SEO}} - W_{g_{SEO}} = \dot{M}_{CV} + W_{BF} - W_{GT} - W_{AN} \quad (F-11)$$

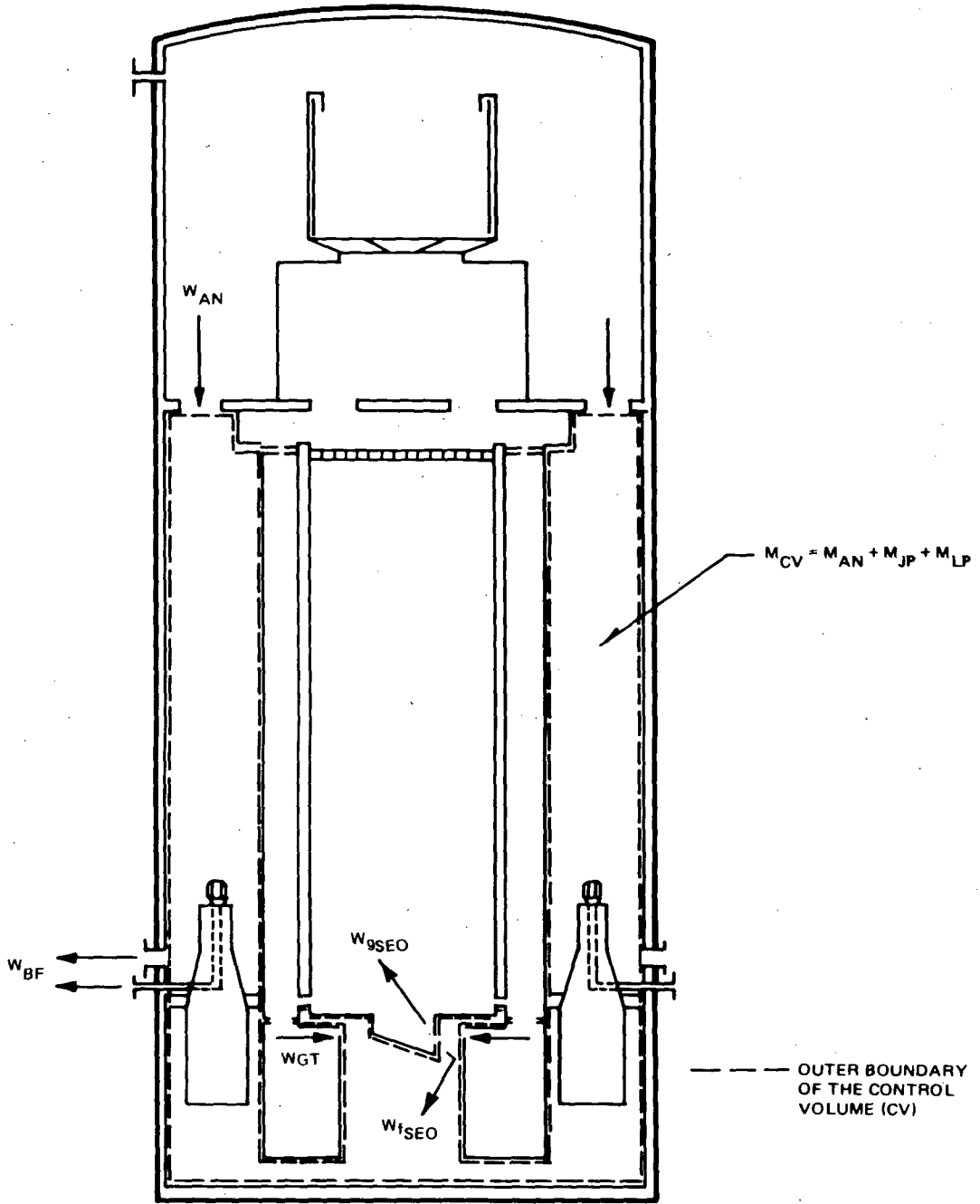


Figure F-2. Control Volume around the Annulus, Jet Pumps, and Lower Plenum.

where

\dot{M}_{CV} = change in liquid mass within the control volume

W_{BF} = break flow rate

W_{AN} = mass flow rate from the steam separator and steam dome to the annulus
(~ 0 lbm/sec)

In order to calculate the SEO flow rates, Equation F-11 must be solved simultaneously with a CCFL correlation which is a function of flow rates instead of dimensionless volumetric fluxes. This CCFL correlation is produced by combining Equations F-1, F-2, F-3, and F-4:

$$\left(\frac{W_g}{\rho_g} \right)^{1/2} + m \left(\frac{W_f}{\rho_f} \right)^{1/2} = bA^{1/2} [gg_c \sigma (\rho_f - \rho_g)]^{1/8} \quad (F-12)$$

$W_{f_{SEO}}$ and $W_{g_{SEO}}$ are found by solving Equations F-11 and F-12 simultaneously and substituting values derived from the test data in Appendix J.

F-4.2 UTP Flow Rates

After HPCS injection begins and before CCFL breakdown at the bypass outlet occurs, an upper plenum mass balance is used to find $W_{g_{UTP}}$ and $W_{f_{UTP}}$, the vapor and liquid flow rates at the UTP. During this period, the liquid flow at the bypass outlet is negligible because of CCFL. Figure F-3 shows the upper plenum as a control volume from which the following equation is derived:

$$W_{f_{UTP}} - W_{g_{UTP}} = W_{CS} - \dot{M}_{CV} - W_{UP} \quad (F-13)$$

where

W_{CS} = core spray flow rate

W_{UP} = flow from upper plenum to separator (~ 0 lbm/sec)

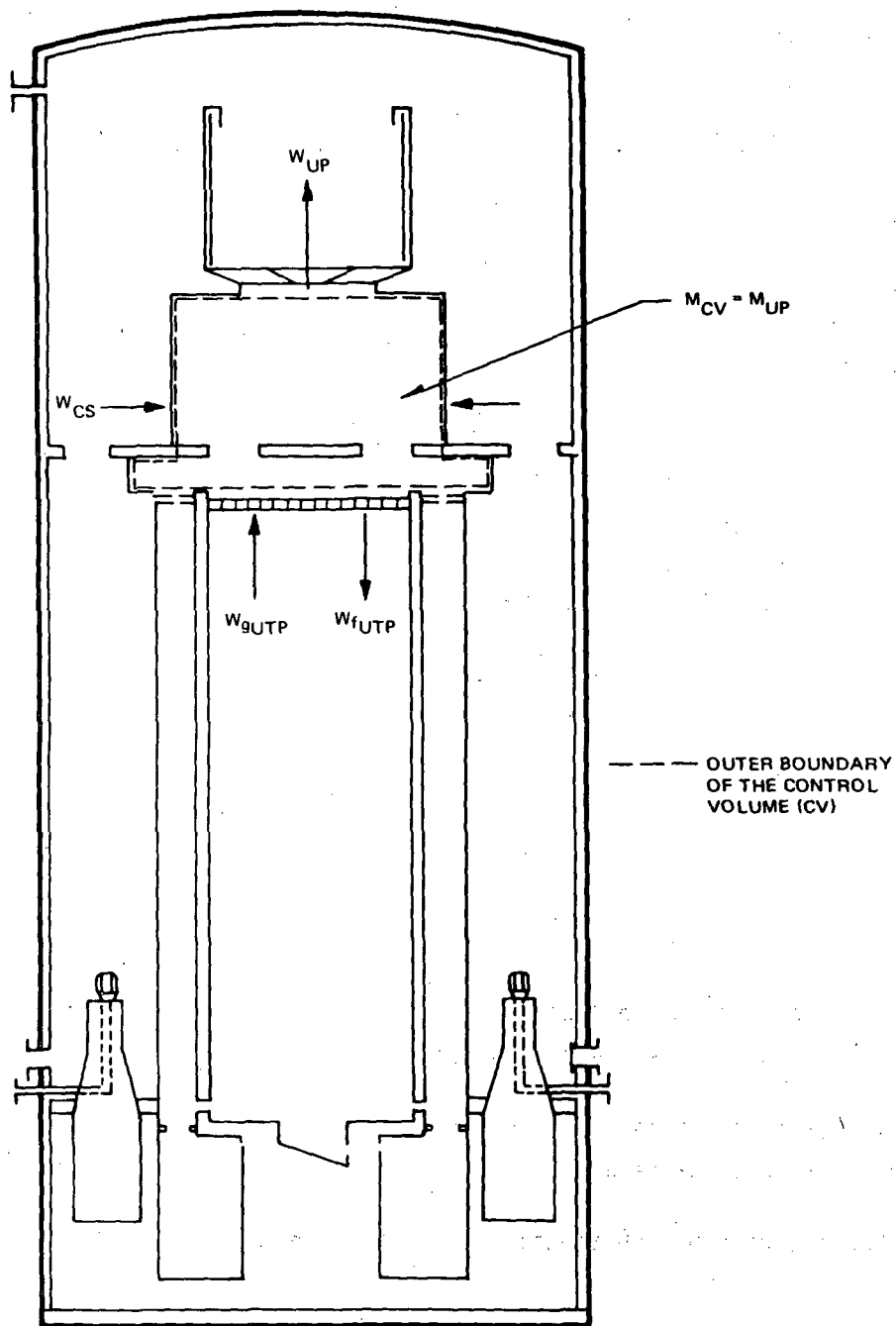


Figure F-3. Upper Plenum Control Volume

$W_{f_{UTP}}$ and $W_{g_{UTP}}$ are found by solving Equations F-12 and F-13 simultaneously and substituting values derived from the test data in Appendix J.

F-4.3 Bypass Outlet Flow Rates

The vapor flow at the bypass outlet, $W_{g_{BYO}}$, is found from a vapor mass balance for the bypass/guide tubes. Assuming the bypass leakage vapor flow is negligible, the following equation is derived:

$$W_{g_{BYO}} = W_{fg_{BY}} + W_{fg_{GT}} - W_{GT} - W_{LPCI} P_{LPCI} \quad (F-14)$$

where

$W_{fg_{BY}}$ = vapor generation from flashing in the bypass tubes (defined by Equation F-10)

$W_{fg_{GT}}$ = vapor generation from flashing in the guide tubes (defined by Equation F-10)

W_{LPCI} = LPCI flow rate

P_{LPCI} = condensing potential of the LPCI fluid (defined by Equation F-8)

$W_{g_{BYO}}$ is calculated using values found from the test data in Appendix J. Before LPCI injection begins, the bypass vapor flow is much greater than the corresponding limiting vapor flow; therefore the bypass liquid flow, $W_{f_{BYO}}$, is essentially zero.

After LPCI injection begins, the condensing potential of the LPCI fluid is sufficiently large to cause a rapid CCFL breakdown. $W_{f_{BYO}}$ is calculated during

this breakdown period by substituting $W_{g_{BYO}}$ into the modified CCFL correlation, Equation F-12.

F-5. REFERENCES

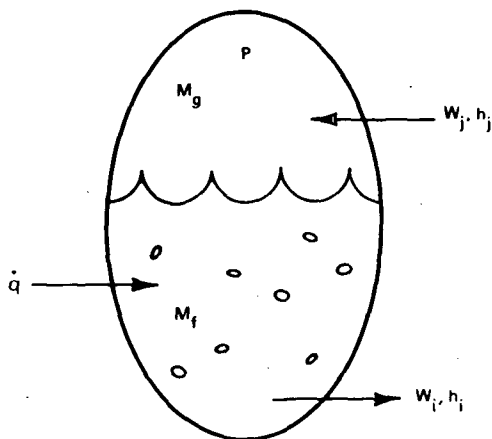
- F-1. D. D. Jones, Subcooled Counter-Current Flow Limiting Characteristics of the Upper Region of a BWR Fuel Bundle, General Electric Company, 1977 (NEDE-23549).
- F-2. D. D. Jones, Test Report - TLTA Components CCFL Tests, General Electric Company, December 1977 (NEDG-23732).
- F-3. M. Naitoh, K. Chino, and R. Kawabe, "Restrictive Effect of Ascending Steam on Fading Water during Top Spray Emergency Core Cooling," J. of Nuclear Science and Technology, Vol. 15, 11, p. 806 (1978).
- F-4. C. Hsieh et al., Counter-Current Air/Water and Steam/Water Flow along a Perforated Plate, Northwestern University, November 1980 (NUREG/CR-1808).

Appendix G

THE SYSTEM DEPRESSURIZATION EQUATION

G-1. DERIVATION OF THE VESSEL DEPRESSURIZATION RATE

The system depressurization equation is derived from the First Law of Thermodynamics. Consider the system as depicted below:



G-1.1 Mass Balance

From a mass balance on the control volume*:

$$V = m_f v_f + m_g v_g = \text{CONSTANT} \quad (\text{G-1})$$

The total mass is:

$$m = m_f + m_g \quad (\text{G-2})$$

*Nomenclature for the equations is included at the back of this Appendix.

G-1.2 Mass Rate

From continuity we can write:

$$\frac{dm_g}{dt} = \sum_j w_{gj} - \sum_i w_{gi} + W_{fg} \quad (G-3)$$

where

$$\begin{aligned} w &= \text{mass flow rate} \\ W_{fg} &= \text{net flashing rate} \end{aligned}$$

(The subscript j corresponds to inflow while i refers to the outflow from the control volume evaluated at the thermodynamic conditions within the control volume.)

Also,

$$\frac{dm_f}{dt} = \sum_j w_{fj} - \sum_i w_{fi} - W_{fg} \quad (G-4)$$

G-1.3 Energy Rate

From the First Law of Thermodynamics:

$$(\text{net inflow of energy}) - (\text{net outflow}) = (\text{net change})$$

$$\begin{aligned} & \left(\dot{q} + \sum_j w_{fj} h_{fj} + \sum_j w_{gj} h_{gj} \right) - \left(\sum_i w_{fi} h_{fi} + \sum_i w_{gi} h_{gi} \right) \\ &= \frac{d}{dt} (m_f h_f + m_g h_g - VP) \end{aligned} \quad (G-5)$$

The right hand side of Equation G-5 is expanded using the chain rule (note that $\dot{V} = 0$):

$$\frac{d}{dt} (m_f h_f + m_g h_g - VP) = \left[m_g \frac{dh_g}{dP} + m_f \frac{dh_f}{dP} - V \right] \frac{dP}{dt} + h_g \frac{dm_g}{dt} + h_f \frac{dm_f}{dt} \quad (G-6)$$

G-1.3 Flashing Rate

Substituting Equations G-3 and G-4 into G-6:

$$\begin{aligned} \frac{d}{dt} (m_f h_f + m_g h_g - VP) &= \left[m_g \frac{dh_g}{dP} + m_f \frac{dh_f}{dP} - V \right] \frac{dP}{dt} \\ &+ h_g \left[\sum_j w_{g_j} - \sum_i w_{g_i} + W_{fg} \right] \\ &+ h_f \left[\sum_i w_{f_j} - \sum_i w_{f_i} - W_{fg} \right] \end{aligned} \quad (G-7)$$

Substituting

$$h_{fg} = h_g - h_f \quad (G-8)$$

into Equation G-7 and putting the results back into G-5:

$$\begin{aligned} \left[m_f \frac{dh_f}{dP} + m_g \frac{dh_g}{dP} - V \right] \frac{dP}{dt} + h_{fg} W_{fg} + h_f \sum_j w_{f_j} - h_f \sum_i w_{f_i} + h_g \sum_j w_{g_j} \\ - h_g \sum_i w_{g_i} = \dot{q} + \sum_j w_{f_j} h_{f_j} + \sum_j w_{g_j} h_{g_j} - \sum_i w_{f_i} h_{f_i} - \sum_i w_{g_i} h_{g_i} \end{aligned} \quad (G-9)$$

Solving for W_{fg} , we obtain:

$$\begin{aligned} W_{fg} = \frac{1}{h_{fg}} \left\{ \dot{q} + \sum_j w_{f_j} h_{f_j} + \sum_j w_{g_j} h_{g_j} - \sum_i w_{f_i} h_{f_i} \right. \\ \left. - \sum_i w_{g_i} h_{g_i} - \left[m_f \frac{dh_f}{dP} + m_g \frac{dh_g}{dP} - V \right] \frac{dP}{dt} - h_f \sum_j w_{f_j} \right. \\ \left. + h_f \sum_i w_{f_i} - h_g \sum_j w_{g_j} + h_g \sum_i w_{g_i} \right\} \end{aligned} \quad (G-10)$$

Now because the flow issuing from the control volume has the same thermodynamic properties as the fluid in that volume, then:

$$h_{f_i} = h_f ; h_{g_i} = h_g$$

and Equation G-10 can be rearranged to yield:

$$\begin{aligned} w_{fg} = \frac{1}{h_{fg}} & \left\{ \dot{q} + \sum_j w_{f_j} h_{f_j} + \sum_j w_{g_j} h_{g_j} - h_f \sum_j w_{f_j} - h_g \sum_j w_{g_j} \right. \\ & - \sum_i w_{f_i} (h_{f_i} - h_{f_i}) - \sum_i w_{g_i} (h_{g_i} - h_{g_i}) \\ & \left. - \left[m_f \frac{dh_f}{dP} + m_g \frac{dh_g}{dP} - V \right] \frac{dP}{dt} \right\}. \end{aligned} \quad (G-11)$$

This reduces to:

$$\begin{aligned} w_{fg} = & \left\{ \frac{1}{h_{fg}} \dot{q} + \sum_j w_{f_j} h_{f_j} + \sum_j w_{g_j} h_{g_j} - h_f \sum_j w_{f_j} - h_g \sum_j w_{g_j} \right. \\ & \left. - \left[m_f \frac{dh_f}{dP} + m_g \frac{dh_g}{dP} - V \right] \frac{dP}{dt} \right\} \end{aligned} \quad (G-12)$$

G-1.4 Vessel Depressurization Rate

To arrive at an expression for the depressurization rate we start by obtaining the derivative of Equation G-1 for $V = 0$:

$$m_g \frac{dv_g}{dt} + v_g \frac{dw_g}{dt} + m_f \frac{dv_f}{dP} + v_f \frac{dm_f}{dt} = 0 \quad (G-13)$$

Applying the chain rule we obtain:

$$v_g \frac{dm_g}{dt} + v_f \frac{dm_f}{dt} + \left[m_f \frac{dv_f}{dP} + m_g \frac{dv_g}{dP} \right] \frac{dP}{dt} = 0 \quad (G-14)$$

Using the expressions for dm_g/dt and dm_f/dt from Equations G-3 and G-4 we have:

$$v_g \left[\sum_j w_{g_j} - \sum_i w_{g_i} + W_{fg} \right] + v_f \left[\sum_j w_{f_j} - \sum_i w_{f_i} - W_{fg} \right] + \left[m_f \frac{dv_f}{dP} + m_g \frac{dv_g}{dP} \right] \frac{dP}{dt} = 0. \quad (G-15)$$

Substituting the expression for W_{fg} into Equation G-15:

$$v_g \left[\sum_j w_{g_j} - \sum_i w_{g_i} \right] + v_f \left[\sum_j w_{f_j} - \sum_i w_{f_i} \right] + \left[m_f \frac{dv_f}{dP} + m_g \frac{dv_g}{dP} \right] \frac{dP}{dt} + \frac{v_{fg}}{h_{fg}} \left\{ \dot{q} + \sum_j w_{g_j} h_{g_j} + \sum_j w_{f_j} h_{f_j} - h_g \sum_j w_{g_j} - h_f \sum_j w_{f_j} - \left[m_f \frac{dh_f}{dP} + m_g \frac{dh_g}{dP} - V \right] \frac{dP}{dt} \right\} = 0. \quad (G-16)$$

Combining like terms and solving for dP/dt :

$$\frac{dP}{dt} = - \left[\frac{f_1(P) + f_2(P)}{f_3(P)} \right] \quad (G-17)$$

where

$$f_1(P) = v_f \left[\sum_j w_{f_j} - \sum_i w_{f_i} \right] + v_g \left[\sum_j w_{g_j} - \sum_i w_{g_i} \right] \quad (G-18)$$

$$f_2(P) = \frac{v_{fg}}{h_{fg}} \left[\dot{q} + \sum_j w_{g_j} h_{g_j} + \sum_j w_{f_j} h_{f_j} - h_g \sum_j w_{g_j} - h_f \sum_j w_{f_j} \right] \quad (G-19)$$

$$f_3(P) = \left\{ m_f \frac{dv_f}{dP} + m_g \frac{dv_g}{dP} - \frac{v_{fg}}{h_{fg}} \left[m_f \frac{dh_f}{dP} + m_g \frac{dh_g}{dP} - V \right] \right\} \quad (G-20)$$

G-1.5 System Depressurization Equation for TLTA

After 20 seconds into the blowdown transient in TLTA, the flows into and out of the pressure vessel are from the ECCS and out the break. The ECC flows are of subcooled water, and so a simple subscript "e" is used. The break flow is from the vessel so that the saturated water and steam out the break are the same as those in the vessel, and no subscript is used. Equation G-17 then takes the following form:

$$-\frac{dP}{dt} = \frac{V_g W_g + V_f W_f - V_e W_e + (V_{fg}/h_{fg}) [\dot{q} + W_e (h_f - h_e)]}{\left[\frac{V_{fg}}{h_{fg}} \left(m_f \frac{dh_f}{dp} + m_g \frac{dh_g}{dp} - V \right) + \left(m_f \frac{dv_f}{dp} + m_g \frac{dv_g}{dp} \right) \right]} \quad (G-21)$$

If heat addition is neglected, Equation G-21 becomes:

$$-\frac{dP}{dt} = \frac{V_g W_g + V_f W_f - V_e W_e + V_{fg} W_e (h_f - h_e)/h_{fg}}{\left[\frac{V_{fg}}{h_{fg}} \left(m_f \frac{dh_f}{dp} + m_g \frac{dh_g}{dp} - V \right) + \left(m_f \frac{dv_f}{dp} + m_g \frac{dv_g}{dp} \right) \right]} \quad (G-22)$$

G-2. EFFECT OF SYSTEM MASS ON DEPRESSURIZATION

The liquid mass in TLTA-5A is lower than the mass in TLTA-5 after 20 seconds because of the isolation of the excess liquid volume in Recirculation Loop 1 in TLTA-5A.

Because the system mass is an important parameter in the depressurization equation, a difference in masses between TLTA-5 and TLTA-5A leads to a difference in depressurizations, if all other factors are equal.

A ratio of depressurizations from TLTA-5 and TLTA-5A at one particular pressure is found by knowing that the ECC flows and enthalpies, break flows and qualities, and heat transfer rates to the surroundings are similar in both TLTA configurations for the same transient. Using Equation G-17 to define depressurization, the ratio is derived:

$$\frac{(dP/dt)_{TLTA\ 5A}}{(dP/dt)_{TLTA\ 5}} = + \frac{[f_3(P)]_{TLTA\ 5}}{[f_3(P)]_{TLTA\ 5A}} \quad (G-21)$$

where

$$[f_1(P)]_{TLTA\ 5} = [f_1(P)]_{TLTA\ 5A} \quad (G-22)$$

$$[f_2(P)]_{TLTA\ 5} = [f_2(P)]_{TLTA\ 5A} \quad (G-23)$$

Substituting Equation G-20 for $f_3(P)$ and rearranging, Equation G-21 becomes:

$$\begin{aligned} \frac{(dP/dt)_{TLTA\ 5A}}{(dP/dt)_{TLTA\ 5}} = & \left[m_{f,TLTA\ 5} \left(\frac{dv_f}{dP} - \frac{v_{fg}}{h_{fg}} \frac{dh_f}{dP} \right) + m_{g,TLTA\ 5} \left(\frac{dv_g}{dP} - \frac{v_{fg}}{h_{fg}} \frac{dh_g}{dP} \right) \right. \\ & \left. + V_{TLTA\ 5} \frac{v_{fg}}{h_{fg}} \right] \div \left[m_{f,TLTA\ 5A} \left(\frac{dv_f}{dP} - \frac{v_{fg}}{h_{fg}} \frac{dh_f}{dP} \right) \right. \\ & \left. + m_{g,TLTA\ 5A} \left(\frac{dv_g}{dP} - \frac{v_{fg}}{h_{fg}} \frac{dh_g}{dP} \right) + V_{TLTA\ 5A} \frac{v_{fg}}{h_{fg}} \right] \quad (G-24) \end{aligned}$$

Using Equation G-1 for $V_{TLTA\ 5}$ and $V_{TLTA\ 5A}$, Equation G-24 is further reduced to:

$$\begin{aligned} \frac{(dP/dt)_{TLTA\ 5A}}{(dP/dt)_{TLTA\ 5}} = & \left[m_{f,TLTA\ 5} \left[\frac{dv_f}{dP} - \frac{v_{fg}}{h_{fg}} \left(\frac{dh_f}{dP} - \frac{v_f v_{fg}}{h_{fg}} \right) \right. \right. \\ & \left. \left. + m_{g,TLTA\ 5} \left[\frac{dv_g}{dP} - \frac{v_{fg}}{h_{fg}} \left(\frac{dh_g}{dP} - \frac{v_g v_{fg}}{h_{fg}} \right) \right] \right] \div \right. \\ & \left[m_{f,TLTA\ 5A} \left[\frac{dv_f}{dP} - \frac{v_{fg}}{h_{fg}} \left(\frac{dh_f}{dP} - \frac{v_f v_{fg}}{h_{fg}} \right) \right. \right. \\ & \left. \left. + m_{g,TLTA\ 5A} \left[\frac{dv_g}{dP} - \frac{v_{fg}}{h_{fg}} \left(\frac{dh_g}{dP} - \frac{v_g v_{fg}}{h_{fg}} \right) \right] \right] \right] \quad (G-25) \end{aligned}$$

Assuming $m_{g,TLTA\ 5} \ll m_{f,TLTA\ 5}$ and $m_{g,TLTA\ 5A} \ll m_{f,TLTA\ 5A}$, the pressure ratio simplifies to:

$$\frac{(dP/dt)_{TLTA\ 5A}}{(dP/dt)_{TLTA\ 5}} \sim \frac{m_{f,TLTA\ 5}}{m_{f,TLTA\ 5A}} \quad (G-26)$$

G-3. SENSITIVITY STUDY OF THE DEPRESSURIZATION EQUATION

The following partial derivatives of the depressurization Equation G-22 were evaluated with the aid of a simple time-share program for conducting the study:

$$\frac{\partial \dot{P}}{\partial (A_B)}, \frac{\partial \dot{P}}{\partial (\dot{q})}, \frac{\partial \dot{P}}{\partial (h_\ell)}, \frac{\partial \dot{P}}{\partial (W_\ell)}, \frac{\partial \dot{P}}{\partial (X_B)}$$

where

- A_B = break area (ft²)
- \dot{q} = heat transfer to coolant (BTU/sec)
- h_ℓ = ECCS enthalpy (BTU/lb)
- W_ℓ = ECCS flow rate (lb/sec)
- X_B = break quality

The input quantities which could be varied to study their effects are:

- V ~ system volume (ft³)
- P ~ system pressure (psia)
- A_B ~ break area (ft²)
- X ~ total system quality
- X_B ~ quality of the break flow
- W_ℓ ~ ECCS flow rate (lb/sec)
- h_ℓ ~ ECCS enthalpy (BTU/lb)
- \dot{q} ~ heat transfer to coolant (BTU/sec)

Results of the study have been summarized in Table 3-13 (Subsection 3.4.3).

G-4. NOMENCLATURE

- h enthalpy
- m mass in vessel
- M initial mass in vessel
- P absolute pressure
- t time

v specific volume
V total vessel (control) volume
w mass flow rate
 W_{fg} flashing rate

Subscripts

e ECC
f saturated liquid property
g saturated vapor property
i exit
j inlet

Appendix H

TLTA BLOWDOWN FLOW MEASUREMENTS AND UNCERTAINTIES (D. W. Danielson, H. Ngo, L. S. Lee)

The blowdown mass flow rate for two TLTA tests was assessed by making use of four independent methods of flow rate measurement. Blowdown flow was calculated from (1) inventory loss from the pressure vessel, (2) suction line flow-limiting nozzle measurements, (3) combined drag disc and turbine meter measurements, and (4) the mass increase in the suppression tank. Each of these methods is discussed in more detail below with measurement results presented and evaluated. Break flow measurement devices are depicted in Figure H-1.

Tests evaluated were the reference test (6425/2 average power, average ECC) and the average power, no ECC test (6426/1). To summarize the blowdown flow measurement results, a comparison of flow rates from both tests using the most accurate method, the vessel inventory method, is shown in Figure H-2. In addition, comparisons of flow rates determined using the other methods are included in Table H-1 for Test 6425 and in Table H-2 for Test 6426.

H-1. FLOW RATE MEASUREMENT METHODS

H-1.1 Vessel Inventory Method

Nodal differential pressure transducers are installed in many places in the pressure vessel for use in measuring nodal mass inventory. The method for deriving nodal mass from the nodal differential pressure is explained in detail in Appendix C-2. A summation of the nodal masses yields the total mass inventory in the vessel. As discussed in Appendix C-3, the blowdown flow rate is determined from the rate of change of vessel inventory after adjustment for other flows in or out of the vessel.

If flow rates are high (such as at test initiation), the dynamic effects of spatial and temporal acceleration can affect the accuracy of the density determined from DP measurements. For these high-flow periods, a more accurate estimate of vessel inventory is obtained from the change in the system liquid level, where the fluid state is determined using pressure and temperature measurements.

Table H-1

BLOWDOWN FLOW ESTIMATE COMPARISON TEST 6425 RUN 2 (AVG POWER, AVG ECC)

Time (sec)	DPT Method							Drag Disc Turbine Meter Method				Blowdown Nozzle Method* (Drive Flow from TM/DD)			Suppression Tank Method				
	Net Vessel Inventory Σ DPT LBM	Loss of Inventory from Σ DPT LBM	Σ ECC Added LBM	Added from Loop #1 LBM	Loss from Steam Line LBM	Net Total Blowdown LBM	Average Blowdown Flow LBM/sec	Suction Line LBM	Drive Line LBM	Total LBM	Average Rate LBM/sec	Blowdown Nozzle LBM	Drive Line Flow Assumed from DD/TM LBM	Combined Total	Average Combined Flow LBM/sec	Tank Mass Increase LBM	Less Piping Mass LBM	Combined Total LBM	Average Flow LBM/sec
0	731	0	0	0	0	0	26.2	0	0	0	23.8	0	0	0	22.0	0	0	0	31.0
10	419	312	0	0	-50	262	9.6	189	49	238	7.5	171	49	220	9.2	360	-50	310	17.9
30	258	473	0	30	-50	453	2.4	305	82	387	2.2	322	82	404	2.3	818	-150	668	4.4
100	196	535	104	30	-50	605	2.3	421	121	542	3.9	447	121	568	1.85	1126	-150	976	1.7
200	282	449	423	30	-50	852		769	162	931		591	162	753		1298	-150	1148	

*Assumes 20% void fraction model.

Table H-2

BLOWDOWN FLOW ESTIMATES COMPARISON FOR TEST 6426 RUN 1 (AVG POWER, NO ECC)

Time (sec)	DPT Method							Drag Disc Turbine Meter Method				Blowdown Nozzle Method* (Drive Flow from TM/DD)			Suppression Tank Method				
	Net Vessel Inventory ΣDPT LBM	Loss of Inventory from ΣDPT LBM	ΣECC Added LBM	Added from Loop #1 LBM	Loss from Steam Line LBM	Net Total Blowdown LBM	Average Blowdown Flow LBM/sec	Suction Line LBM	Drive Line LBM	Total LBM	Average Rate LBM/sec	Blowdown Nozzle LBM	Drive Line Flow Assumed from DD/TM LBM	Combined Total	Average Combined Flow LBM/sec	Tank Mass Increase LBM	Less Piping Mass LBM	Combined Total LBM	Average Flow LBM/sec
0	685	0	0	0	0	0	26.7	0	0	0	26.8	0	0	0					
10	368	317	0	0	50	267	7.6	195	73	268	9.7	157	73	230			N/A		
30	246	439	0	30	50	419	1.9	313	149	462	1.7	309	149	458					
100	115	570	0	30	50	550	0.26	412	170	582	0.38	428	170	598					
200	89	596	0	30	50	576		441	179	620		468	179	642					

*Assumes 20% void fraction model

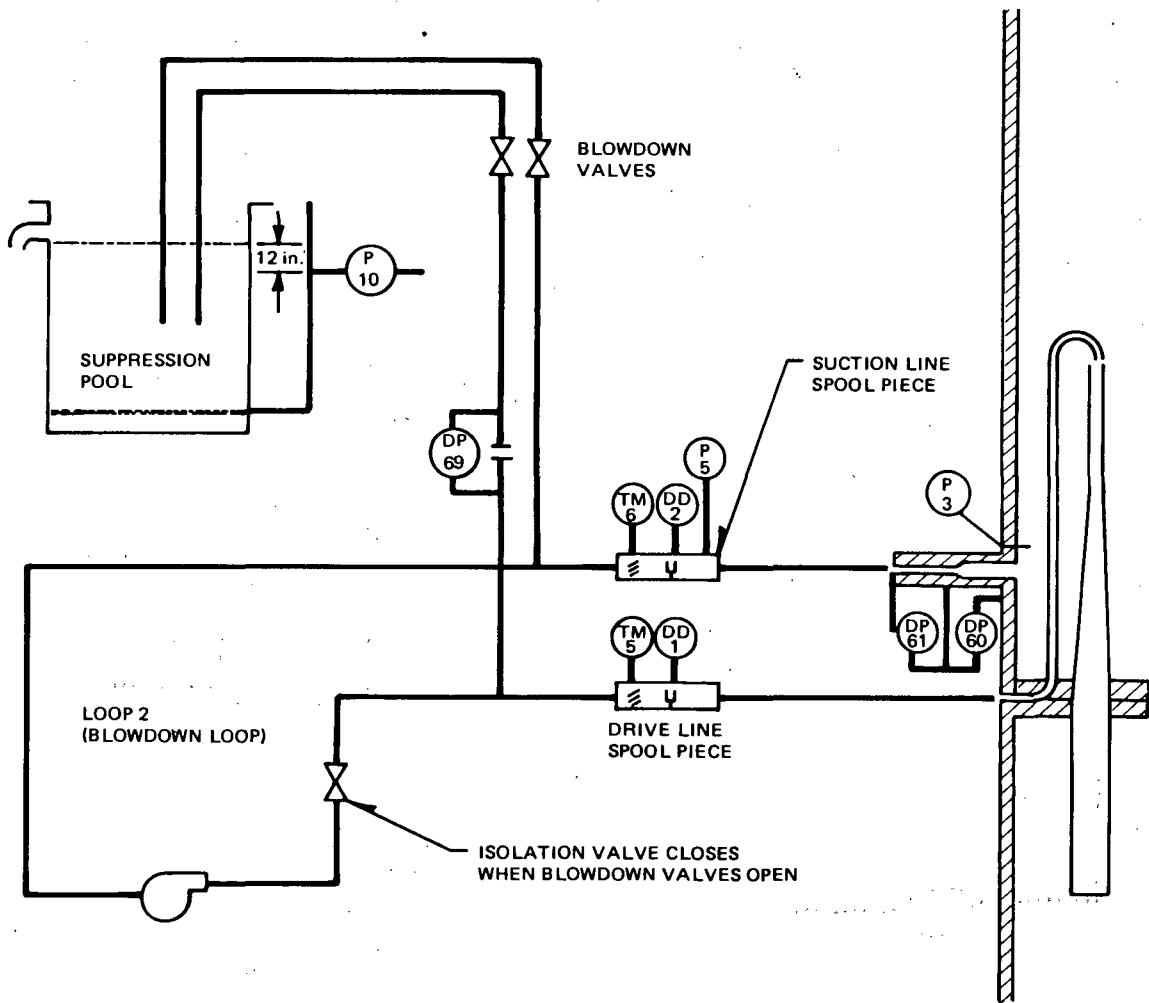


Figure H-1. Blowdown Loop Break Flow Measurements in TLTA 5A

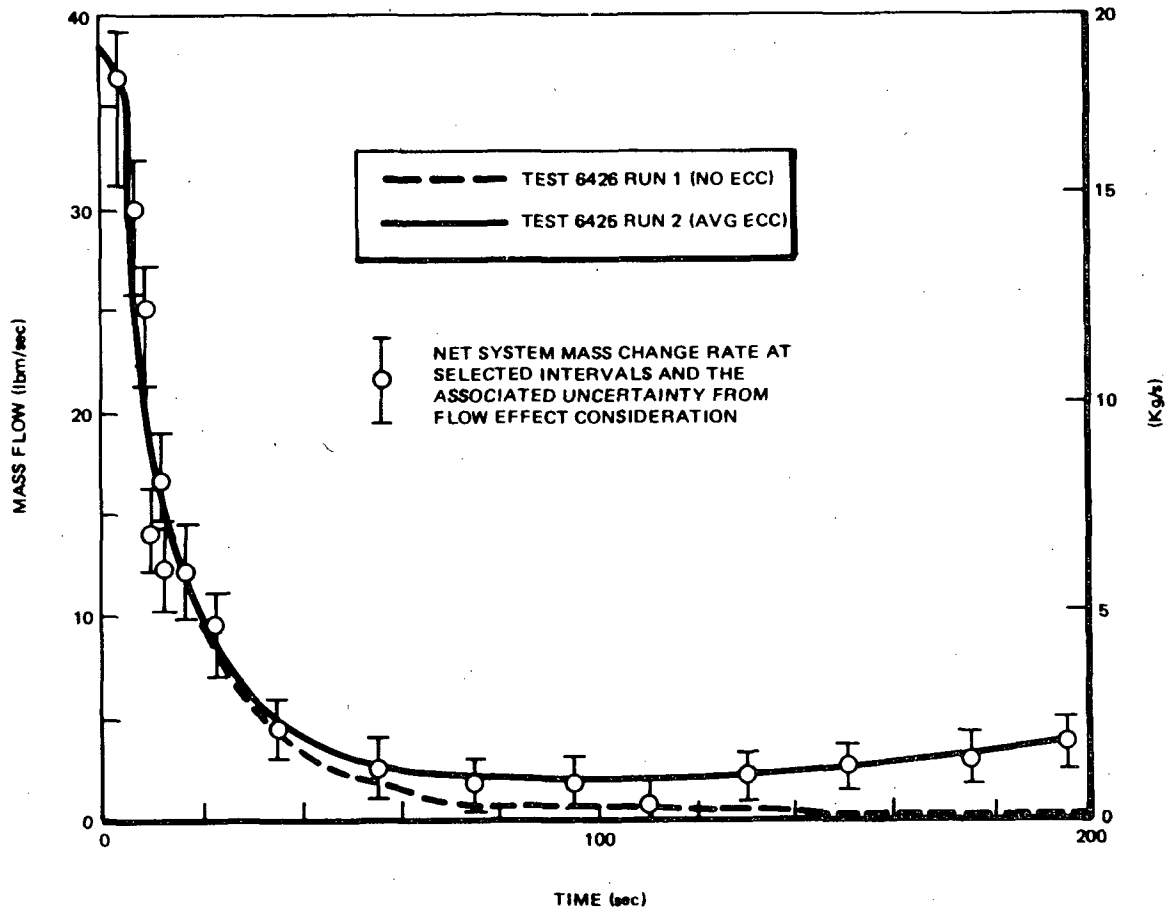


Figure H-2. Total Break Flow Determined from Inventory Method for Average Power Tests with (6425/1) and without (6426/1) ECC

H-1.2 Drag Disc/Turbine Meter Method

Separate measurements in spool pieces in the suction line and the drive line yield momentum flux and volumetric flow rate data. The mass flow rate and density through each line are calculated using the following expressions:

$$W = \frac{(\rho v^2)_{\text{drag disc}} (A)^2}{(Q)_{\text{turbine meter}}} \quad (\text{H-1})$$

$$\rho = \frac{(\rho v^2)_{\text{drag disc}} (A)^2}{(Q)^2_{\text{turbine meter}}} \quad (\text{H-2})$$

where

ρ = blowdown flow density - lb_m/ft^3

W = mass flow rate - lb_m/sec

ρv^2 = momentum flux from drag disc - $lb_m/ft \text{ sec}^2$

A = flow area - ft^2

Q = volumetric flow rate from turbine meter - ft^3/sec

H-1.3 Blowdown Nozzle Method

The suction line blowdown flow rate is estimated from pressure drop measurements at the flow-limiting nozzle. The basic equation used is the energy equation, by assuming adiabatic, isentropic flow and quasisteady-state conditions. Referring to Figure H-3, inlet fluid enthalpy and entropy at Point 1 are defined by the pressure and density and by assuming homogeneous, equilibrium conditions. The fluid is assumed to be saturated throughout the blowdown except initially when subcooling exists. For subcooled fluid, it is required to have a measurement of temperature along with the pressure to find the inlet enthalpy and entropy. The flow velocity at Point 1 is assumed to be negligible.

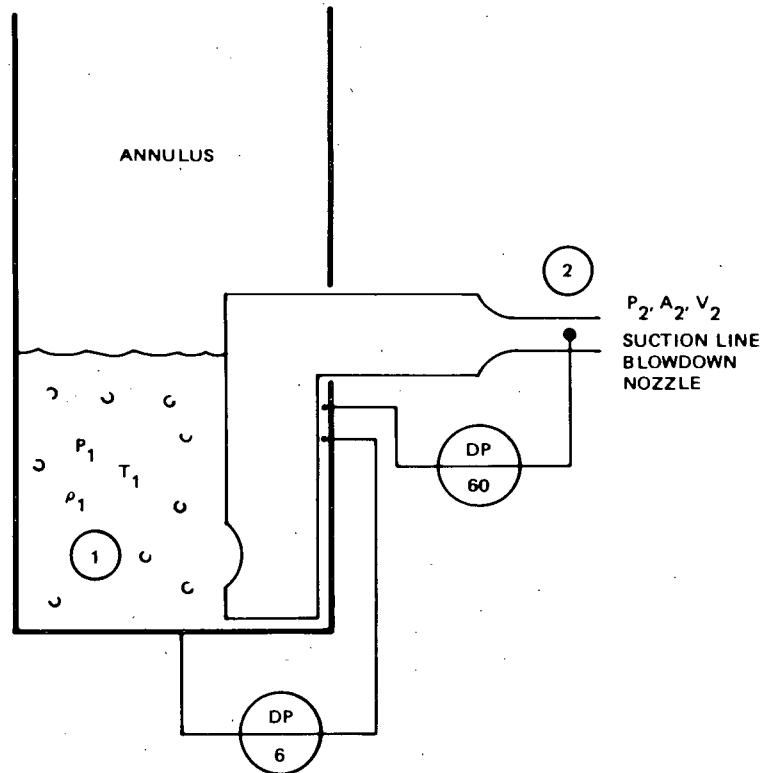


Figure H-3. TLTA Blowdown Flow Measurements

The pressure at Point 2 is found by subtracting the nozzle pressure drop from the pressure at Point 1. The outlet quality is determined by assuming isentropic flow from Point 1 to Point 2. Assuming saturated, homogeneous equilibrium conditions at the nozzle exit, the outlet enthalpy is determined by using the calculated outlet pressure and quality. Knowing the outlet enthalpy and using the energy equation for this system, an equation for the two-phase, homogeneous velocity in the nozzle at Point 2 is derived:

$$V_2 = [2 g_c (h_1 - h_2)]^{1/2} \quad (H-3)$$

where

V_2 = velocity in the nozzle (ft/sec)

g_c = 32.174 lb_m/ft/lb_f-sec²

h_1 = specific enthalpy in the annulus (ft-lb_f/lb_m)

h_2 = specific enthalpy in the nozzle (ft-lb_f/lb_m)

The standard nozzle flow equation was used for all the liquid flow at pretest conditions. The mass flow rate is then determined:

$$W = \rho_z A_z V_z \quad (H-4)$$

where

ρ_z = density at the nozzle exit (lb_m/ft³)

A_z = nozzle exit area (ft²)

One limitation of this method is that it is difficult to determine the actual blowdown line inlet density at Point 1. It is seen from Figure H-3 that the blowdown pipe inlet location is within Node 6. An average nodal density for Node 6 is determined, using the procedure detailed in Appendix C-2, from DP6, a differential pressure transducer measurement. When the two-phase level in the annulus is above Node 6, the inlet density is assumed to be the same as the average nodal density. However, when the two-phase level is within Node 6, the inlet density is found from the estimated two-phase level, the average nodal density, and the saturated liquid and steam densities.

To calculate the two-phase level within Node 6, the fluid in the node is assumed to have a 20 percent void fraction. This assumption is an approximation based upon typical observed void fractions. For example, data from the reference test in Figure H-4 show that the void fraction holds at about 20 percent in Node 6 between 200 and 300 seconds, while the next higher node, Node 7, is filling.

Figure H-5, showing the blowdown line inlet density for the reference test, was generated using the above density approximation methods.

H-1.4 Suppression Tank Method

In the TLTA system, all the blowdown flow is condensed in the suppression tank so that a measurement of the rate of increase of fluid mass in the tank is also a measurement of the blowdown flow rate. Compensation must be made for the fluid mass entering from the steam line during the first few seconds, the initial fluid mass in the blowdown piping, and the flashing fluid from the recirculation loop. These flows all add to the blowdown flow and result in an added level increase in the suppression tank. A special pressure averaging probe was used to sense tank fluid mass using a differential pressure transducer to minimize measurement errors of level during transient conditions. In Test 6426, it was necessary to keep supplying cooling water to minimize the temperature rise in the suppression tank. For this test it was impractical to use this method for estimating blowdown flow.

H-2. BLOWDOWN (BREAK) FLOW DETERMINATION

The flow rates were determined for Tests 6425 and 6426 using all four methods. A plot of both runs based on the vessel inventory method is shown in Figure H-1. The flow rates are similar, as expected, except for the time period when Test 6425 showed some added flow from the ECC sources.

The drag disc/turbine meter method data for Test 6425 are plotted in Figures H-6 through H-11, with Test 6426 plotted in Figures H-12 through H-17. The individual drag disc and turbine meter outputs for both the drive line and the suction line are included, as well as the resultant mass flow rates. When comparing the results from tests, it is seen that the volumetric flow rate is higher, but the mass flow rate is lower for Test 6426, which is due to the absence of the lower enthalpy ECC fluid at the break exit.

6-H

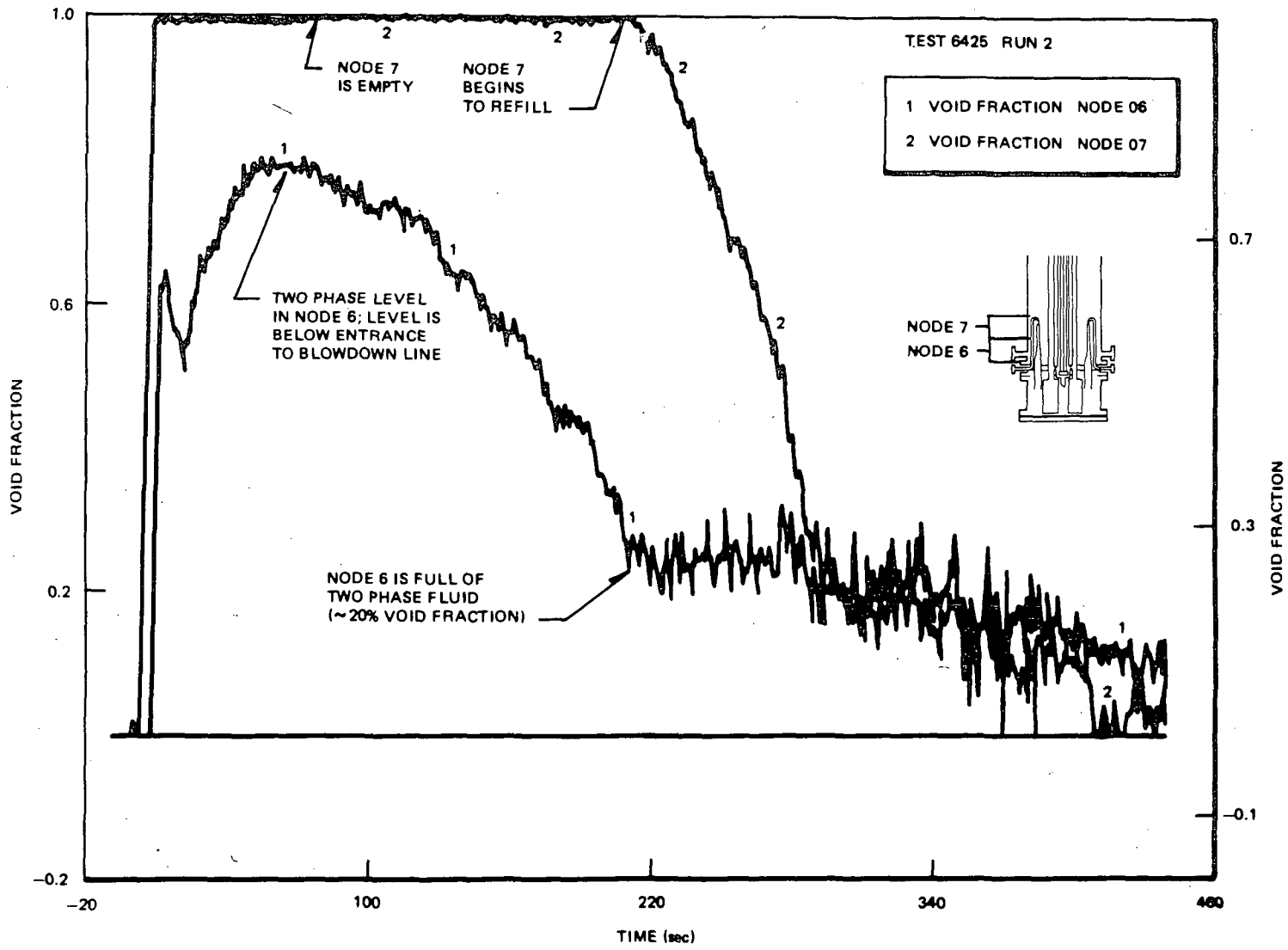


Figure H-4. Void Fraction at Nodes Upstream of Break for Test 6425 Run 2 (Avg. Power, Avg. ECC)

H-10

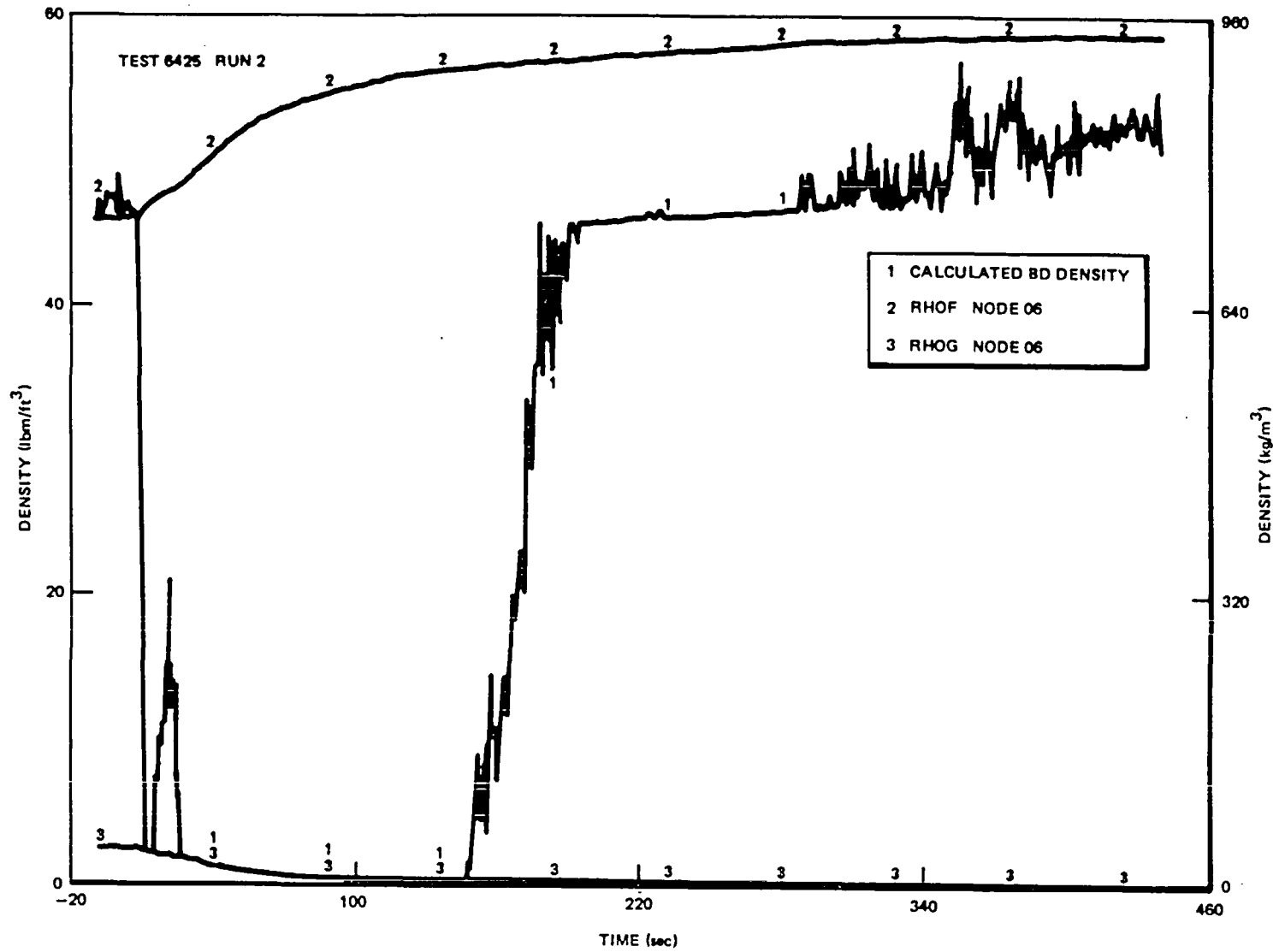


Figure H-5. Fluid Density Estimated for Break Flow through Nozzle of Test 6425 Run 2 (Avg. Power, Avg. ECC)

II-11

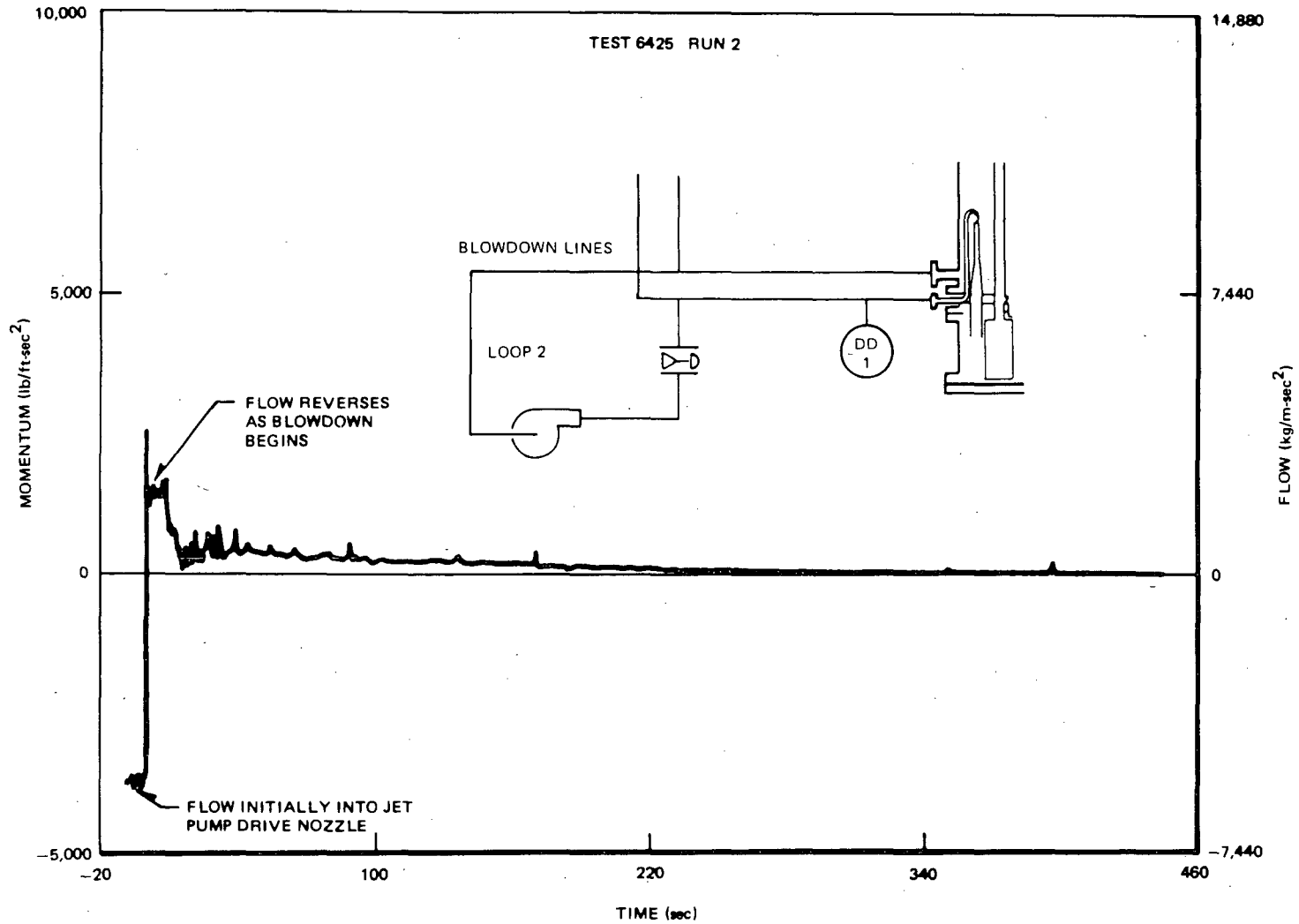


Figure H-6. Drive Line Drag Disc Momentum for Test 6425 Run 2 (Avg. Power, Avg. ECC)

H-12

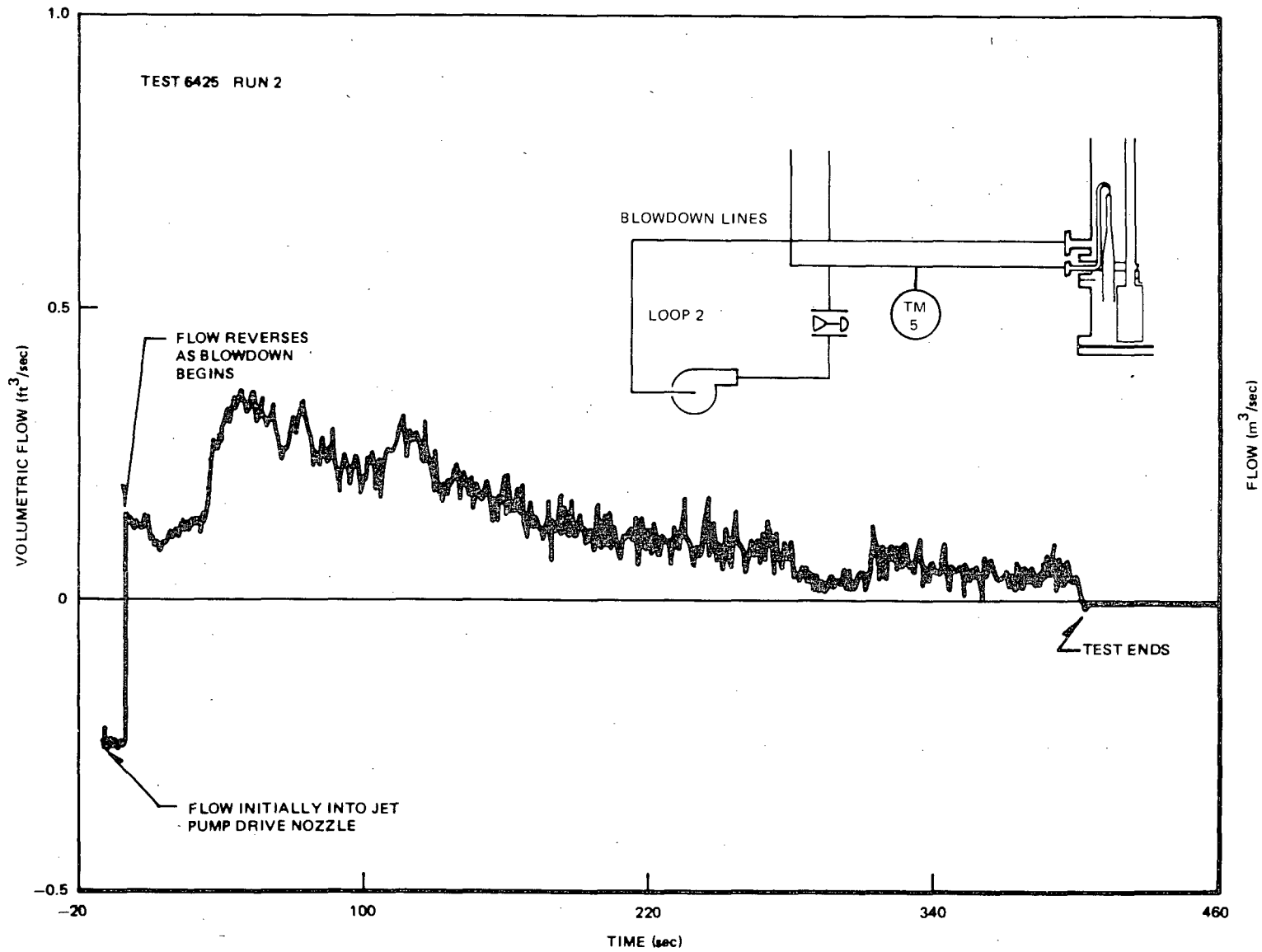


Figure H-7. Drive Line Turbinemeter Volumetric Flow for Test 6425 Run 2 (Avg. Power, Avg. ECC)

H-13

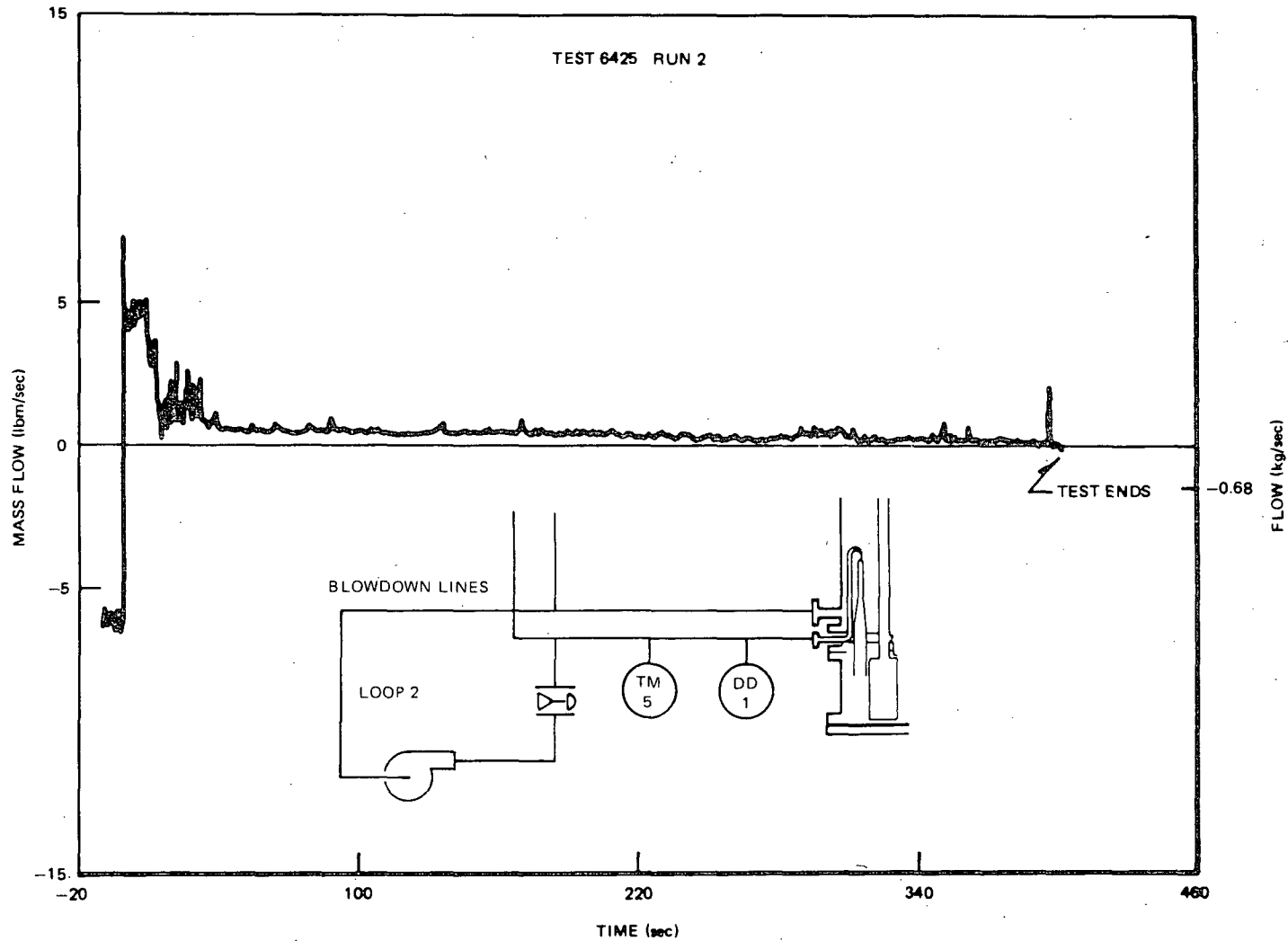


Figure H-8. Drive Line Break Flow Based on TM/DD Measurements for Test 6425 Run 2 (Avg. Power, Avg. ECC)

H-14

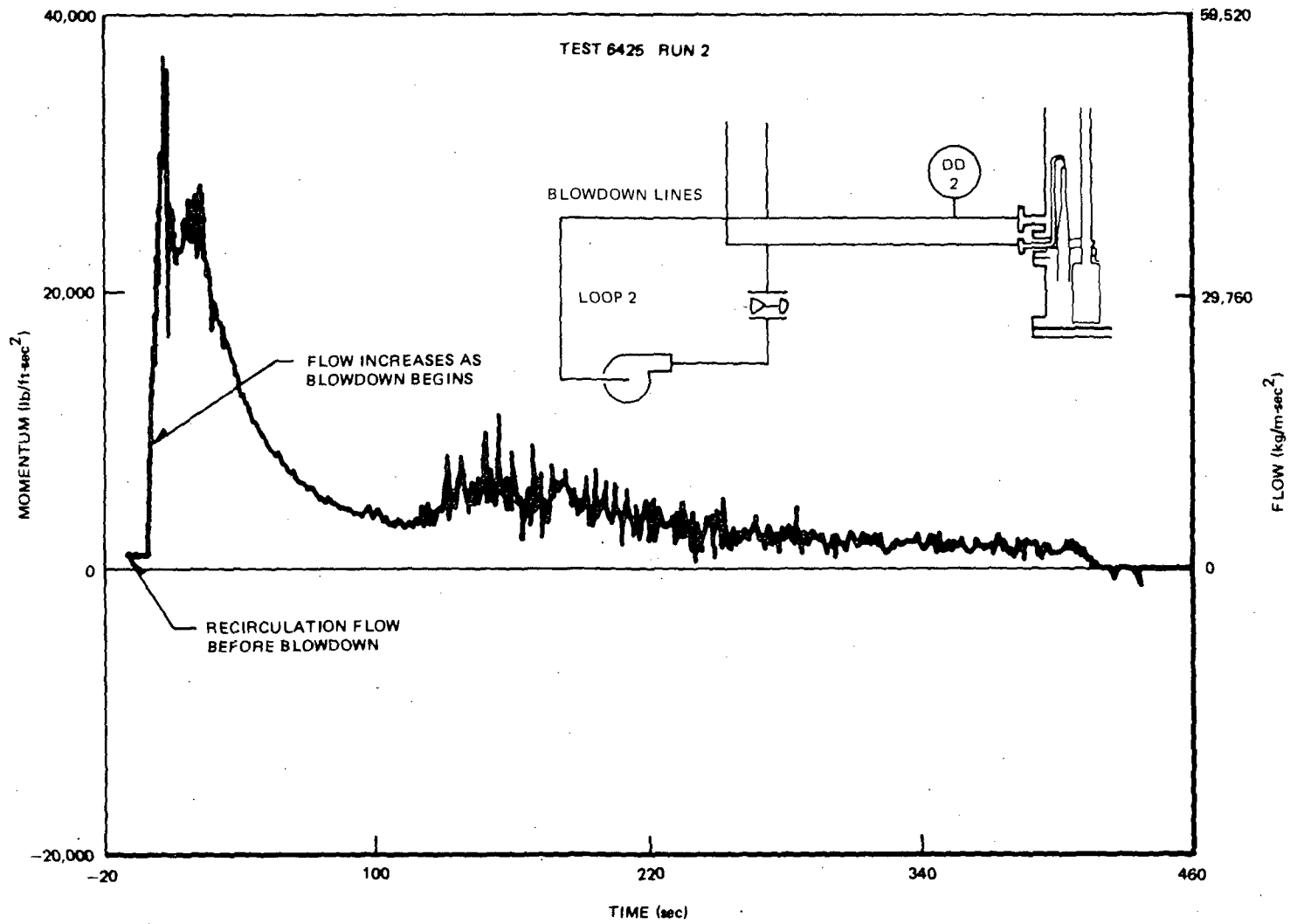


Figure H-9. Suction Line Drag Disc Momentum for Test 6425 Run 2

H-15

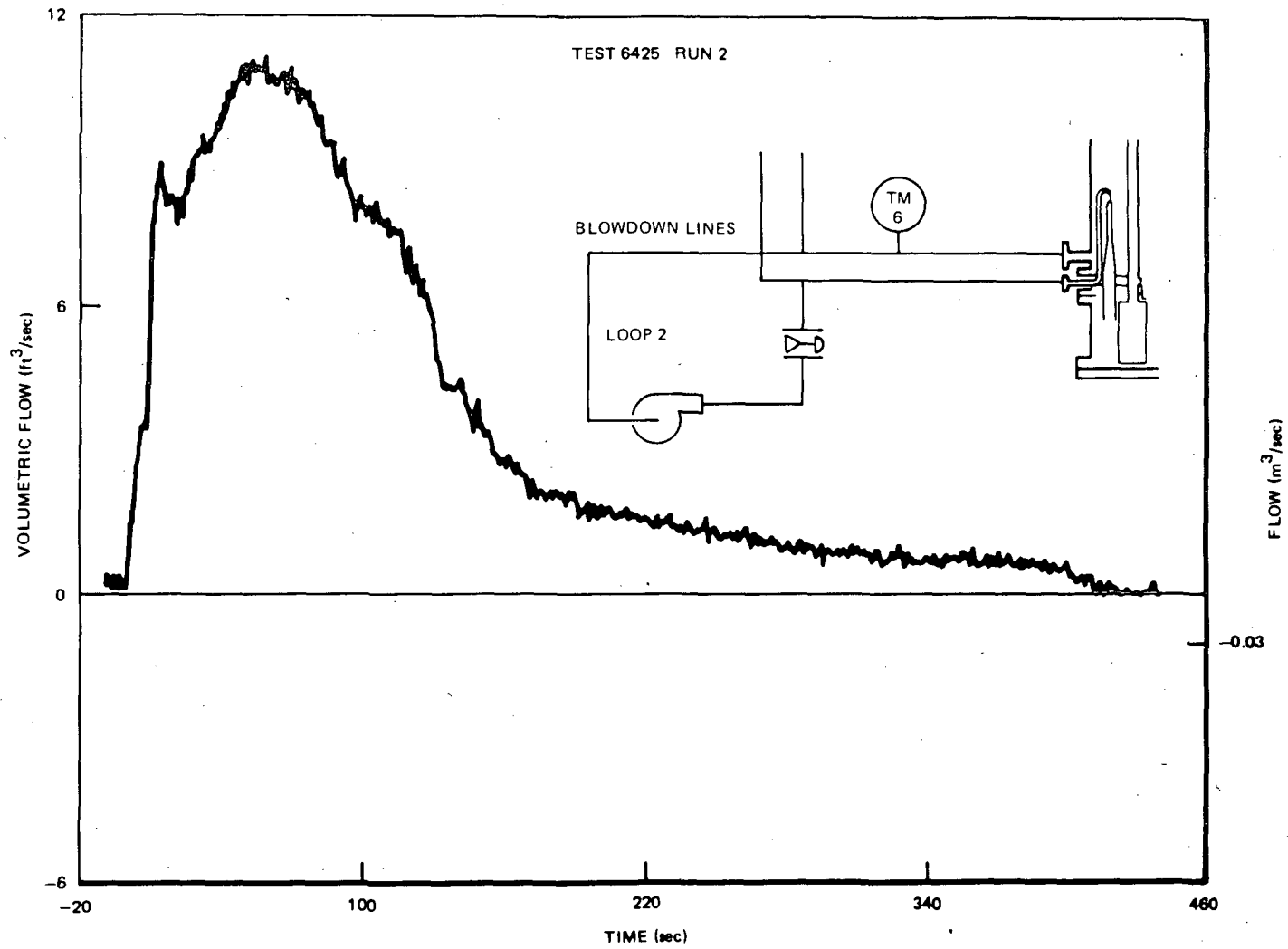


Figure H-10. Suction Line Turbinemeter Volumetric Flow for Test 6425 Run 2 (Avg. Power, Avg. ECC)

H-16

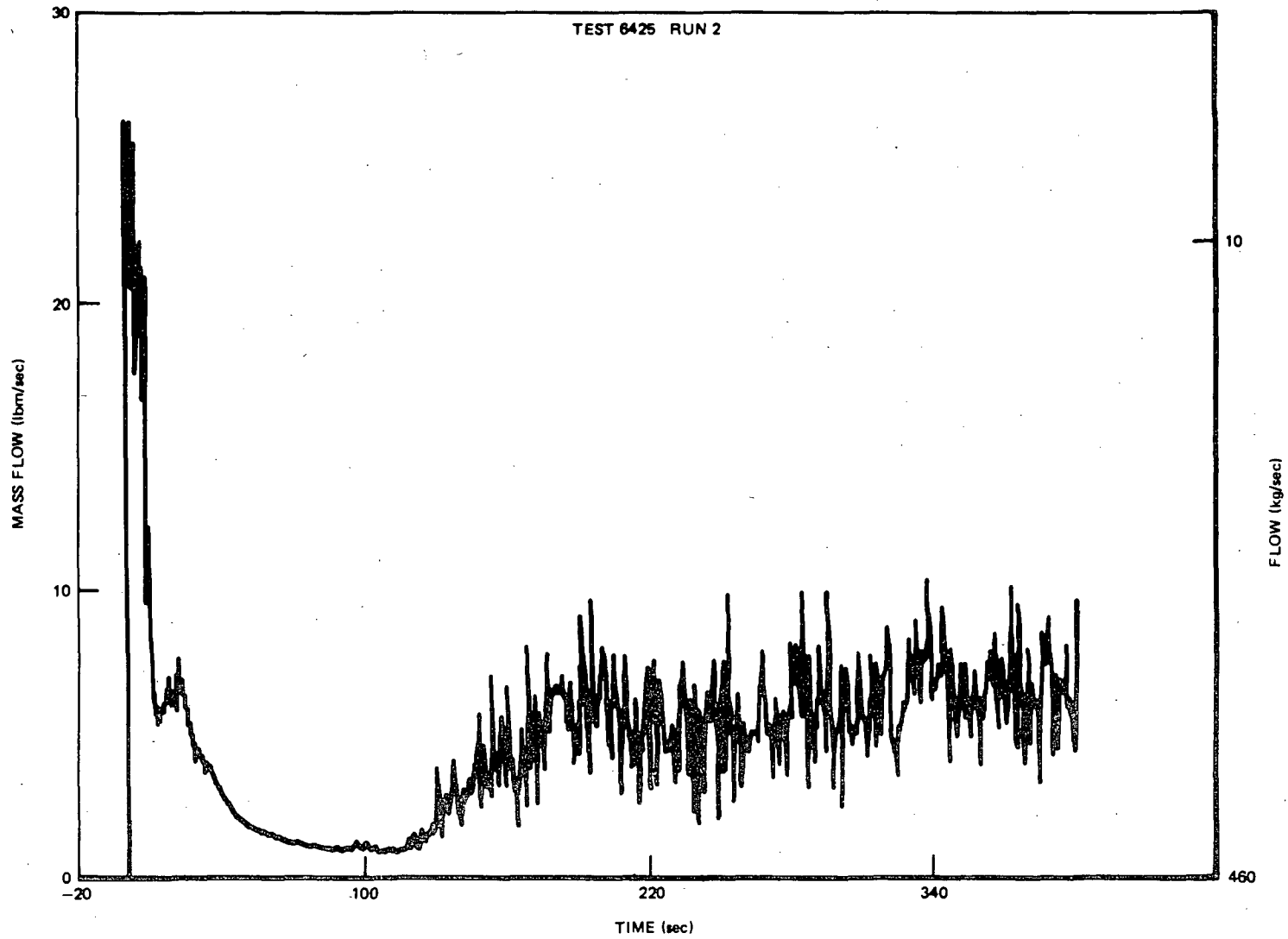


Figure H-11. Suction Line Break Flow Based on TM/DD for Test 6425 Run 2 (Avg. Power, Avg. ECC)

H-17

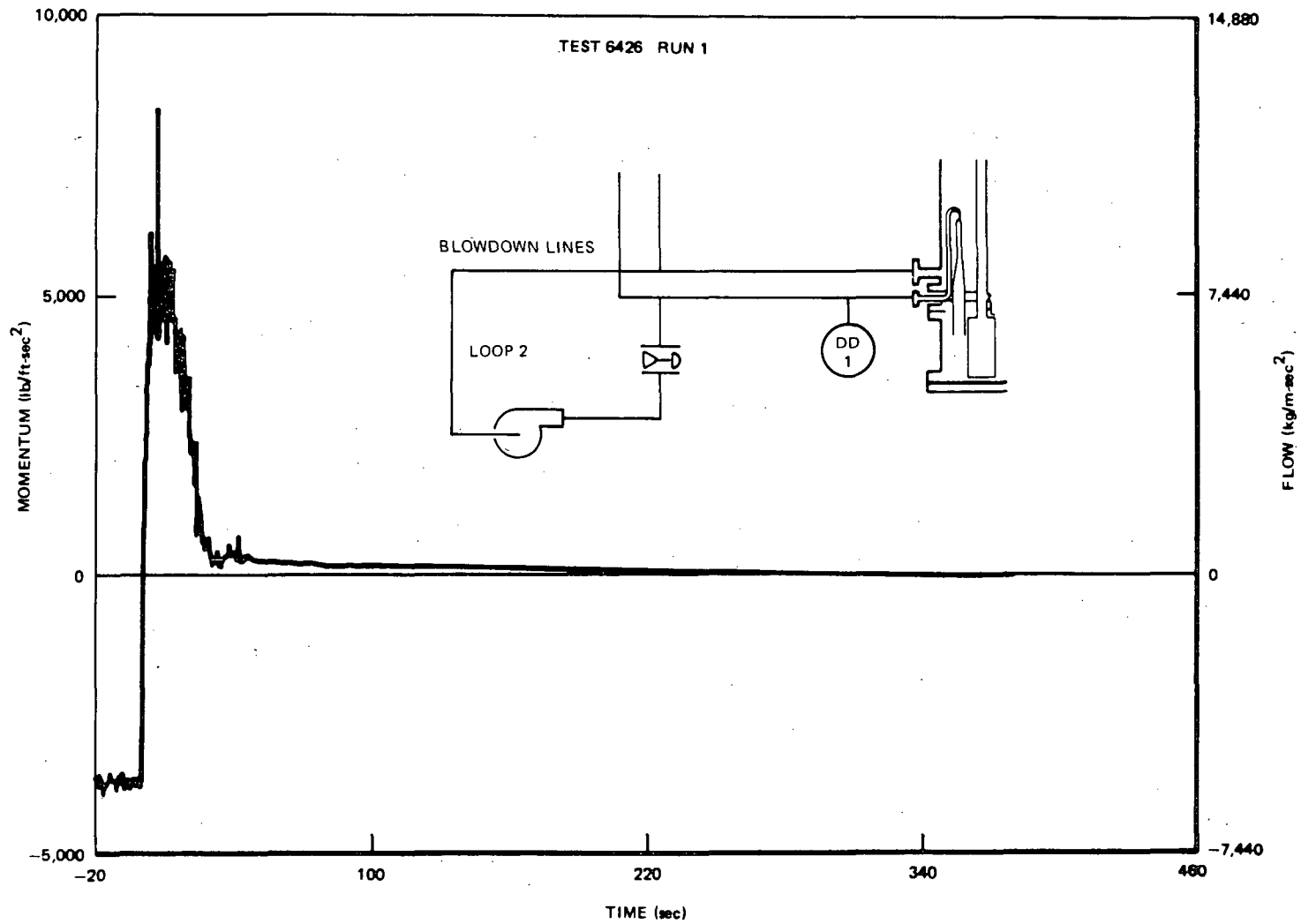


Figure H-12. Drive Line Drag Disc Momentum for Test 6426 Run 1 (Avg. Power, No ECC, Valve Failure)

81-H

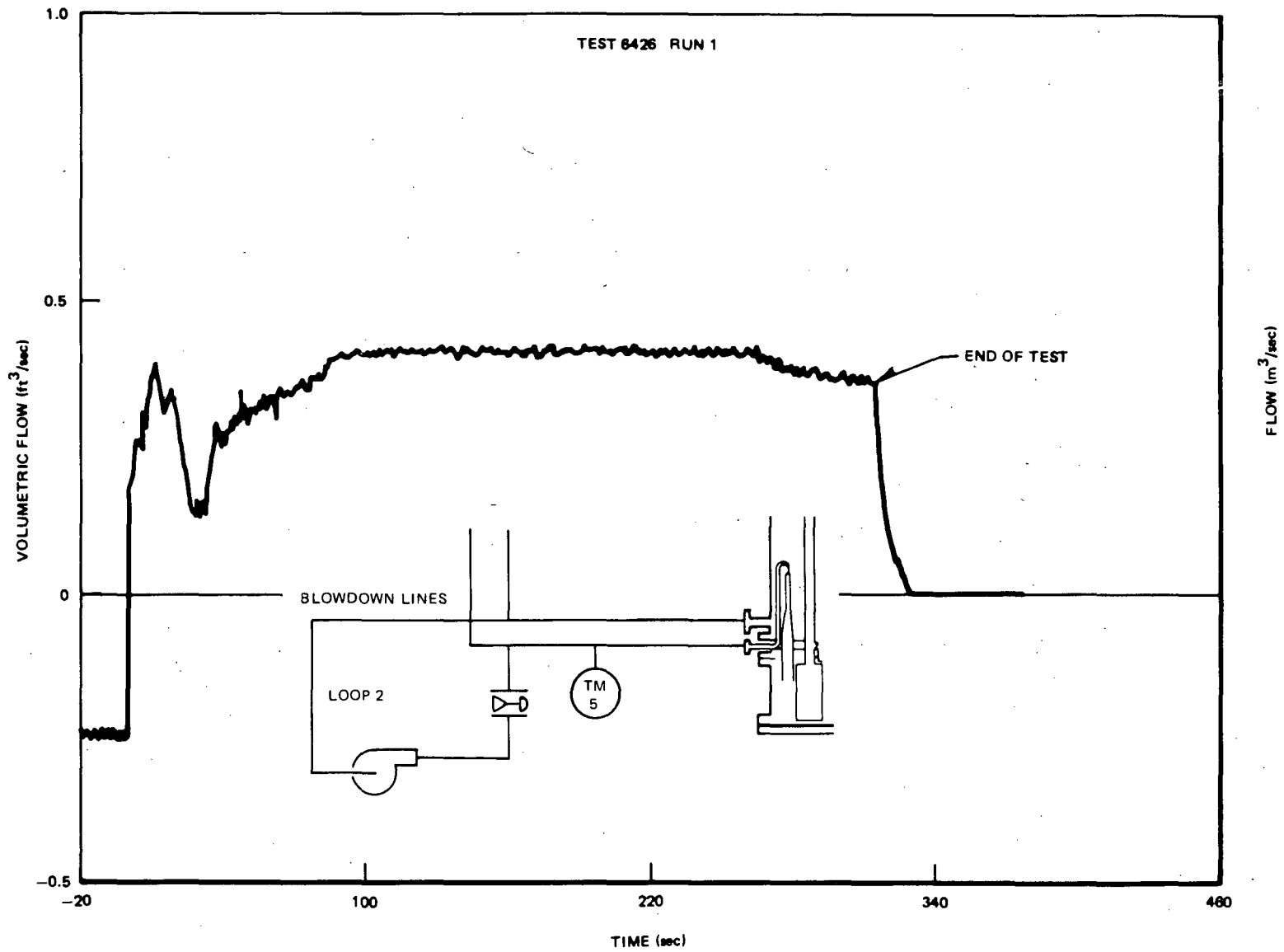


Figure H-13. Drive Line Turbinemeter Volumetric Flow for Test 6426 Run 1 (Avg. Power, No ECC, Valve Failure)

6I-H

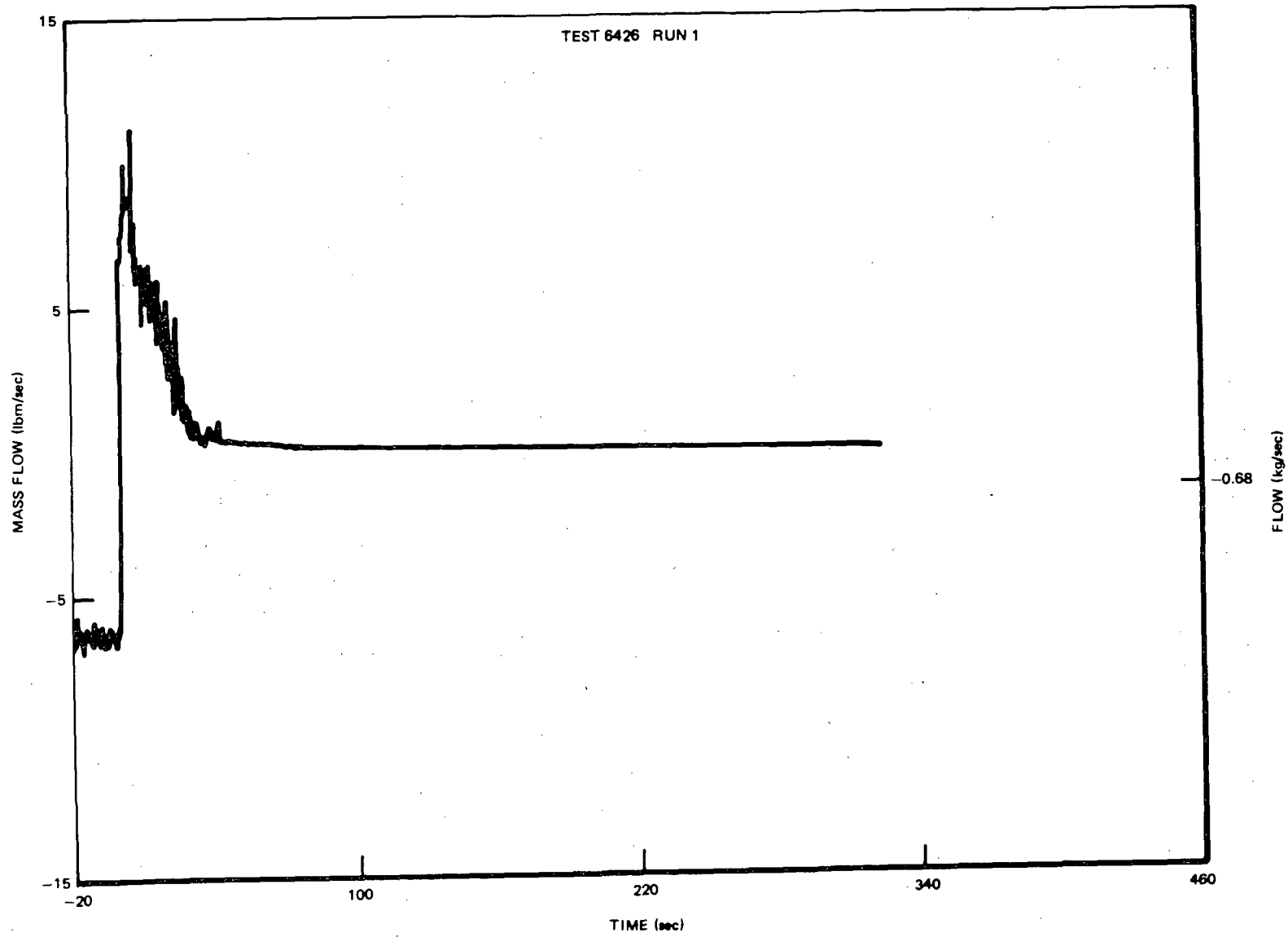


Figure H-14. Drive Line Break Flow Based on TM/DD for Test 6426 Run 1 (Avg. Power, No ECC, Valve Failure)

H-20

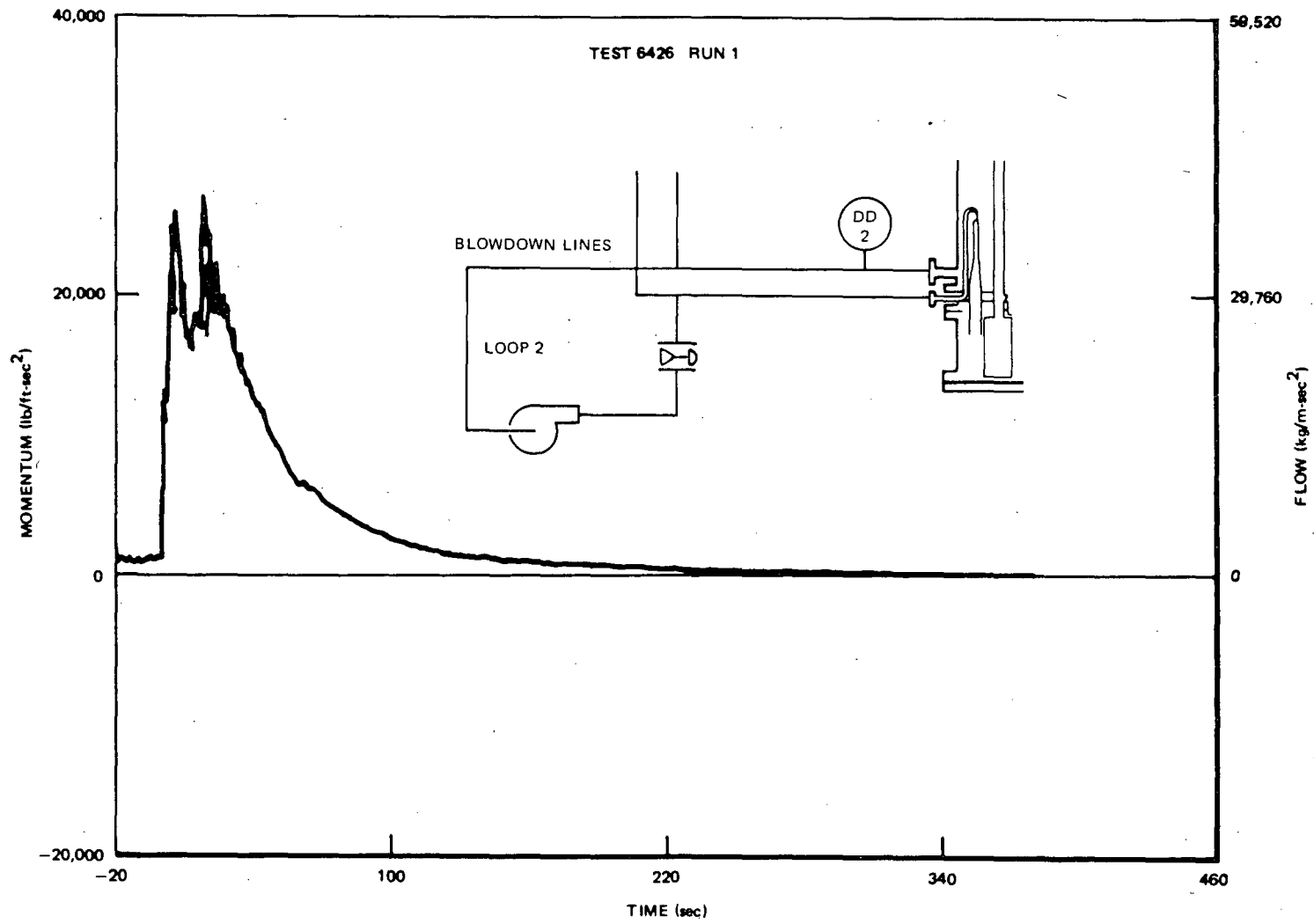


Figure H-15. Drag Disc Momentum at Suction Line for Test 6426 Run 1 (Avg. Power, No ECC, Valve Failure)

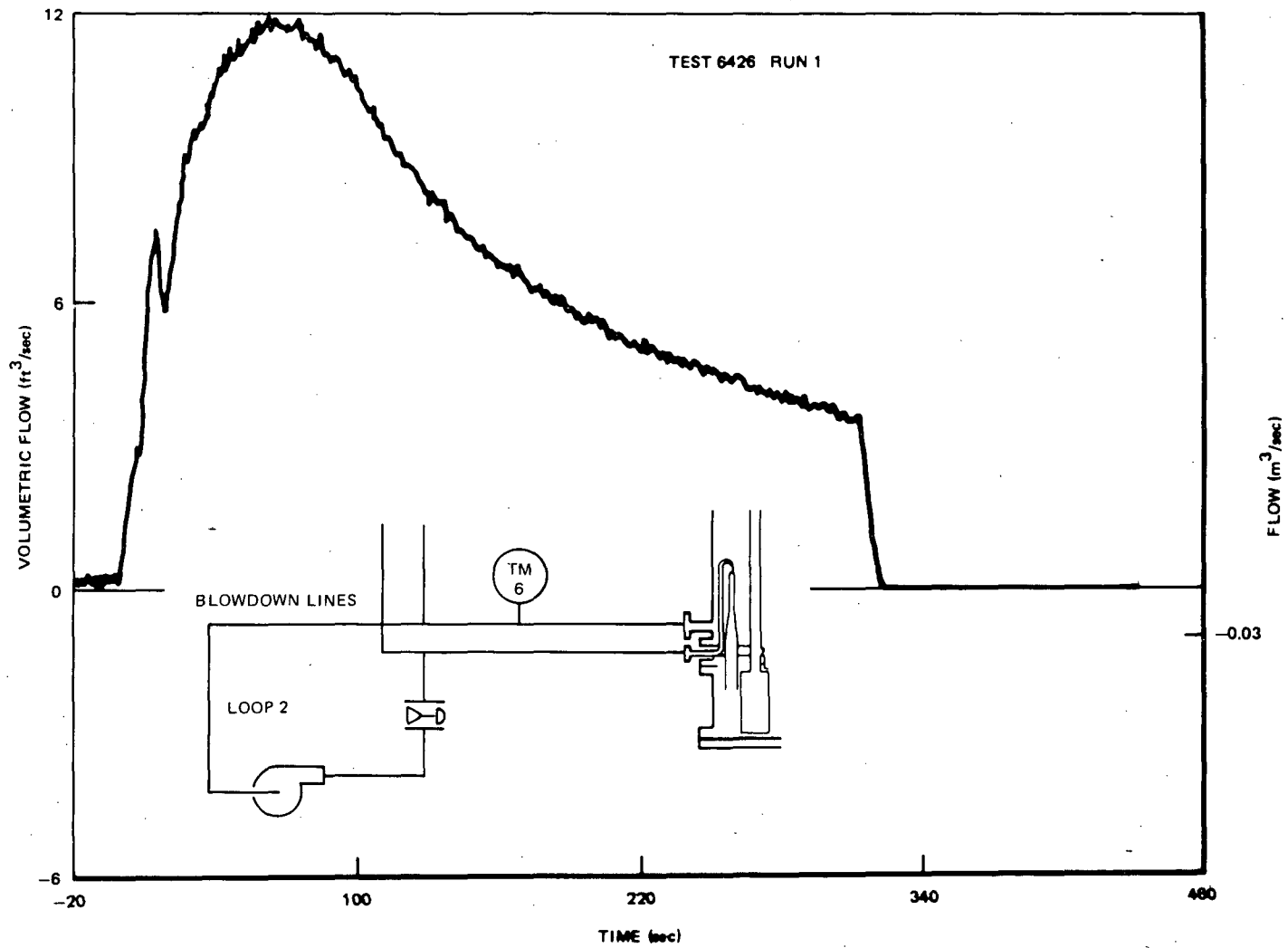


Figure H-16. Turbinometer Volumetric Flow at Suction Line for Test 6426 Run 1 (Avg. Power, No ECC, Valve Failure)

H-22

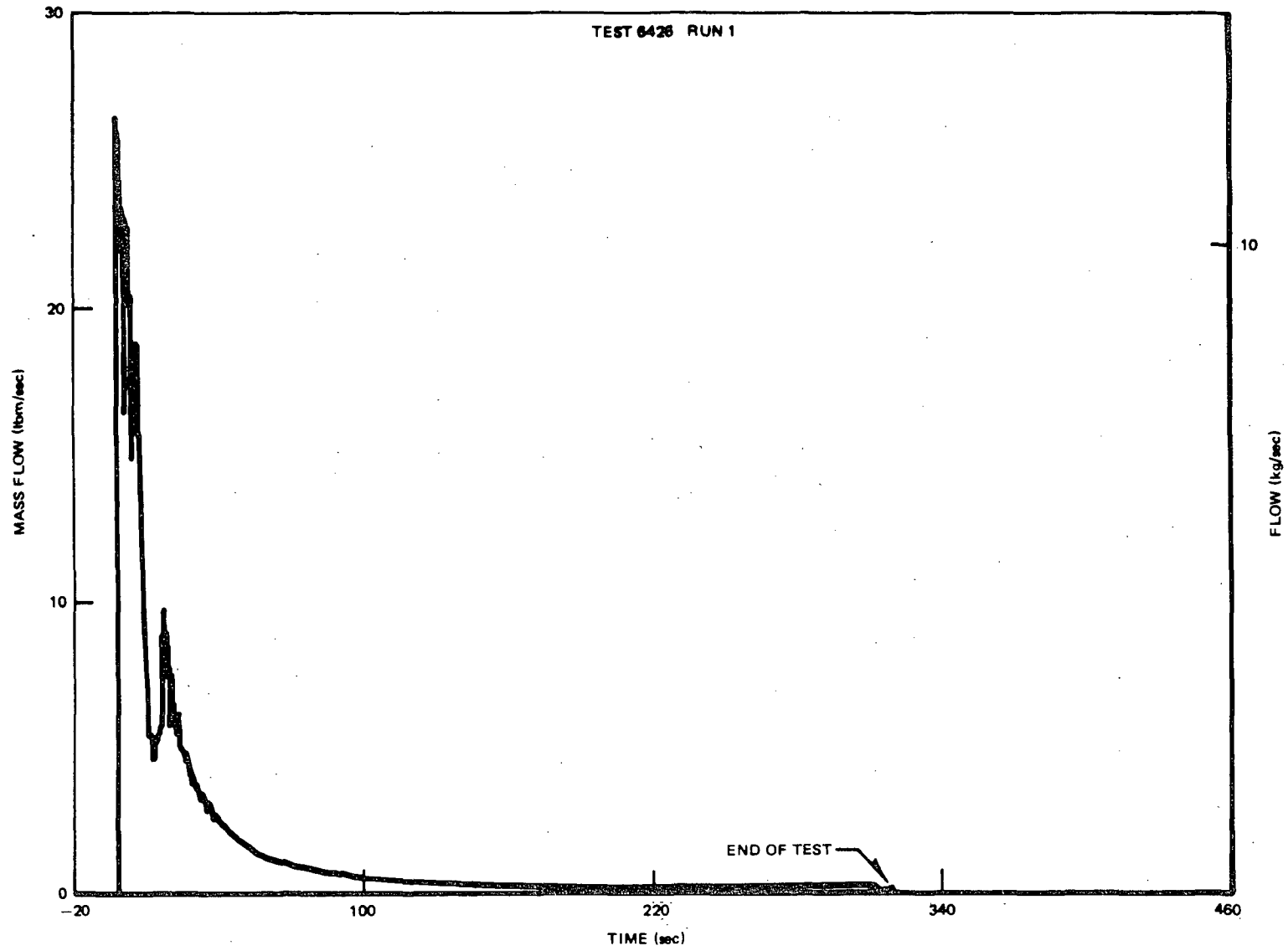


Figure H-17. Suction Line Break Flow Based on TM/DD for Test 6426 Run 1

Calculated data for the blowdown Nozzle flow (suction line only) are included as Figures H-18 and H-19 for Tests 6425 and 6426, respectively. As expected, the two flow rates are similar except for the latter portion of the runs.

The results for all methods have been summarized in Table H-1 for Test 6425 and Table H-2 for Test 6426. The total mass flow and average flow rate are presented for each of four time intervals. The time intervals were chosen to represent different portions of the blowdown as identified in Table H-3.

The blowdown nozzle flow calculation represents only the suction line blowdown and may be compared directly to the drag disc/turbine meter suction line flow. In Tables H-1 and H-2 the blowdown nozzle method requires addition of the drive line flow, taken from the drag disc/turbine meter data, to obtain a total blowdown flow for comparison to other methods.

The suppression tank results are not presented for Test 6426 because the tank cooling water supply was kept in operation during the test.

H-3. GENERAL COMPARISON OF METHODS AND UNCERTAINTY

As evidenced in Tables H-1 and H-2, the vessel inventory, drag disc/turbine meter, and blowdown nozzle methods all give reasonably consistent results for each test. The suppression tank method is included to show that the method does have some potential but needs optimization if accurate results are to be obtained. The blowdown flow for both tests is nearly the same except for the last time interval (100-200 sec) when some ECC-injected water was available for discharge through the blowdown line in Test 6425.

Table H-3
FLOW INTERVALS

<u>Time</u>	<u>Flow Type</u>
0-10 seconds	slightly subcooled liquid
10-30 seconds	steam plus saturated liquid from lower plenum flashing
30-100 seconds	primarily steam
100-200 seconds	steam plus liquid from ECC injection (if applicable)

H-24

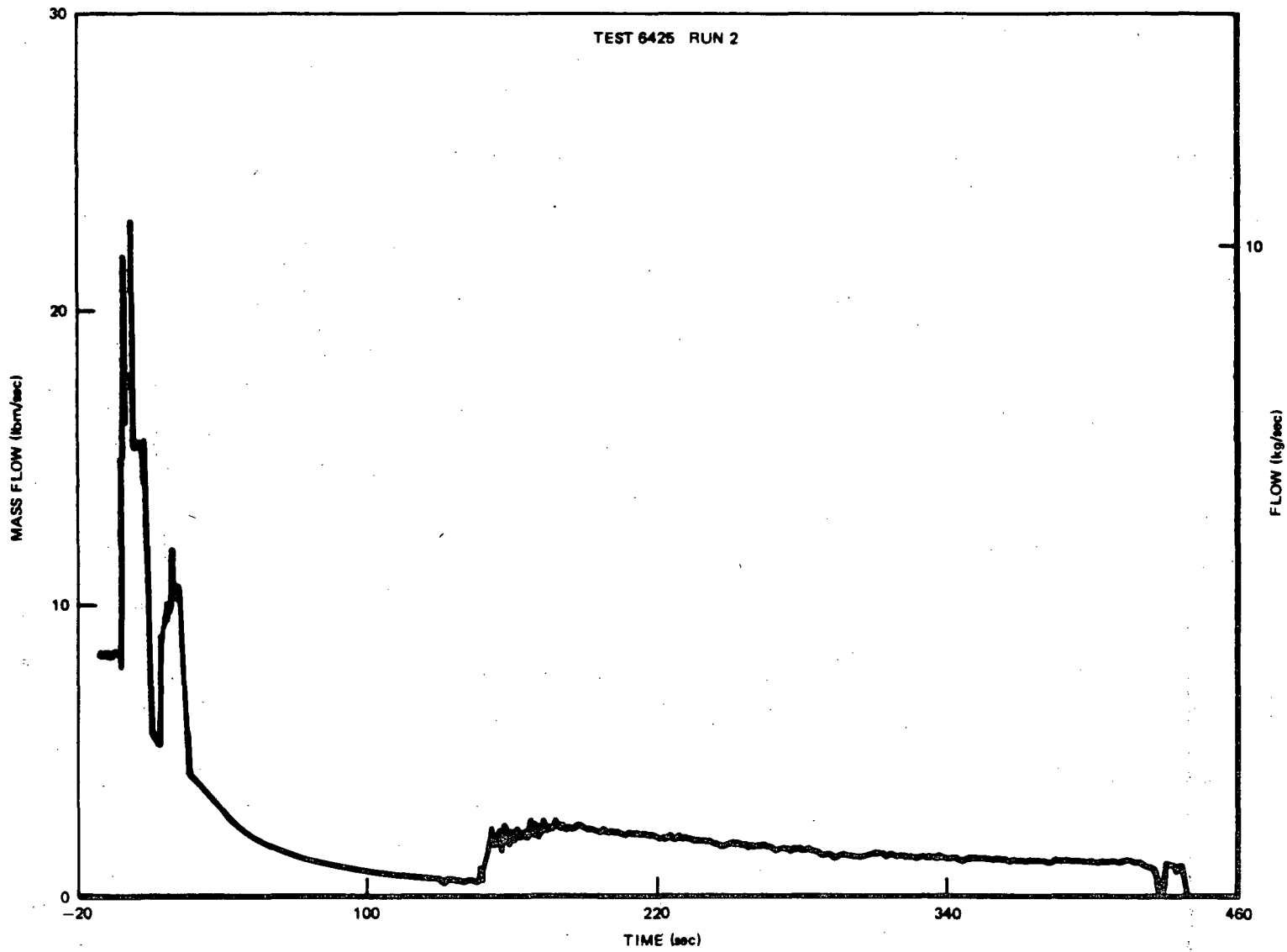


Figure H-18. Blowdown Nozzle Flow for Test 6425 Run 2 (Avg. Power, Avg. ECC)

H-25

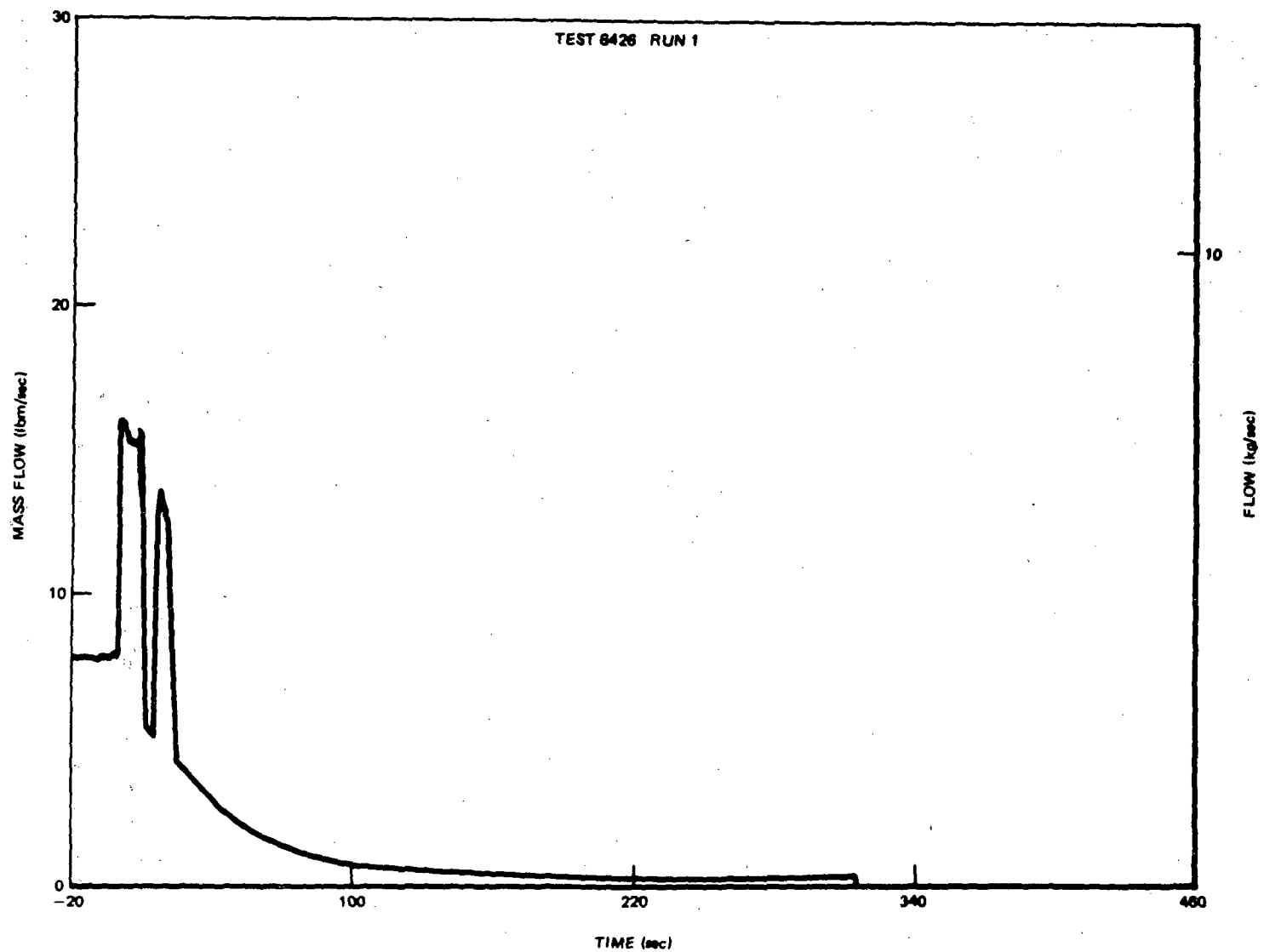


Figure H-19. Blowdown Nozzle Flow for Test 6426 Run 1 (Avg. Power, No ECC, Valve Failure)

The vessel inventory method is considered the reference or more accurate method of giving average rates over the entire transient because it is based upon proven techniques for measurement of density from vessel nodal differential pressure. The best estimate of overall uncertainty in integrated mass is $\pm 15\%$ after corrections such as are made for dynamic flow effects on the density measurements at the initial conditions just prior to the start of the blowdown. This method is most accurate during the latter part of the transient when dynamic flow effects inside the vessel are minimal.

The drag disc/turbine meter method agrees with the vessel inventory method within about $\pm 25\%$ except after 100 seconds when the drag disc/turbine meter flow is 50 to 70 percent higher. For that time period, the suction line DD/TM appears to yield results which are too high.

The accuracy of the drag disc/turbine meter method is limited by the fact that homogeneous flow is assumed. A separate density measurement is needed to obtain data for estimating individual liquid and vapor phase velocities for use in a more detailed treatment such as the Rouhani model.* Such an enhancement would be expected to yield more accurate results. Even with its present limitations, the drag disc/turbine meter method continues to provide the best transient mass flow indication and enables comparison of volumetric flow rate vs. mass flow rate.

The blowdown nozzle method results are actually more consistent with the reference method results than expected. The method is handicapped by a non-ideal arrangement of instruments to measure blowdown pipe inlet fluid density because pressure taps are not available on the vessel at the optimum locations. The results in terms of integrated flow for the given time intervals are within $\pm 30\%$ of the same suction line blowdown flow as calculated by the drag disc/turbine meter method except for the 100-200-second interval for Test 6425. For that time period, the blowdown flow agrees more closely with the reference vessel inventory method.

*H. Estrada, Jr. and J. D. Sheppard, Some Aspects of Interpreting Two-Phase Flow Measurements in Instrumented Piping Spool Pieces, U.S. Nuclear Regulatory Commission, June 1977 (NUREG-0280/NRC-2).

DISTRIBUTION

Division of Reactor Safety Research
U.S. Nuclear Regulatory Commission
Washington, DC 20555
Attn: W. D. Beckner (5)

Division of Reactor Licensing
U.S. Nuclear Regulatory Commission
Washington, DC 20555
Attn: R. K. Frahm

Electric Power Research Institute
4312 Hillview Avenue
Palo Alto, CA 94303
Attn: S. P. Kalra

Argonne National Laboratory
9700 Cass Avenue
Argonne, IL 60439
Attn: P. Lottes, RSR Heat Transfer Coordinator

EG & G
550 Second Street
Idaho Falls, ID 83401
Attn: R. J. Dallman

Safety and Systems Analysis
Nuclear Power Generation Division
Babcock & Wilcox
P. O. Box 1260
Lynchburg, VA 24505
Attn: Dr. B. E. Bingham

Reactor Development Center
Babcock & Wilcox
P. O. Box 1260
Lynchburg, VA 24505
Attn: Mr. D. Montgomery

Safeguards Development
Pressurized Water Reactor Systems Division
P. O. Box 355
Pittsburgh, PA 15230
Attn: Dr. L. E. Hochreiter

C-E Power Systems
Combustion Engineering, Inc.
1000 Prospect Hill Road
Windsor, CT 06095
Attn: Mr. J. D. Crawford

Librarian, General Atomic
P. O. Box 81608
San Diego, CA 92138

Department of Nuclear Engineering
University of California at Berkeley
Berkeley, CA 94720

Department of Nuclear Engineering
Massachusetts Institute of Technology
77 Massachusetts Avenue
Cambridge, MA 02139

Engineering Library
Stanford University Campus
Stanford, CA 94305

Los Alamos Scientific Laboratory
Los Alamos, NM 87544
Attn: C. W. Hirt, Group T-3

Environmental Protection Agency
P. O. Box 15027
Las Vegas, NV 89114

U. S. Nuclear Regulatory Commission
Reactor Analysis Section/Analysis Branch
Washington, DC 20555
Attn: W. Hodges

Mr. Kenneth Randen
ASEA Atom 1
Box 53
S-721 04
Vaesteraas 1, Sweden

Dr. T. Kawai
Hitachi, Limited
Hitachi Works
3-1-1 Saiwai-Cho
Hitachi-Shi, Ibaraki-Ken 317, Japan

Mr. Dieter Ewers
Kraftwerk Union AG
Postfach 700649
D-6000 Frankfurt (Main) 70
Federal Republic of Germany

Dr. H. Hashimoto
Tokyo Shibaura Electric Company
Toshiba Mita Building
13-12, 3-Chome Mita, Minato-Ku
Tokyo, 108, Japan

Mr. E. Annino
AMN Impianti Termici e Nucleari
Casella Postale 190
16151 Genova Sampierdarena
Italy

NRC FORM 335 (11-81)		U.S. NUCLEAR REGULATORY COMMISSION BIBLIOGRAPHIC DATA SHEET		1. REPORT NUMBER (Assigned by DDC) NUREG/CR-2229, Vol. 1 EPRI NP-1783 GEAP-24962-1	
4. TITLE AND SUBTITLE (Add Volume No., if appropriate) BWR Large Break Simulation Tests -- BWR Blowdown/Emergency Core Cooling Program				2. (Leave blank)	
7. AUTHOR(S) L.S.Lee, G.L. Sozzi, and S.A. Allison				3. RECIPIENT'S ACCESSION NO.	
9. PERFORMING ORGANIZATION NAME AND MAILING ADDRESS (Include Zip Code) Nuclear Engineering Division General Electric Company 175 Curtner Ave. San Jose, California 95125				5. DATE REPORT COMPLETED MONTH YEAR March 1981	
12. SPONSORING ORGANIZATION NAME AND MAILING ADDRESS (Include Zip Code) Division of Accident Evaluation Office of Nuclear Regulatory Research U.S. Nuclear Regulatory Commission Washington, D.C. 20555				6. (Leave blank)	
13. TYPE OF REPORT Technical Report				7. (Leave blank)	
15. SUPPLEMENTARY NOTES				8. (Leave blank)	
16. ABSTRACT (200 words or less) The BD/ECC Program is an experimentally based program jointly sponsored by the Nuclear Regulatory Commission, The Electric Power Research Institute, and The General Electric Company. The BD/ECC 1A Test Phase of this program involves investigating the integral systems effects of emergency core coolant injection during a hypothetical LOCA. Tests were conducted in a BWR system simulator, the Two-Loop Test Apparatus (TLTA), which features a full-sized electrically heated bundle. Fluid delivery systems were included to simulate emergency coolant injections. Tests conducted under this program include large break (design basis accident), small break, and core uncover under slow loss-of-coolant (boil-off) transients. Three separate topical reports are issued, one for each type of test. This topical covers the large break results.				9. (Leave blank)	
17. KEY WORDS AND DOCUMENT ANALYSIS BWR LOCA TLTA		10. PROJECT/TASK/WORK UNIT NO.			
17b. IDENTIFIERS/OPEN-ENDED TERMS		11. FIN NO. FIN B3014			
18. AVAILABILITY STATEMENT Unlimited		13. TYPE OF REPORT Technical Report		PERIOD COVERED (Inclusive dates) 1976-1981	
19. SECURITY CLASS (This report) Unclassified		14. (Leave blank)			
20. SECURITY CLASS (This page) Unclassified		15. SUPPLEMENTARY NOTES			
21. NO. OF PAGES		16. ABSTRACT (200 words or less) The BD/ECC Program is an experimentally based program jointly sponsored by the Nuclear Regulatory Commission, The Electric Power Research Institute, and The General Electric Company. The BD/ECC 1A Test Phase of this program involves investigating the integral systems effects of emergency core coolant injection during a hypothetical LOCA. Tests were conducted in a BWR system simulator, the Two-Loop Test Apparatus (TLTA), which features a full-sized electrically heated bundle. Fluid delivery systems were included to simulate emergency coolant injections. Tests conducted under this program include large break (design basis accident), small break, and core uncover under slow loss-of-coolant (boil-off) transients. Three separate topical reports are issued, one for each type of test. This topical covers the large break results.			
22. PRICE S		17. KEY WORDS AND DOCUMENT ANALYSIS BWR LOCA TLTA			

UNITED STATES
NUCLEAR REGULATORY COMMISSION
WASHINGTON, D. C. 20555

OFFICIAL BUSINESS
PENALTY FOR PRIVATE USE, \$300

POSTAGE AND FEES PAID
U.S. NUCLEAR REGULATORY
COMMISSION

